

**KARADENİZ TECHNICAL UNIVERSITY
THE GRADUATE SCHOOL OF NATURAL AND APPLIED SCIENCES**

ELECTRICAL AND ELECTRONICS ENGINEERING GRADUATE PROGRAM

**AN INTELLIGENT CONTROLLED NOVEL POWER CONDITIONING FOR
WAVE ENERGY CONVERTER SYSTEMS**

Ph.D. THESIS

Emre Özkop, M.Sc.E.

**FEBRUARY 2012
TRABZON**

KARADENİZ TECHNICAL UNIVERSITY
THE GRADUATE SCHOOL OF NATURAL AND APPLIED SCIENCES
ELECTRICAL AND ELECTRONICS ENGINEERING GRADUATE PROGRAM

**AN INTELLIGENT CONTROLLED NOVEL POWER CONDITIONING FOR
WAVE ENERGY CONVERTER SYSTEMS**

Emre Özkop, M.Sc.E.

**This Thesis is Accepted to Give the Degree of
"DOCTOR OF PHILOSOPHY IN ELECTRICAL ENGINEERING
By
The Graduate School of Natural and Applied Sciences
at Karadeniz Technical University**

**The date of Submission : 21.02.2012
The date of examination : 12.03.2012**

Thesis Supervisor : Prof. Dr. İsmail Hakkı Altaş

Trabzon 2012

Karadeniz Technical University
The Graduate School of Natural and Applied Sciences
Electrical and Electronics Engineering Graduate Program

The thesis entitled:

**AN INTELLIGENT CONTROLLED NOVEL POWER CONDITIONING FOR
WAVE ENERGY CONVERTER SYSTEMS**

Prepared by Emre Özkop

has been accepted as a thesis of

DOCTOR OF PHILOSOPHY

**after the examination by the jury assigned by the Administrative Board of the
Graduate School of Natural and Applied Sciences with the decision number 1445/6
dated February 21, 2012.**

Examining Committee Members

Supervisor : Prof. Dr. İsmail Hakkı Altaş

Member : Prof. Dr. Liuchen Chang

Member : Assoc. Prof. Dr. Cemal Köse

Member : Asst. Prof. Dr. Halil İbrahim Okumuş

Member : Asst. Prof. Dr. Fatih Mehmet Nuroğlu

Prof. Dr. Sadettin KORKMAZ
Director

Karadeniz Teknik Üniversitesi Fen Bilimleri Enstitüsü
Elektrik-Elektronik Mühendisliği Ana Bilim Dalında
Emre ÖZKOP Tarafından Hazırlanan

DALGA ENERJİSİ DÖNÜŞTÜRÜCÜ SİSTEMLERİNDE AKILLI DENETİMLİ
YENİ BİR GÜÇ DÜZENLEYİCİ UYGULAMASI

başlıklı bu çalışma, Enstitü Yönetim Kurulunun 21 / 02 / 2012 gün ve 1445/6 sayılı kararıyla oluşturulan jüri tarafından yapılan sınavda

DOKTORA TEZİ
olarak kabul edilmiştir.

Jüri Üyeleri

Başkan : Prof. Dr. İsmail Hakkı ALTAŞ

Üye : Prof. Dr. Liuchen CHANG

Üye : Doç. Dr. Cemal KÖSE

Üye : Yrd. Doç. Dr. H. İbrahim OKUMUŞ

Üye : Yrd. Doç. Dr. Fatih M. NUROĞLU

Prof. Dr. Sadettin KORKMAZ
Enstitü Müdürü

FOREWORD

There are times that one gives many things to reach the targeted goal. Graduate studies consume an important part in academician life. Completing PhD seems to be the end of it. However, I think its a pass way to harder studies rather than being an end. A good research in PhD leads to better ones afterwards. I hope this thesis and the research I have done will bring a similar effect on my future studies.

I would like to give my thanks to my supervisor Dr. İsmail Hakkı Altaş for his guidance, support, and enthusiasm during my studies. I will remain in intellectual debt to Dr. Altaş throughout my life, not only for guiding me in this dissertation, but also in my academic and professional life throughout this decade. I would like to deeply express my sincere thanks to Dr. Adel M. Sharaf for his novel ideas and guidance, which inspired me in many parts of this thesis. Also, special thanks go to my committee members: Dr. Cemal Köse, Dr. Halil İbrahim Okumuş and Dr. Fatih Mehmet Nuroğlu for their constructive feedback and timely inspiration in this journey. I also would like to thank to Dr. Liuchen Chang for accepting to be a member of my examining committee. I also wish to express my sincere thanks to Dr. A. Sefa Akpınar who supervised me during way M.Sc.E studies.

To all member of the Department of Electrical and Electronics Engineering, both past and present, I want to give very sincere thanks to them for their support of my research and continuing friendship. I enjoyed every minute of working with them and wish them all the best. I especially would like to thank Topaloğlu, Sevim, Hacıoğlu, Akyazı for all of the good times, both in and out of the department.

Thanks to Karadeniz Technical University Scientific Research Projects Unit (Project No: 2008.112.004.1) and TÜBİTAK for the project supporting and providing a scholarship via 2211-National Scholarship Programme for PhD Students, respectively.

Finally, my greatest thanks go to my mother, Zehra, my sisters, Emine, Emel and my brother, Ekrem, for their ongoing love and encouragement; I could not have done this without you.

I want to dedicate this thesis to my father, Sadettin who could not wait to see the completion of this thesis.

Emre Özkop
Trabzon 2012

THESIS STATEMENT

I declare that, this PhD thesis, I have submitted with the title “An Intelligent Controlled Novel Power Conditioning for Wave Energy Converter Systems” has been completed under the guidance of my PhD supervisor Prof. Dr. İsmail Hakkı Altaş. All the data used in this thesis are obtained by simulation and experimental Works done as parts of this work in our research labs. All referred information used in the thesis has been indicated in the text and cited in reference list. I have obeyed all research and ethical rules during my research and I accept all responsibility if proven otherwise. 21/02/2012

Emre Özkop

TABLE OF CONTENTS

	<u>Page No</u>
FOREWORD.....	IV
THESIS STATEMENT.....	V
TABLE OF CONTENTS	VI
ÖZET.....	X
SUMMARY	XI
LIST OF FIGURES.....	XII
LIST OF TABLES	XVII
LIST OF SYMBOLS.....	XVIII
LIST OF ABBREVIATIONS	XXI
1. INTRODUCTION.....	1
1.1. World Energy Demands.....	1
1.2. Renewable Energy	2
1.3. Objectives of This Dissertation.....	4
1.4. Organization of This Dissertation.....	5
2. WAVE ENERGY	6
2.1. Introduction.....	6
2.2. Wave Energy Systems	6
2.3. Control in Wave Energy Systems	10
2.4. Power and Electrical Equipment in Wave Energy Systems	12
3. SYSTEM MODELING AND SIMULATION.....	17
3.1. Introduction.....	17
3.2. Wave Energy Converter System.....	19
3.2.1. The Wave Model.....	19
3.2.1.1. Approximated Model of the Wave Dynamics	19
3.2.1.2. Stochastic Model of the Wave Dynamics	21
3.2.2. Generator Model	22
3.2.2.1. Ideal Model	22
3.2.2.2. Dynamic Model.....	25
3.3. Power Electronic Converters	28

3.3.1.	AC/DC Rectifier	28
3.3.2.	DC-DC Buck Converter.....	29
3.3.3.	DC/AC Inverter.....	31
3.3.4.	Green FACTS Interface (SPF-GP)	33
3.4.	Control Strategy	35
3.4.1.	Introduction.....	35
3.4.2.	Conventional (P, PI and PID) Controls.....	35
3.4.3.	Sliding Mode Control.....	37
3.4.4.	Fuzzy Logic Control	39
3.4.5.	Application of the Controllers.....	40
3.5.	Backup Units.....	42
3.5.1.	Photovoltaic Energy Conversion System.....	42
3.5.2.	Battery.....	43
3.5.2.1.	Battery Management System (BMS)	44
3.5.2.2.	Battery State of Charge Estimation.....	45
3.5.2.3.	Current Based SOC Estimation.....	46
3.6.	Loads.....	48
4.	EXPERIMENTAL STUDIES.....	49
4.1.	Introduction.....	49
4.2.	Wave Energy Conversion Emulator (WECE)	50
4.2.1.	Computer Based Wave Energy Conversion Emulator (CBWECE)	50
4.2.1.1.	Wave Energy Converter Output Voltage Waveform Model	51
4.2.1.2.	Three Phase Wave Energy Converter Output Voltage Modeling.....	53
4.2.1.3.	Signal Filtering.....	54
4.2.1.4.	Signal Amplification.....	56
4.2.1.5.	Power Supply Stage	57
4.2.1.5.1.	Low-voltage/Low-current Power Stage.....	57
4.2.1.5.2.	High-voltage/High-current Power Stage	58
4.2.1.6.	Computer Based Wave Energy Conversion Emulator Output Waveforms.....	59
4.2.2.	Machine Based Wave Energy Conversion Emulator (MBWECE)	60
4.3.	Switched Power Filter-Green Plug (SPF-GP).....	64
4.4.	Design of Power Electronic Converters.....	64
4.4.1.	DC-DC Buck Converter Design	64

4.4.2.	DC-DC Chopper Design	66
4.4.2.1.	Power Supply	66
4.4.2.2.	Driver	67
4.4.2.3.	Current Control	68
4.4.2.4.	Current Protection	70
4.4.2.4.1.	Upper Transistor Current Protection	70
4.4.2.4.2.	Lower Transistor Current Protection and Regulation	70
4.4.3.	DAQ Output Isolation Circuit	71
4.4.4.	DC/AC Inverter Design	74
4.4.4.1.	Integrated Power Module	74
5.	SIMULATION AND EXPERIMENTAL RESULTS	76
5.1.	Experimental Results for the Wave Energy Converter System	76
5.1.1.	Introduction	76
5.1.2.	Experimental Results for Different Scenarios	76
5.1.2.1.	A Novel Switched Power Filter-Green Plug (SPF-GP) Scheme for Wave Energy Systems	76
5.1.2.1.1.	Experimental Set-up for the WEC System Laboratory Testing	78
5.1.2.1.2.	Novel Error Driven Controller	79
5.1.2.1.3.	Digital Simulation	80
5.1.2.1.4.	Experimental Implementation	83
5.1.2.1.5.	Digital Simulation and Experimental Results	84
5.1.2.2.	Novel Switched Power Filter-Green Plug (SPF-GP) Intelligent Controllers for Wave Energy Converter System: Experimental Results	91
5.1.2.2.1.	The Wave Energy Conversion System	91
5.1.2.2.2.	Experimental Implementation	92
5.1.2.2.3.	Experimental Results	94
5.1.2.2.4.	Conclusion	102
5.1.2.3.	A Novel Switched Power Filter-Green Plug (SPF-GP) Scheme for Wave Energy System with Hybrid Loads	104
5.1.2.3.1.	The Wave Energy Conversion with Hybrid Loads	104
5.1.2.3.2.	Controllers	106
5.1.2.3.3.	Digital Simulation	108
5.1.2.3.4.	Experimental Implementation	110
5.1.2.3.5.	Digital Simulation and Experimental Results	113

5.1.2.3.6. Conclusion	120
5.2. Summary	121
6. CONCLUSIONS AND FUTURE WORKS	123
6.1. Conclusions.....	123
6.2. Future Work	124
7. REFERENCES.....	125
8. APPENDICES	146
CURRICULUM VITAE	

Doktora Tezi

ÖZET

DALGA ENERJİSİ DÖNÜŞTÜRÜCÜ SİSTEMLERİNDE AKILLI DENETİMLİ YENİ BİR
GÜÇ DÜZENLEYİCİ UYGULAMASI

Emre ÖZKOP

Karadeniz Teknik Üniversitesi
Fen Bilimleri Enstitüsü
Elektrik-Elektronik Mühendisliği Anabilim Dalı
Danışman: Prof. Dr. İsmail Hakkı ALTAŞ
2012, 145 Sayfa, 18 Sayfa Ek

Dalga enerjisi, dünyadaki en fazla bulunan fakat yeterince kullanılmayan enerji kaynaklarından biridir. Ancak, dalga enerjisi dönüşüm sisteminin karmaşık yapısı, deniz koşulları, mekanik zorluklar ve oldukça yüksek maliyetten dolayı, dalga enerjisi dönüşüm sistemi yeteri kadar yaygın değildir. Yine de alternatif enerji kaynaklarının kullanımına duyulan ihtiyaç, çeşitli kaynakların enerji dönüşüm tasarımlarının geliştirilmesinde etkin olmuştur. Dalga enerjisi, umut vadeden enerji kaynaklarından bir tanesidir ve dünyanın bazı bölgelerinde dalga enerjisi dönüştürücü sistemler kuruludur. Dalga enerjisinin karakteristik yapısının zaman içerisinde kararlı ve önceden kestirilebilir olmaktan çok düzensiz olması sebebiyle dalga enerjisi dönüştürücülerinden elde edilen elektrik enerjisi de düzensiz yapıya sahiptir. Bu sebeple, dalga enerjisi dönüşüm sistemleri, dalga enerjisinin düzgün olmayan özelliklerini gidermek için güç düzenleyici ara yüzüne gerek duymaktadır.

Bu çalışmada, kaynak tarafı düzensizliklerini gidermek ve yük kısmından yalıtılmak için Anahtarlamalı Güç Filtresi-Yeşil Fiş olarak isimlendirilen yeni bir Esnek Alternatif Akım İletim güç koşullandırıcısı sunulmaktadır. Bu anahtarlamalı güç filtresi-yeşil fiş, yeni bir DA-DA Esnek Alternatif Akım İletim cihazıdır ve geliştirilen uygun anahtarlama anları ile kontrol edilmektedir. Kaynak tarafındaki düzensizlik ile uyumlu çalışmak için uyarlanabilir akıllı denetleyicilerin geliştirilmesi gereklidir. Bu sebeple, klasik, bulanık ve klasik-bulanık birleştirilmiş denetleyiciler de irdelenerek, gerilim, akım ve güç gibi kontrol parametrelerinin değişimine dayalı adaptif yapılı denetim tasarlanmış ve kullanılmıştır. Geliştirilen bütün sistem modelleri hem benzetim hem de deneysel olarak test edilmiştir. Sistem performansları ve model doğrulama için benzetim modeli sonuçları, uygulamadan elde edilenler ile karşılaştırılmıştır.

Anahtar Kelimeler: Dalga enerjisi, Akıllı kontrol, Anahtarlamalı Güç Filtresi, FACTS, Yeşil yenilenebilir enerji kullanımı

PhD. Thesis

SUMMARY

AN INTELLIGENT CONTROLLED NOVEL POWER CONDITIONING FOR WAVE
ENERGY CONVERTER SYSTEMS

Emre Özkop

Karadeniz Technical University
The Graduate School of Natural and Applied Sciences
Electrical and Electronics Engineering Graduate Program
Supervisor: Prof. Dr. İsmail Hakkı Altaş
2012, 145 Pages, 18 Pages Appendix

The wave energy is the biggest and untapped energy sources on planet Earth. However, the wave energy conversion is not ubiquitous enough due to its structure complexities, sea conditions and high cost. However, the need of using alternative energy sources has an impact on developing energy conversion schemes from various sources that seems to be costly but have promising future. The wave energy is one of these promising energy sources and has been installed in some specific sites around the world. Since the characteristic behavior of the wave energy is irregular rather than being stable and predictable for time durations, the electrical power obtained by wave energy converters has an irregular behavior, as well. Therefore wave energy conversion systems require interfacing power conditioners to compensate the irregular characteristics of the wave power.

A novel power conditioner FACTS device, called Switched Power Filter - Green Plug is introduced in this study in order to compensate and isolate the load side electrical quantities from the source side irregularities. The novel SPF-GP is a DC-DC type FACTS device and controlled by developing proper switching sequences. In order to comply the irregularity on the source side, adaptive based intelligent controllers are required to be developed. Therefore classical, fuzzy, and classical-fuzzy combined controllers are also studied to be operated by including adaptively in terms of the variations in control parameters such as voltage, current, and power. All system models are developed and tested both by simulation and implementation. Simulation model results are compared with those of obtained from implementation for model validation and system performances.

Key Words: Wave energy, Intelligent control, Power filter, FACTS, Green renewable energy utilization

LIST OF FIGURES

	<u>Page No</u>
Figure 3.1. Wave Energy Conversion system with the novel FACTS (SPF-GP).....	18
Figure 3.2. A progressive surface wave shape.....	19
Figure 3.3. Surface particle velocity profile	21
Figure 3.4. Pierson Moskowitz wave spectral density representing summer conditions.....	22
Figure 3.5. The phase to neutral voltage.....	25
Figure 3.6. PMLG dynamic Simulink model.....	27
Figure 3.7. Circuit diagram of the rectifier used in the thesis.....	28
Figure 3.8. A classification of DC-DC converter technologies	29
Figure 3.9. A general buck DC/DC converter schematic	30
Figure 3.10. The designed DC-DC buck converter general circuit diagram	31
Figure 3.11. The DC-AC inverter system block diagram.....	32
Figure 3.12. The SPF-GP FACTS scheme	34
Figure 3.13. The two operating states of the novel FACTS SPF-GP system	34
Figure 3.14. The switching waveforms for normal operation.....	35
Figure 3.15. The PI controller.....	40
Figure 3.16. The PID controller.....	40
Figure 3.17. The classical FLC	40
Figure 3.18. The Self-Scaled FLC (SSFLC).....	41
Figure 3.19. The classical SMC.....	41
Figure 3.20. The Fuzzy Tuned SMC (FTSMC).....	41
Figure 3.21. The Self-Scaled Fuzzy Tuned PI Controller (SSFTPIC)	41
Figure 3.22. One diode equivalent parameters PV model	42
Figure 3.23. Charge stages of lead acid battery	44
Figure 3.24. BMS flow chart	45
Figure 3.25. Simulation diagram of the system with DC and AC motor type loads	48
Figure 4.1. The experimental setup.....	50
Figure 4.2. The general system block diagram	50
Figure 4.3. The wave energy waveform Matlab/Simulink model	51

Figure 4.4. Wave velocity model.....	52
Figure 4.5. Phase-neutral voltage.....	52
Figure 4.6. The WEC output voltage waveform with the RTWT.....	52
Figure 4.7. The output waveforms of the DAQ card analog outputs.....	53
Figure 4.8. The phase shift circuit diagram	53
Figure 4.9. The input (V_{in}) and output (V_{out}) signals of the phase.....	54
Figure 4.10. The shift circuit output voltage waveforms.....	54
Figure 4.11. The second order low-pass Chebyshev filter circuit diagram	55
Figure 4.12. The input ($V_{C2} - V_{C1}$) and output (V_{A3}) signals of the filter circuit.....	56
Figure 4.13. The system circuit diagram (phase shift, signal filtering and amplification circuits).....	57
Figure 4.14. The low power stage circuit diagram	58
Figure 4.15. The high power stage circuit diagram	58
Figure 4.16. Wave energy converter system emulator block diagram.....	59
Figure 4.17. The wave energy converter emulator waveform (a) The DAQ card analog output (b) The adjustment stages output (x10).....	59
Figure 4.18. A general view of the wave energy converter test bed.....	60
Figure 4.19. The WECE test block diagram for Case I	61
Figure 4.20. Phase to phase AC voltage waveform (x137)	61
Figure 4.21. The dc-bus voltage waveform (x137).....	61
Figure 4.22. The WECE test block diagram for Case II.....	62
Figure 4.23. The dc-bus voltage waveform (x137) (C=1200uF, 45Vdc).....	62
Figure 4.24. The WECE test block diagram for Case III and Case IV.....	63
Figure 4.25. The dc-bus voltage (x137) (DC load: 12V DA, 0.16A).....	63
Figure 4.26. The dc-bus voltage (x137) (DC load: 12V DA, 0.16A) (C=1200uF, 45Vdc).....	63
Figure 4.27. Experimental circuitry view of the SPF-GP system.....	64
Figure 4.28. The designed DC-DC buck converter general circuit diagram	65
Figure 4.29. The converter system detailed circuit diagram.....	65
Figure 4.30. The block scheme of controller power supply.....	67
Figure 4.31. The driver connection diagram.....	68
Figure 4.32. Current control block diagram.....	69
Figure 4.33. Upper transistor current production circuit diagram	70
Figure 4.34. Lower transistor current production circuit diagram.....	71

Figure 4.35. Isolation circuit diagram	72
Figure 4.36. The designed DC-DC chopper circuit diagram	73
Figure 4.37. The DC-AC inverter system block diagram	75
Figure 5.1. Wave Energy Conversion system without the SPF-GP	77
Figure 5.2. Wave Energy Conversion system with the SPF-GP	78
Figure 5.3. A general view of WEC system experimental set-up	78
Figure 5.4. Single-loop voltage control scheme	79
Figure 5.5. A novel multi-loop dynamic error driven control scheme	80
Figure 5.6. The system Simulink operational block diagram without the SPF-GP	81
Figure 5.7. The system Simulink operational block diagram with the SPF-GP	82
Figure 5.8. The main control stages of the test system: (a) without the SPF-GP (b) with the SPF-GP	83
Figure 5.9. Experimental setup	84
Figure 5.10. WEC voltage (PI)	86
Figure 5.11. DC bus voltage (V_d) (PI)	86
Figure 5.12. PMDC motor voltage (V_m) (PI)	87
Figure 5.13. WEC voltage (PI)(Case III-IV)	87
Figure 5.14. DC bus voltage (V_d) (PI)	87
Figure 5.15. PMDC motor voltage (V_m) (PI)	87
Figure 5.16. WEC voltage	88
Figure 5.17. DC bus voltage (V_d)	88
Figure 5.18. PMDC motor voltage	88
Figure 5.19. WEC voltage	88
Figure 5.20. DC bus voltage (V_d)	89
Figure 5.21. PMDC motor voltage	89
Figure 5.22. The sample study system diagram (without SPF-GP)	91
Figure 5.23. The sample study system diagram (with SPF-GP)	92
Figure 5.24. Data acquisition and Simulink modeling of for single loop PI controller the system without the SPF-GP	93
Figure 5.25. Data acquisition and Simulink modeling of three loop dynamic error driven PI controller for the system with SPF-GP	93
Figure 5.26. WEC voltage	95
Figure 5.27. WEC current	95
Figure 5.28. DC bus voltage (V_d)	96

Figure 5.29. DC bus current (I_d)	96
Figure 5.30. PMDC motor voltage (V_m)	96
Figure 5.31. PMDC motor current (I_m)	96
Figure 5.32. WEC voltage	98
Figure 5.33. WEC current	98
Figure 5.34. DC bus voltage (V_d)	98
Figure 5.35. DC bus current (I_d)	98
Figure 5.36. PMDC motor voltage (V_m)	99
Figure 5.37. PMDC motor current (I_m)	99
Figure 5.38. WEC voltage	100
Figure 5.39. WEC current	100
Figure 5.40. DC bus voltage (V_d)	101
Figure 5.41. DC bus current (I_d)	101
Figure 5.42. PMDC motor voltage (V_m)	101
Figure 5.43. PMDC motor current (I_m)	101
Figure 5.44. Wave Energy Conversion system without the SPF-GP	105
Figure 5.45. The three phase AC motor voltage control with SSFTPIC block diagram	106
Figure 5.46. The PMDC motor speed control with PID controller block diagram	107
Figure 5.47. The battery charge control with FLC block diagram	107
Figure 5.48. The three-loop dynamic error driven control with PI controller for the SPF-GP system diagram	108
Figure 5.49. The Simulink operational block diagram of the system without the FACTS (SPF-GP)	109
Figure 5.50. The Simulink operational block diagram of the system with the FACTS (SPF-GP)	109
Figure 5.51. The main control stages of the test system without the FACTS (SPF-GP)	111
Figure 5.52. The main control stages of the test system with the FACTS (SPF-GP)	112
Figure 5.53. WEC phase-phase voltage	115
Figure 5.54. WEC phase current	115
Figure 5.55. Load side bus voltage, V_{lsb}	116
Figure 5.56. Load side bus current, I_{lsb}	116
Figure 5.57. Battery voltage, V_b	116

Figure 5.58. Battery charge current, I_b	116
Figure 5.59. Battery net current, I_{bnc}	117
Figure 5.60. Battery SOC.....	117
Figure 5.61. PMDC motor speed	117
Figure 5.62. 3 phase AC motor phase-phase voltage (rms).....	117
Figure 5.63. WEC phase-phase voltage	118
Figure 5.64. WEC phase current.....	118
Figure 5.65. Load side bus voltage, V_{lsb}	118
Figure 5.66. Load side bus current, I_{lsb}	118
Figure 5.67. Battery voltage, V_b	119
Figure 5.68. Battery charge current, I_b	119
Figure 5.69. Battery net current, I_{bnc}	119
Figure 5.70. Battery SOC.....	119
Figure 5.71. PMDC motor speed	120
Figure 5.72. 3 phase AC motor phase-phase voltage (rms).....	120

LIST OF TABLES

	<u>Page No</u>
Table 1.1. Comparison of renewable energy technologies.....	4
Table 2.1. Wave energy converter systems with controls in literature.....	14
Table 3.1. Application parts of the controllers in the Wave Energy Conversion system.....	42
Table 3.2. The comparison of the commonly used rechargeable battery systems	43
Table 3.3. The energy and cost comparison in rechargeable batteries	43
Table 3.4. The comparison of the different techniques for SOC estimation	46
Table 3.5. The history of SOC development	47
Table 4.1. Switch states and current values	69
Table 5.1. The three different system scenarios for the real time experimental studies.	85
Table 5.2. The system scenarios for the real time experimental studies	94
Table 5.3. The three different system scenarios for the real time experimental studies.	113

LIST OF SYMBOLS

B	DC motor friction
C	Phase velocity
C_d	SPF-GP capacitor
C_f	Load side bus filter capacitor
C_1	Buck converter input filter capacitor
C_2	Buck converter input filter capacitor
C_3, C_4	Buck converter snubber capacitors
C_5	Buck converter filter capacitor
d	Displacement
d_c	Duty cycle
d_G	Maximum generator travel
d_w	Wave depth
D_1	Buck converter freewheeling diode
D_2	SPF-GP freewheeling diode
e_{dcmlv}	DC motor load voltage error signal
e_{I_d}	Loop error of DC bus current dynamic error
$e_{I_{lsb}}$	Loop error of load side bus current dynamic error
e_m	DC motor induced voltage
e_{P_d}	Loop error of DC bus power dynamic error
$e_{P_{lsb}}$	Loop error of load side bus power dynamic error
e_{t_B}	Total control error
e_{V_d}	Loop error of DC bus voltage error
$e_{V_{lsb}}$	Loop error of load side bus voltage error
F	Force for PMLG
f_e	Peak electrical frequency
$f_{mono-loop}$	Mono-loop switching frequency
f_{spf-gp}	SPF-GP switching frequency
H	Wave height
i_a	DC motor armature current

i_d	d-axis current
i_q	q-axis current
I_{bat}	Battery current
I_c	Cell output current
I_d	DC bus current
I_{dcmlc}	DC motor load current
I_{lsb}	Load side bus current
I_o	Reverse saturation current of diode
I_{ph}	Photo current, function of irradiation level and junction temperature
J	DC motor nonlinear inertia
k	Wave number
$K_{I(dcmlv)}$	Mono-loop PI controller I parameters
K_T	Torque constant
$K_{P(dcmlv)}$	Mono-loop PI controller P parameters
L	Wave length
L_f	Load side bus filter inductance
L_m	DC motor inductance
L_1	Buck converter input filter inductor
L_2	Buck converter filter inductor
N	Number of turns per coil
p	Number of poles of a machine
P_d	DC bus power
Q	Rated capacity
r	Radius of machine
R_m	Coil resistance in PMLG
R_{dcm}	DC motor resistance
R_s	Series resistance
R_1, R_2	Buck converter snubber resistances
$S(\omega)$	Spectra form
S_A, S_B	Controller B PWM output signals
S_x	Ambient irradiation
T	Wave period

T_e	DC motor electromagnetic torque
T_{em}	Electrical torque
T_L	DC motor load torque
T_0	Low-pass filter time delay
T_x	Ambient temperature
V_{bat}	Battery voltage
V_c	Cell output voltage
v_d	d-axis voltage
V_d	DC bus voltage
V_{dcmlc}	DC motor load voltage
V_{dcmlv}	DC motor load voltage
$V_{dcmlv(ref)}$	DC motor load reference voltage
V_{lsb}	Load side bus voltage
v_q	q-axis voltage
\hat{V}	Peak phase-neutral voltage
ω_c	Vertical velocity
ω_m	Wave frequency
ω_{mech}	Rotational mechanical frequency
ω_{mo}	DC motor angular velocity
ω_s	Vertical particle velocity
γ_{I_d}	Loop weight gain of current tracking loop
γ_{P_d}	Loop weight gain of power tracking loop
γ_{V_d}	Loop weight gain of voltage tracking loop
λ	Magnetic wavelength
λ_{fd}	Excitation linkage flux of a machine
σ	Sliding surface
σ_w	Wave angular frequency
τ	Pole pitch
α	Sliding surface slope
$\hat{\Phi}$	Peak flux
θ	Phase displacement angle

LIST OF ABBREVIATIONS

AWS	Archimedes Wave Swing
BMS	Battery Management System
CBWECE	Computer Based Wave Energy Conversion Emulator
CCM	Continuous Conduction Mode
DCM	Discontinuous Conduction Mode
FACTS	Flexible AC Transmission System
FLC	Fuzzy Logic Controller
FTSMC	Fuzzy Tuned Sliding Mode Controller
LIMPET	Land Installed Marine Power Energy Transmitter
MBWECE	Machine Based Wave Energy Conversion Emulator
OB	Oscillating Body
OWC	Oscillating Wave Column
PCB	Printed Circuit Board
PECS	Power Electronic Converters
PID	Proportional-Integral-Derivative
PM	Permanent Magnet
PMDC	Permanent Magnet DC Motor
PMLG	Permanent Magnet Linear Generator
PV	Photovoltaic
PWM	Pulse Width Modulation
SMC	Sliding Mode Controller
SOC	State of Charge
SPF-GP	Switched Modulated Power Filter-Green Plug
SSFLC	Self-Scaled Fuzzy Logic Controller
SSFTPIC	Self-Scaled Fuzzy Tuned PI Controller
VSCS	Variable Structure Control System
VSS	Variable Structure System
WEC	Wave Energy Converter
WECE	Wave Energy Conversion Emulator
WSE	Wave Star Energy

1. INTRODUCTION

1.1. World Energy Demands

Energy is key to economic and social development. While world population and national economic growth continue to impact energy and electricity demand, over 80% of the world's energy demand is still supplied by fossil fuels (petroleum, natural gas, and coal) and this energy demand could double or much more by 2050 [1]. It is assumed that global energy demand increases by one-third from 2010 to 2035 [2, 3]. Renewables and natural gas are collectively expected to reach nearly two-thirds of rising energy demand for 2010-2035 [2]

Increase in oil demand and oil market uncertainties cause price volatility with oil import price expected to reach 210 \$/barrel by 2035. In addition, there is a prediction that US oil imports will surpass those of the EU and China by 2035 [2, 3].

It seems that natural gas share in the market is increasing and will continue to increase over the period to 2035. As well, indicators show that Russia continues to be the leader as a gas producer until 2035. Although natural gas is the cleanest of the fossil fuels, increasing use of it will not solve the carbon emissions problem.

In the first decade of the 21st century, coal use continued to rise [2, 3]. In international coal markets, pricing has become increasingly sensitive to developments in Asia, with India overtaking China as the biggest coal importer by 2020. A different point of view on energy shows that there is still an energy deficit in the world with 1.3 billion people, around 20% of the world's population still live without electricity [3].

As described above, the world oil supply diversity is diminishing and popularity of natural gas is growing with the consumption point shifting from one conventional source (coal) to another (natural gas). Thus, countries having resources become role players in the world energy market. However, when any turmoil takes place in source regions such as Middle East and North Africa, doubts on the reliability of energy supply emerge and economic concerns divert attention from energy policy. Countries with limited energy resources have planned to rely on nuclear power. On the other hand, the effects of the earthquake on Fukushima Daiichi nuclear power plant have caused doubts on reliability of nuclear power.

Increased concerns about environmental pollution, overpopulation, desire of developing countries to have same life standards as developed countries, unevenly distributed fossil fuel resources, imbalance in consumption, energy crisis, and rising or fluctuating costs of fossil fuels around the world forces people to reduce consumption, greenhouse gas emissions, environmental pollution and dependency on oil and natural gas by controlling the population growth with implementation of policies on energy sources.

The world consumption relies primarily on oil, coal, natural gas, nuclear and water power. The most of the energy sources have been extracted via difficult methods and long processes. The fossil fuels such as oil, coal and gas are not sustainable and also the lifetime of fossil fuels is limited.

It is obvious that energy is an important need for quality life standards and strategic development for the nations. Therefore alternative energy is always in the scope of the research topics for current and future energy planning. In order to mitigate the potential crises caused by the limited resources as well as the disputes between countries, many nations have targeted investment on renewable energy as an alternative to the conventional sources.

1.2. Renewable Energy

Main renewable energy sources are solar, wind, bioenergy, geothermal, hydro, tide, waves, hydrogen and so on. Renewable energy gives hope to lessen environmental concerns and to increase source diversities. Many countries have announced regulations to providing incentives towards the renewable energy utilization. During the last decade, the use of renewable energy such as wind and solar has been increased tremendously so that some countries are supplying about 4-20% of their energy needs from wind and solar resources. Although it is not used as much as solar and wind, the wave and tidal energy has also become an alternative to the conventional ones as a usable energy source lately as the devices are developed to resolve the power quality problems. Since one of the main problems in renewable energy applications is interfacing the generating units with the user side, the interface devices take an important role in renewable energy utilization. In addition to the technical problems, the investors of the renewable energy systems are still facing other problems such as feed-in tariffs, renewable portfolio standards, local regulations, financial supports, etc.

In order to underline the importance of renewable and alternative energy, it will probably be good to take a look at world's primary energy outlook.

The share of the primary energy sources in the world primary energy supply in 2005 was indicated as 25.3% coal, 35.0% oil, 20.6% natural gas, 6.3% nuclear, 2.6% hydro, 9.9% renewable combustibles and wastes. Besides, the product shares in the world renewable energy supply in 2005 were recorded as 78.6% renewable combustibles and waste (75.6% solid biomass/charcoal, 0.9% gas from biomass), 0.6% wind, 17.4% hydro, 0.3% solar/tide, and 3.2% geothermal [4, 5].

Renewable sources have grown to supply about 16% of global final energy consumption. At least 100 countries have renewable energy policy targets or support policies. Moreover, total global investment in renewable energy in 2010 has increased 32% compared to the previous year. As the renewable energy capacity has grown, the costs have decreased accordingly. At least 61 countries and 26 states/provinces worldwide enact feed-in tariff programs. Many policies have been implemented to popularize renewable energy applications, such as direct capital investment subsidies and grants, tax incentives, credits, and public financing [5]. Wind and solar energies are two of most common renewable energy sources in use.

The sun is the main source of renewable energies and provides wind, bio, wave and hydro energies to arise. Solar energy is plentiful. The amount of incoming solar energy in one day is sufficient to afford the world's total energy needs for one year. The solar power used for heating and lighting until the eighteenth century has been utilized to get electricity via solar cell invention in 1883 [6]. A photovoltaic (PV) cell is used to convert sunlight into electricity in solar energy applications. It has many advantages such as working anywhere that the sun shines. However, high cost and intermittency (no power generation during nights) are serious drawbacks of PV solar energy. There are many PV applications such as residential, industrial, utility-scaled power, despite the high cost. PV utilization has been increased over the years, while PV demand worldwide was 2.83 GW in 2007, it has showed a 110% increase in 2008 [7]. Solar power use is predicted to grow thousand-fold until 2050 [4].

Wind energy is one of the most popular energy technologies with the earliest utilization of wind energy dating to 5000 B.C. Wind energy was used for boat propelling, water pumping, grain grinding in its early applications, and electricity generation from wind energy began in the early 1880s [6, 7]. Installed wind power capacity has increased

so fast over the years that over 70 countries are using wind energy. From 2000 to 2007, the global wind power capacity has increased to approximately five times of its previously recorded data [6]. The wind power electricity generating capacity in the world is about 198 GW as of 2010 [5]. 23% of electricity is generated by wind in Denmark, 6% in Germany and approximately 8% in Spain [7]. There is a prediction that 12% of global electricity will be provided from wind power by 2050 [4]. Environmental factors such as visual impact, noise, and risk of bird collisions and disruption of wild life should be taken into consideration during wind energy power system realization.

Mainly wind and solar renewable energy sources have been competitive with fossil fuels through technological improvements in performance and cost. A comparison of renewable energy technologies is given in Table 1.1 [8].

Table 1.1. Comparison of renewable energy technologies

Technology	Typical levelized costs (US cents per kWh)	Advantages	Problems
Wind	4-5	Widespread resource, scalable	Difficult to site, intermittent
Photovoltaic	20-40	Ubiquitous source, silent, long lifetimes, scalable	Very expensive, intermittent
Biomass	4-9	Dispatchable, large resource	Has air emissions, expensive
Hydropower	4	Dispatchable, can be inexpensive	Has land, water, and ecological impacts
Geothermal	5-6	Dispatchable, can be inexpensive	Limited resource, depletable
Wave	20-30	Widespread resource, high density, few aesthetic and noise concerns	Immature technology, expensive, unpredictable environment

Note: Net cost to install a renewable energy system divided by its expected life-time energy output
Levelized means including first (capital), operating, maintenance, and fuel costs

1.3. Objectives of This Dissertation

The purpose of this study is to reduce the interfacing power quality problems, improve the energy utilization of Wave Energy Converter (WEC) systems, design and realize of a novel power stage and effective control strategies. The main focus is given to modeling, validation and control for a wave energy converter system, a novel Switched Modulated Power Filter-Green Plug (SPF-GP) Scheme adapted into a wave energy converter system and loads exhibiting variable characteristics. The ultimate goal of this dissertation is to set up experimental prototype models of the wave energy converter

system, the proposed SPF-GP system and error driven controllers to verify the digital simulation model by comparing the results which validate the effectiveness of the proposed interfacing device and the control algorithms. Both the simulation and the experiments are done for several cases and results of the same operating conditions from both platforms are compared for model validation as well as system performances. Effectiveness of the proposed Flexible AC Transmission System (FACTS) power filter compensator and control strategies on eliminating stochastic wave effects on load side voltage and load variations on source side by reducing voltage sags and swells is also investigated.

1.4. Organization of This Dissertation

A review and background information on the wave energy is given in Chapter Two. The modeling and simulation of the proposed wave energy conversion system is developed and given in Chapter Three. The conversion system parts, which are wave energy converter system, power electronic converters, proposed FACTS device, controllers, back up units and loads are dealt with regards to modeling. Chapter Four describes the experimental design and realization of the overall system described in previous chapter. In Chapter Five the simulation and experimental results for the wave energy converter system are presented. Chapter Six reviews the results, provides concluding remarks, and addresses the future work.

2. WAVE ENERGY

2.1. Introduction

Over 70% of the earth's surface is covered by oceans, which are the world's largest solar collectors. Moreover, the oceans are the biggest and untapped energy sources on planet Earth. One of the energy harvesting methods from ocean is based on taking advantage of waves, which are result of wind blowing over the water surface. The power density of wave energy is much higher than that of wind or solar energy. The environmental concerns in the use of wave systems for generating energy are also less. Waves can travel long distances and lose little energy during travelling. Depending on sea surface, weather conditions, shore structure and location on earth, the magnitude and periodic characteristic of the waves may vary. Magnitude and duration of the waves occurring consecutively may not be the same each time. The occurrence of the waves may be periodic with the same peaks however, this is not guaranteed every time and it is not suggested to rely on this behavior of the wave characteristics. On the other hand, waves show periodic occurrence with the same magnitudes for some certain durations in time. Waves show different characteristics from season to season, day to night, day to day, even hour to hour during the same day.

Depending on design and usage, the wave energy converter can produce power up to 90% of the time while wind and solar power systems produce 20-30% [9-12].

2.2. Wave Energy Systems

The energy in waves around the world has a considerable amount of potential. The useful worldwide wave power resource has been estimated to be greater than 2 TW [9]. The estimated annual global wave electricity potential is 300 TWh [4]. Annual average wave power levels differ in various parts of the world. The wave energy potential is about 1 TWh/day at the coastal waters of the British Isles and the same amount of energy supplies British Isles electricity demand for an average day. Estimates indicate that approximately 15-25% of the United Kingdom (UK) energy demand can be supplied by the wave energy [11]. Wave energy potential in Europe is about 320 GW [7]. The wave

energy can effectively contribute to world energy demands. At least 25 countries are engaged in wave energy development [5].

Although there are a number of mechanisms such as attenuator, terminator and point absorber to capture wave energy and prototypes, few commercial projects are realized [7, 9-11, 13]. As wave energy conversion is complex and not ubiquitous and subject to varying sea conditions, wave energy converter system cost is considerably high [6]. There are over 1000 patents on wave energy conversion techniques presented in Europe, Japan, and North America [11]. The most common wave energy technologies are categorized as shown below [12, 14, 15]:

Oscillating Water Column

Fixed:

Isolated: Pico [16, 17], LIMPET [18-20]

Breakwater: Sakata [21], Mutriku [22]

Floating: Mighty Whale [23, 24], Sperboy [25], Spar Buoy [26], Oceanlinx [27, 28]

Oscillating Bodies

Floating:

Translation: AquaBuoy [29-31], IPS Buoy [32- 34], FO3 [35], Wavebob [36, 37],
PowerBuoy [38-41]

Rotation: Pelamis [42-47], PS Frog [48], SEAREV [49-51]

Submerged:

Translation: AWS [52-54]

Rotation: WaveRoller [55, 56], Oyster [57, 58]

Overtopping

Floating: Wave Dragon [59-62]

Fixed:

Shoreline: TAPCHAN [63, 64]

Breakwater: SSG [65, 66]

Although the first patent dates back to 1799, the oil crisis of the 1970s led to greater interest in utilization from waves with the world's first commercial wave farm (2.25 MW) built in 2005 in Portugal [9, 11, 12].

The wave energy devices can be categorized as shoreline, nearshore, and offshore [67]. In offshore energy technologies, the wave energy conversion system is located away from the shore and a floating or fixing body is used to absorb wave energy. Nearshore technologies are adapted into the shore. Channel/reservoir/turbine and air-driven turbine methods are applied to harvest wave energy. Each mechanism has a variety of advantages and disadvantages. For instance, whilst locations for land installations for oscillating water column (OWC) systems are more limited than offshore systems, land installations are easier to construct and maintain. Although the shoreline wave devices have advantages such as easy installation and maintenance, the wave energy extracted potential is lower than other schemes. As the nearshore devices are positioned in less than 20 m water depths, the offshore devices are more typical in deep water (>40 m).

There are some fuzzy matters and problems, such as environmental impacts, test and measurement standards, resources assessment, energy production forecasting and design tools that must be illuminated [4, 67-69].

In the wave energy systems, energy conversion devices such as linear or rotational generators, compressors, turbines, and pumps can be used to convert mechanical energy of wave to electrical energy. There are many studies about wave energy converter systems, operation mode, generator types like wave-activated linear, linear, synchronous, longitudinal-flux permanent magnet (PM), three-phase synchronous, and radial flux PM synchronous generators, switched reluctance machines, turbine models such Wells, Self-pitch-controlled blades, Kaplan, mechanical part shapes [6].

There are many possibilities to harness waves through a variety of means with device parts such as floats, flaps, ramps and liquid pistons. They can be installed at the surface, the sea bed or anywhere and use oil, air, water, steam, gearing depends on wave energy system types [9, 10]. OWC, Overtopping devices, Pelamis, Wave Dragon, Archimedes Wave Swing (AWS), and Wave Star Energy (WSE) are mainly used technologies to convert wave power into electricity. Each technology incorporates advantages and disadvantages with regards to power limits, efficiency, maintenance, installation and operation costs, and installation difficulties [6, 9, 12, 14]. Some of the wave energy technologies are summarized below:

The studies on OWC started in the 1970s and then a number of systems have been built in various places, such as Japan, UK, Australia, India, and Norway up to now. The system turbine size changes between 250 kW to 1 MW. The OWC system to require large

area is one of disadvantages. On the other hand, there is no direct connection between turbine, generator and water, no requirement of deep-water anchorages and long submarine electrical cables [6, 12]. Thus, the mechanical parts are protected against water corrosion. The Wells turbine and the Impulse turbine considered, as two of the most popular types of air turbines are used in OWC systems [9]. Wavegen's Land Installed Marine Power Energy Transmitter (LIMPET) (250 kW) and Pico Plan (400 kW) are commercial applications of fixed-structure OWC wave energy conversion system [9].

Pelamis is a hinged contour device and applied in offshore applications. It consists of many different functional components. The cables are used to transfer energy from sea side to the land side.

Wave Dragon developed in 1986 is an overtopping device to be placed in water depths above 20 m and also a floating offshore converter. This model was first made in Denmark. It seems that Wave Dragon has a promising future in terms of power capacity. The rated power for each unit is 4-11 MW. The size is big and weight is huge [13]. Negative effects on the device are lessened by the means of the device size and also maintenance cost and downtime are reduced.

The AWS emerged in 1994 and is an offshore submerged device. The surface waves cause the oscillations of pressure, and the device starts to operate. PM linear synchronous machines are used in the AWS applications and energy storage technologies can be used to improve the efficiency of the AWS. Firstly, a 1:20 model was tested in 1995 and then experimental tests were performed for different situations. In 2004, a 2 MW rated capacity pilot plant was submerged and tested in a variety of sea states and operation conditions [9, 13].

A WSE developed by the WSE Company looks like a millipede and is called a multipoint absorber. Since 2006, real time implementations of WSE have continued. There are individual hydraulic cylinders for each absorber. To provide continuous energy conversion, the device length holds several wavelengths. The WSE involves a storm protection system to lessen the undesired mechanical forces.

There are different wave device classification methods. It is not easy to encompass all device categories. Another device classification method is based on the present status of a device, the development time-scale and economic investment cost [9]. This device classification categorizes the systems as first, second and third generation systems. Onshore and nearshore OWC devices, which are installed currently or under development,

are members of the first generation systems. The float pump devices are accepted as second generation systems. Offshore and nearshore devices, which can capture high level power, are parts of the second generation systems. The large-scale offshore device, both with regards to physical size and power output are defined as third generation systems.

Wave energy can be described as a highly promising renewable energy source for the future. Strategies should be advanced to increase the use of wave energy converter systems commercially. For instance, the wave energy systems in use can be modified, developed and improved, and then promising systems can be built. However, government supports may be required to promote and encourage the use of wave energy converter system. Up to now, a number of prototypes have been proposed and tested, but few systems put forth the effort to reach commercial deployment levels [6].

For future, a number of projects are planned in various countries. In the United Kingdom, total of 41.4 MW consisting of prototypes and projects are deployed and awarded. A test park consisting of five power systems totaling 600 kW will be built over two years and a 52 MW capacity wave energy conversion system will be installed in Turkey. Various wave energy projects in Indonesia, Italy, and LaReunion in the India Ocean are planned and will be realized in the near future [5]. Many countries are making contributions for research and development activities of wave technologies. Research studies show a hopeful future for the wave energy market.

2.3. Control in Wave Energy Systems

For Oscillating Body (OB) and OWC converters, a natural frequency of oscillation should coincide with the frequency of the incoming waves since maximum efficiency is attained at resonance. It is not easy to maintain a resonant condition because real waves are comprised of multiple frequencies and incompatibility in body dimension.

The studies to control wave energy converter systems have been proposed for the mid 1970s. Firstly, it was proposed to control the reactive power so as to maximize the active power for a Power Take Off (PTO) device and this method is named as an optimum phase control [70]. Later, approximate optimum phase control was developed to use in discrete time unlike the optimum phase control in continuous mode.

Many studies were executed both theoretically and experimentally for OB and OWC types wave energy conversion technologies in the 1980s. Optimum phase and amplitude

conditions with constrained or unconstrained options were referred to get maximum power. Optimization should be done with keeping in mind the conditions mentioned above and economic constraints. Some alternative control methodologies have been proposed, where system physical quantities are omitted. This situation causes a reduction on maximum power point of WEC systems. Nevertheless, if control methodologies are implemented with discrete cases, the system performances can be enhanced in many applications [11, 70].

Active control of WEC dynamics can improve the efficiency of WECs [11]. One of the active control methods is the latching control, which is firstly examined in 1980 showing discrete and highly non-linear characteristics. The device's motion is stalled at its extreme position (when velocity is zero) and released when the wave forces are in good phase. If the natural frequency is bigger than the excitation wave frequency, the control method can be applicable. Reference [71] proposes the discrete latching control to improve the efficiency of the PTO system. In [72], an oscillating-body wave energy converter with hydraulic PTO system is controlled with a latching control. The hydraulic feature is simplified to realize the control. The results were reasonable.

Since the behavior of real sea waves is nonlinear, some assumptions have to be done during the modeling of WECs and control strategies. A time-domain model of WEC system is utilized to observe the effect on performance of a dynamically changing wave frequency and to predict the real system output efficiency. A frequency based model is not adequate to model the system characteristics [73, 74]. The WEC system linear model can be used in WEC system simulation where the wave frequency is stable. However, the linear model approximation becomes insufficient under variable system conditions. So, the Pierson–Moskowitz spectrum is preferred to model the behavior of real sea waves [75]. In [76], an offshore OWC is modeling and the combination of control techniques (energy quality, amplitude and phase controls) are proposed. Simulation results obtained with Matlab/Simulink and power utilization could be advanced by 500%. The experiments made for regular waves are reported in [76].

2.4. Power and Electrical Equipment in Wave Energy Systems

Wave energy conversion systems utilize different types of generators such as a conventional rotating generator or direct-drive linear generator to get electrical energy. In many applications (OB, OWC), mechanical interfaces (air and water turbines and hydraulic motors) are used to convert alternating motion to a continuous unidirectional movement. On the other hand, linear generators, which do not need a mechanical interface, have been implemented in wave energy converter systems since 1970s. Rotating electrical generators driven by mechanical turbines such as a hydraulic turbine or motor, air turbine are preferred in most wave energy converters [12].

It is a difficult, slow and expensive process to reach the wave systems for commercial applications. Firstly, theoretical and numerical system modeling is worked on and then a small model is tested. After the time consuming and expensive task, the system is tested in real operation conditions. Since the process from idea to market is long and complex, the operation should be supported by governments to lessen the difficulties.

The studies based on WECs control are scanned in literature and classified in terms of Generator, Implementation, Wave, Validation and Control types are summarized in Table 2.1. While 36 paper refers to rotational generator, 17 studies are about linear generator type. An energy utilization control of the WEC systems can be mechanical or electrical. The number of papers about the implementation type is same just as implying in generator types. The WEC control is investigated with only regular, only irregular or both irregular and regular wave forms. The validation of the WEC systems is done by only experiment, only simulation, or both experiment and simulation. The WEC system output power control has been carried out with different control methods as given in Table 2.1. The most preferred control type is a phase control.

There are different types of power electronics interface topologies used in wave energy conversion systems to provide the requirements between energy system and load. In [124], DC-DC buck converter topologies are implemented to both charge battery and supply loads. In [102], H-bridge and Miller's converter are considered to install in a wave energy conversion system. A three-phase full-wave passive rectifier circuit is proposed to utilize power from a wave energy converter in [112]. A D-STATCOM device is adapted to smooth power oscillation in [88]. An electrical power is regulated by power electronics AC/DC/AC converter in [122].

An AC/DC rectifier followed by a DC/AC converter is used to extract the output power in [100]. Reference [116] applies AC/DC/AC converters including active or passive mode in AC/DC stage with transformers to adjust maximum power to transmit to the consumer. In [101, 110, 111, 115], an active AC/DC/AC inverter topology is applied to get power from WEC to a grid. Reference [96] uses AC/DC converter, high voltage direct current (HVDC) and DC/AC inverter to transfer power through loads. A rectifier charged a battery and inverter converts DC power into AC load in [87]. A three phase passive diode rectifier is connected with a WEC and the rectifier output feeds a dc load in [93]. Reference [113] prefers to use a passive diode rectifier and a capacitor filter to get smoother power output. Two different topologies based on AC/DC passive diode rectifier are examined in [99]. The power electronics interface devices mentioned above have superiorities to each other in terms of a high efficiency, low cost, high reliability, complying with standards, smaller total harmonic distortion, and so on.

When we look at the previous work we see that these works mainly deal with the followings:

- Power management by mechanical parts.
- Using resistive type loads without considering power quality issues.
- Using phase balance and latching as control methods.
- Usually simulations are done rather than experimental works.
- There are also a few works using power electronics interfacing units in WECs.

Table 2.1. Wave energy converter systems with controls in literature

Reference No	WEC type	Control Type	Generator type	Implementation type	Wave type	Simulation/ Experimental	Year
[77]	OWC	PID	Linear	Mechanical	Irregular	Experimental	1997
[78]	Heaving-buoy WEC	Phase	-----	Mechanical	Irregular	Simulation	1998
[79]	OWC	Optimal, sub-optimal, semi-optimal	-----	Mechanical	Irregular	Simulation	1999
[80]	OWC	Air flow	-----	Mechanical	Regular/Irregular	Simulation	1999
[81]	OWC	Reactive control	Rotary	Mechanical	Irregular	Simulation	1999
[82]	OWC	Reactive and latching controls, Time domain control	Rotary	Mechanical	Irregular	Experimental	2000
[83]	Deep water floating wave energy devices	Latching	Linear	Mechanical	Regular/Irregular	Simulation	2002
[84]	OWC	Optional control	Rotary	Mechanical	Irregular	Simulation	2002
[85]	OWC	Optimal rotational speed control	Rotary	Mechanical	Irregular	Simulation	2002
[86]	Heaving wave energy device	Latching	-----	Mechanical	Regular/Irregular	Simulation	2004
[87]	OWC	-----	Rotary	Electrical	Irregular	Simulation/ Experimental	2004
[88]	OWC	Feed-forward control	Rotary	Electrical	Irregular	Simulation	2004
[89]	PTO	Latching	Rotary	Mechanical	Irregular	Simulation/ Experimental	2006
[90]	A heaving buoy and SEAREV	Latching	Rotary	Mechanical	Regular/Irregular	Simulation	2006
[91]	Oscillating-body WEC	Flow, liquid	Rotary	Mechanical	Regular/Irregular	Simulation	2007
[92]	Archimedes Wave Swing	Latching, phase and amplitude, reactive, feedback linearisation	Linear	Mechanical	Regular/Irregular	Simulation	2007
[93]	PTO	No Control	Linear	Electrical	Irregular	Simulation	2007
[94]	Oscillating-body WECs with hydraulic PTO system	Phase	-----	Mechanical	Regular/Irregular	-----	2008
[95]	AWS	Neural network (NN) with control strategies (phase, amplitude, internal model and switching)	Linear	Mechanical	Irregular	Simulation	2008

Table 2.1 (continued)

Reference No	WEC type	Control Type	Generator type	Implementation type	Wave type	Simulation/ Experimental	Year
[96]	OWC	-----	Rotary	Electrical	Regular	Simulation	2008
[97]	Point-absorbing WEC	Latching	-----	Mechanical	Regular/Irregular	Simulation/ Experimental	2009
[98]	PTO	Declutching	-----	Mechanical	Regular/Irregular	Simulation	2009
[99]	Point absorber	No control	Linear	Electrical	Irregular	Simulation/ Experimental	2009
[100]	Heaving-buoy WEC	Current PI controller	Linear	Electrical	Regular	Simulation	2009
[101]	AWS	PI	Linear	Electrical	Regular/Irregular	Simulation	2009
[102]	PTO	Phase	Linear	Electrical	Regular	Simulation/ Experimental	2009
[103]	OWC	-----	Rotary	Mechanical	Regular	Experimental	2009
[104]	Wave energy hyperbaric converter, Oscillating body systems	Phase, A proportional-proportional integral (P-PI) cascade controller	Rotary	Mechanical	Regular/Irregular	Simulation	2010
[105]	Point absorber, PTO	Quiescent period predictive	-----	Mechanical	Irregular	Simulation	2010
[106]	A floating wave energy converter (PTO)	Phase	Rotary	Mechanical	Irregular	Simulation	2010
[107]	Heaving-buoy WEC	Phase	Linear	Mechanical	Irregular	Simulation	2010
[108]	Heaving point absorber WEC	Optimal	Rotary	Mechanical	Regular/Irregular	Simulation	2010
[109]	Point-absorber WEC	Latching	-----	Mechanical	Irregular	Simulation	2010
[110]	PTO (SEAREV)	Latching, Power leveling	Rotary	Electrical	Irregular	Simulation	2010
[111]	PTO	Phase, amplitude, combined phase and amplitude	Linear	Electrical	Regular	Experimental	2010
[112]	PTO	No Control	Linear	Electrical	Irregular	Simulation	2010
[113]	PTO	No Control	Linear	Electrical	Irregular	Simulation/ Experimental	2010

Table 2.1 (continued)

Reference No	WEC type	Control Type	Generator type	Implementation type	Wave type	Simulation/ Experimental	Year
[114]	OWC	rotational speed control	Rotary	Mechanical	Regular/Irregular	Simulation	2010
[115]	PTO (Wave Dragon)	Direct Torque control with space vector control (PI control), Direct Power control with space vector control (PI control)	Rotary	Electrical	Regular/	Simulation/ Experimental	2010
[116]	PTO (Wave Dragon)	Frequency control, current control	Rotary	Electrical	Irregular	Simulation	2010
[117]	Variable liquid-column oscillator (VLCO)	-----	Rotary	Mechanical	-----	Simulation	2011
[118]	A heaving-buoy WEC	-----	Linear	Mechanical	Irregular	Simulation	2011
[119]	Two-body wave energy device (PTO)	Phase	-----	Mechanical	Regular/Irregular	Simulation	2011
[120]	Point absorber, SEAREV	-----	Rotary	Mechanical	Regular/Irregular	Simulation	2011
[121]	PTO	-----	Rotary	Electrical	Regular	Simulation	2011
[122]	PTO	Field-oriented control (FOC) with space vector control (PI)	Rotary	Electrical	Regular/Irregular	Simulation	2011
[123]	OWC	PID, phase, amplitude	-----	Mechanical	Regular/Irregular	Simulation	2011
[124]	OWC	PI control	Rotary	Electrical	Irregular	Experimental	2011
[125]	Generic oscillating body	Wave power prediction, novel forecasting method	-----	Mechanical	Irregular	Experimental	2012
[126]	Hydraulic power take-off	-----	Linear	Mechanical	Irregular	Simulation	2012
[127]	Floating-buoy WEC	Fuzzy	Rotary	Mechanical	Regular	Simulation	2012
[128]	Point absorber WEC	-----	-----	Mechanical	Regular/Irregular	Experimental	2012
[129]	PTO	Phase	Rotary	Mechanical	Regular/Irregular	Simulation	2012

3. SYSTEM MODELING AND SIMULATION

3.1. Introduction

The modeling and simulation of the proposed wave energy system is developed and given in this chapter. As shown in Figure 3.1 the scheme has various parts from input to output. An emulator model of the wave energy conversion system is placed on the upper left corner. The emulator consists of a DC motor a speed reducer and a PM generator. The DC motor and speed reducer are used to emulate the wave dynamics in a closed laboratory environment. The complete scheme is divided into the following sub categories:

1. The wave energy converter system
2. Power electronic converters
3. Proposed FACTS device
4. Controllers
5. Back up units
6. Loads

The proposed renewable energy scheme consists of only the wave energy converter system as the power source. Actually these sorts of systems typically require additional sources for sustainability. For example a photovoltaic and/or wind power generation system may be used together with the wave energy converter system to maintain the sustainability. A PV power generation system is considered to be used as a backup system to charge the battery as well as supply power to the load as long as the weather conditions permit. Since the PV systems are well discussed in literature and have many applications widespread around the world, it will not be discussed here keeping in mind that it can be added to the wave energy converter system easily. The generated electrical power is stored in a battery backup unit and then used to feed the loads. The modeling process of each part of the system listed above will be explained one by one by in following sections. The simulation of the complete system shown in Figure 3.1 will be given in the next chapter followed by implementation in the chapter afterword.

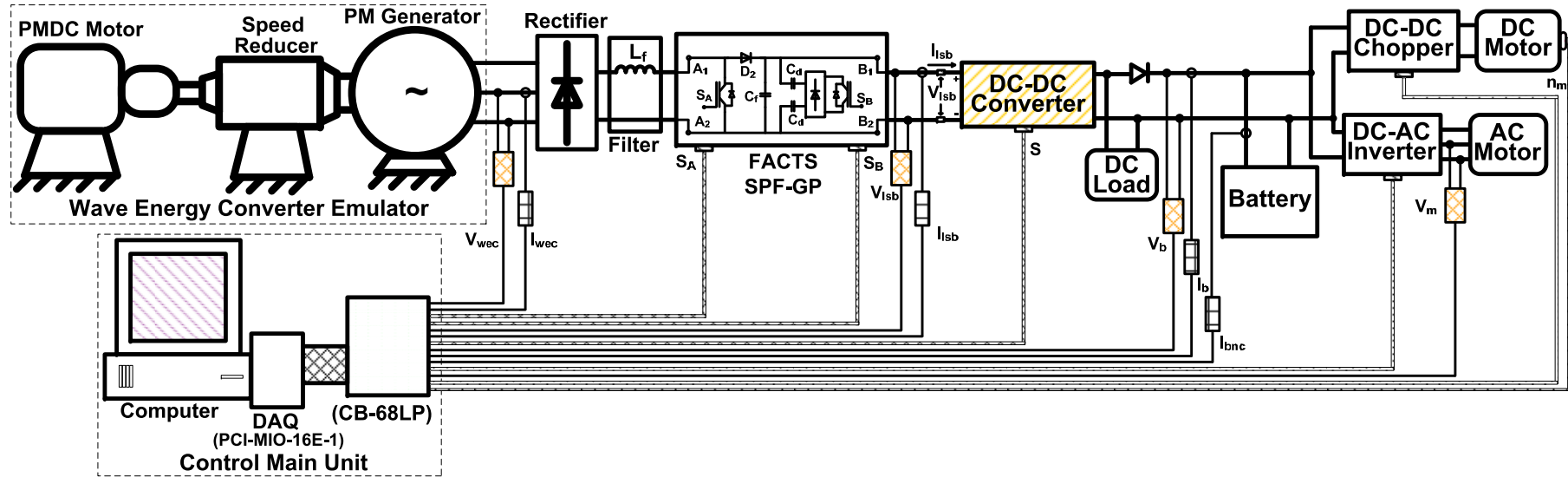


Figure 3.1. Wave Energy Conversion system with the novel FACTS (SPF-GP)

3.2. Wave Energy Converter System

Since the main energy source of the electricity from wave energy systems starts from the sea surface, the first modeling in this chapter is started with the mathematical background and simulation model of the wave energy converter system, which includes two main parts as surface wave and the electrical generator. The mathematical model of the surface wave and the generator are obtained separately and adapted to Matlab/Simulink/SimPower Software environment for simulation. After the models of all the components are developed and adapted to be operated as a combined whole system, then the simulation studies of wave energy converter system together with the other parts are carried out for various controllers under different operation conditions.

3.2.1. The Wave Model

3.2.1.1. Approximated Model of the Wave Dynamics

A progressive surface wave shape is given in Figure 3.2 for a monochromatic wave travelling [130]. The wave is assumed to be traveling with constant length and constant average height.

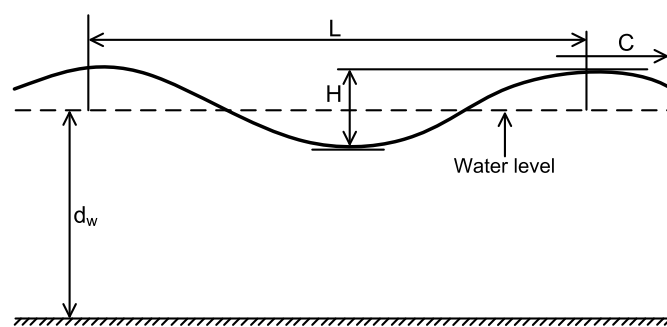


Figure 3.2. A progressive surface wave shape

The parameters in Figure 3.2 are defined as;

C : phase velocity

H : wave high, (m)

L : wave length, (m)

d_w : wave depth, (m)

The phase velocity is defined by:

$$C = \frac{L}{T} \quad (3.1)$$

where T is wave period and L is wave length.

The water wave is comprised of the particle activities. So, if the particle velocity profile is clearly defined, the wave model can be obtained easily. The vertical forces generated by the waves are used in this thesis as the base force input to the mechanical systems. The vertical particle velocity generating the force is defined as,

$$\omega_s = \frac{\pi H}{T} e^{kz} \sin(kx - \sigma_w t) \quad (3.2)$$

where k and σ_w are wave number and wave angular frequency, respectively, and are defined as

$$k = \frac{2\pi}{L} \quad (3.3)$$

$$\sigma_w = \frac{2\pi}{T} \quad (3.4)$$

The maximum value of the velocity is obtained when the position z is equal to 0 (zero). In this case, the vertical velocity can be written in equation (3.5).

$$\omega_c = \frac{\pi H}{T} \sin(kx - \sigma t) \quad (3.5)$$

where $\frac{\pi H}{T}$ is the maximum value of the velocity.

While the wave height is $H = 1\text{ m}$, water depth is 40 m and wave period is $T = 5\text{ s}$ at an arbitrary position, $x = 0$, the surface particle velocity waveform is obtained as shown in Figure 3.3. The maximum velocity is obtained when the *sinus* function is equal to 1. Thus the peak linear velocity can be written as

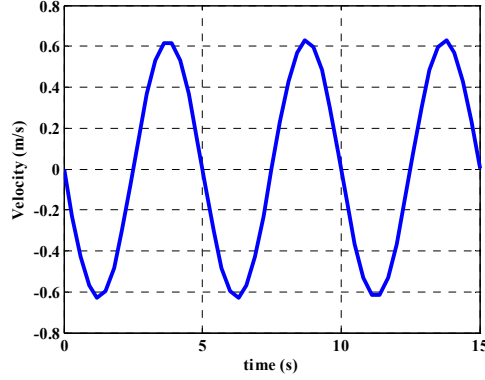


Figure 3.3. Surface particle velocity profile

$$\omega_c = \frac{\pi H_c}{T_c} \quad (3.6)$$

where H_c and T_c are the wave height and wave period corresponding to the peak linear velocity, respectively.

3.2.1.2. Stochastic Model of the Wave Dynamics

To realize the real world environment for a wave energy converter system, the stochastic wave model should be used. A random wave environment for various wave frequencies is constituted by the stochastic model. To do this the wave spectral density data should be available. The data can be obtained by different methods. One of them is given by Pierson-Moskowitz (1964) calculating the wave spectra for various wind speeds. The spectra form is given as follows

$$s(\omega) = \frac{\alpha g^2}{\omega^2} \exp \left[-\beta \left(\frac{\omega_0}{\omega} \right)^4 \right] \quad (3.7)$$

where $\omega = 2\pi f$, f is the wave frequency in Hz, $\beta = 0.74$, $\alpha = 7.9 \times 10^{-3}$, $\omega_0 = g/U_{17.5}$, and $U_{17.5}$ is the wind speed at a height of 17.5 m above the sea surface, the anemometers height on the weather ships used by Pierson-Moskowitz in 1964. To calculate the spectra from a known wave height equation (3.8) can be used.

$$H_{1/3} = 0.21 \frac{(U_{17.5})^2}{g} \quad (3.8)$$

The amplitudes and frequencies are acquired for all of the component waves in the ocean by the generated wave spectra. The *Pierson Moskowitz Wave Spectral Density* is obtained using an input $H_{1/3}$ of 1.5 m, representing summer conditions as shown in Figure 3.4.

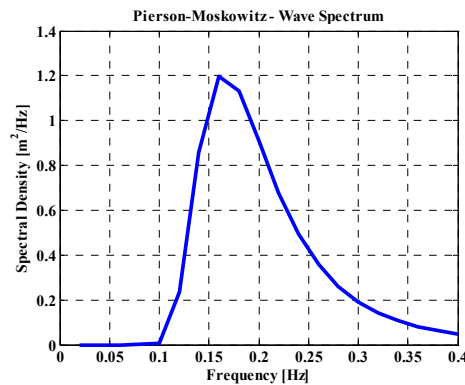


Figure 3.4. Pierson Moskowitz wave spectral density representing summer conditions

3.2.2. Generator Model

3.2.2.1. Ideal Model

There are various generator types used in wave energy conversion systems. In this section, a Permanent Magnet Linear Generator (PMLG) is considered and modeled. In ideal model, firstly the monochromatic wave will be used and then the stochastic wave model will be adapted.

The vertical displacement of generator depends on the maximum range associated with the generator feature. The vertical displacement, $y(t)$ with the maximum generator travel d_G and wave frequency ω_m are given in equations (3.9) and (3.10), respectively, where the wave frequency in rad/sec and d_G is the maximum generator travel in meter.

$$y(t) = \frac{d_G}{2} \sin(\omega_m t) \quad (3.9)$$

$$\omega_m = 2\pi f_m = \frac{2\pi}{T_m} \quad (3.10)$$

The permanent magnets produce a variable flux out depending on the vertical displacement and magnetic wavelength. The variable flux can be defined as in equation (3.11), where λ is the magnetic wavelength in meters and $\hat{\Phi}$ is the peak flux in Tesla.

$$\phi(t) = \hat{\Phi} \sin\left(\frac{2\pi}{\lambda} y(t)\right) \quad (3.11)$$

The induced voltage in the coils is expressed as a function of the flux deviation with time as

$$V(t) = N \frac{d\phi}{dt} \quad (3.12)$$

where N is the number of turns per coil.

Equation (3.12) leads to the phase to neutral voltage described as

$$V(t) = \hat{V} \cos(\omega_m t) \cos\left(\frac{\pi d_G}{\lambda} \sin(\omega_m t) + \theta\right) \quad (3.13)$$

where \hat{V} is the peak phase-neutral voltage and the phase displacement angle θ has the following values.

$$\theta = 0, -\frac{2\pi}{3}, +\frac{2\pi}{3}$$

Since three-phase voltages will have a 120° displacement phase angle, they are defined as follows.

$$\begin{aligned}
 V_a(t) &= \hat{V} \cos(\omega_m t) \cos\left(\frac{\pi d_G}{\lambda} \sin(\omega_m t)\right) \\
 V_b(t) &= \hat{V} \cos(\omega_m t) \cos\left(\frac{\pi d_G}{\lambda} \sin(\omega_m t) - \frac{2\pi}{3}\right) \\
 V_c(t) &= \hat{V} \cos(\omega_m t) \cos\left(\frac{\pi d_G}{\lambda} \sin(\omega_m t) + \frac{2\pi}{3}\right)
 \end{aligned} \tag{3.14}$$

The peak electrical frequency is obtained by using the magnetic wavelength and the translator peak speed as given in equation (3.15).

$$\hat{f}_e = \frac{\text{velocity}_{peak}}{\lambda} \tag{3.15}$$

$$\text{where } \hat{\omega}_e = \frac{2\pi}{\lambda} \left(\frac{dx}{dt}\right)_{max}$$

Since the magnetic wavelength represents a complete cycle from north to south, the peak electrical frequency is expected as equation (3.15).

Using the wave and permanent magnet linear generator models together, the ideal wave source model is obtained as substituting $\lambda = 0.140$, $d_G = 1 \text{ m}$, $T_m = 5 \text{ sec}$, and $\hat{V} = 220 \text{ V}$ in equation (3.14). The phase to neutral voltage output for phase A is obtained as shown in Figure 3.5.

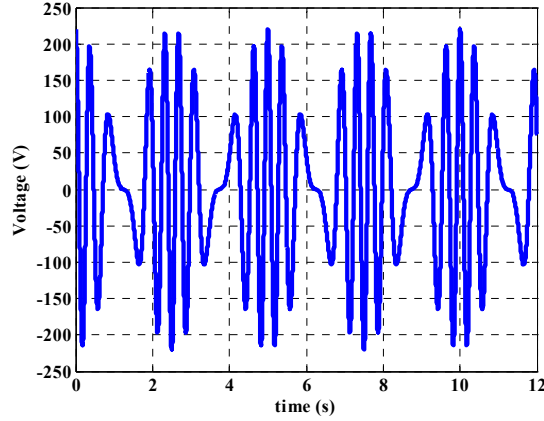


Figure 3.5. The phase to neutral voltage

3.2.2.2. Dynamic Model

The dynamic model equations are similar to that of rotary permanent magnet synchronous generator. There are some differences in the torque and force equations. The dq-axis equations for a linear generator are given as;

$$v_{sq} = R_s i_{sq} + \frac{d}{dt} \lambda_{sq} + \omega_m \lambda_{sd} \quad (3.16)$$

$$v_{sd} = R_s i_{sd} + \frac{d}{dt} \lambda_{sd} - \omega_m \lambda_{sq} \quad (3.17)$$

$$\lambda_{sq} = L_s i_{sq} \quad (3.18)$$

$$\lambda_{sd} = L_s i_{sd} + \lambda_{fd} \quad (3.19)$$

$$L_s = L_{ls} + L_m \quad (3.20)$$

where R_s is the coil resistance, ω_m is the electrical angular frequency, i_q is the q-axis current, i_d is the d-axis current and λ_{fd} is the excitation linkage flux of the stator due to flux produced by the magnets. v_d and v_q are d and q axes voltages, respectively [131].

If equation (3.18) and (3.19) are substituted into equation (3.16) and (3.17), the dq-axis voltages can be represented as

$$v_{sq} = R_s i_{sq} + \frac{d}{dt} L_s i_{sq} + \omega_m L_s i_{sd} \quad (3.21)$$

$$v_{sd} = R_s i_{sd} + \frac{d}{dt} (L_s i_{sd} + \lambda_{fd}) - \omega_m L_s i_{sq} \quad (3.22)$$

where $\omega_m = \frac{p}{2} \omega_{mech}$, p is the number of poles of the machine, ω_m is the electrical frequency in rad/sec, ω_{mech} is the rotational mechanical frequency in rad/sec, λ_{fd} is the flux linkage of the stator d-winding due to the flux produced by the rotor magnets.

The electrical torque can be defined as;

$$T_{em} = \frac{p}{2} (\lambda_{sd} i_{sq} - \lambda_{sq} i_{sd}) \quad (3.23)$$

If the equations (3.18) and (3.19) are substituted into equation (3.23), the output torque as a function of the q-axis current and magnet excitation flux linkage can be obtained as follows

$$T_{em} = \frac{p}{2} ((L_s i_{sd} + \lambda_{fd}) i_{sq} - L_s i_{sq} i_{sd}) = \frac{p}{2} \lambda_{fd} i_{sq} \quad (3.24)$$

Equations (3.25) and (3.26) express the length of the linear generator stator and the circumference of a rotary synchronous generator, respectively.

$$l = (\text{phasen number}) \tau p \quad (3.25)$$

$$c = 2\pi r \quad (3.26)$$

where τ is pole pitch and p is the number of poles.

Since the length and circumference are equal, the radius of a machine can be defined as

$$r = \frac{3\tau p}{2\pi} \quad (3.27)$$

The radius of a 2 pole machine, 1 pole pair is given in equation (3.28)

$$r = \frac{3\tau}{\pi} \tag{3.28}$$

The torque output for a rotary machine with 2 poles is represented by

$$T_{em} = \lambda_{fd} i_{sq} \tag{3.29}$$

The relation between torque and force can be expressed as

$$F = \frac{T_{em}}{r} = \frac{\pi}{3\tau} \lambda_{fd} i_{sq} \tag{3.30}$$

The force output of the linear synchronous machine is directly proportional to the number of poles, like the case in a rotary machine. A general equation to represent the force can be derived as

$$F = \frac{p\pi}{6\tau} \lambda_{fd} i_{sq} \tag{3.31}$$

Equations (3.16) to (3.31) are combined by using the operational dynamic block library in Matlab/Simulink. The combined Simulink model of the PMLG for dynamic simulation studies is given in Figure 3.6.

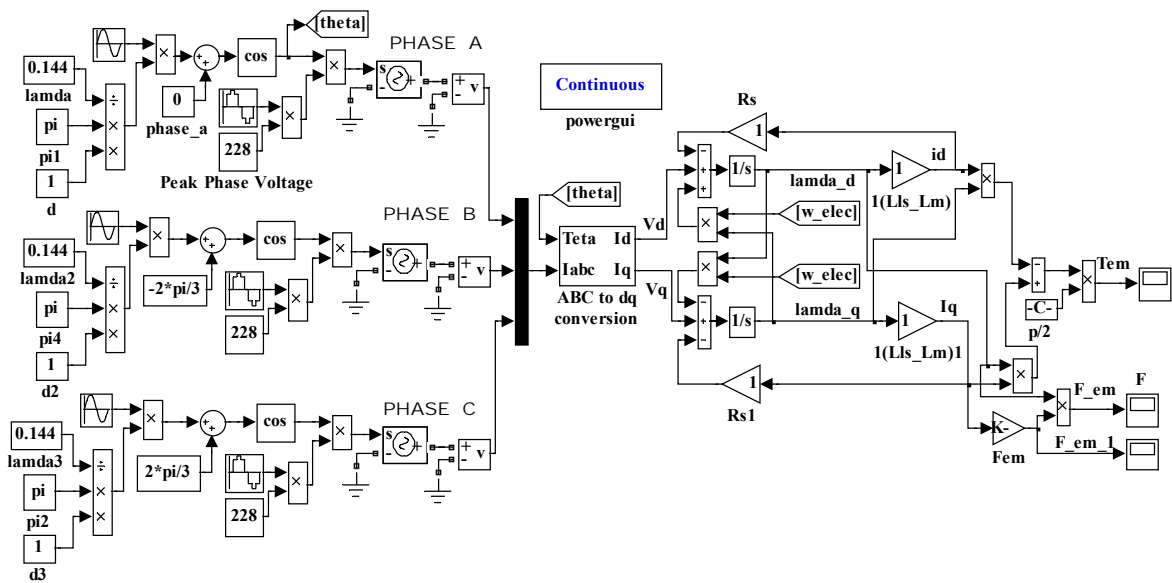


Figure 3.6. PMLG dynamic Simulink model

3.3. Power Electronic Converters

As shown in Figure 3.1, there is a AC/DC rectifier right after the PM generator, a DC-DC converter after the proposed FACTS device and DC-DC chopper at DC motor load terminals and DC/AC inverter at AC motor load terminals. The proposed Modulated SPF–GP is also a power electronic device. However, it will be treated separately from the others because it is one of the contributed parts of the thesis.

3.3.1. AC/DC Rectifier

An AC/DC rectifier is used to convert the AC output voltage of the PM linear generator to DC voltage, which will be conditioned by the proposed SPF-GP FACTS interface device before being controlled by a DC-DC chopper. The circuit diagram of the 6-pulse diode rectifier used in the system is given in Figure 3.7. Since the simulation model of the diode rectifier is already available in Matlab/Simulink/SimPower utility library, the parameters of the rectifier used in the thesis are entered into the model in Simulink/SimPower toolbox instead of developing a new model for the rectifier. The parameters used in simulation are given in Appendix 1.

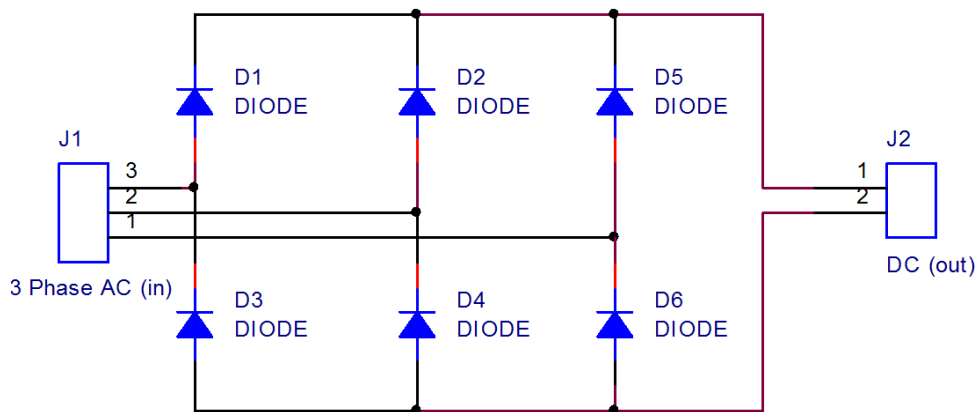


Figure 3.7. Circuit diagram of the rectifier used in the thesis

3.3.2. DC-DC Buck Converter

The DC-DC converters, which are widely used in power supplies, in control of the DC to DC energy flow, and in industrial applications, transfer electrical energy from one level to another [132]. Low-power and low-voltage DC-DC converter applications have been developed in such diverse areas as telecommunications, notebook, industrial instrumentation in recent years [133]. Figure 3.8 shows a classification of DC-DC converter technologies [133-135].

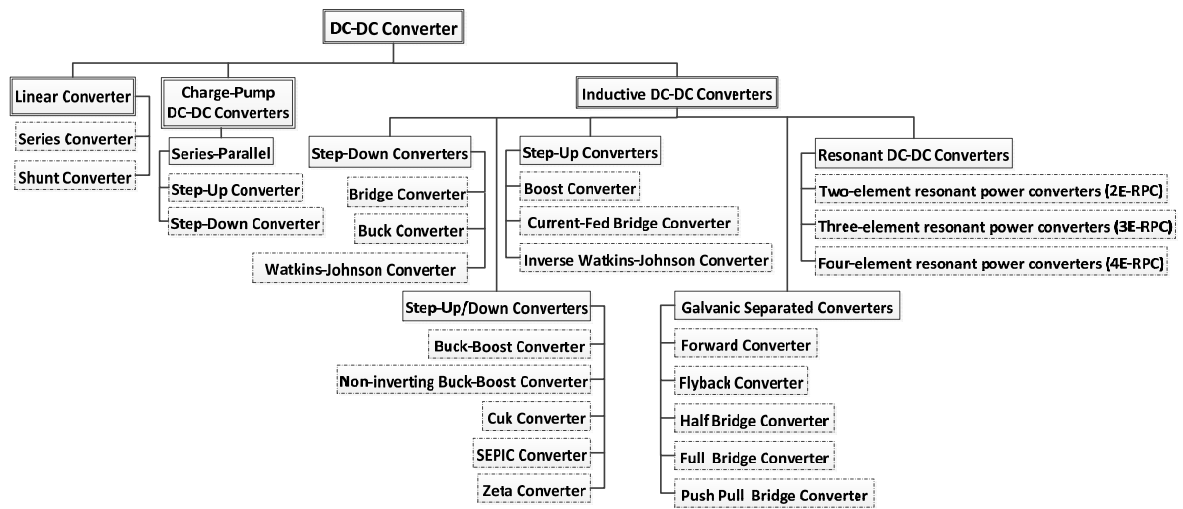


Figure 3.8. A classification of DC-DC converter technologies

The linear converter is a resistive divider and can convert an input voltage into a lower output voltage. In spite of a simple implementation of a linear converter, it is inefficient since the DC-DC voltage conversion is realized by power dissipation in a resistor. On the other hand, modified topologies can be used to improve the power efficiency [136, 137].

The maximum power conversion efficiency can be achieved at the optimal voltage conversion ratio and the output voltage can be increased or decreased with depending on demand in a charge-pump DC-DC converter. The converter is adapted into fixed frequency operation and rated load current modes generally [138]. To improve power efficiency and decrease the input and output ripples, an adaption should be done into the converter [139].

Inductive DC-DC converters are separated in non-galvanic and galvanic topologies. The non-galvanic topology covers step-down, step-up, resonant and step-up/down

converters. The galvanic separated converters are fundamentally derived from the main types of non-galvanic DC-DC converters such as step-down, step-up converters. Figure 5.8 summarizes the DC-DC converter types, clearly. There are many advantages and drawbacks of the converter topologies depending on application areas and studies to improve the converter performances [140-145]. In this part, a buck converter is studied.

A circuit diagram of a buck converter is shown in Figure 3.9. This converter is used to regulate the dc power supply by controlling the switching sequences of the switch S_{dd} . The buck converter output voltage is always smaller than the converter input voltage since the duty cycle d_c is defined between the interval $[0, 1]$ as $0 \leq d_c \leq 1$.

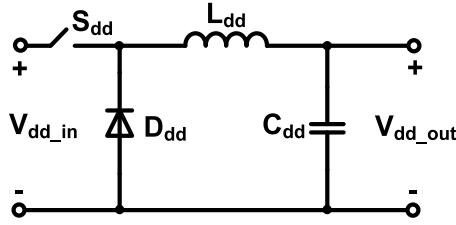


Figure 3.9. A general buck DC/DC converter schematic

The average output voltage value can be represented as:

$$V_{dd_out} = d_c V_{dd_in} \quad (3.32)$$

The output voltage can be regulated by controlling the duty cycle (d_c). The buck converter is composed of a diode (D_{dd}), an inductor (L_{dd}), a switch (S_{dd}) and a capacitor (C_{dd}). During the on-state, where the switch is in the turned-on position, the current flows through the inductor and capacitor while the diode remains reverse biased. During the off-state, where the switch is in the turned-off position, the source current flow is zero, thus the stored energy in the inductor is dissipated as the current flows through the inductor, capacitor and the diode loop. The inductor value can be determined by considering continuous conduction mode (CCM) and discontinuous conduction mode (DCM) [146].

$$L_{dd} = \frac{(1-d_c)R}{f} \quad (3.34)$$

For typical values of $d_c = 0.5$, $R = 10 \Omega$, and $f = 100 \text{ kHz}$, the boundary is $L_{dd} = 25 \mu\text{H}$. For $L > L_{dd}$, the converter operates in the CCM. To limit the output voltage ripple value (V_r), the capacitance C_{dd} must be greater than minimum capacitance value (C_{min}) given below

$$C_{min} = \frac{(1-d_c)V_{dd_out}}{8V_r L f^2} \quad (3.35)$$

At $d_c = 0.5$, $V_r/V_{dd_out} = 1\%$, $L_{dd} = 25 \mu\text{H}$, and $f = 100 \text{ kHz}$, the minimum capacitance is $C_{min} = 25 \mu\text{F}$.

DC-DC buck converter used in this study is shown in Figure 3.10. Contrary to the general circuit diagram given in Figure 3.9, the DC-DC buck converter used in the thesis consists of input and output filtering as shown in Figure 3.10. The circuit diagram given in Figure 3.10 is also modeled in Matlab/Simulink/SimPower along with the other components. The simulation results of the combined system is given and discussed in the chapter about the results.

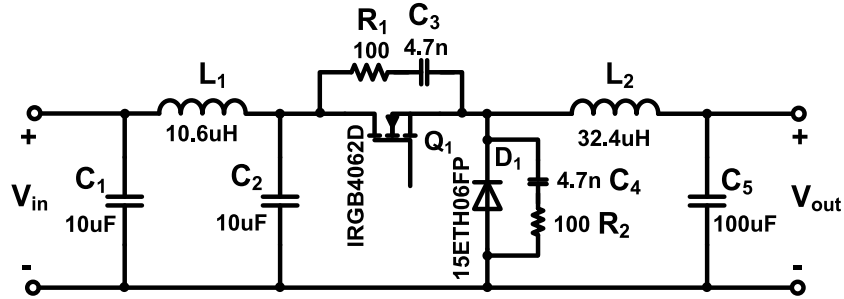


Figure 3.10. The designed DC-DC buck converter general circuit diagram

3.3.3. DC/AC Inverter

A DC/AC converter is used to supply power to the AC loads. The inverter used in the thesis is realized using the circuit diagram shown in Figure 3.11. The circuit design details are given in the next chapter about the implementation. Although the inverter used here is built up in lab and combined with the main scheme, there is no special and novel design or application features different from the ones commercially available in the market. Therefore the simulation model of the inverter is not different than the one given in

Simulink/SimPower application library. Therefore the inverter model from Simulink/SimPower is adapted to this study by modifying the parameters.

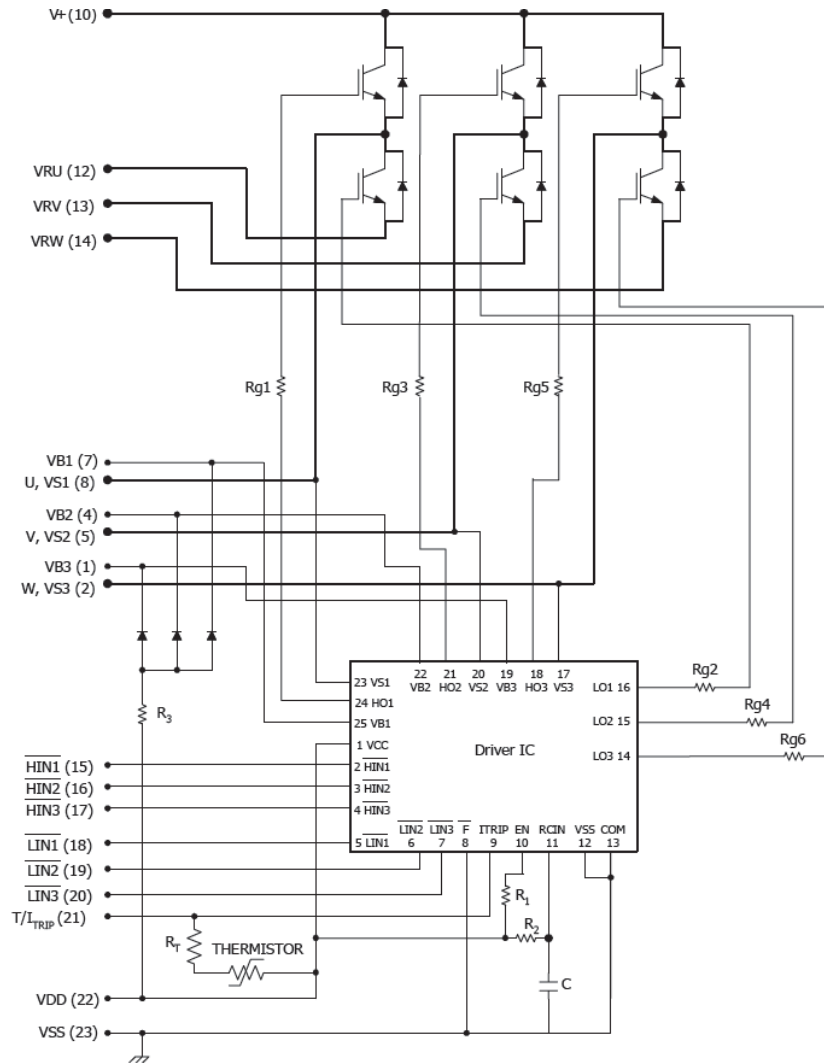


Figure 3.11. The DC-AC inverter system block diagram

The inverter is controlled to keep three phase output RMS voltages at constant voltage and frequency values determined by loads. As for the other controlled components in the system, the inverter is also controlled by the controllers developed in the thesis. The simulation models of the controllers are discussed later in this chapter.

3.3.4. Green FACTS Interface (SPF-GP)

The voltage generated by a PMLG is not the same as the one generated by round rotor synchronous generator. As given in Figure 3.5, the generated phase to ground voltage has an alternating nature but pure sine wave. Since waves on the sea do not have a constant or regular regime, the magnitude and the frequency of the generated voltage are not constant. Therefore it is required to convert the alternating voltage with the irregular wave shape. The DC voltage at the output terminals of the AC/DC rectifier reflects the wave shape depicted in Figure 3.2. The irregular shape of the DC voltage affects the voltage applied to the loads either DC or AC. For both load types the voltage will include pulse wise effects resulting in undesired operational problems such as noise in motors and dimming of lights.

Actually, irregular waves mean irregular voltage shape and irregular power condition from generation to dissipation. This irregularity must be eliminated and an isolation unit should be installed between the wave energy conversion unit and the load. The isolation unit acts as a power conditioner between the WEC system and the load to ensure the power quality and voltage stabilization in the system.

The common concerns of power quality and voltage stabilization are long duration voltage variations (overvoltage, under voltage, and sustained interruptions), short duration voltage variations (interruption, sags (dips), and swells), voltage imbalances, waveform distortions (DC offsets, harmonics, inter harmonics, notching and noise), voltage fluctuations (voltage flickers), and power frequency variations [147, 148]. To prevent undesirable states and reduce power consumption, FACTS compensators are typically applied.

A SPF-GP FACTS scheme is introduced here as the power conditioning filter device. The SPF-GP FACTS device is one of the major contributions of the thesis in the field. This device developed and applied to the WEC scheme. The basic circuit diagram of the SPF-GP is given in Figure 3.12. This circuit is realized and adapted to the WEC system in the experimental part of the study. A simulation model is also developed to be used in the simulation studies. The simulation model of the SPF-GP FACTS device is based on the diagram given in Figure 3.12.

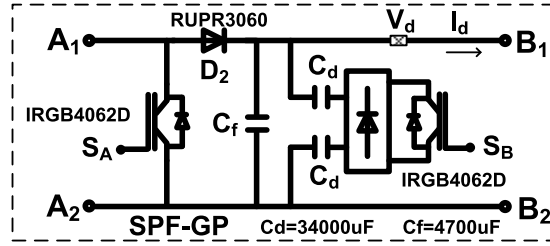


Figure 3.12. The SPF-GP FACTS scheme

There are two operating states of the SPF-GP system depending on the operating modes of switches S_A and S_B where S_B is the negation of S_A ($S_B = \overline{S_A}$). These stages are shown in Figure 3.13. In State-I, the IGBT (S_A) is OFF and the IGBT (S_B) is ON, therefore the current flows through the diode D_2 , capacitors C_f , C_d and terminals B_1B_2 and back to the source. In State-II, while the IGBT (S_A) is ON and the IGBT (S_B) is OFF, the diode (D_2) does not conduct and the capacitor maintains the output voltage at a constant.

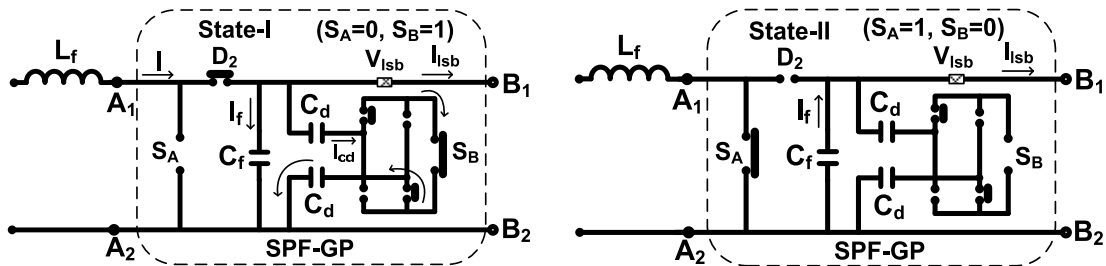


Figure 3.13. The two operating states of the novel FACTS SPF-GP system

Energy storages such as flywheels and battery can be used to smooth the voltage on the load side bus (V_{Isb}), but cost of energy storage is expensive and they need periodic maintenance. On the other hand, a capacitor offers a zero maintenance solution [149, 150]. The voltage and current waveforms of the novel FACTS SPF-GP are shown in Figure 3.14. The inductor (L_f) operates at discontinuous conduction mode and the output voltage is regulated at desired reference output voltage. The Printed Circuit Board (PCB) and experimental circuitry of the SPF-GP system are given in the next chapter.

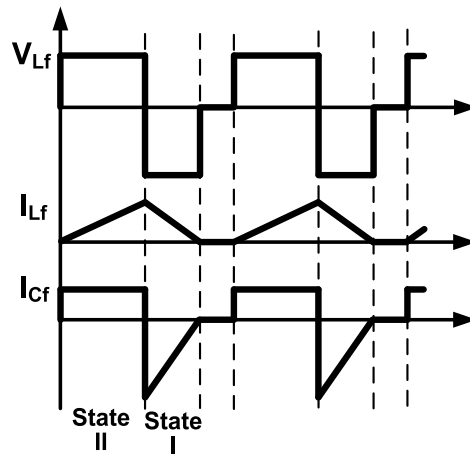


Figure 3.14. The switching waveforms for normal operation

3.4. Control Strategy

3.4.1. Introduction

Controllers have been the heart of engineering applications for many years. There are many variable controller techniques to improve the system performance. In this chapter some types of controllers will be reviewed and compared in terms of their performances. The controllers studied here are the ones used in the WEC system proposed and work through the thesis, starting with the classical Proportional plus Integral plus Derivative (PID), Fuzzy Logic Controller (FLC) and Sliding Mode Controller (SMC).

3.4.2. Conventional (P, PI and PID) Controls

Demands on controllers are to ensure fast response, less or zero overshoot, zero steady-state error, high stability margin, and provide an increase in productivity by improving quality, and reducing maintenance requirements [151].

The PID control, invented at the beginning of the 1900s, has been used in many different areas with advancement of control technology, such as modern, optimal, robust and adaptive control theories. Particularly, the PID type control is preferred in the most of the process control applications [152, 153]. 333 published Transactions, Journals, and Proceedings papers from IEEE (Institute of Electrical and Electronics Engineers), IFAC (International Federation of Automatic Control), and other international control societies

were determined in nineties [154]. 97% of regulatory controllers are PID type in the refining, chemicals and pulp and paper industries [155]. Over eleven thousand publications on PID control were cited by ScienceDirect scientific database from 1995 to 2006 [156].

There are many reasons why the PID controller is in the various industry applications, as it is easy to understand and pre-programmed in control system [155, 157].

A standard PID controller is comprised three terms, which are K_p , the proportional gain, K_I , the integral gain, and K_D , the derivative gain. Each terms of the PID controller affects the system performance in different ways. The proportional part produces a control signal directly proportional to the control error. The integral part facilitates the elimination of steady-state error, the step response of type zero systems. The derivative part allows the controller to anticipate changes in the desired value. The PID controller obtains data from present, past and future error signals.

Although the derivative term improves the system stability robustness and enhances the performance, the derivative part is by-passed because the derivative part introduces noise to the system and requires filtering in order to eliminate this noise. The additional filtering process brings difficulties into the design of PID controllers in practice [151].

Trial-and-error tuning is a technique, which is used widely in industrial practice to determine the PID controller parameters via observing the dynamic behavior of the system output. The effects of the control parameters on system behavior should be fully understood to perform effective trial-and-error tuning [156]. After initial guess of the control parameters are assigned, they are modified until a desired system output is observed. The chance of success on determination the controller parameters depends on user's knowledge, skill and experience [158]. The desirable performance for complex systems containing higher-order and nonlinearities cannot be obtained with trial-and-error approaches [159]. Undesirable affects such as nonlinearities, complicated dynamics, process uncertainty and varying parameters of the systems decrease the PID controller efficiencies. On the other hand, the PID parameter tuning does not guarantee the stability of the control system. Therefore, new ideas to improve the PID controller performance on the applications have been released.

It is claimed that 80% of PID controller parameters are poorly tuned [160]. Adjustment of PID controller parameters can be done with various types of analytical, heuristic, frequency, optimization and adaptive methods [151, 158, 161-164]. There are over 100 patented tuning methods on PID controllers recorded from 1970 to 2011 [165,

166]. In addition, the number of proposed PID controller tuning rules has surpassed one thousand and still increasing, with 293 of the 408 separately explored tuning rules reported between 1992 and 2006 [167, 168].

The PID control performance assessment should be done for each PID controller where the parameters are tuned to maximize trade-offs between them [169].

Up to now, there are many various studies done for PID control strategies, but the PID controller is still an open research area since technology does not stand still.

3.4.3. Sliding Mode Control

The SMC is a nonlinear controller and a type of variable structure control system (VSCS). The term “sliding mode” was firstly used by Nikol’skii in 1934 [170, 171]. Variable structure system (VSS) with sliding mode control was first proposed in the early 1950s [172-174]. VSS got widespread acceptance among engineering with technological development after the 1960s [175-177]. There are many types of application areas of SMC such as process control, robotics, aerospace applications, motion control, power converter, power system, economy, electric drives, automobile applications and medical applications [171, 176, 178-186]. The interest in SMC has increased, modified and adapted day by day [187-189]. One of the proofs is that the term “sliding mode control” is cited by *Google Scholar* database over 440 000 items (as of May 28, 2009) and 860.000 items (as of December 26, 2011) [190].

Main advantages of the SMC are to provide stability and robustness against parameter, line, and load uncertainties, to have applicability to multiple-input-multiple-output systems, well-established design criteria for discrete-time systems, a high degree of flexibility, order reduction, simplicity in design and application and good performance [172, 175, 176, 178, 191-196].

Some disadvantages of SMC in practical applications are high frequency oscillation in the controller output signal called chattering, insensitive on measurement of noise, possibility of unnecessarily large control signals, and difficulty in the calculation of equivalent control and unmodeled dynamics [117, 119, 121, 137, 144]. Many studies and approaches such as boundary layer, chaos control, high gain control, state observers, 2-sliding mode control, Lipschitz-like condition technique and continuous approximation method have been carried out to solve chattering problem [170, 175, 176, 178, 181, 185,

190, 193, 196, 198-201]. The earliest available sliding observer studies were observed in the mid 1980s [175].

There is a wide utilization of SMCs in various application fields such as fault detection, fault reconstruction, condition monitoring [175, 191]. Although implementation of the SMC needs less effort than other types of nonlinear controllers [191], it is observed that implementation of SMC in the power electronic areas has many difficulties such as the integrated circuit of SMC is not practicable, regular design methodologies are not applicable, its high and variable switching frequency causes excessive power losses, it generates electromagnetic interference and has complicated filter design, and has weak validation of practical worthiness of use [171, 191, 202].

An Infinite switching frequency must be used in SMC to acquire desired steady-state operation and dynamic response at power electronic applications. This situation causes an increase in losses. Therefore, the switching frequency should be limited via methods like hysteresis, constant ON time, etc [191]. On the other hand, several techniques are proposed to remove or lessen the disadvantages like a boundary-layer approach and a provident control, which are required to exactly defined the system mathematical model and also advanced control strategies based on fuzzy logic, neural networks, evolutionary computation (Genetic algorithm, Particle Swarm Optimization algorithm, Ant Colony Optimization algorithm etc), and other techniques adapted from artificial intelligence [203]. SMC with advanced control methods offers facilities to overcome imprecision, uncertainty, disturbances and to improve flexibility, and to deal with partial truth and approximation [185, 190, 204-206]. Google Scholar searches (as of December 26, 2011) of the key words "sliding mode" with "fuzzy", "neural network", and "genetic algorithm", which regained over 38000, 21700, and 6600 items, respectively.

The combination of sliding mode control and advanced control can be used to combine the advantages of both control techniques [203, 207], although it can be difficult to choose which advanced control to use for a given application [203, 206].

3.4.4. Fuzzy Logic Control

After the idea of fuzzy logic was firstly published by Lotfi Asker Zadeh in 1965, many applications have been implemented in diverse fields. Fuzzy Logic (FL) has been used in many different areas such as communications, automatic controls, consumer electronics, data processing, house hold appliances, data processing, expert systems, computer vision, signal processing, computer vision, traffic management, manufacturing organization, medical applications, power systems, robotics, management, pattern recognition, and so on [208-228]. More than 2000 commercially available products are in use actively [229]. Academic and industrial communities have focused on fuzzy logic control with theory and application techniques and many books on the topic have been published [230-248].

The first industrial application of Fuzzy Logic appeared in early 1970's with the development of a FLC by Mamdani and his colleagues [249, 250]. Later, efficient realization techniques for fuzzy logic control systems have been deeply researched since 1977 with the increase in fuzzy logic applications and awareness. After the first fuzzy chip was reported in 1985, research laboratories have been increasingly established [220, 227, 228]. The hardware implementations of the FLC have been studied and various strategies have been developed [209, 251].

The fuzzy logic control system performance depends on many different parameters such as software speed, number and precision of inputs, outputs, number of rules, fuzzification, defuzzification strategies, fuzzy membership function, fuzzy set and so on [209, 228, 252, 253].

Due to limitations of conventional control due to plant non-linearity, plant uncertainty, multi-variable structures, multi-loops and environmental constrains, uncertainty in measurements, and temporal behaviors, it is preferred to apply the FLC [213, 214, 220, 254, 255]. The FLC has some superiority on the conventional controllers [210, 213, 220, 228, 256]. Some of the advantages of fuzzy logic control approach are to fuse quantitative and qualitative information, to trade off potentially conflicting objectives, to provide a flexible control structure, and to deal with nonlinear input/output relationships [218, 222, 251].

Whilst many studies have been done to enhance the design and performance of the FLC, extensive work on combinations of FLC and conventional controllers, such as PI-

fuzzy control, PD-fuzzy control, PID-fuzz adaptive fuzzy PD or artificial intelligence techniques, such as a fuzzy sliding control, fuzzy gain scheduling, self-tuning and self-organizing FLCs, adaptive fuzzy control, genetic algorithm with fuzzy logic, fuzzy-sliding mode control, Takagi-Sugeno model-based fuzzy control and neuro-fuzzy logic control have increased day by day [210, 213, 214, 221, 223, 224, 227, 228, 254-258].

3.4.5. Application of the Controllers

In this thesis, a classical PI and PID controllers, a classical SMC, a classical FLC, a Self-Scaled Fuzzy Tuned PI Controller (SSFTPIC), a Self-Scaled FLC (SSFLC), a Fuzzy Tuned SMC (FTSMC) are used for different parts of the Wave Energy Conversion system. The control structures used are shown in Figures 3.15-3.21. Application parts of the controllers in the thesis are summarized in Table 3.1.



Figure 3.15. The PI controller



Figure 3.16. The PID controller

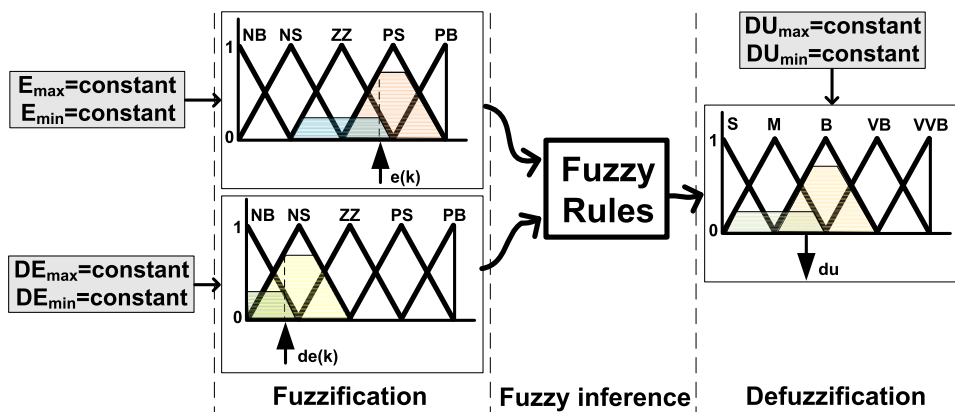


Figure 3.17. The classical FLC

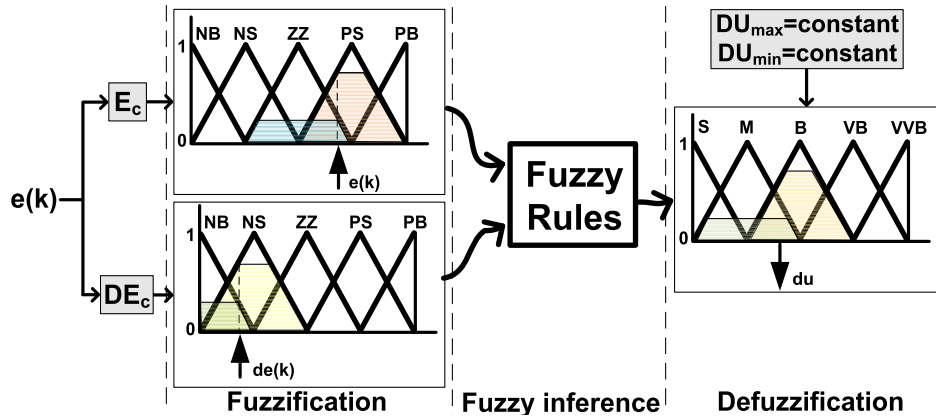


Figure 3.18. The Self-Scaled FLC (SSFLC)

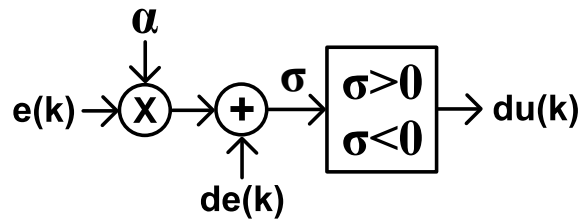


Figure 3.19. The classical SMC

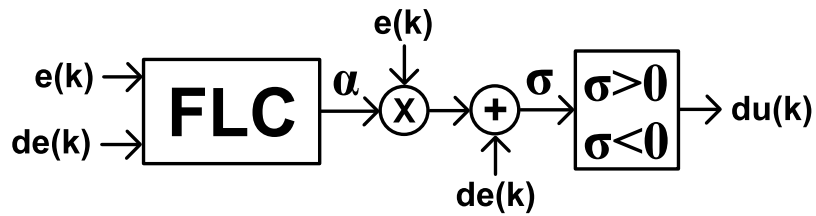


Figure 3.20. The Fuzzy Tuned SMC (FTSMC)

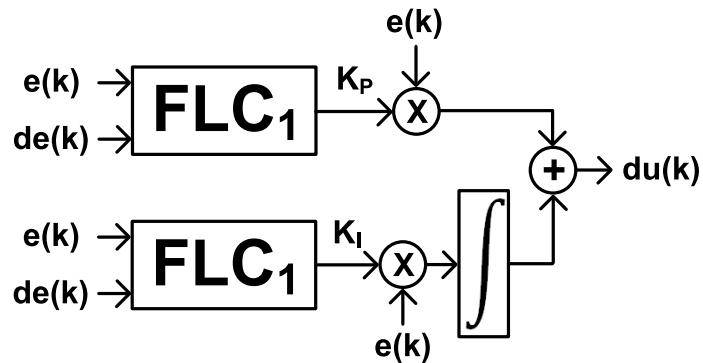


Figure 3.21. The Self-Scaled Fuzzy Tuned PI Controller (SSFTPIC)

Table 3.1. Application parts of the controllers in the Wave Energy Conversion system

Application Controller	PMDC Motor		AC Motor Voltage Control	Battery Charge Control	SPF-GP Load Side Voltage Control
	Speed Control	Voltage Control			
PI	x				x
PID	x				
SMC					x
FLC		x			
SSFLC				x	
FTSMC					x
SSFTPIC			x		x

3.5. Backup Units

3.5.1. Photovoltaic Energy Conversion System

The PV power has many advantages like short lead time for design and installation, high energy density, no noise and CO₂ emission, long life time, highly mobile and portable, and minimal maintenance requirements [259]. PV systems have been studied well in literature [260]. Many PV power generation stations have been installed in many countries [5]. The PV system in this thesis is considered as a backup system to the wave energy conversion system and will not be discussed in detail. However one of the PV models used widely in literature is adapted [261-264] to combine with the models of the other parts of the proposed scheme for complete simulation. The PV system is represented by the equivalent circuit shown in Figure 3.22 and given in equation (3.36).

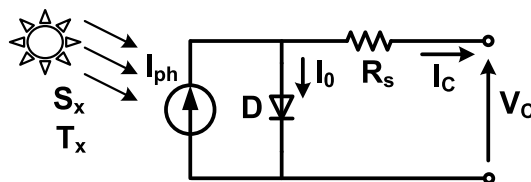


Figure 3.22. One diode equivalent parameters PV model

$$V_c = \frac{AKT_c}{e} \left(\frac{I_{ph} + I_0 - I_c}{I_0} \right) - R_s I_c \quad (3.36)$$

3.5.2. Battery

Batteries have different performance characteristics. Batteries can be used in various operating conditions. During some conditions, batteries can be damaged. It is required to keep in mind the battery manufacturer's recommended regulation values, to provide an appropriate system design and to realize efficient charging control. The most commonly used consumer and industrial batteries are NiCd, NiMH, Lead Acid, and Li-ion/polymer. The comparison of the five most commonly used rechargeable battery systems is given in Table 3.2. The energy and cost comparison in rechargeable batteries are given in Table 3.3 [265].

Table 3.2. The comparison of the commonly used rechargeable battery systems

	NiCd	NiMH	Lead Acid	Li-ion	Li-ion polymer
Energy density (Wh/kg)	45-80	60-120	30-50	110-160	100-130
Cycle life	1500	300-500	200-300	500-1000	300-500
Fast Charge Time	1h typical	2-4h	8-16h	2-4h	2-3h
Overcharge Tolerance	Moderate	Low	High	Very low	Low
Operating Temperature	-40/60 °C	-20/60 °C	-20/60 °C	-20/60 °C	0/60 °C
Typical Battery Cost	\$50 (7.2V)	\$60 (7.2V)	\$25 (6V)	\$100 (7.2V)	\$100 (7.2V)
Commercial use since	1950	1990	1970	1991	1999

Table 3.3. The energy and cost comparison in rechargeable batteries

	NiCd (AA Cell)	NiMH (AA Cell)	Lead Acid (typical pack)	Li-ion (18650 Cell)
Capacity	600 mAh	1000 mAh	2000 mAh	1400 mAh
Battery Voltage	7.5V	7.5V	12V	7.2V
Energy per cycle	4.5Wh	7.5Wh	24Wh	8.6Wh
Cycle life	1500	500	250	500
Cost per battery	\$50	\$70	\$50	\$100
Cost per kWh	\$7.5	\$18.5	\$8.5	\$24.0

3.5.2.1. Battery Management System (BMS)

Batteries can be charged in various methods. The quality of the chargers determines the performance and longevity of batteries. A lead acid battery is used in this section. Therefore, the battery charge control system must be designed with considering battery type to expand battery life. Lead acid battery is most economical for large power applications where weight is of little concern [265]. Charge time of a sealed lead acid is 12 to 16 hours. Charge time can be reduced with higher current and variable charge ways. Charge stages of lead acid battery are shown in Figure 3.23 [265]. It entails charging the battery in two stages, referred to as the constant current charge (bulk charge), constant voltage (float charge). The bulk charge provides the battery with sufficient charging current to return the battery to 90% State of Charge (SOC). The float charge (constant voltage) maintains the battery at full charge. The most energy transfer happens during the constant current charge (bulk charge) stage.

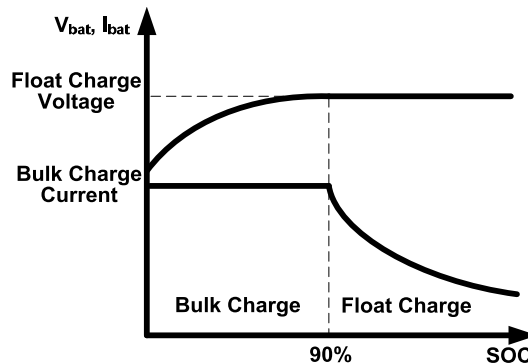


Figure 3.23. Charge stages of lead acid battery

The Battery Management System (BMS) has following features:

- i. Flexible control of the rate of battery charging
- ii. Overcharge and over discharge protection of batteries
- iii. Limitations on the charging current/voltage and discharging current/voltage

While the battery is in charging state, the BMS controls the battery situation and protects the battery against overcharging and regulates the charging current or voltage according to the SOC. While the battery is in discharging state, the BMS protects the

battery against discharging. The battery voltage (V_{bat}) and the battery current (I_{bat}) are used as control variables in the battery charging control system.

There are two different modes in the charging operation. The net current flowing in and out of the battery bank is calculated to determine its SOC. While the SOC is lower than 90%, the battery will be under a constant current. On the other hand, while the SOC is higher than 90%, the battery will be charged under constant voltage. BMS algorithm flowchart is shown in Figure 3.24.

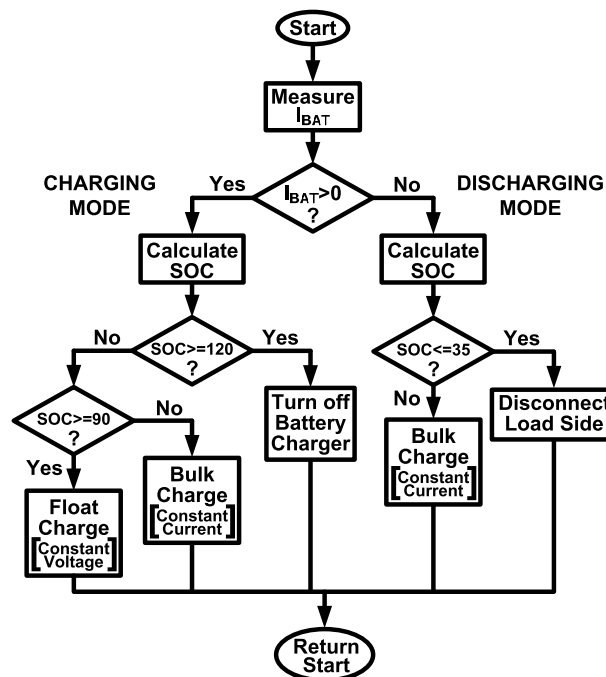


Figure 3.24. BMS flow chart

3.5.2.2. Battery State of Charge Estimation

A SOC expresses the level of charge that a battery retains: A fully charged battery is indicated with a 100% SOC, and a dead battery is indicated with a 0% SOC. The SOC calculation is very important to apply the battery charging control scenarios. There are different methods to estimate the SOC such as a direct measurement, specific gravity measurement, voltage based SOC estimation, current based SOC estimation and other methods. The comparison of the different techniques for SOC estimation and the history of SOC development are given in Table 3.4 and 3.5, respectively [266, 267].

Table 3.4. The comparison of the different techniques for SOC estimation

Technique	Field of application	Advantages	Drawbacks
Discharge test	All battery systems	Easy and accurate, independent of SOH	Offline, time intensive, loss of energy
Ah balance	All battery systems	Online, easy	Needs a model for the losses and regular re-calibration points. Sensitive to parasite reactions.
Physical properties of electrolyte	Lead, possibly Zn/Br and Va	Online Gives information about SOH	Low dynamic. Sensitive to temperature and impurities.
Open circuit voltage	Lead, possibly Zn/Br and Va	Online, cheap	Low dynamic, error if acid stratification. Problem of parasite reaction.
Linear model	Lead PV	Online, easy	Needs reference data for fitting parameters.
Artificial neural network	All battery systems	Online	Needs training data of a similar battery.
Impedance spectroscopy	All systems	Gives information about SOH and quality.	Temperature sensitive, cost intensive.
DC Internal resistance	Lead, Ni/Cd	Gives information about SOH and cheap, easy	Good accuracy, but only for low SOC.
Kalman filter	All battery systems	Online, dynamic	Needs large computing capacity and a suitable battery model. Problem of determining initial parameters.

3.5.2.3. Current Based SOC Estimation

The current based SOC estimation is widely used to determine the SOC of a battery due to simplicity of implementation. The measurement of net battery current has a critical importance to calculate the remaining battery capacity. The SOC of battery can be calculated by following equation [266].

$$SOC = SOC_{init} + \frac{1}{Q} \int_{t_{init}}^t (I_{bat} - I_{los}) d\tau \quad (3.37)$$

where Q : Rated capacity, I_{bat} : Battery current, I_{los} : Current consumed by the loss reactions, SOC_{init} : Initial SOC value.

Table 3.5. The history of SOC development

Year	Researcher/ Company	Method
1938	Heyer	Voltage measurement
1963	Curtis	Voltage measurements and threshold in voltage levels
1970	Lerner	Comparison between two batteries (one with a known SOC)
1974	Brandwein	Voltage, Temperature and current measurement
1975	Christianson	OCV
1975	Dowgiallo	Impedance measurements
1975	Finger	Coulomb counting
1978	Eby	OCV and voltage under load
1980	Kikuoka	Book-keeping
1981	Finger	Voltage relaxation
1984	Peled	Look-up tables based on OCV and T measurements
1985	Muramatsu	Impedance spectroscopy
1986	Kopmann	Look-up tables based on V, I, and T measurements
1988	Seyfang	Book-keeping and adaptive system
1992	Aylor	OCV, OCV prediction and coulometric measurements
1997	Gerard	Voltage and Current Measurements, Artificial Neural Networks
1999	Salkind	Coulomb counting, Impedance spectroscopy, fuzzy logic
2000	Garche	Voltage and Current Measurements, Kalman filters
2000	Bergveld	Book-keeping, over potential

There are several drawbacks in this method: an incorrect current measurement causes error and all current supplied to the battery cannot be consumed by charging. The method drawbacks can be relieved with investing money and different approaches. On the other hand, there are some assumptions and limitations in the current based SOC estimation [268].

Assumptions:

- The capacity of the battery doesn't change with the amplitude of the current.
- The temperature doesn't affect the model's behavior.
- The self-discharge of the battery is not represented.
- The battery has no memory effect.

Limitations:

- The minimum no-load battery voltage is 0V and the maximum capacity is not limited.
- The minimum capacity of the battery is 0Ah and the maximum capacity is not limited. Therefore, the maximum SOC can be greater than 100% if the battery is overcharged.

3.6. Loads

DC and AC motor type loads are used in the study. Since the purpose of this study is to develop the interfacing power conditioner FACTS device and proper controllers, the load modeling is not done from scratch, the models developed in other studies are used instead. Both DC and AC Motor models are adapted from literature [269, 270] and modeled in Matlab/Simulink/SimPower. A closed type simulation diagram of the system with DC and AC motor loads is given in Figure 3.25. Simulation results are given in the chapter where the results are discussed along with those of implementation.

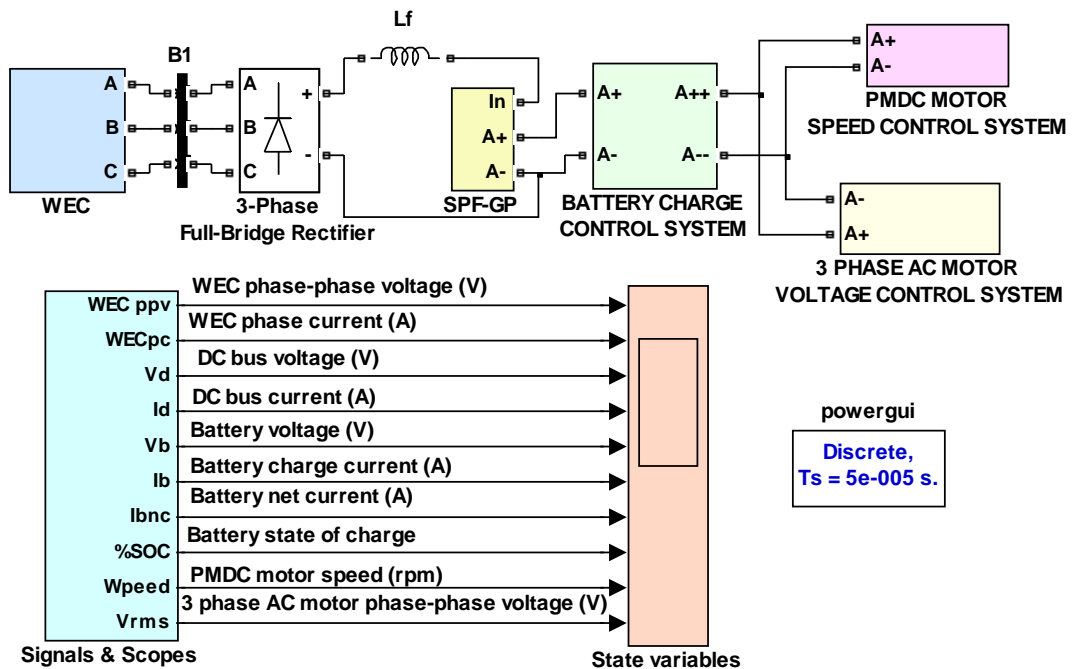


Figure 3.25. Simulation diagram of the system with DC and AC motor type loads

4. EXPERIMENTAL STUDIES

4.1. Introduction

This chapter explains the experimental design and realization of the overall system described in previous chapter.

The experimental setup of the WEC studied in the thesis consists of numerous machinery devices, circuitry and computer software as shown in Figure 4.1. Some of the machinery and devices are bought commercially while some others are designed especially for this thesis in the lab.

A WEC emulator has been built by assembling a permanent magnet dc (pmdc) motor, a speed reducer and a three phase PM generator. All of the power electronic circuits and devices are designed and realized for this study and assembled to the experimental setup. The proposed SPF-GP and the controller are also designed experimentally. All of the controllers used in the study are developed digitally in computer and implemented with data acquisition (DAQ) processes as described in this chapter.

The experimental studies are divided into following sections.

- * Wave Energy Conversion Emulator (WECE)
- * Switched Power Filter-Green Plug (SPF-GP)
- * Power Electronic Converters (PECS)
- * Loads
- * Controllers

The operational behaviors and specifications of all these components are described in previous section when the simulation models are developed and discussed. Therefore only the experimental setup and circuitry realizations of the above sections will be given in this chapter in order to avoid repetition.



Figure 4.1. The experimental setup

4.2. Wave Energy Conversion Emulator (WECE)

4.2.1. Computer Based Wave Energy Conversion Emulator (CBWECE)

The general system block diagram is shown in Figure 4.2.

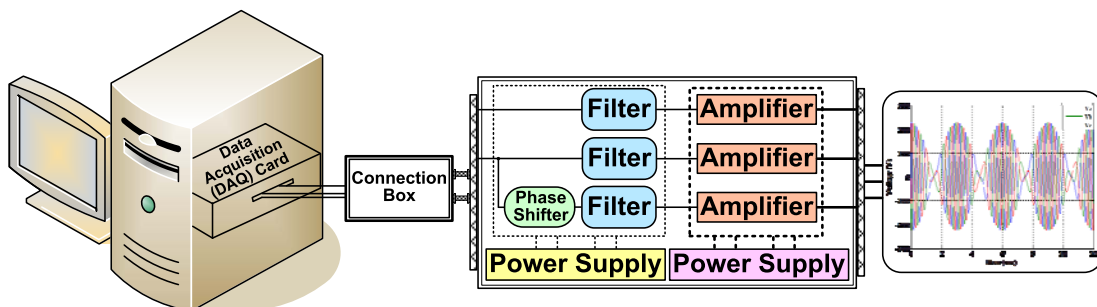


Figure 4.2. The general system block diagram

The real time implementation of the system is done using the Real-Time Windows-Target (RTWT) available in Matlab/Simulink toolbox, which provides an opportunity to create and control real time executable commands for real time applications through Matlab/Simulink. A PCI-6070E (PCI-MIO-16E-1) multifunction DAQ card is used in this study in order to establish communication on data acquisition between the real time part of the study and the computer, which contains the digital modeling of the wave energy converter output voltage waveform. The PCI-6070E DAQ card's features are given in Appendix 1.

4.2.1.1. Wave Energy Converter Output Voltage Waveform Model

The wave and permanent magnet linear motion generator models are used to model the wave energy converter output voltage waveform via Matlab/Simulink/SimPowerSystems environment as shown in Figure 4.3.

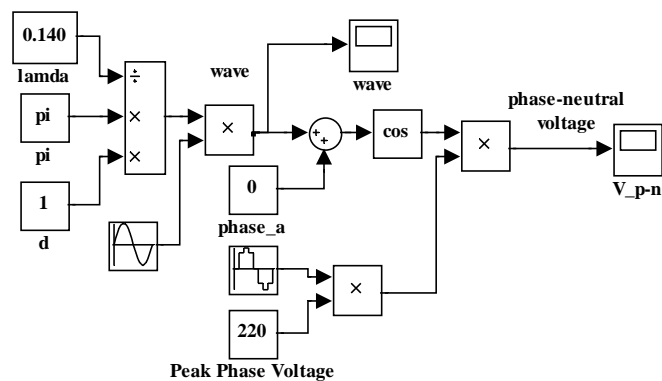


Figure 4.3. The wave energy waveform Matlab/Simulink model

The system parameters for the model: $H = 1\text{ m}$, $\lambda = 0.140$, $d = 1\text{ m}$, $T_m = 5\text{ sec}$, $\hat{V} = 220\text{ V}$. The system output waveforms are shown in Figures 4.4 and 4.5.

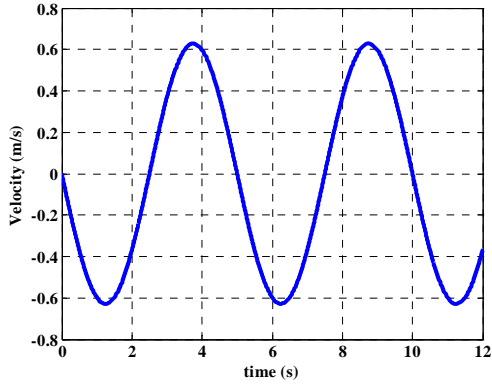


Figure 4.4. Wave velocity model

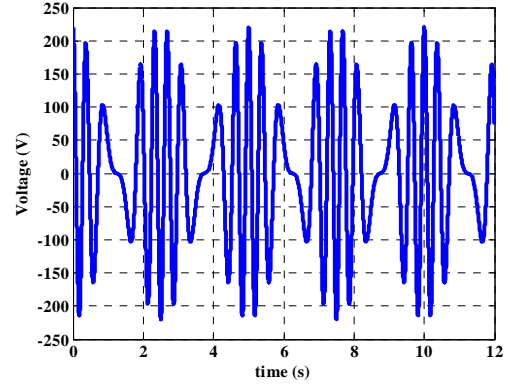


Figure 4.5. Phase-neutral voltage

The wave energy converter output voltage waveform constituted via Matlab environment is transferred into the DAQ card analog output by the RTWT shown in Figure 4.6.

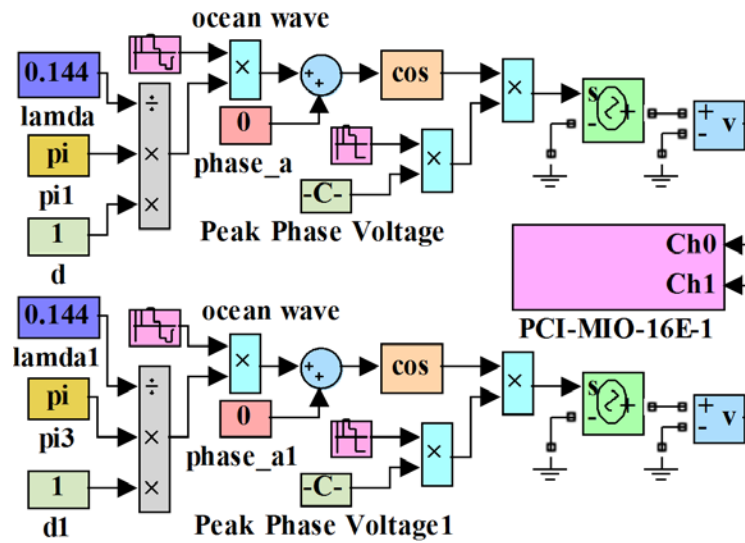


Figure 4.6. The WEC output voltage waveform with the RTWT

The wave energy converter output voltage waveforms are observed at analog outputs of the DAQ card. Since there are two analog outputs in the DAQ card, only two phase voltage waveforms can be taken. The output waveforms of the analog outputs of the DAQ card are shown in Figure 4.7.

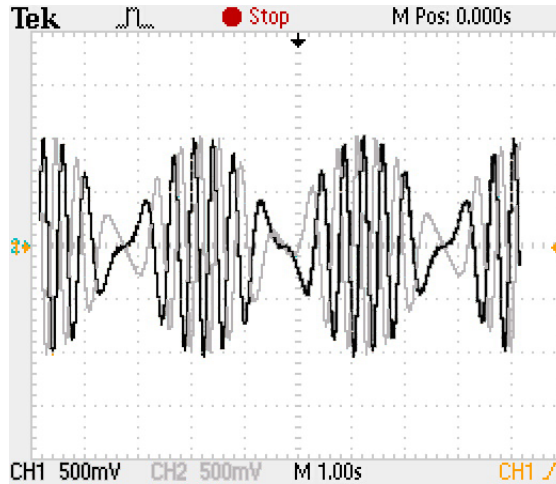


Figure 4.7. The output waveforms of the DAQ card analog outputs

4.2.1.2. Three Phase Wave Energy Converter Output Voltage Modeling

The analog outputs of the DAQ card do not provide the supply needed since the wave energy converter output is three phase. Therefore, one of signals from the analog outputs must be used to generate another signal, which is $2\pi/3$ radians (120° , $1/3$ of a cycle) offset in time with the signal taken from the analog outputs.

The phase shift circuit diagram designed is shown in Figure 4.8. The phase shift circuit transfer function is given in equation (4.1) [269].

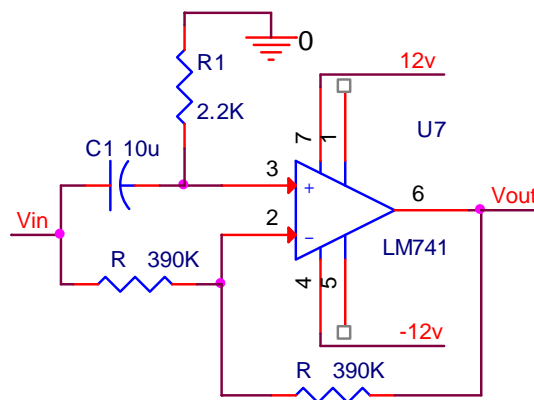


Figure 4.8. The phase shift circuit diagram

$$\frac{V_{out}}{V_{in}} = \frac{s - \frac{1}{R_1 C_1}}{s + \frac{1}{R_1 C_1}} \quad (4.1)$$

Phase shifting angle can be calculated as given in equation (4.2).

$$\text{Angle (rad)} = \tan^{-1} \left[\frac{\frac{2\omega}{R_1 C_1}}{\omega^2 - \left[\frac{1}{R_1 C_1} \right]^2} \right] \quad (4.2)$$

where, ω : frequency in rad/s ($\omega = 2\pi f$, f : Hz), R: 390 k Ω , R1: 2.2 k Ω , C1: 10 μ F

The one of the analog outputs is applied to the phase shift circuit and input (V_{in}) and output (V_{out}) signals are observed as shown in Figure 4.9. The three phase output voltage waveforms of the wave energy converter are shown in Figure 4.10.

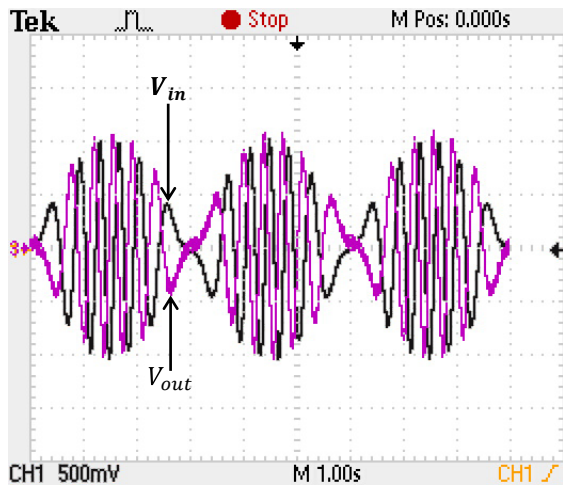


Figure 4.9. The input (V_{in}) and output (V_{out}) signals of the phase

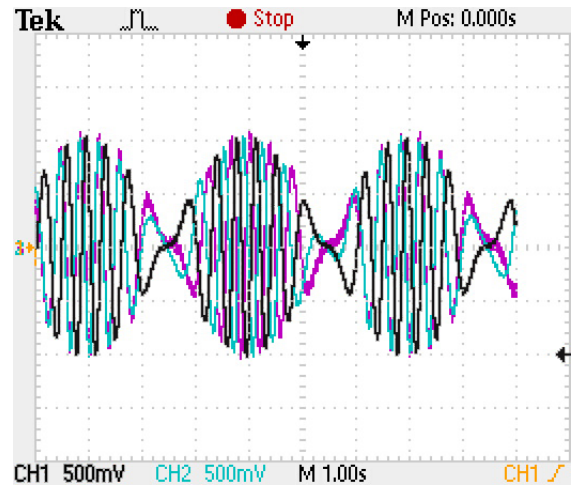


Figure 4.10. The shift circuit output voltage waveforms

4.2.1.3. Signal Filtering

There are three types of analog filters commonly used in applications. They are *Bessel*, *Butterworth* and *Chebyshev* filters. The number of poles in the filters determines performance of the filters. The increase in number of poles requires an increase in the number of the electronic components in the circuit and provides better performance in applications [270]. In this study, a second order low-pass *Chebyshev* filter is used and its circuit diagram is shown in Figure 4.11.

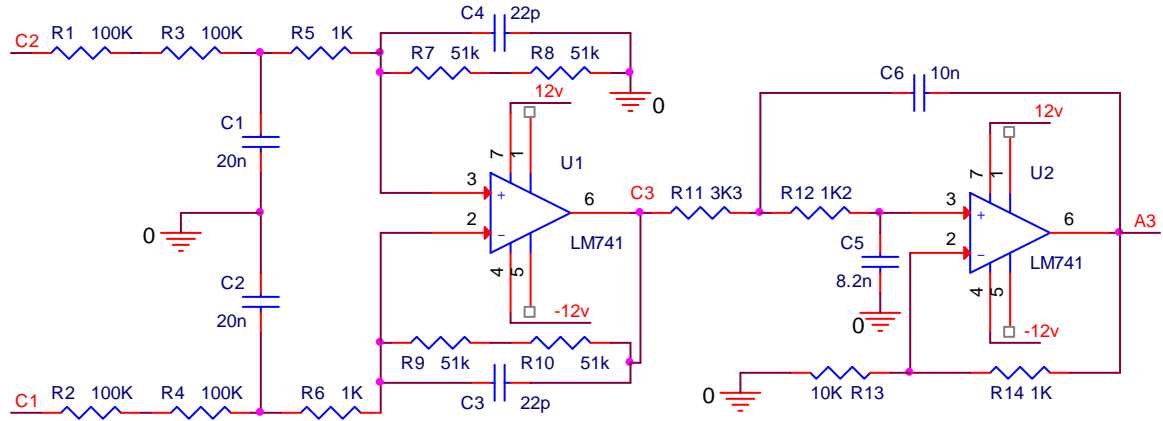


Figure 4.11. The second order low-pass Chebyshev filter circuit diagram

The filter transfer function is given in Equations (4.3) and (4.4)

$$\frac{V_{C3}}{V_{C2} - V_{C1}} = \frac{\frac{R_2}{R_0 + R_1}}{1 + s \frac{R_2}{R_0 + R_1} C_0} = \frac{K}{1 + s\tau}, \quad K = \frac{R_2}{R_0 + R_1} \quad (4.3)$$

If $K = 1$, $\frac{1}{\tau} = \frac{R_0 + R_1}{R_0 R_1} C_0 = 2\pi f_{max}$ and also

$$\frac{V_{A3}}{V_{C3}} = \frac{1 + \frac{R_6}{R_5}}{C_2 C_3 R_4 R_3 s^2 + \left[(R_4 + R_3) C_3 - \frac{R_6}{R_5} R_3 C_2 \right] s + 1}, \quad K = 1 + \frac{R_6}{R_5}$$

$$\omega_n = \frac{1}{\sqrt{C_2 C_3 R_4 R_3}} = 2\pi f, \quad Z = \frac{\omega_n}{2} \left[(R_4 + R_3) C_3 - \frac{R_6}{R_5} R_3 C_2 \right] \quad (4.4)$$

The input ($V_{C2} - V_{C1}$) and output (V_{A3}) signals are observed as shown in Figure 4.12.

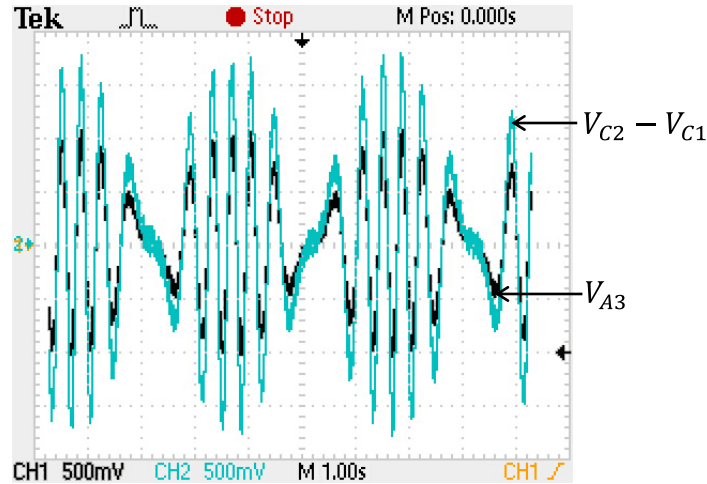


Figure 4.12. The input ($V_{C2} - V_{C1}$) and output (V_{A3}) signals of the filter circuit

4.2.1.4. Signal Amplification

The filtered wave energy converter output voltage waveforms are transferred into the amplification circuit part. In the amplification part, the amplifier parameters are adjusted to get the desired voltage value from the amplifier circuit output. The high-voltage/high-current operational amplifier (OPA549) is used to design the amplification circuit part. The features of the amplifier are given in Appendix 1 [271].

The circuit diagram of the system consisting of a phase shift, signal filtering and amplification circuits is shown in Figure 4.13. The PCB and photo of the system consisting of a phase shift, signal filtering and amplification circuits are given in Appendix 2.

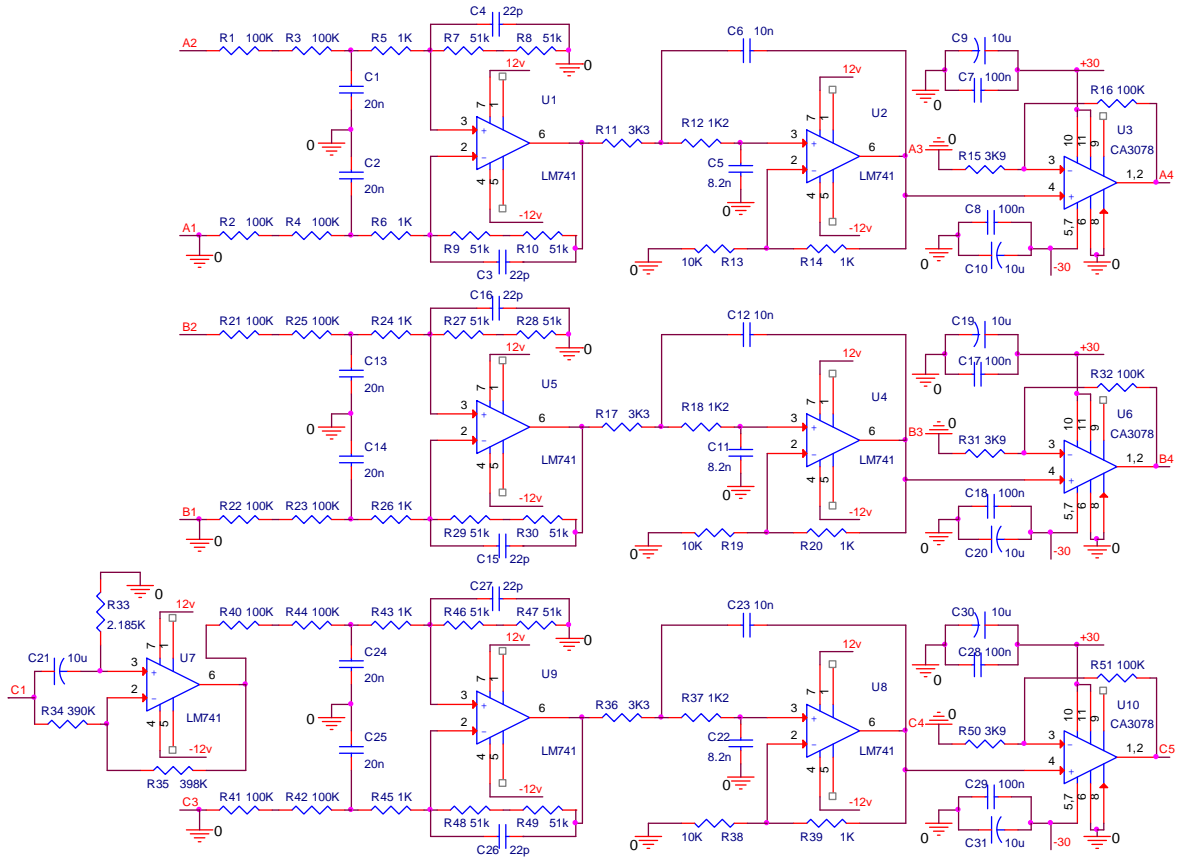


Figure 4.13. The system circuit diagram (phase shift, signal filtering and amplification circuits)

4.2.1.5. Power Supply Stage

The Wave Energy Conversion Emulator is supplied through two types of power stages. Low-voltage/low-current and high-voltage/high-current power stages are designed separately.

4.2.1.5.1. Low-voltage/Low-current Power Stage

As shown Figure 4.14, there are a total of seven low-voltage/low-current operational amplifiers used in the system circuit including phase shift, signal filtering and amplification circuits.

The low power stage is designed taking into consideration the power consumption of amplifiers [272]. The circuit diagram is shown below and the low power stage PCB and photo are given in Appendix 2.

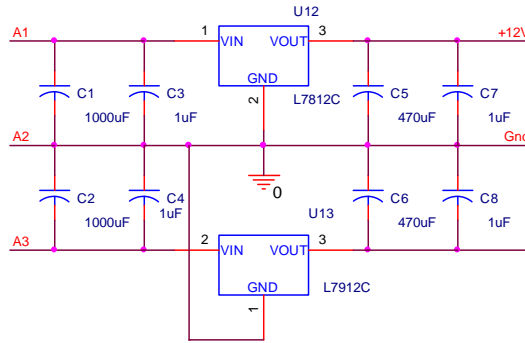


Figure 4.14. The low power stage circuit diagram

4.2.1.5.2. High-voltage/High-current Power Stage

There are three high-voltage/high-current operational amplifiers used in the amplification circuits. The circuit diagram is shown below and the low power stage PCB and photo are given in Appendix 3.

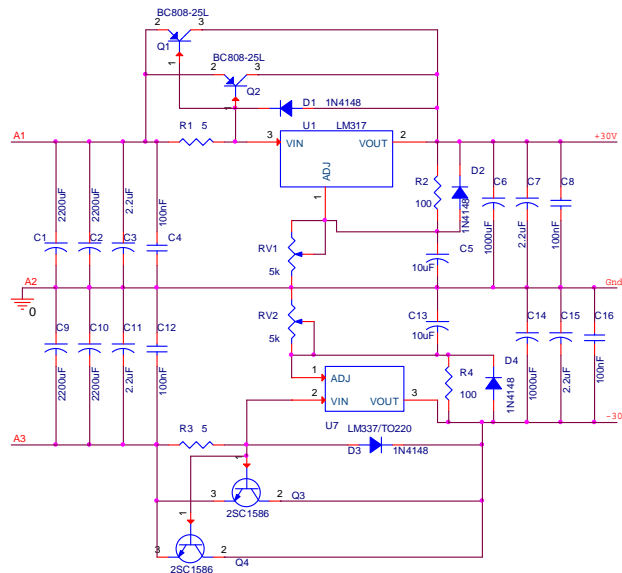


Figure 4.15. The high power stage circuit diagram

4.2.1.6. Computer Based Wave Energy Conversion Emulator Output Waveforms

The system block diagram is shown in Figure 4.16. The wave converter output waveforms are built in Matlab/Simulink environment and then transferred into the DAQ card analog output channels. The signals are put through the phase shift, filtering and amplification stages. The waveforms observed from the DAQ card analog output and the output of the adjustment stages are shown in Figure 4.17.

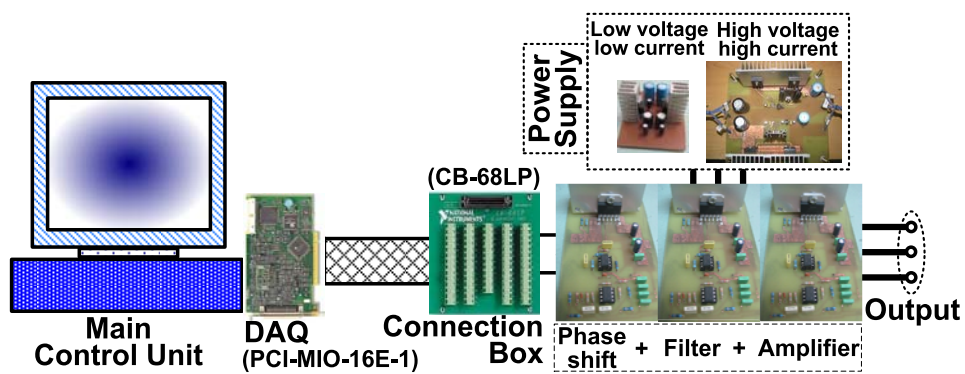


Figure 4.16. Wave energy converter system emulator block diagram

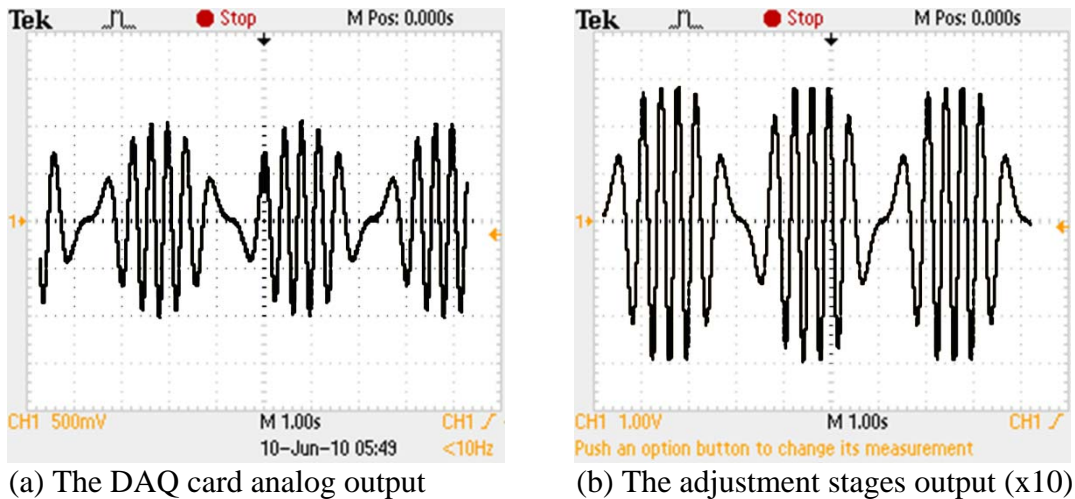


Figure 4.17. The wave energy converter emulator waveform

4.2.2. Machine Based Wave Energy Conversion Emulator (MBWECE)

The machine based wave energy conversion emulator is shown in Figure 4.18. It consists of a Permanent Magnet DC (PMDC) motor, a reducer, a three phase permanent magnet generator and couplings.



Figure 4.18. A general view of the wave energy converter test bed

The PMDC motor and the reducer are used to emulate the wave turbine capable of producing waving speeds and torque input to 3-phase PM generator. The parameters of these components are given in Appendix 4.

Well known dynamic model of PMDC motor is used in simulation software together with the models of the reducer and three-phase PM generator in order to develop a complete model for the proposed wave energy converter system. This simulation model is already discussed in previous chapter.

The wave energy conversion emulator is used to realize different operating conditions. The output of the WECE system is connected to a three phase passive rectifier to transfer the power to a dc-bus. The dc-bus provides interfacing to SPF-GP and the other equipment in the setup as given in Figure 3.1 and shown in Figure 4.1.

The emulator developed to represent the wave energy conversion system is tested with four different cases as:

Case I: No-load condition

Case II: Capacitor connected in parallel with the rectifier no-load condition

Case III: DC load connected in parallel with the rectifier condition

Case IV: Capacitor and DC load connected in parallel with the rectifier condition

Firstly, the system performance is observed for the no-load condition. The experimental setup diagram shown in Figure 4.19 is used for the Case I in order to observe the output voltage waveforms of the generator.

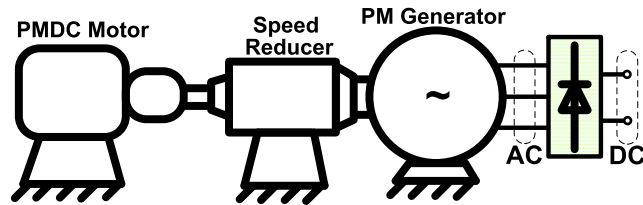


Figure 4.19. The WECE test block diagram for Case I

As shown in Figure 4.20 the resultant voltage wave form at the output terminals of the generator comprise with those of obtained from Simulation studies and reported in literature. The rectified voltage at the output terminals of the diode bridge rectifier is given in Figure 4.21 where the discontinuity of the wave dynamics are reflected in the rectified voltage waveform by the voltage sags. In order to eliminate these voltage sags and obtain a sag free dc voltage, a capacitor is connected in parallel to the output terminals of the rectifier as the operating Case II, which is given in Figure 4.22. The capacitor across the rectifier acts as a voltage depositor and eliminates the voltage sags resulting in a proper dc voltage waveform as shown in Figure 4.23.

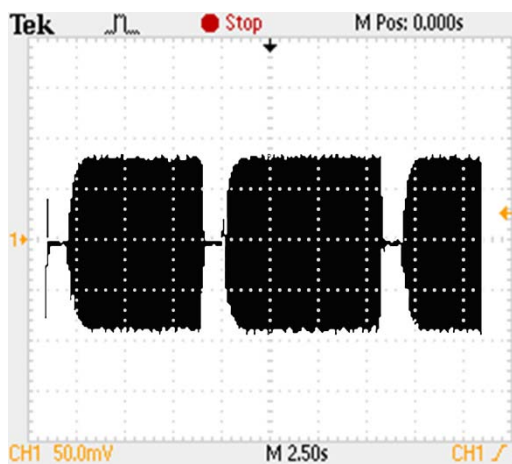


Figure 4.20. Phase to phase AC voltage waveform (x137)

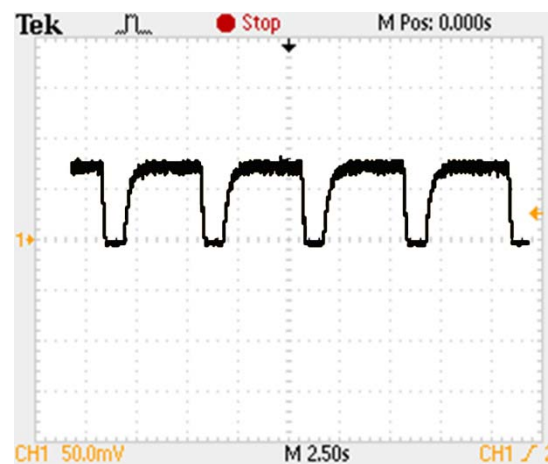


Figure 4.21. The dc-bus voltage waveform (x137)

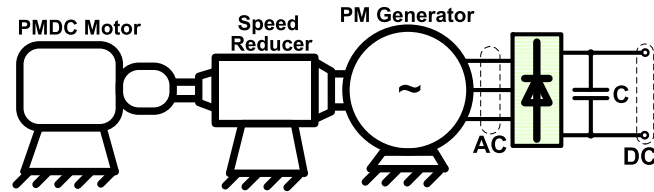


Figure 4.22. The WECE test block diagram for Case II

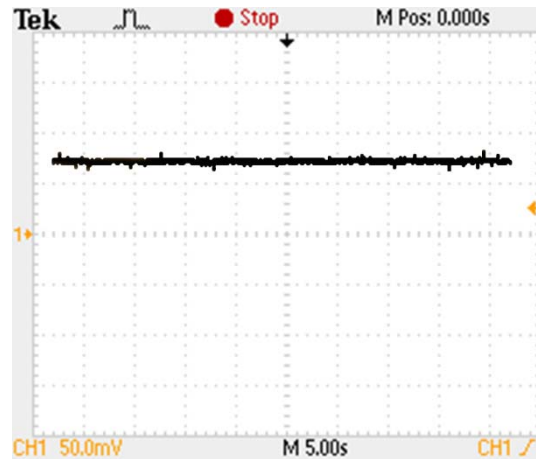


Figure 4.23. The dc-bus voltage waveform (x137)
($C=1200\mu\text{F}$, 45V_{dc})

Due to the stochastic nature of the wave kinetic characteristics, the generated voltage shows variations and extensive oscillations, which are not exactly periodic. In order to reduce these oscillations in the generated voltage with variable frequency and amplitude, the WEC output voltage is rectified and the power is collected on a dc-bus, where a capacitor is connected in parallel in Case II. In order to complete the observation of the WECE operating performance a dc motor type load is connected as shown in Figure 4.24 to the rectifier output. The motor load is operated with and without the voltage storage capacitor. It has been observed that the dc-bus voltage under load without the capacitor is similar to the voltage obtained in Case I. The dc-bus voltage has voltage sags shown in Figure 4.25 are required to be improved. The connection of the capacitor under dc motor type load is able to improve the voltage waveform as in Case II. However, the improvement under loaded condition is not as good as it is under no-load condition. As shown in Figure 4.26, the voltage sags are reduced but not completely improved. When there is a load connected to the output of the rectifier with the storage capacitor, the load causes a discharge in the capacitor during discontinuous period of the generated voltage.

Therefore the capacitor should be selected properly so that the voltage sags can be eliminated.

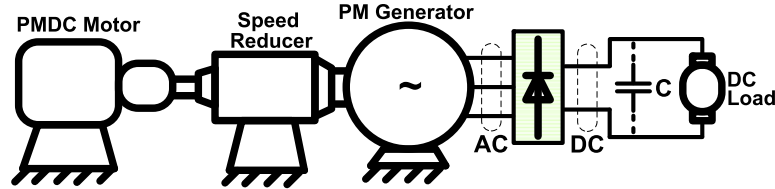


Figure 4.24. The WECE test block diagram for Case III and Case IV

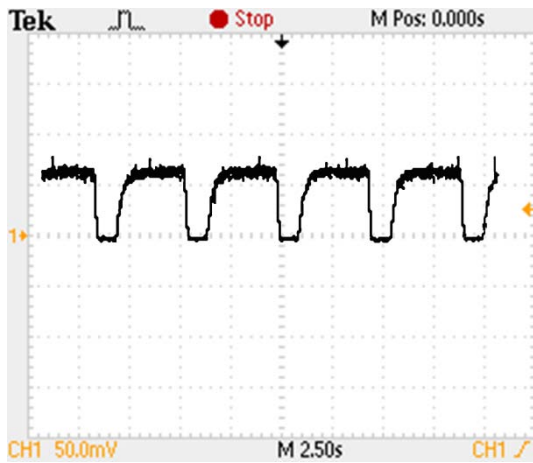


Figure 4.25. The dc-bus voltage (x137)
(DC_{load} : 12V DA, 0.16A)

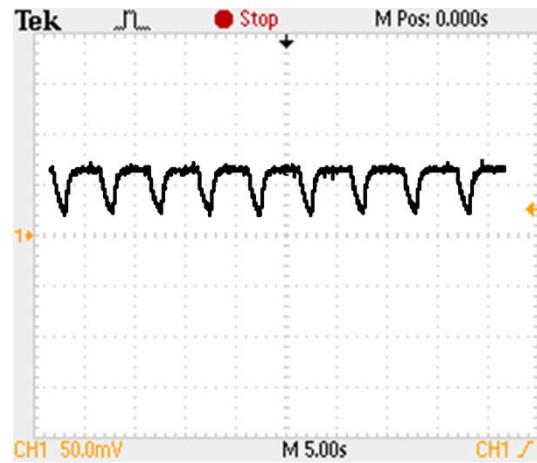


Figure 4.26. The dc-bus voltage (x137)
(DC_{load} : 12V DA, 0.16A)
($C=1200\mu\text{F}$, $45V_{dc}$)

As the tests show, the emulator developed to represent the wave energy conversion system is able to generate the required voltage waveforms. Its operating characteristics show that when the WEC system is directly connected to the loads, some precautions should be taken to operate the loads without problems, otherwise the voltage sags will cause undesirable effects on the loads. Therefore a SPF-GP is proposed and utilized to overcome these undesirable effects. Experimental design of the proposed SPF-GP is given next.

4.3. Switched Power Filter-Green Plug (SPF-GP)

A novel FACTS device called Switched Power Filter-Green Plug (SPF-GP) is designed to eliminate generator side voltage sags and oscillations not to effect the load side. This FACTS device has been suggested by Dr. Adel M. Sharaf, who has cooperative studies with the supervisor of this thesis, Dr. Altas. The circuit diagram of SPF-GP is given in Figure 3.12. Therefore, it is not going to be repeated here.

The experimental circuitry of the SPF-GP system is shown in Figures 4.27.



Figure 4.27. Experimental circuitry view of the SPF-GP system

4.4. Design of Power Electronic Converters

4.4.1. DC-DC Buck Converter Design

The next device after the SPF-GP is a DC-DC converter. This device is used to supply a constant voltage to a dc bus at its output. The DC-DC converter circuit is designed as the one shown in Figure 4.28. The DC-DC buck converter has an input voltage range of 12-100V and a constant output voltage as 24V. Detailed circuit diagram of the converter system consisting of a DC-DC buck converter and power supply stage is shown in Figure 4.29. The PCB and photo of the system are given in Appendix 5. The DC-DC buck converter is controlled by employing the controllers given in Subsection 3.4 in previous chapter.

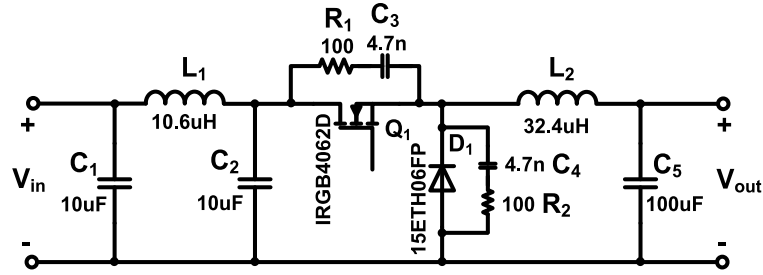
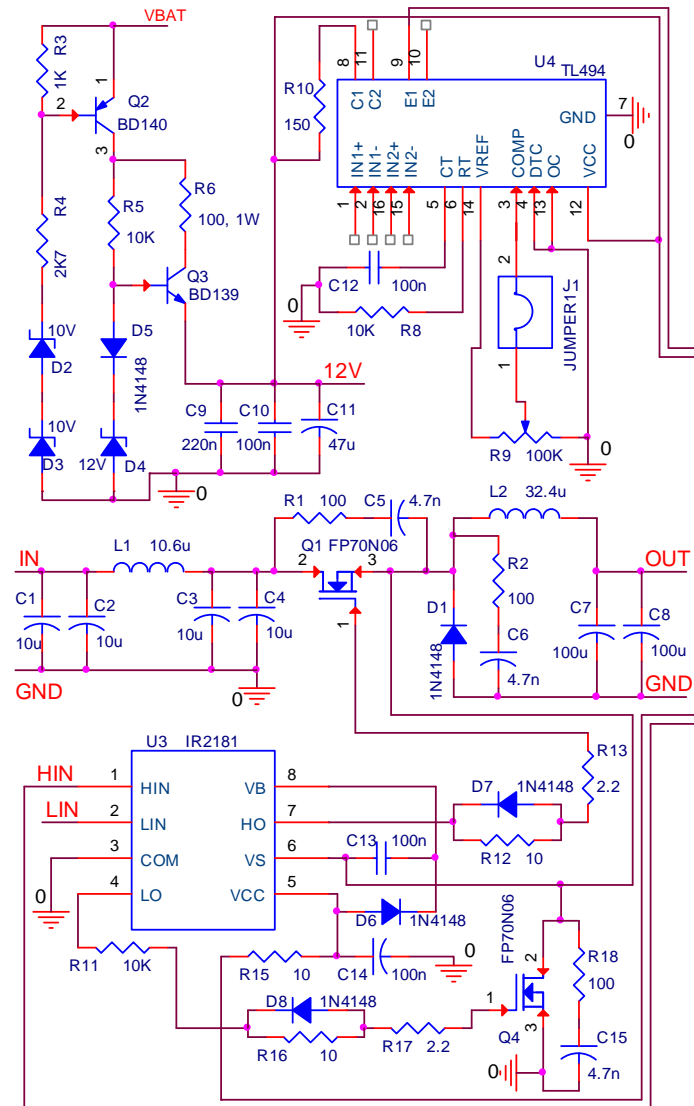


Figure 4.28. The designed DC-DC buck converter general circuit diagram



Title		
Prof.Dr. Ismail H. Altas & Emre Ozkop		
Size	Document Number Custom <Doc>	Rev
Date:	Monday, January 09, 2012	Sheet 1 of 1

Figure 4.29. The converter system detailed circuit diagram

4.4.2. DC-DC Chopper Design

A special DC-DC chopper is designed to be used with DC motor type loads. The chopper is designed to ensure constant input voltage to DC motor such that the DC-DC chopper operates as both a voltage controller and an isolation device between the WEC system and the load. The design scheme of the DC-DC chopper consists of the followings;

- Power supply for control circuits
- Driver units
- Current control unit
- Current protection unit
- DAQ output isolation unit

The details of these designs are given below.

4.4.2.1. Power Supply

The circuit diagram of chopper feeding is shown in Figure 4.30. The working principle of the system follows: The voltage drop in zener diodes ($D1$ and $D2$) will be equal to 20 V and if enough voltage is present, $Q1$ will be ON and there will be an output voltage to feed the controller. In this application, the battery voltage (V_{supply}) is equal to 24 V . If $V_{BAT} < 24\text{ V}$ or

$$\left(\frac{V_{supply}-20}{R_2-R_1}\right) \times R_1 < V_{BE(Q1)}, \quad Q1 \text{ is OFF} \quad (4.5)$$

If we assume $V_{BE(Q1)} = 0.6\text{ V}$:

When $V_{supply} \geq 24\text{ V}$, output voltages ($V_{driver, ICs}$) is equal to 12 V :

$$\left(\frac{24-20}{R_2+R_1}\right) \times R_1 = 0.6 \text{ so } \frac{R_2}{R_1} = 6 \quad (4.6)$$

The limit can be adapted depending on the battery type by changing R_2 and R_1 . The chosen resistances values are: $R_1 = 1\text{ k}\Omega$ and $R_2 = 2.7\text{ k}\Omega$. The PCB and general view of the supply are given in Appendix 5.

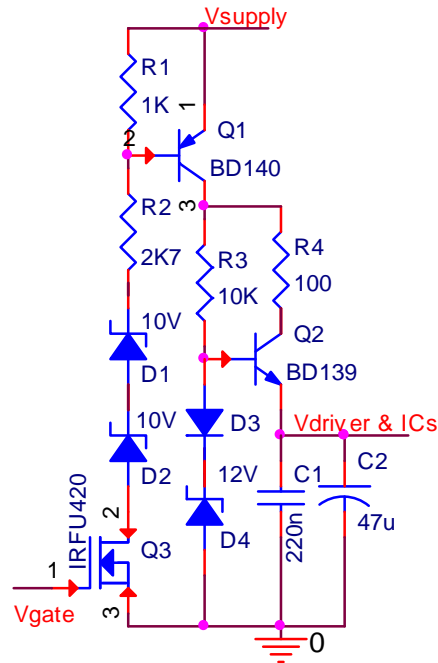


Figure 4.30. The block scheme of controller power supply

4.4.2.2. Driver

The gate drive circuit forms the interface between the DAQ control card and the power MOSFETs. The gate drive circuit has two purposes. Firstly, it buffers the gate signals generated by the DAQ card. The DAQ card can only source a maximum of 50 mA from each pin. The peak charging current required to turn MOSFETs may be as high as 1 A. This is due to the high switching frequency used along with the inherent gate capacitance of the MOSFET.

The second purpose of the gate circuit is to generate the gate voltages required to activate the topside transistor. To turn on an N-channel FET, the gate source voltage must be 10 to 15 V. In this application, *IR2181* was used as a driver. The driver connection diagram is shown in Figure 4.31. The *IR2181* is a high voltage; high speed power MOSFETs and IGBT driver with independent high and low side referenced output channels [273]. *C1* is a bootstrap capacitor and *D1* is a bootstrap diode. The operation of the bootstrap capacitor and diode system is as follows: When *V_S* is pulled down to ground (either through the low side FET or the load, depending on the circuit configuration), the bootstrap capacitor (*C1*) charges through the bootstrap diode (*D1*) from the *V_{CC}* supply. Thus providing a supply to *V_{C1}*. The *V_{C1}* voltage provides the supply to the high side driver

circuitry of IR2181. The bootstrap diode ($D1$) needs to be able to block the full power rail voltage, which is seen when the high side device is switched on. It must be a fast recovery device to minimize the amount of charge fed back from the bootstrap capacitor into the VCC supply, and similarly the high temperature reverse leakage current would be important if the capacitor has to store charge for long periods of time. The bootstrap diode is 1N4148. Resistors $R5$ and $R6$ are $2.2\ \Omega$ series current limiting resistors.

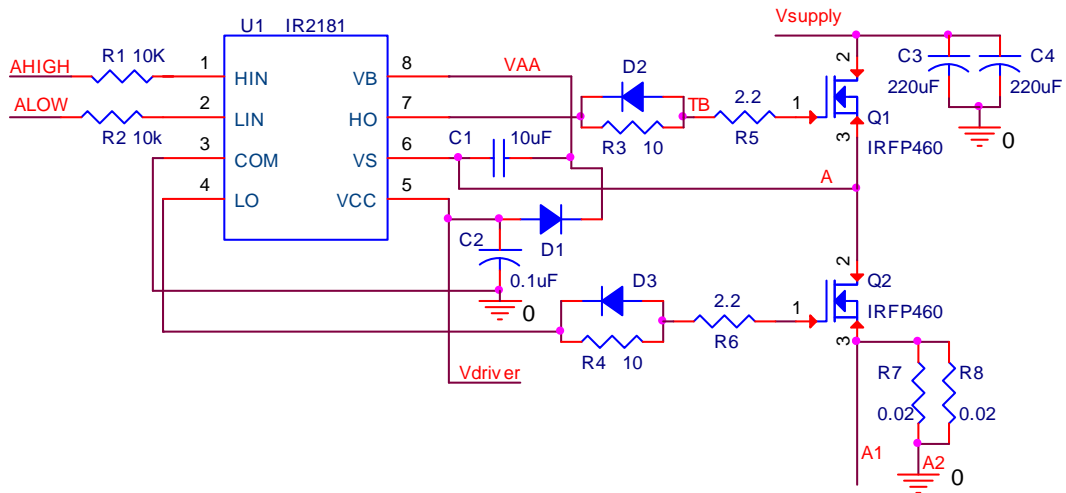


Figure 4.31. The driver connection diagram

4.4.2.3. Current Control

While a current flows in the motor, the current is compared with the reference voltage value in the operational amplifier ($TLC272$). If the current value is bigger than the reference value, operational amplifier output ($TLC272$, pin 1) will be zero. The gate voltage of $Q3$ shown in Figure 4.30 becomes low and thus the output voltage to feed the driver will be zero. The current control block diagram is shown in Figure 4.32.

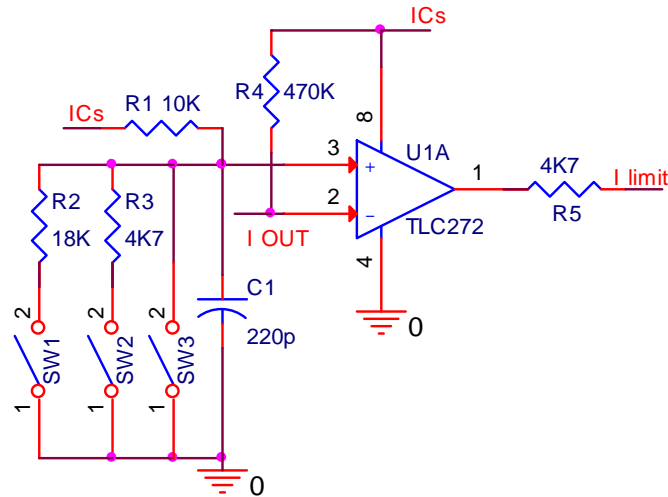


Figure 4.32. Current control block diagram

We put three switches to control the current limit. We can obtain four different states:

1. When SW1, SW2 and SW3 are OFF, the current value 15 A is obtained.
2. When SW1 is ON, SW2 and SW3 are OFF, the current value 10 A is obtained.
3. When SW2 is ON, SW1 and SW3 are OFF, the current value 5 A is obtained.
4. When SW3 is ON, SW1 and SW2 are OFF, the current value 0 A is obtained, and the motor does not work.

These states are shown in Table 4.1.

Table 4.1. Switch states and current values

Current (A)	SW1	SW2	SW3
0	OFF	OFF	ON
5	OFF	ON	OFF
10	ON	OFF	OFF
15	OFF	OFF	OFF

4.4.2.4. Current Protection

4.4.2.4.1. Upper Transistor Current Protection

The upper transistor current protection circuit diagram is shown in Figure 4.33. The transistor, which is connected to the upper MOSFET has a relationship with each phase separately. We choose one leg to explain work principle clearly.

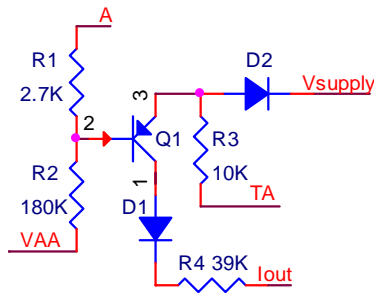


Figure 4.33. Upper transistor current production circuit diagram

The condition, which is explained below must be verified to work a leg upper transistor current protection circuit in cold state:

$$\left(\frac{V_{AA}-A}{R_2-R_1}\right) \times R_2 < V_{BE(Q1)} + V_{E(Q1)} \quad (4.7)$$

If this condition is not verified, there is no current flow from the transistor ($Q1$) collector to the diode ($D1$). If the condition is verified, current flows and generates voltage drop in resistor ($R4$) and then the current value is obtained as a voltage in current control part.

4.4.2.4.2. Lower Transistor Current Protection and Regulation

In this application, for the current control and lower transistor current protection which was shown in Figure 4.34, we used a *TLC274*, which has 4 operational amplifiers. Three of the operational amplifiers were used to amplify the sensed current in the sensed

resistors ($R1$, $R2$), and then we can calculate the maximum current value. There is an amplifier in parallel to the current sensed resistors to magnify the low voltage value in these resistors. It is a differential amplifier with two RC low pass filters in both inputs to filter the high frequency. The three amplifier outputs are joined to obtain always one value of I_{OUT} . $D1$ diode was used to eliminate the drop of $D2$ diode. The capacitor $C2$ was used to limit the spikes on the current signal.

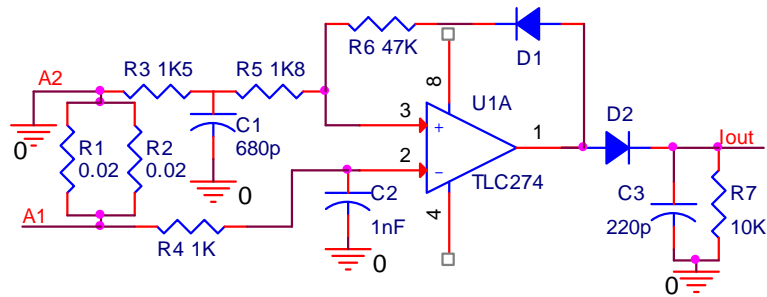


Figure 4.34. Lower transistor current production circuit diagram

4.4.3. DAQ Output Isolation Circuit

The pulse width modulation (PWM) signals generated in the Matlab/Simulink environment and the encoder output signal are isolated to suppress the noise with the isolation circuit. The DAQ output isolation circuit diagram is shown in Figure 4.35.

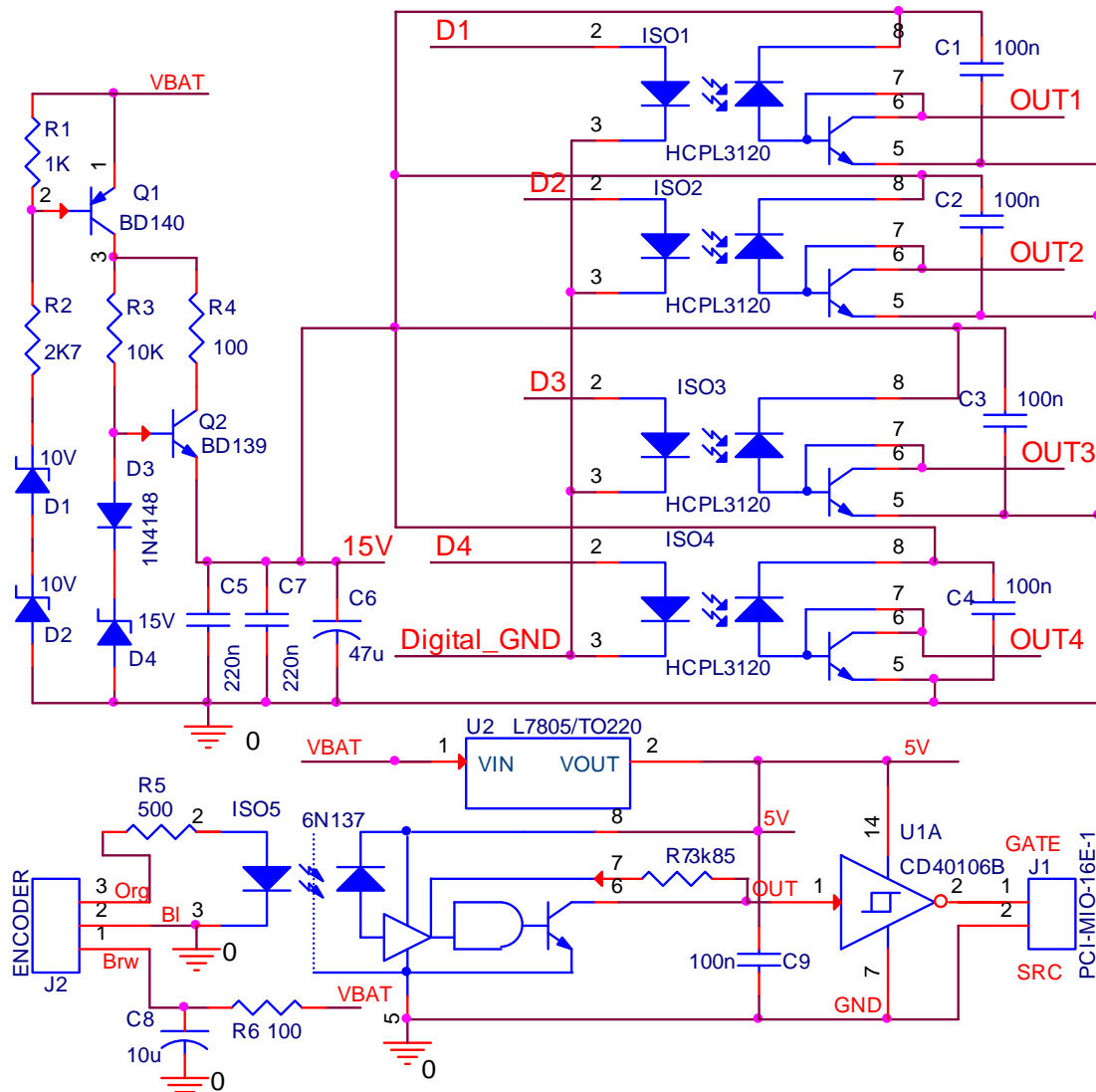


Figure 4.35. Isolation circuit diagram

The designed DC-DC chopper circuit diagram is shown in Figure 4.36, and its PCB and general view are given in Appendix 5.

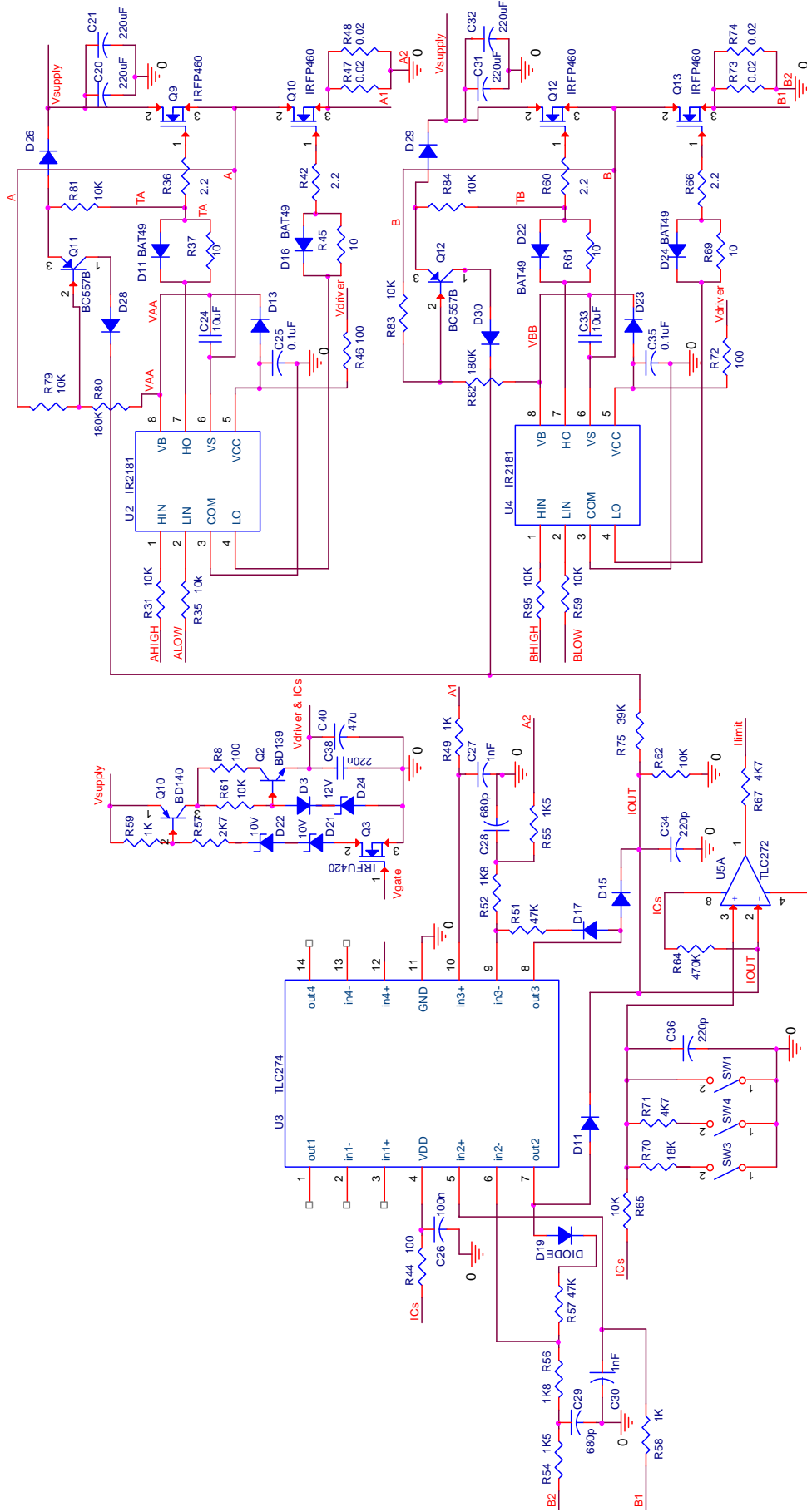


Figure 4.36. The designed DC-DC chopper circuit diagram

4.4.4. DC/AC Inverter Design

4.4.4.1. Integrated Power Module

The electronics industry is steadily moving toward one compact package technology to achieve high power density and low profile. The improvements in power semiconductors have provided variable solutions for high switching loss and high stress. Due to packaging technology, the parasitic inductance and capacitance causes stress and an undesirable noise problem. Thermal and noise problems also greatly affect the performance of IC. With advancement of the packing technology, different types of power modules have been constituted. One of them is an Integrated Power Module (IPM) including advanced packaging technology.

In this application, International Rectifier's *IRAMX20UP60A* (a 20A, 600V Integrated Power Hybrid IC) is used to realize the DC/AC inverter circuit. The features of the IPM is given Appendix 6. There are 6 signal inputs, where 3 signal inputs are high side gate driver and 3 signal inputs are low side gate driver.

3 PWM signals generated in the Matlab/Simulink environment are transferred into the DC/AC inverter system via the DAQ card (PCI-MIO-16E-1). In the DC/AC inverter circuit, the signals pass through the isolation circuit (HCPL-3120) to eliminate the noise.

The Schmitt Trigger integrated circuit (*CD40106*) is used to produce negative signals of the input signals. The 6 signals comprising negative and positive PWM signals are connected to the IPM circuit. The DC/AC inverter system block diagram is shown in Figure 4.37. The PCB and general view of the DC/AC inverter system are given in Appendix 6.

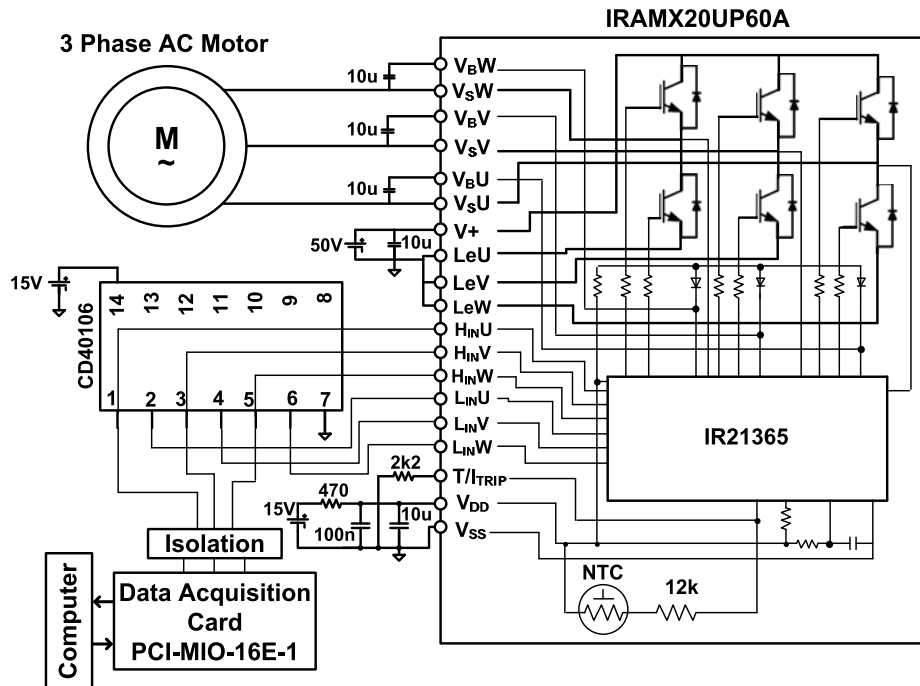


Figure 4.37. The DC-AC inverter system block diagram

5. SIMULATION AND EXPERIMENTAL RESULTS

5.1. Experimental Results for the Wave Energy Converter System

5.1.1. Introduction

In this chapter the simulation and experimental results for the wave energy converter system are presented. A Switched Modulated Power Filter-Green Plug (SPF-GP) Scheme is adapted into a wave energy converter system. A novel multi-loop dynamic error driven controller is used to control the novel SPF-GP scheme. A classical PI and Self-Scaled Fuzzy Tuned PI (SSFTPI) controllers are firstly utilized. The utilization of the proposed PI and SSFTPI controllers with the novel SPF-GP switched power filter compensator and dynamic error driven control strategy is examined via simulation model developed in Matlab/Simulink/Simpower Software Environment and experimental prototype model. The performances of wave energy converter system with the SPF-GP are observed with different controller types (PI, SMC, a Fuzzy Tuned SMC (FTSMC) and a Self-Scaled Fuzzy Tuned PI Controller (SSFTPIC)) in experimental platforms. Finally, the wave energy converter system is connected with loads exhibiting variable characteristics. The wave energy converter system with hybrid loads model is developed and analyzed in both simulation and experiment modes for different operation conditions and cases.

5.1.2. Experimental Results for Different Scenarios

5.1.2.1. A Novel Switched Power Filter-Green Plug (SPF-GP) Scheme for Wave Energy Systems

The proposed wave energy conversion utilization system is shown in Figures 5.1 and 5.2 without and with the novel FACTS SPF-GP, respectively. The unified system is comprised of a wave energy converter, rectifier, dc filter, SPF-GP system, buck converter and dc motor as the load.

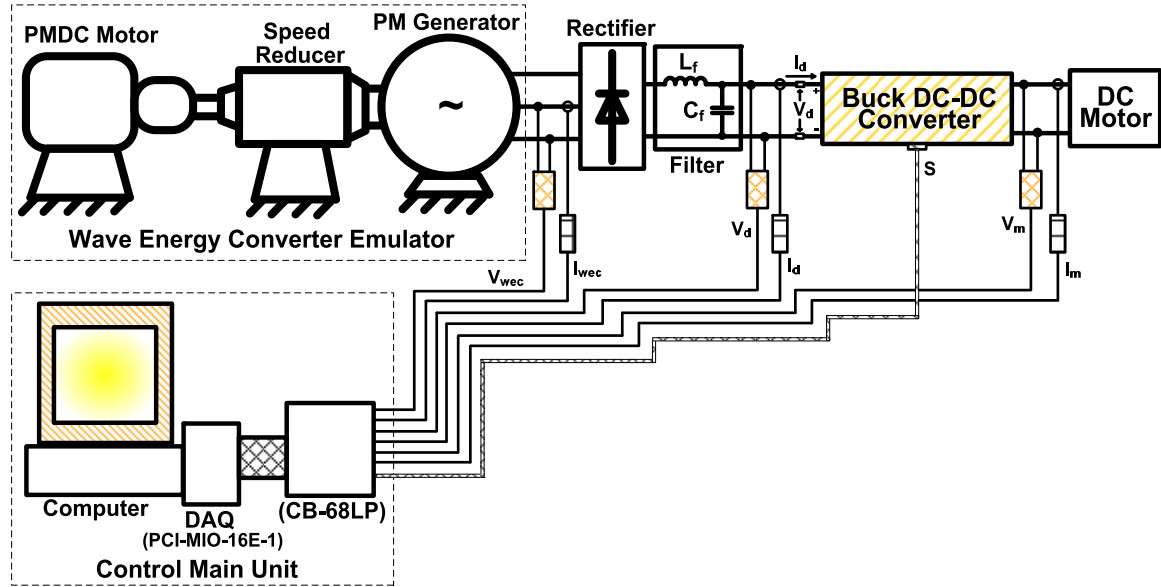


Figure 5.1. Wave Energy Conversion system without the SPF-GP

Due to the stochastic nature of the wave kinetic characteristics, the generated voltage show variations and extensive oscillations, which are not exactly periodic. In order to reduce these oscillations in the generated voltage with variable frequency and amplitude, the WEC output voltage is rectified and the power is collected on a DC bus. A common DC bus is useful for collecting power from other similar WEC systems at one common bus for obtaining more power to supply larger loads. The rectified voltage is transformed and regulated by the SPF-GP converter and power is transmitted to a PMDC motor load through a DC-DC buck converter. Appropriate controllers for the SPF-GP converter and DC-DC buck converter are also developed in the scope of this study. The DC bus voltage is regulated and kept constant by means of using the SPF-GP converter controller. Moreover, the PMDC motor load demand is assured by controlling the DC-DC buck converter.

A set of monochromatic wave travelling parameters representing areas around Trabzon, Turkey are used in the study. Trabzon is a city on the Black Sea coast of north-eastern Turkey and located at a longitude of 39.46 degrees East and latitude of 40.59 degrees North. Wave measurements were done between 1994 and 1998 in NATO TURKISH-WAVES Project. The coastlines around Trabzon have mean power densities in the range of 1.67-8.61 kW/m [274].

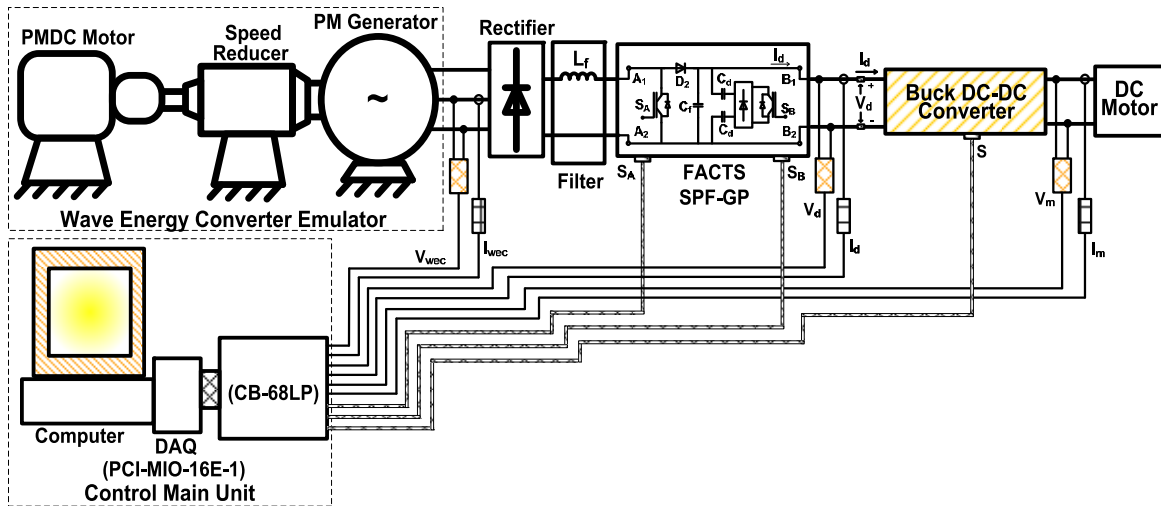


Figure 5.2. Wave Energy Conversion system with the SPF-GP

5.1.2.1.1. Experimental Set-up for the WEC System Laboratory Testing

A laboratory prototype experimental setup of the WEC system is shown in Figure 5.3. A PMDC motor and a reducer are used to emulate the wave turbine capable of producing waving speeds and torque input to 3-phase PM generator.

Well known dynamic model of PMDC motor is used in simulation software together with the models of the reducer and 3-phase PM generator in order to develop a complete model for the proposed WEC so that proposed controllers can be tested by simulation before building the system.



Figure 5.3. A general view of WEC system experimental set-up

5.1.2.1.2. Novel Error Driven Controller

Two control structures are utilized in the study. First a single negative feedback loop consisting of only a dc voltage control and then an alternative multi-loop structure is applied to include dc current and power changes in the controller besides the voltage control. The dc motor load voltage is regulated by the buck converter with the single-loop classical PI controller shown in Figure 5.4.

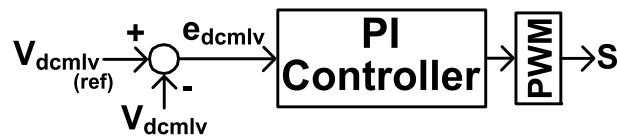


Figure 5.4. Single-loop voltage control scheme

The dc motor load voltage (V_{dmclv}) is measured by a LV-25P voltage transducer and compared with the reference voltage ($V_{dmclv(ref)}$) to yield the voltage error signal (e_{dmclv}), which is applied to a PI controller to generate the required output. The output of the PI controller is applied to PWM switching unit to generate required pulses into the buck converter.

The alternatively proposed control scheme has a multi-loop structure as shown in Figure 5.5. The controller uses the changes in the common DC bus current (I_d), common DC bus voltage (V_d) and changes in common DC bus power (P_d) to generate a total error signal for DC bus voltage control. The changes in DC bus current (e_{I_d}) and power error (e_{P_d}) are obtained by taking the differences, between the current and delayed real input values. The common DC bus current change, the common DC bus voltage error and the power change multiplied by the related weighting factors (γ_{I_d} , γ_{V_d} and γ_{P_d}) and the output summation is the total control error (e_{t_B}). The total error of the multi-loop structure goes into the controller block. The inclusion of the changes in current and power in the total control error signals enables the controller to take action whenever the current and/or power changes due to either the oscillations caused by waves or sudden load changes. The multi-loop dynamic error driven structure of the total effective error enables the controller to decrease the discontinuity on current and voltage of wave energy system. The output

signal of the controller drives a pulse generator to modulate pulses so that converter switching signals S_A and S_B , are generated so that $S_B = \text{not}(S_A)$.

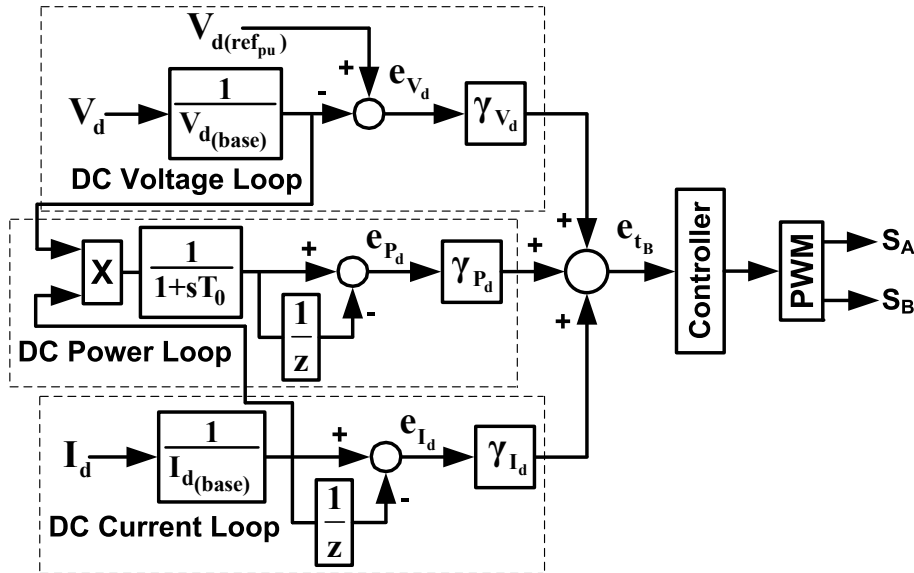


Figure 5.5. A novel multi-loop dynamic error driven control scheme

In this section, a classical PI and SSFTPI controllers are used in a novel multi-loop dynamic error driven control scheme.

5.1.2.1.3. Digital Simulation

The proposed WEC system and all components including controller, filters and auxiliary devices are modeled in Matlab/Simulink and simulated for different operating conditions so that the performances of the system elements can be evaluated. The operational dynamic blocks in Simulink/Simpower library are used in the modeling of the system for simulation studies as shown in Figures 5.6 and 5.7 without and with the SPF-GP, respectively. The data for the diodes, the capacitors and the other semiconductors are set to the same values given in the components datasheets. The simulation system parameters are given in Appendix 7.

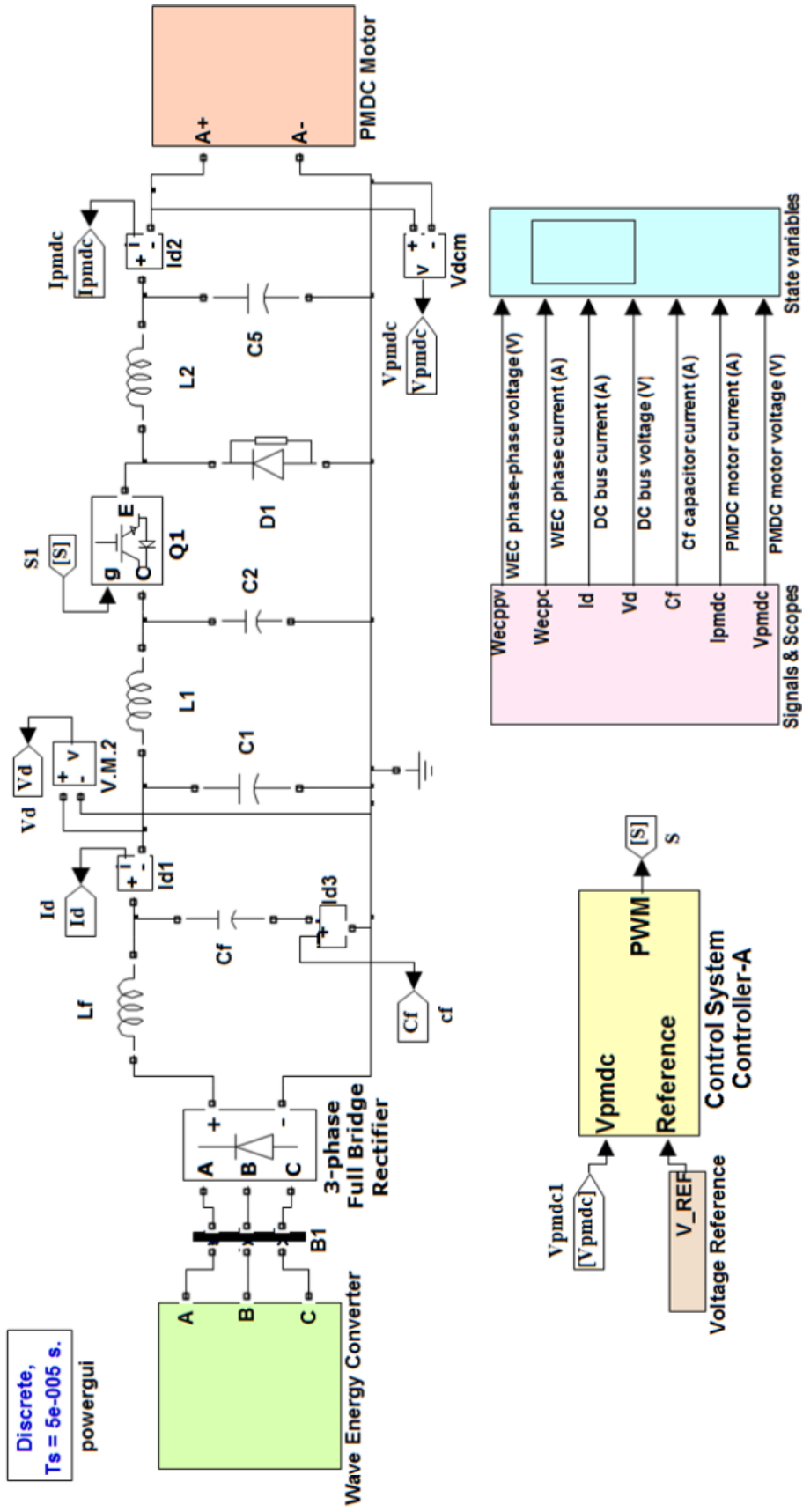


Figure 5.6. The system Simulink operational block diagram without the SPFGP

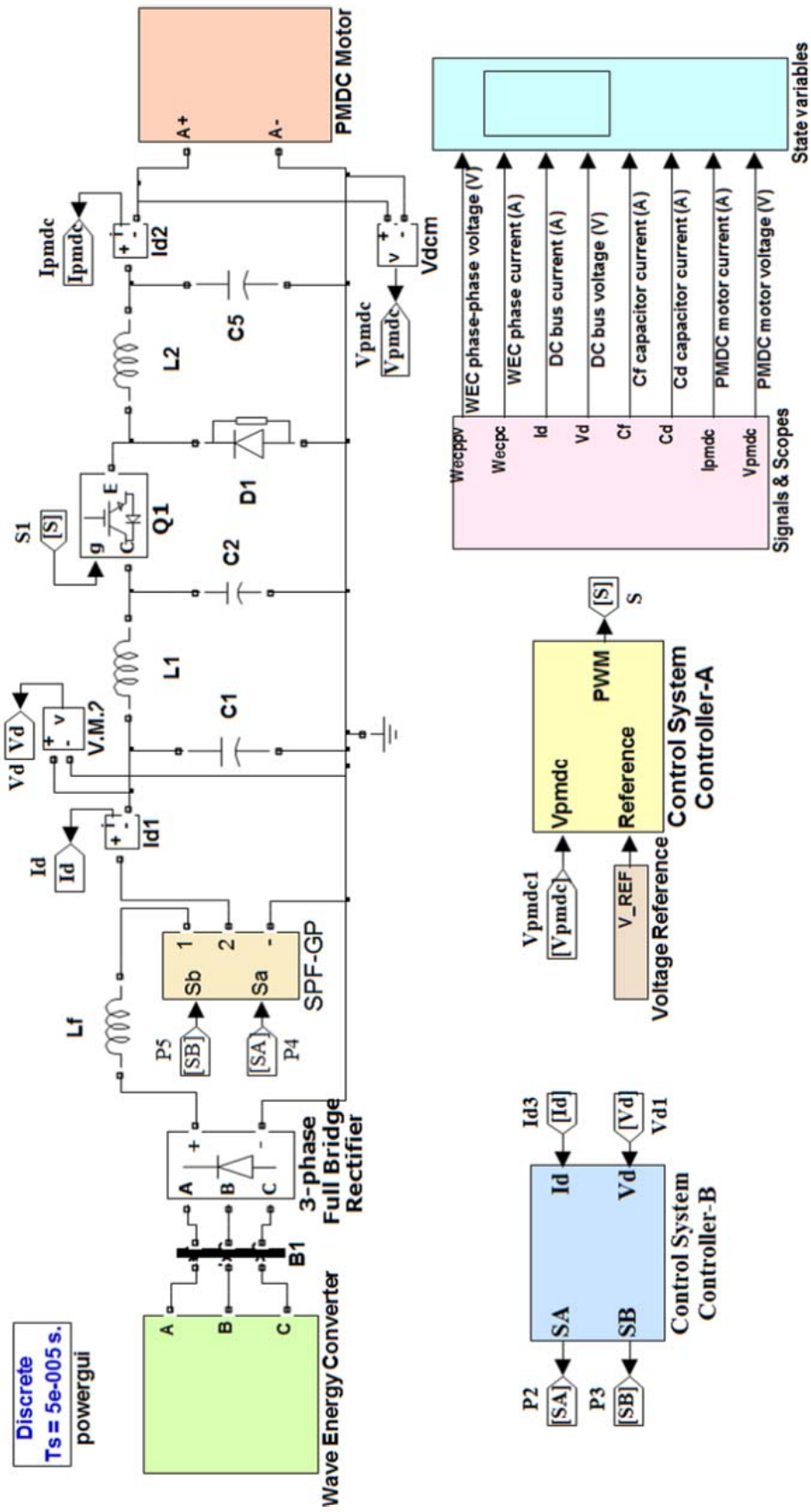


Figure 5.7. The system Simulink operational block diagram with the SPF-GP

5.1.2.1.4. Experimental Implementation

The real time implementation of the unified system is done using the RTWT available in Matlab/Simulink toolbox, which provides an opportunity to create and control real time executable commands for real time applications through Matlab/Simulink [275-286]. A PCI-6070E multifunction DAQ card is used in this study in order to establish communication on data acquisition between the real time part of the study and the computer, which contains the digital modeling of the SPF-GP and the controllers used in complete system. The main control units of the system without SPF-GP are implemented through Matlab/Simulink as shown in Figure 5.8.a. Since an individual driver circuit and an additional control algorithm are required for switching the semiconductors in the rectifier, a passive rectifier is used to reduce the cost and controller complexity while increasing the system robustness. The output voltage wave energy converter emulator is rectified by a three phase full bridge uncontrolled rectifier and then applied to the buck converter, which is controlled for constant voltage and variable voltage trajectory references. The system with the novel FACTS SPF-GP control main unit is modeled in the Matlab/Simulink software as shown in Figure 5.8.b.

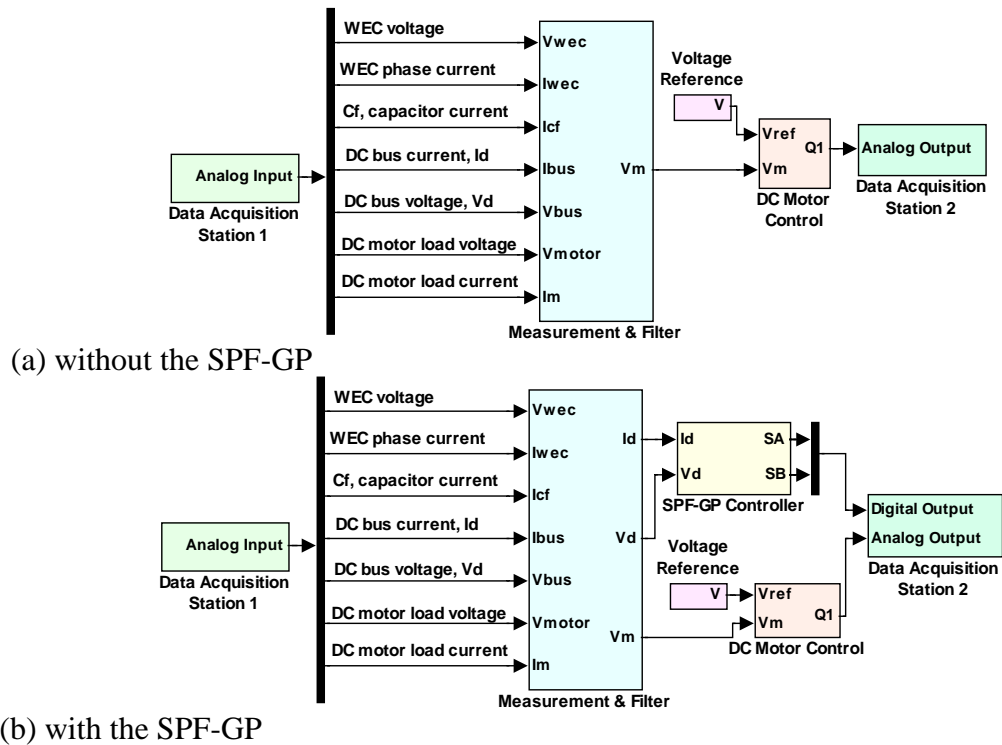
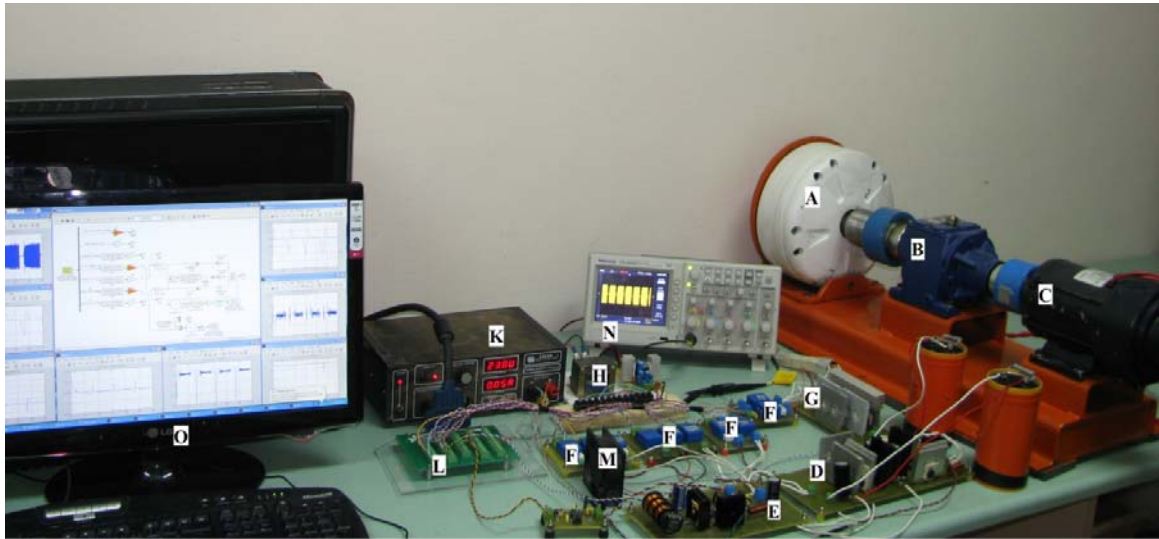


Figure 5.8. The main control stages of the test system

5.1.2.1.5. Digital Simulation and Experimental Results

The experimental setup shown in Figure 5.9 consists of the data acquisition system with five Hall Effect Current Sensors (LEM, LA-25NP), three Hall Effect Voltage Sensors (LEM, LV25-P), and an analog input board (National Instruments PCI-6070E). The computational implementation part of the experimental setup runs in Matlab/Simulink environment, through the data acquisition. The parameters of the system for both simulation and experimental tests are given in Appendix 7.

In order to validate the simulation models of the proposed filters and control algorithms, an experimental set up has been established as shown in Figure 5.9. Both digital simulation models and the experimental test are done under four different cases tabulated in Table 5.1 for observing the systems under different operating conditions.



[A: 3 Phase Permanent Magnet (PM) Generator; B: Reducer; C: PMDC Motor; D: SPF-GP System; E: DC-DC Buck Converter; F: Hall Effect Voltage-Current Sensors; G: 3 Phase AC-DC Rectifier; H: DC Power Supply (Hall Effect Voltage-Current Sensors); K: DC Power Supply (SPF-GP and DC-DC Buck Converter Circuits); L: Data Acquisition System Connector Block; M: DC Motor (Load); N: Oscilloscope; O: Computer]

Figure 5.9. Experimental setup

Firstly, the system performance is observed for a constant voltage trajectory reference with and without the SPF-GP model for a DC bus reference voltage of 20V. Some of resultant figures for the Cases I and II with PI controller and FPI controller are

given in Figures 5.10-5.12 and Figures 5.16-5.18, respectively, and the rest of results are given in Appendix 8.

Table 5.1. The three different system scenarios for the real time experimental studies

	Case I	Case II	Case III	Case IV
PMDC motor voltage trajectory tracking reference ($V_{m(ref)}$)	Constant	Constant	Variable	Variable
DC bus reference voltage ($V_{d(ref)}$)	20V	20V	20V	20V
SPF-GP model	Without	With	Without	With

The phase to phase voltages of the WEC system are shown in Figures 5.10 and 5.16 for SPG-GP scheme with PI controller and SSFTPI controller, respectively. Experimental and Simulation results without and with SPF-GP are depicted in the same figure for providing a better comparison and show the effect of the SPF-GP. Figures 5.10 and 5.16 show that similar voltage waveforms are obtained from simulation and experiments. The effect of the SPF-GP can be seen clearly on the peak to peak voltage waveforms. The peak values of the phase to phase voltages are over 21 Volts with SPF-GP while they are below 21 Volts without the SPF-GP. Figures 5.11 and 5.17 show the DC bus voltage variation from experimental and simulation studies with and without SPF-GP. When SPF-GP is not used, the DC bus voltage and currents have higher drops for each starting instant of the wave cycles. With the use of SPF-GP these drops are reduced and the DC bus voltage is kept constant at 20V. The load voltage is kept nearly constant for these cases as given in Figures 5.12 and 5.18.

Some of resultant figures for the Cases III and IV with PI controller and SSFTPI controller are given in Figures 5.13-5.15 and Figures 5.19-5.21, respectively, and the rest of results are given in Appendix 8. These cases deal with variable voltage trajectory operation of the system. The load voltage is not kept constant for these cases. Stepwise changes are given to the load voltage to analyze the performance of the novel FACTS SPF-GP and controller if the applied voltage of the load changes due to variable power or torque control requirements. The effects of the SPF-GP on voltage is given in Figures 5.14 and 5.20, while the peak values of the WEC voltages are below 21 volts without SPF-GP, they are above 21 volts with the SPF-GP. The voltages of the WEC show similar effects

with the SPF-GP here as in the Cases I and II. The voltage of the WEC is kept constant when the voltage applied to the dc motor has step changes as shown in Figures 5.15 and 5.21. As the load voltage encounters some random step changes, the novel FACTS SPF-GP is employed to keep the common DC bus voltage constant at 20V as given in Figures 5.14 and 5.20. It can be observed from Figures 5.14 and 5.15 that the convergence of the DC bus voltage occurs when the load voltage is low or higher. The SPF-GP system FPI controller performances have been determined by the means of ISE, IAE and ITAE as given in Appendix 9. The improvement is observed in the system performance.

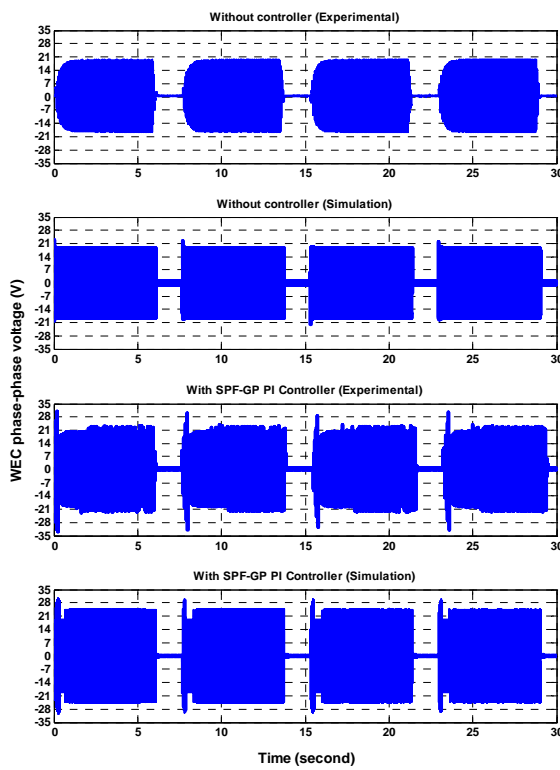


Figure 5.10. WEC voltage (PI)

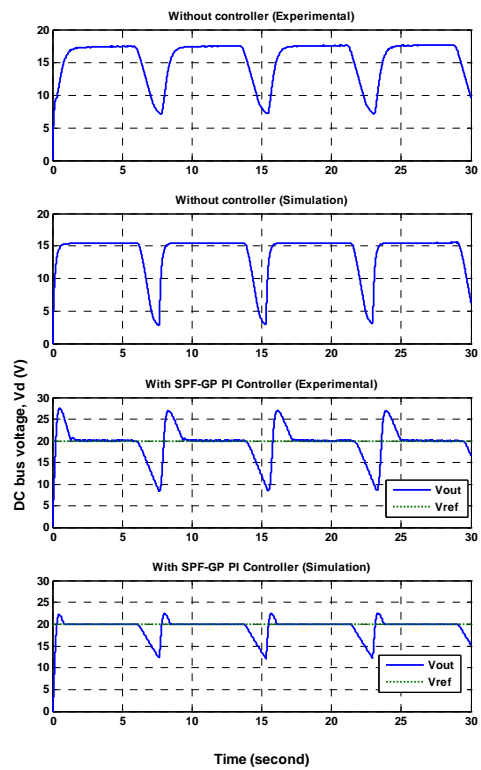


Figure 5.11. DC bus voltage (V_d) (PI)

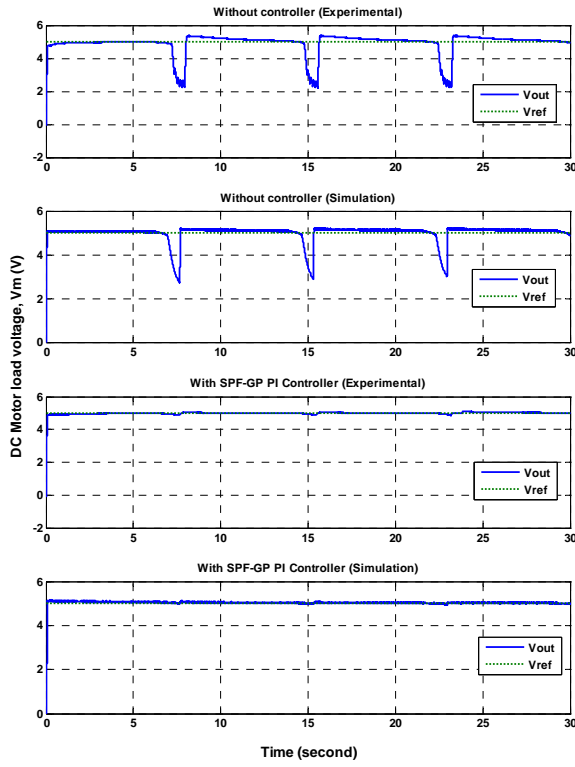


Figure 5.12. PMDC motor voltage (V_m) (PI)

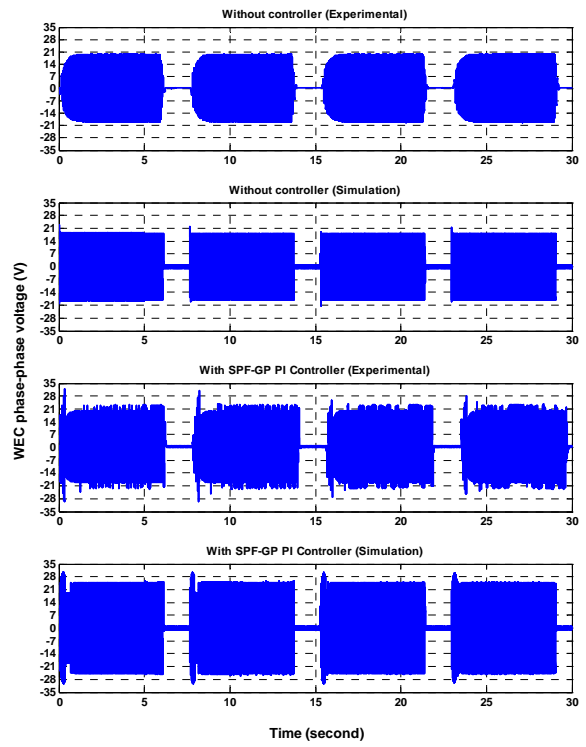


Figure 5.13. WEC voltage (PI)(Case III-IV)

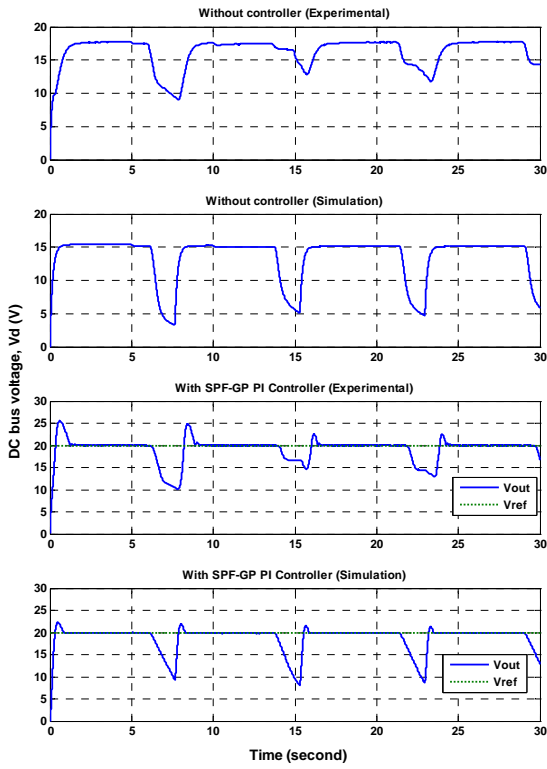


Figure 5.14. DC bus voltage (V_d) (PI)

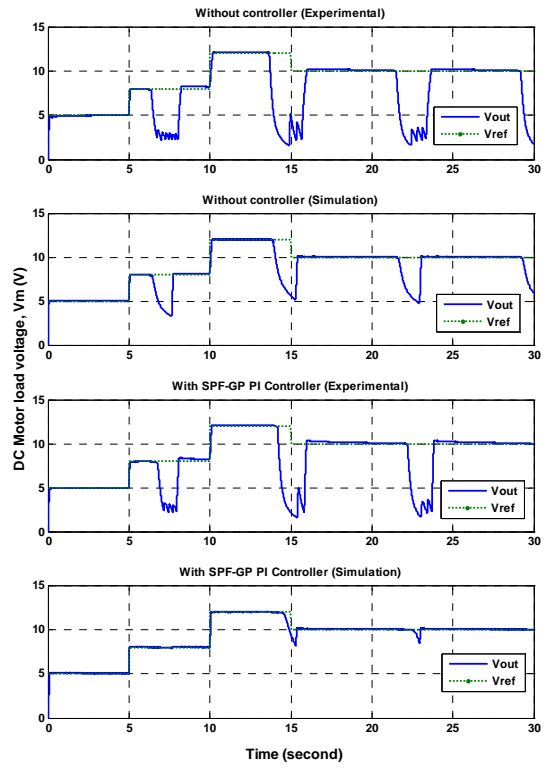


Figure 5.15. PMDC motor voltage (V_m) (PI)

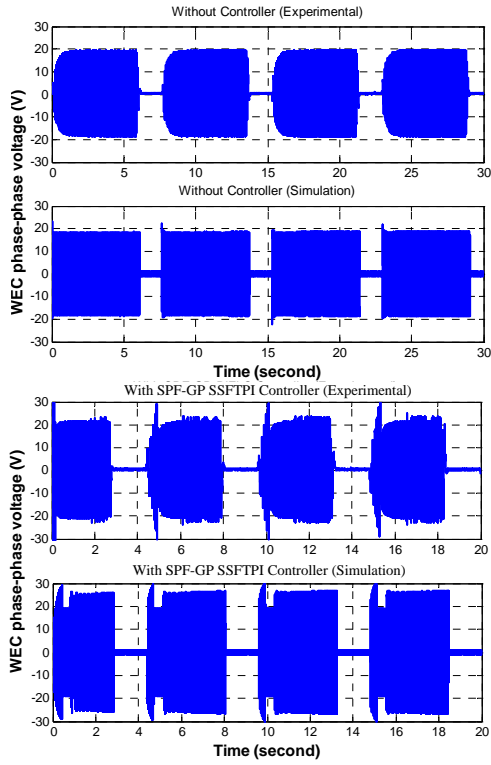


Figure 5.16. WEC voltage

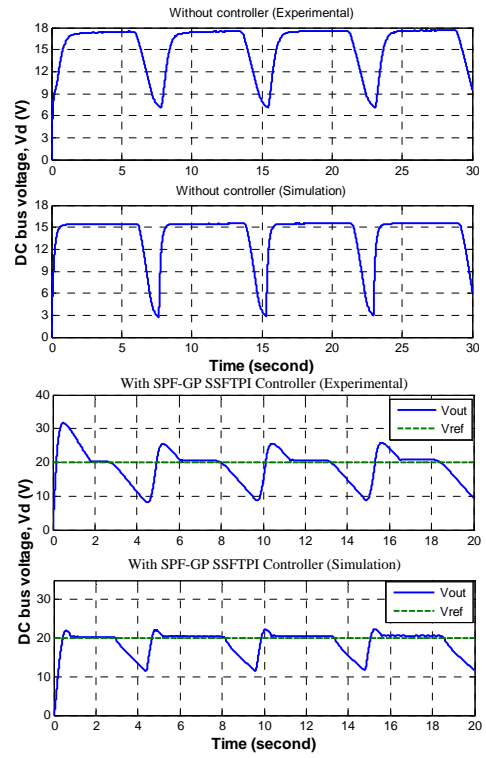


Figure 5.17. DC bus voltage (V_d)

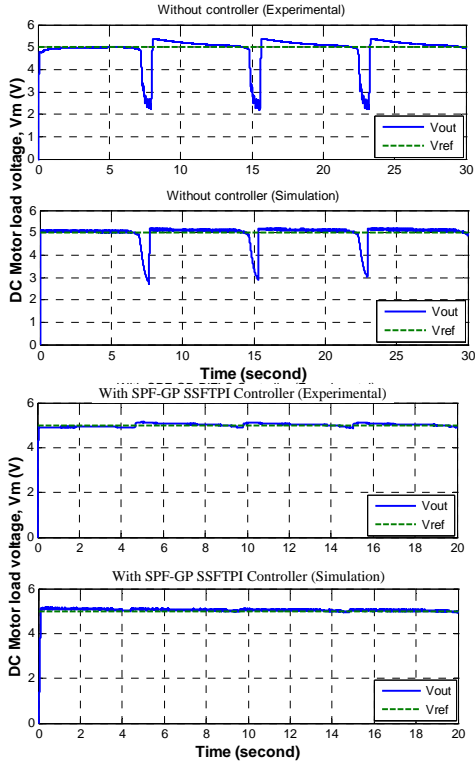


Figure 5.18. PMDC motor voltage

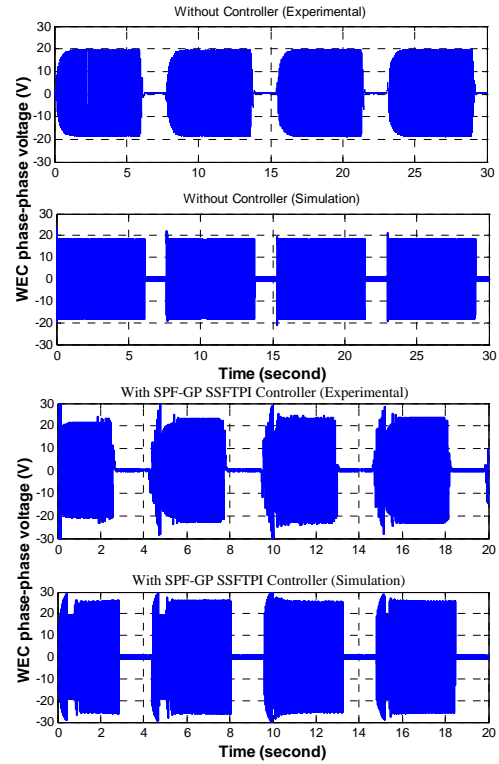


Figure 5.19. WEC voltage

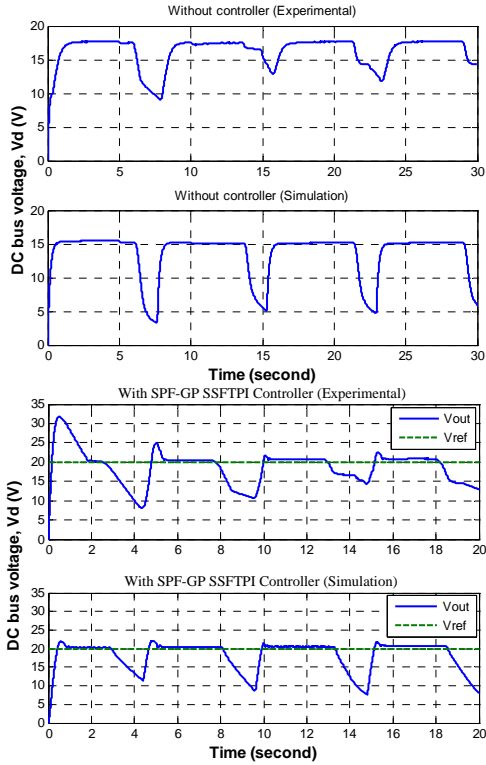
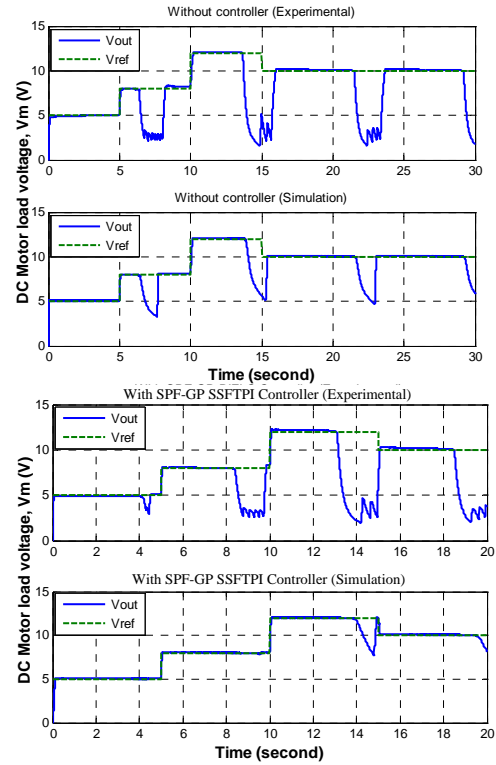
Figure 5.20. DC bus voltage (V_d)

Figure 5.21. PMDC motor voltage

A novel FACTS based SPF-GP scheme regulated by a tri-loop dynamic error driven control algorithm is developed and used to stabilize the wave energy system used as standalone source for DC loads. In order to control and compensate the power flow from wave source to electrical load, a classical PI and Self-Scaled Fuzzy Tuned PI (SSFTPI) controller are developed and used which acts as the power conditioner and stabilization device between the wave source and the load. Since the magnitude, speed and cycle of the sea wave are not constant and unpredictable; the generated power is not reliable due to stochastic variations. Therefore, interfacing devices between the WEC system and the electrical loads are required to ensure power balance and voltage stabilization. The generated AC voltage from WEC system is rectified and applied to a buck converter. Then the buck converter is controlled for constant DC bus voltage whether the load voltage is constant or variable. The PI or SSFTPI controlled FACTS SPF-GP device is fully utilized to provide a stable voltage regulation at the common DC bus. It is shown that the proposed PI and SSFTPI used in the SPF-GP scheme improved the DC bus voltage stabilization so that energy utilization is enhanced. The dynamic error driven scheme uses the DC bus voltage error as the main regulating loop along with the dynamic current and power deviations as the two supplementary/auxiliary loops. The use of this novel control strategy

enables the regulating system to react to any changes in load power and load current to generate the required control action for a constant DC bus voltage. The FACTS SPF-GP scheme regulated by the time-descaled dynamic error driven loops and controller is the main contribution of this study providing the required DC bus voltage stabilization. The proposed scheme and the controller are validated using the developed Matlab simulation model of the unified AC-DC system and compared with those of obtained from the experimental setup of the same system for model validation.

Both digital simulation and laboratory prototype experiments are done for four cases, which are constant load voltage references tracking with and without FACTS SPF-GP scheme and variable DC motor voltage trajectory with and without the SPF-GP scheme. It can be concluded from the comparison of the results from all the test cases that the application of the PI or SSFTPI controlled FACTS SPF-GP scheme and the multi loop error driven fuzzy logic control approach provides a mean constant DC bus voltage for both constant and variable load voltage trajectory test cases. One additional study, which is not considered here, may be the elimination of dc inrush current ripples that occur at the beginning of the each sea-wave cycle. Actually this problem can easily be solved just using a backup battery storage such that the required load demand is managed effectively from the batteries during the beginning of each wave cycle. Since the worst case scenario is considered here, the positive support of any back-up battery storage scheme is not considered. Even without the use of the expensive backup battery storage scheme, the magnitude of the DC bus voltage fluctuations is small.

The same flexible and SSFTPI controlled FACTS SPF-GP scheme can be extended to other AC-DC Interface Schemes using Wind-Photovoltaics, Wave-Microhydro and Hybrid Green Energy utilization systems. Other control strategies based on using soft-computing Artificial-Intelligent Controllers can also be utilized.

5.1.2.2. Novel Switched Power Filter-Green Plug (SPF-GP) Intelligent Controllers for Wave Energy Converter System: Experimental Results

In this study, the SPF-GP intelligent controllers for wave energy conversion systems are presented. In order to reduce the interfacing problems and improve power quality in WEC systems, design and realization of a novel SPF-GP and control approaches are studied. Experimental prototype models of the proposed SPF-GP system and the controllers (PI, SMC, Fuzzy Tuned SMC (FTSMC) and Self-Scaled Fuzzy Tuned PI Controller (SSFTPIC)) have been set up to observe performance by comparing the results, which show the effectiveness of the proposed interfacing device and the control algorithms. The experiments were done for several cases and the results of the same operating conditions from both platforms were compared for system performance. It has been shown that the proposed power filter and control approaches are very effective on eliminating wave effects on load side voltage and load variations on source side by reducing voltage sags and swells.

5.1.2.2.1. The Wave Energy Conversion System

The proposed wave energy conversion utilization system is shown in Figures 5.22 and 5.23 without and with the novel FACTS switched power filter-green plug (SPF-GP), respectively. The unified system is comprised of a wave energy converter, rectifier, dc filter, SPF-GP system, buck converter and dc motor as the load. A laboratory prototype experimental setup of the WECS is shown in Figure 5.3. In this part, there are four different controllers, which are PI, SMC, FTSMC and SSFTPIC, for the Controller B.

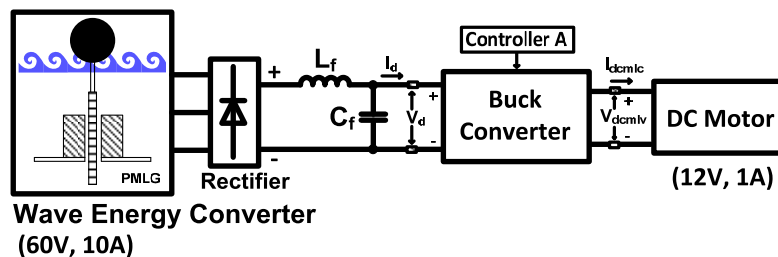


Figure 5.22. The sample study system diagram (without SPF-GP)

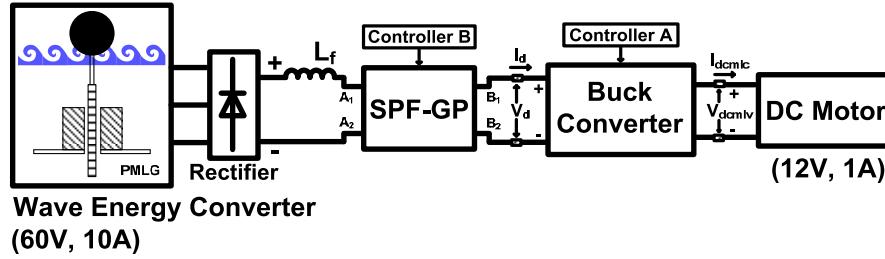


Figure 5.23. The sample study system diagram (with SPF-GP)

5.1.2.2.2. Experimental Implementation

The real time implementation of the system is done using RTWT available in Matlab/Simulink toolbox, which provides an opportunity to create and control real time executable commands for real time applications through Matlab/Simulink. PCI-6070E multifunction DAQ card is used in this study in order to establish communication on data acquisition between the real time part of the study and the computer, which contains the digital modeling of the SPF-GP and the controllers used in complete system.

The system experimental setups are shown in Figures 5.1 and 5.2 for the operation cases without and with the SPF-GP. The main control units of the system without SPF-GP are implemented through Matlab/Simulink as shown in Figure 5.24.

Since an individual driver circuit and an additional control algorithm are required for switching the semiconductors in the rectifier, a passive rectifier is used to reduce the cost and controller complexity while increasing the system robustness. The output voltage wave energy converter emulator is rectified by a three phase full bridge uncontrolled rectifier and then applied to the buck converter, which is controlled for constant voltage and variable voltage trajectory references. The system with the SPF-GP control main unit is modeled in Matlab/Simulink as shown in Figure 5.25.

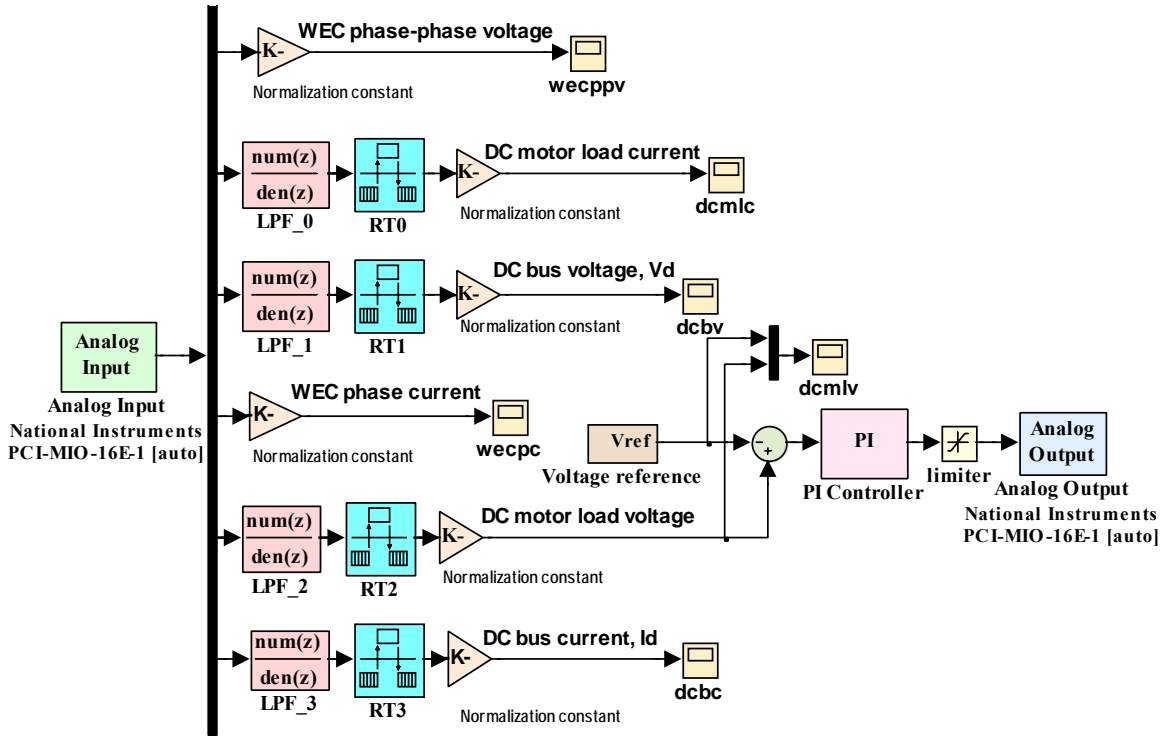


Figure 5.24. Data acquisition and Simulink modeling of for single loop PI controller the system without the SPF-GP

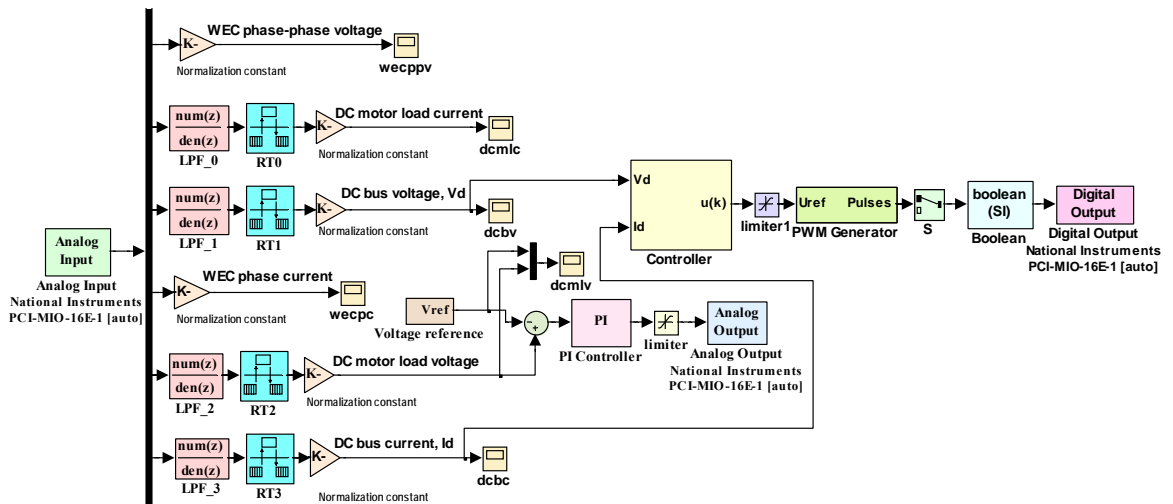


Figure 5.25. Data acquisition and digital Simulink modeling of three loop dynamic error driven PI controller for the system with SPF-GP

5.1.2.2.3. Experimental Results

Experimental tests and simulations are conducted for three different cases in order to observe the performance for different operating conditions. Figure 5.9 illustrates the experimental setup where the data acquisition system consists of five hall effect current sensor (LEM, LA-25NP), three hall effect voltage sensor (LEM, LV25-P), and an analog input board (National Instruments PCI-6070E). The computational implementation part of the setup runs in Matlab/Simulink environment. Four different controller types (PI, SMC, FTSMC and SSFTPIC) are used as a SPF-GP subsystem controller. There are three different system scenarios tabulated in Table 5.2 for the real time experimental studies.

Table 5.2. The system scenarios for the real time experimental studies

	Scenario-I	Scenario-II	Scenario-III
PMDC motor voltage trajectory reference ($V_{m(ref)}$)	Constant	Variable	Variable
DC bus reference voltage ($V_{d(ref)}$)	20V	20V	50V
SPF-GP model	with & without	with & without	with & without

The following performance measures are determined to compare the performances of controllers and given in Appendix 10: rise time (t_r), percent maximum overshoot (%OS), integral square error (ISE), integral of the absolute error (IAE) and integral of time multiplied by absolute error (ITAE).

In Scenario-I, the system performance is observed for a constant voltage trajectory reference ($V_{m(ref)}$) in the system with and without the SPF-GP model during the dc bus reference voltage ($V_{d(ref)}$) is 20V for four different controller types (PI, SMC, FTSMC and SSFTPIC) for Controller-B. The system performance outputs are shown in Figures 5.26-5.31. The WEC phase to phase voltage waveform is affected by the SPF-GP controllers. The peak to peak WEC phase-phase voltage value in the system with the SPF-GP controllers is bigger than the value in the system without the SPF-GP controller shown in Figure 5.26. The WEC phase current peak values in uptime are the smallest in the system with the SPF-GP FTSMC controller shown in Figure 5.27. The DC bus voltage has no overshoot only in the system with the SPF-GP FTSMC controller shown in Figure 5.27.

The controller compares the reference and the actual voltage values and generates the desired value of the SPF-GP voltage to be injected to the bus. Since the WEC output voltage waveform has a discontinuity, it is difficult to provide continuity in the DC bus voltage. At least a discontinuity is partially lessened with the SPF-GP control system. The dc bus current peak values in uptime are the smallest in the system with the SPF-GP FTSMC controller shown in Figure 5.29. The discontinuity in the voltage affects the dc motor load voltage control negatively. If the discontinuity is decreased or removed, the dc motor load voltage control will be better than before. The load voltage is controlled with the buck converter. The dc motor load current varies depending on the dc motor voltage shown in Figure 5.30. The current fluctuation is the smallest in the SPF-GP FTSMC control system shown in Figure 5.31.

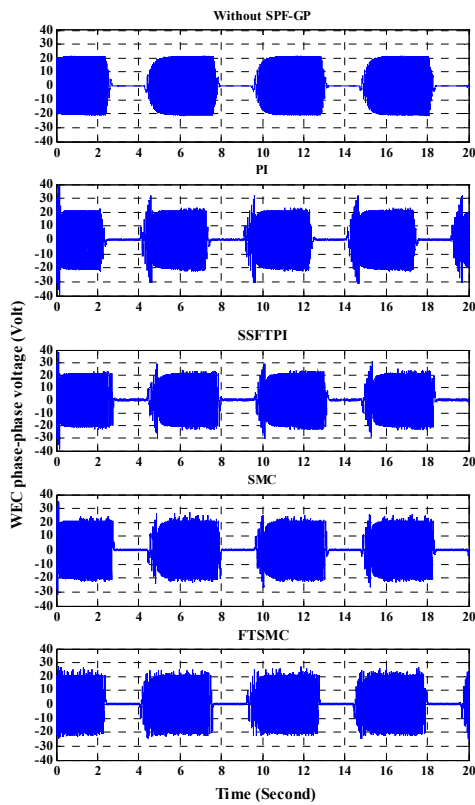


Figure 5.26. WEC voltage

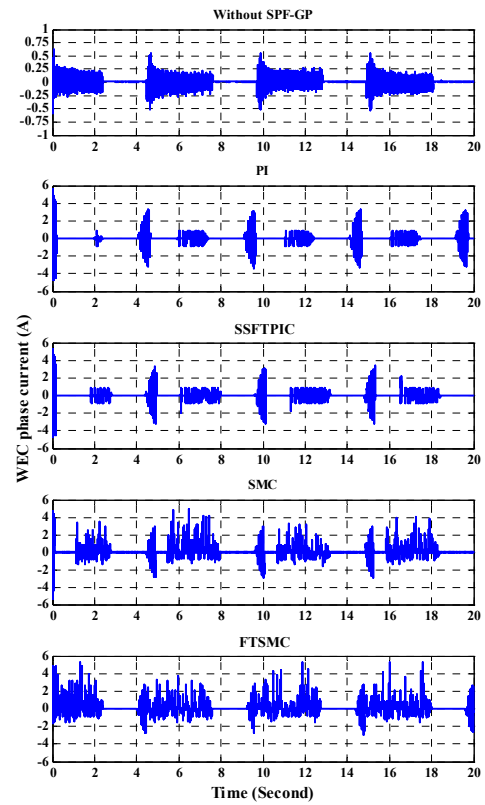


Figure 5.27. WEC current

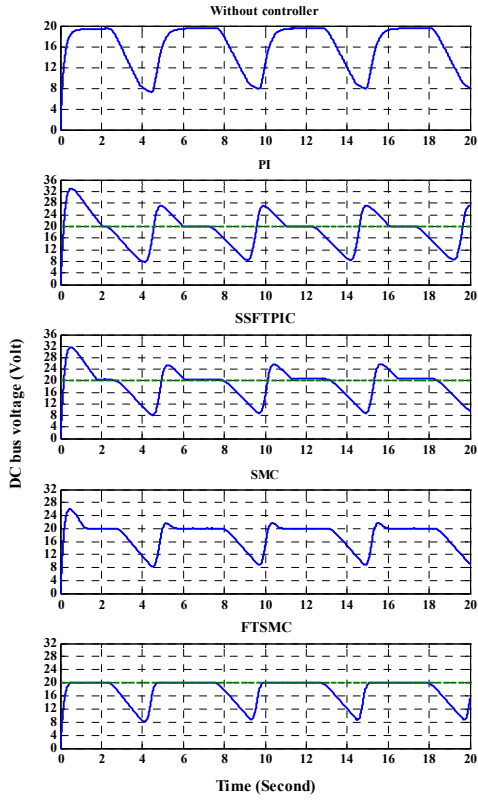


Figure 5.28. DC bus voltage (V_d)

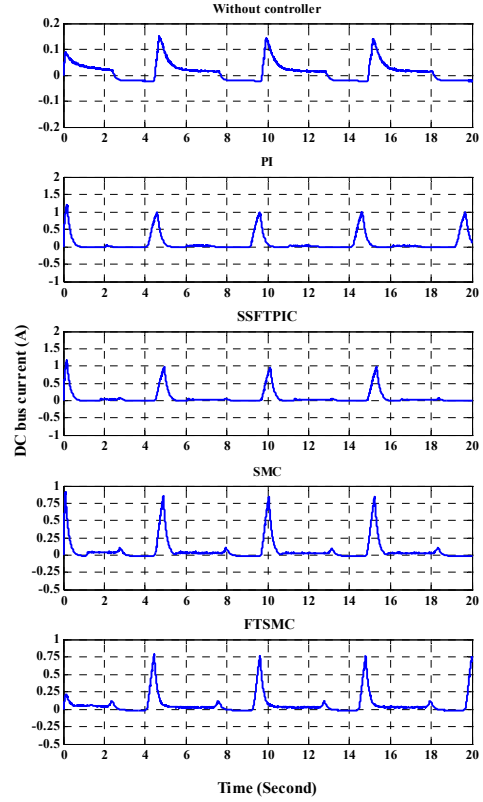


Figure 5.29. DC bus current (I_d)

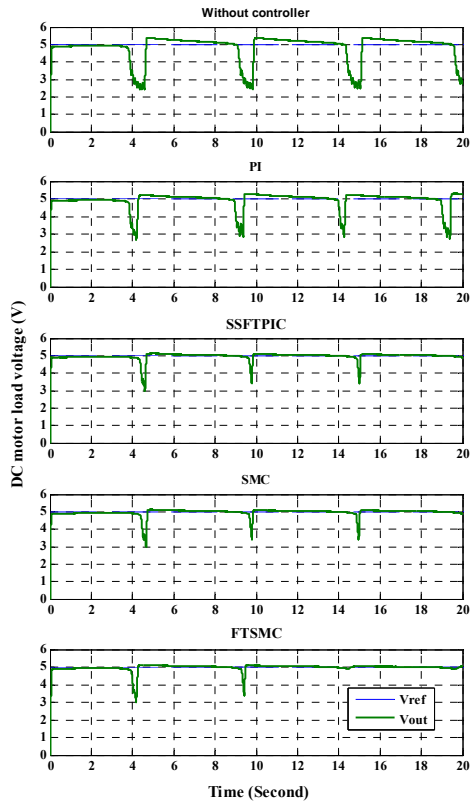


Figure 5.30. PMDC motor voltage (V_m)

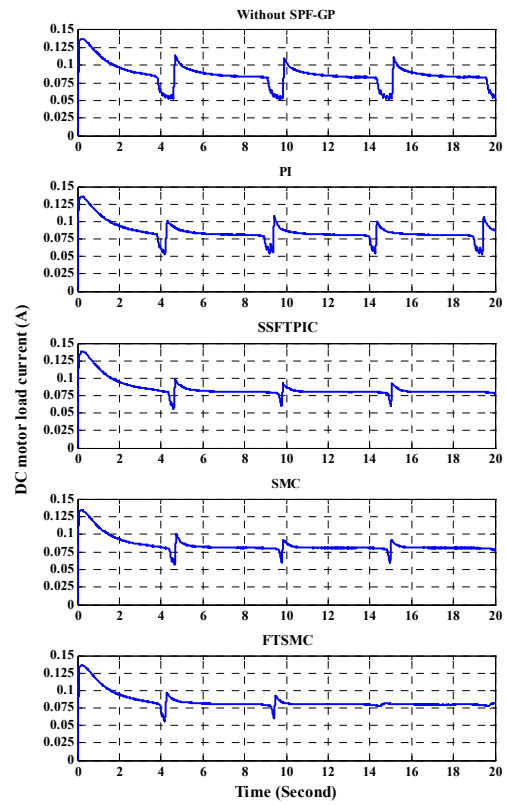


Figure 5.31. PMDC motor current (I_m)

In Scenario-II, the system performance is observed for a variable voltage trajectory reference ($V_{m(ref)}$) in the system with and without the SPF-GP model during the dc bus reference voltage ($V_{d(ref)}$) is constant. The system performance outputs are shown in Figures 5.32-5.37. The performance analysis of the controllers for a Scenario-II is given Appendix 10. The WEC phase to phase voltage waveform is affected by the SPF-GP controllers. The peak to peak WEC phase to phase voltage value in the system with the SPF-GP controllers is bigger than the value in the system without the SPF-GP controller shown in Figure 5.32. The current consumption increases with the SPF-GP control system. The WEC phase current peak values in uptime are the biggest in the system with the SPF-GP FTSMC controller shown in Figure 5.33.

The DC bus voltage waveform has no overshoot only in the system with the SPF-GP FTSMC controller shown in Figure 5.34. Since the WEC output voltage waveform has a discontinuity, it is difficult to provide continuity in the DC bus voltage shown in Figure 5.34. At least a discontinuity is partially lessened with the SPF-GP control system. The dc bus current peak values in uptime are the smallest in the system with the SPF-GP FTSMC controller shown in Figure 5.35. The discontinuity in the voltage affects the dc motor load voltage control negatively. If the discontinuity is decreased or removed, the dc motor load voltage control will be better than before. The load voltage is controlled with the buck converter. When the dc motor load reference voltage increases, to ensure the dc motor load voltage tracks the voltage reference is more difficult as shown in Figure 5.36. To increase the voltage decreases performance of the SPF-GP controller system. So, a discontinuity in the dc motor load voltage waveform is distinctive in parallel with increasing the dc motor load voltage reference. Contrary to the constant dc motor load reference voltage results, the dc motor load current waveforms have same characteristics as shown in Figure 5.37.

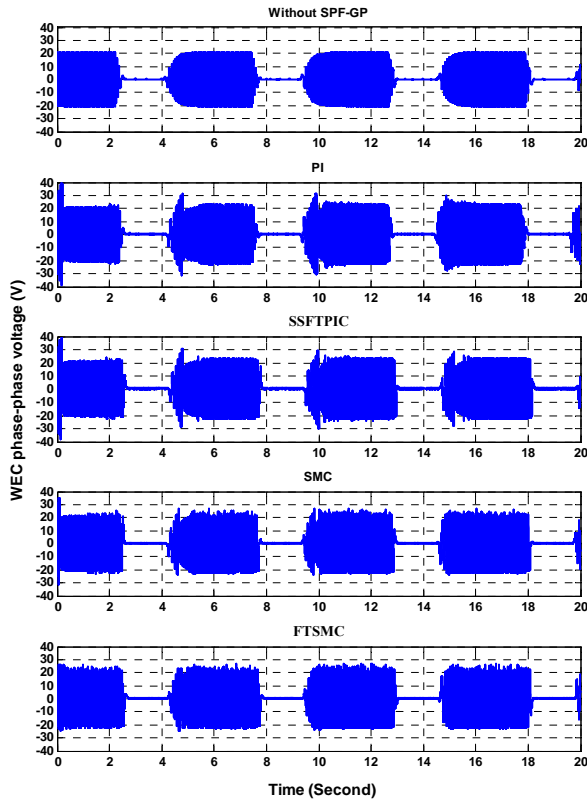


Figure 5.32. WEC voltage

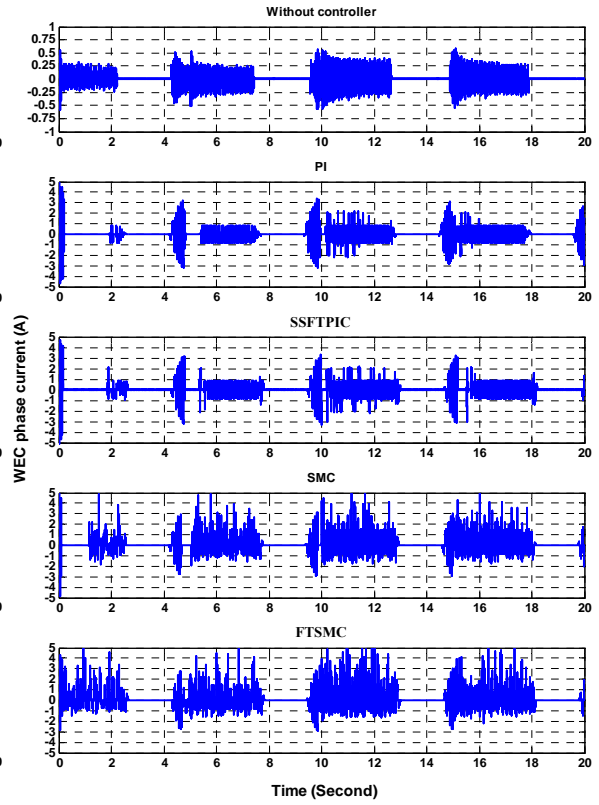


Figure 5.33. WEC current

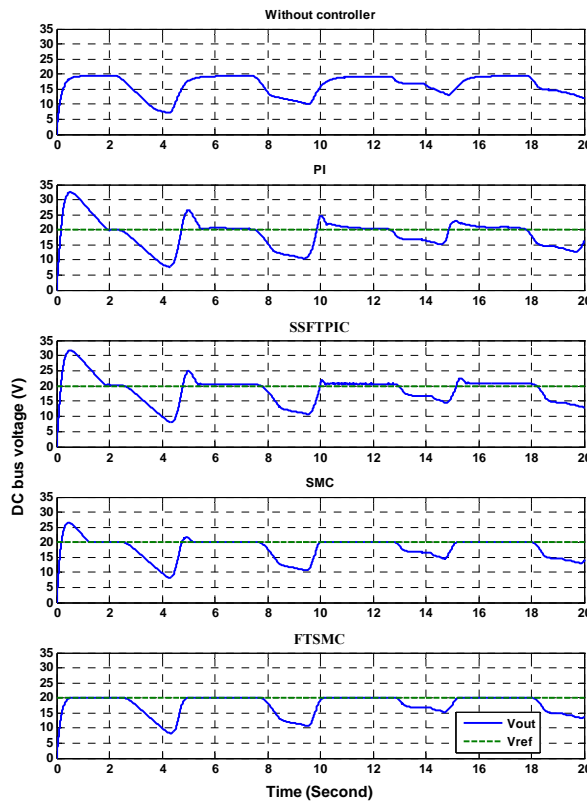


Figure 5.34. DC bus voltage (V_d)

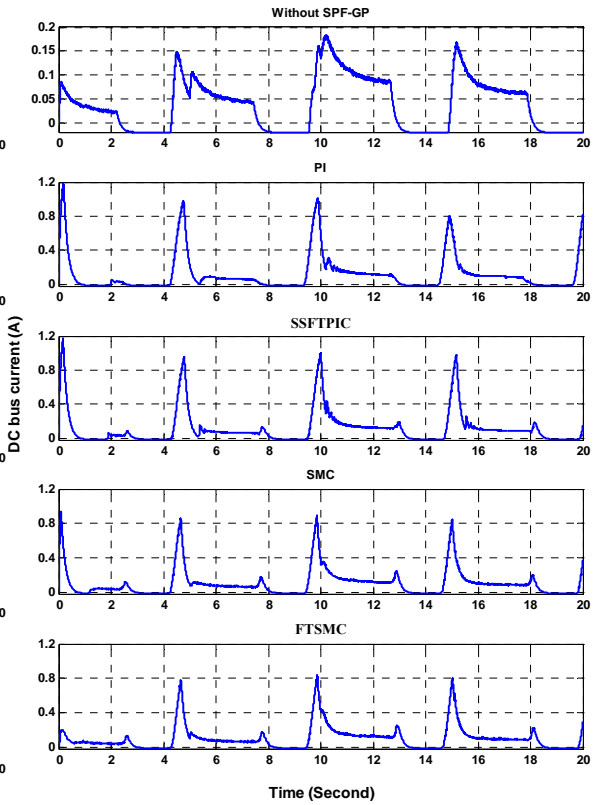
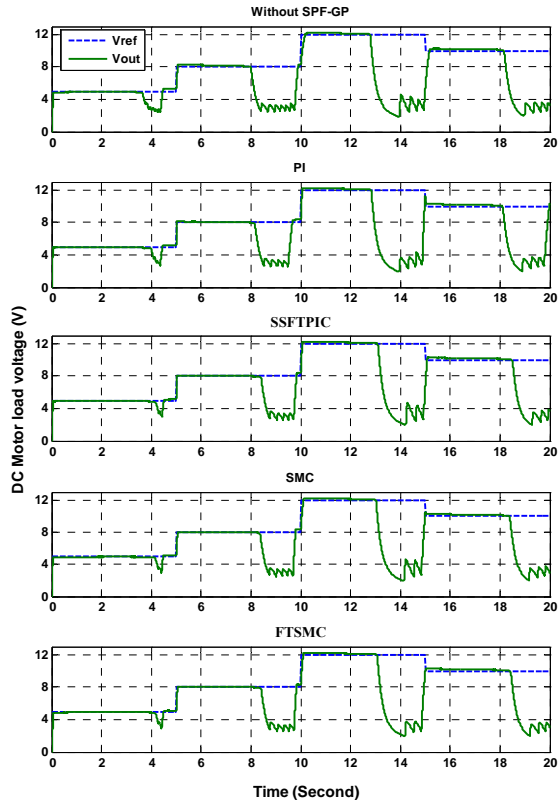
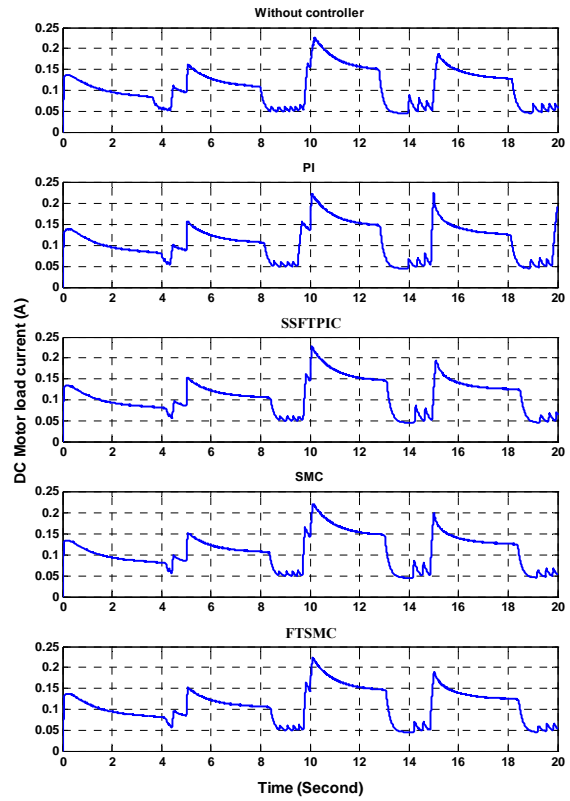


Figure 5.35. DC bus current (I_d)

Figure 5.36. PMDC motor voltage (V_m)Figure 5.37. PMDC motor current (I_m)

In Scenario-III, the system performance is observed for a variable voltage trajectory reference ($V_{m(ref)}$) in the system with and without the SPF-GP model during the DC bus reference voltage ($V_{d(ref)}$) is constant and different from Scenario-II. The system performance outputs are shown in Figures 5.38-5.43. The performance analysis of the controllers for a Scenario-III is given Appendix 10. The real time experimental results for a variable voltage trajectory reference in the system with the SPF-GP controllers are shown in Figures 5.38-5.43 during the DC bus reference voltage is 50V.

The WEC phase-phase voltage waveform is affected by the SPF-GP controllers and then the peak to peak WEC phase-phase voltage value in the system with the SPF-GP controllers is bigger than the value in the system without the SPF-GP controller shown in Figure 5.38. The WEC phase current consumption increases with the SPF-GP FTSMC controller system as shown in Figure 5.39. While dc motor load reference voltage increases, the WEC phase current value ascends too. The DC bus voltage waveform has no overshoot only in the system with the SPF-GP FTSMC controller shown in Figure 5.40. When the comparison is done between the system with and without SPF-GP control, a discontinuity is partially lessened with the SPF-GP control system at least.

The dc bus current peak values in uptime are the smallest in the system with the SPF-GP FTSMC controller as shown in Figure 5.41. The dc motor load voltage follows the voltage trajectory reference effectively as shown in Figure 5.42. The effects of the discontinuity in the WEC phase voltage is eliminated with the SPF-GP control systems. The load current, is shown in Figures 5.43.

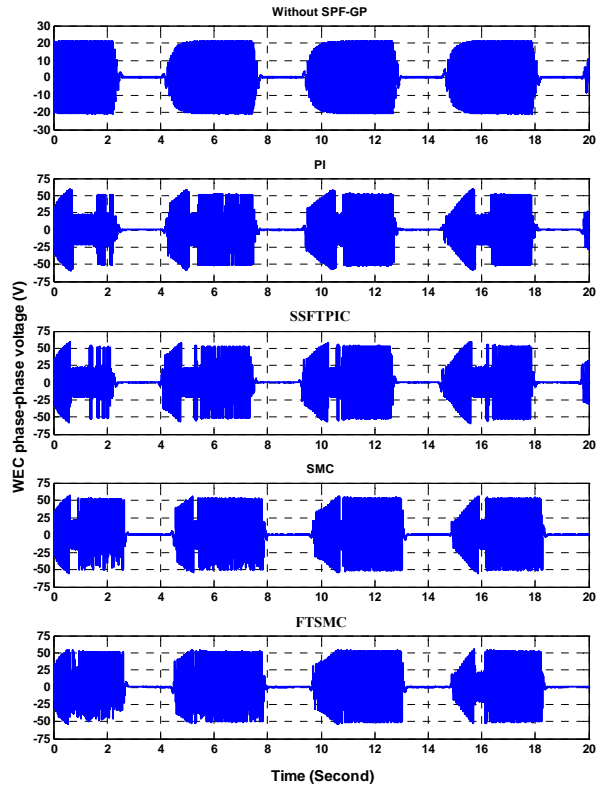


Figure 5.38. WEC voltage

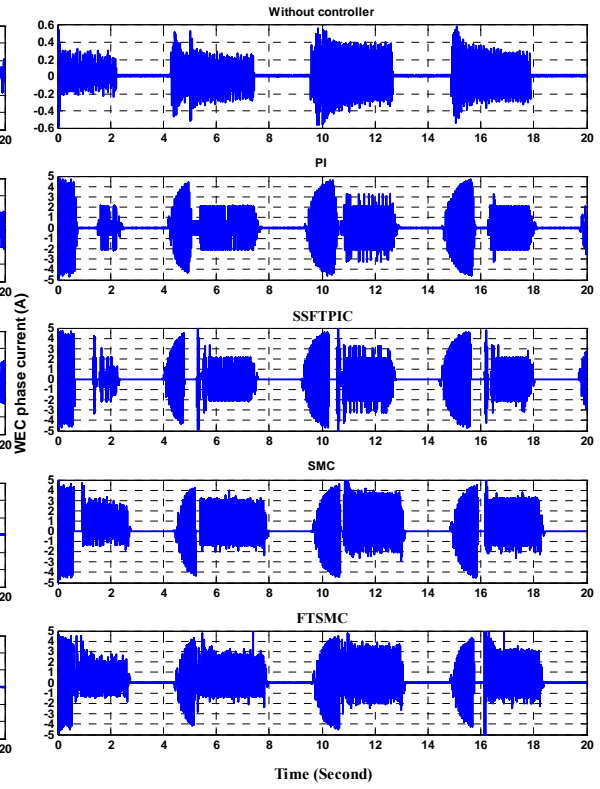


Figure 5.39. WEC current

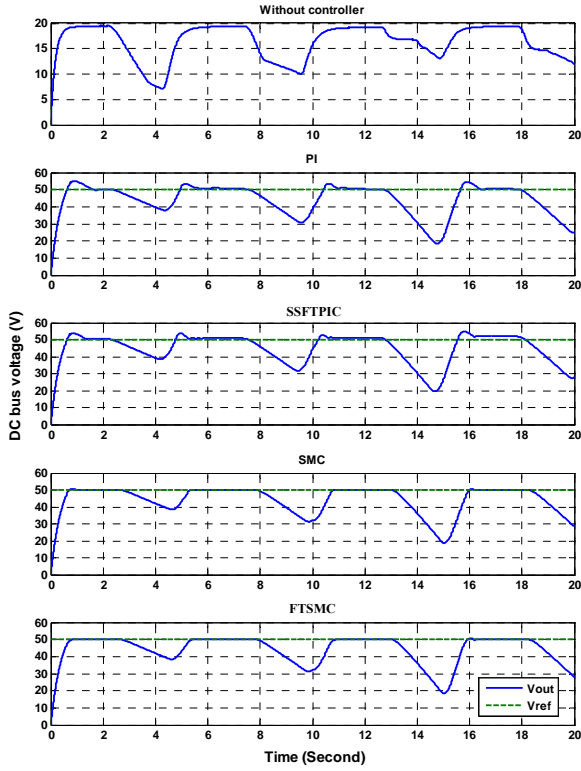


Figure 5.40. DC bus voltage (V_d)

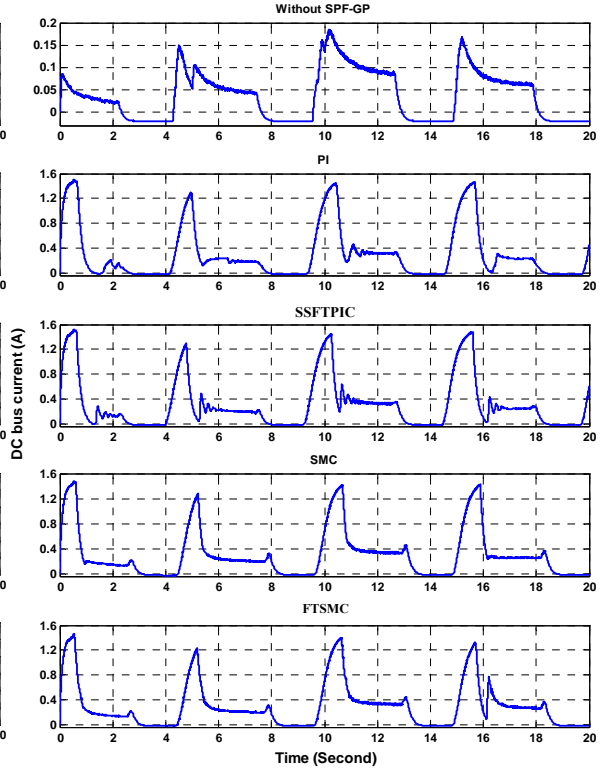


Figure 5.41. DC bus current (I_d)

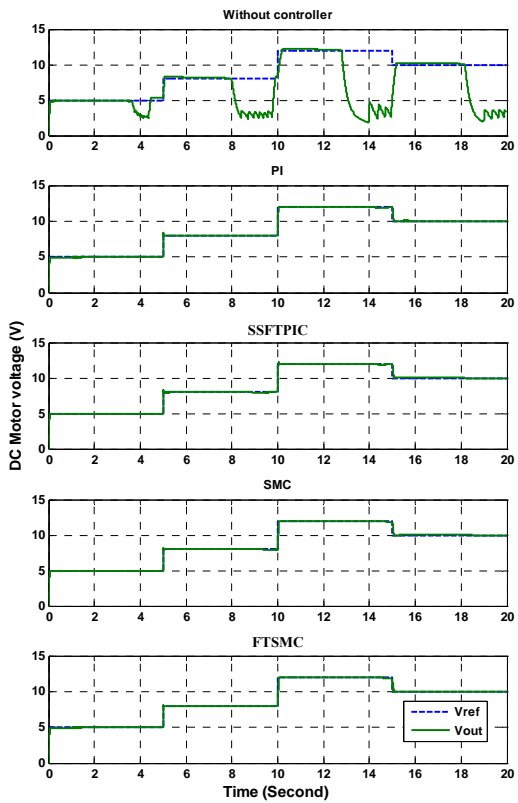


Figure 5.42. PMDC motor voltage (V_m)

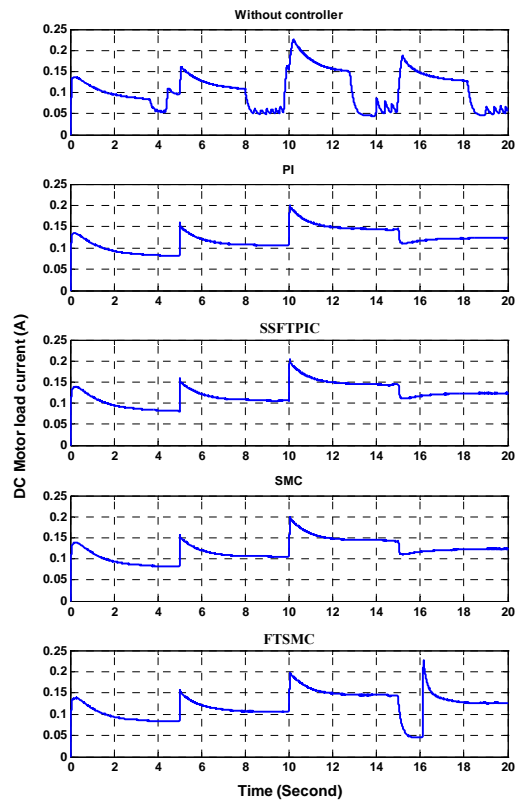


Figure 5.43. PMDC motor current (I_m)

The performance measures are determined, tabulated and graphed as given in Appendix 10 and 11, respectively:

In Scenario-I, while the Controller-A and B are PI controllers, the PMDC motor load voltage rise time is smallest, but the percentage maximum overshoot (%OS) is biggest, and also the load side bus voltage rise time is smallest and %OS is zero for all situations. On the other hand, while there is no SPF-GP system, the load voltage rise time is biggest and the %OS is equal to zero.

In Scenario-II, while the Controller-B is a SMC controller, the PMDC motor load voltage rise time is smallest and if there is no the SPF-GP system, the PMDC motor load and load side bus voltage rise times are biggest and also the load side bus voltage %OS is smallest. On the other hand, if the Controller-B is a SSFTPI controller, the load side bus voltage rise time is smallest. As the controller-B is a PI controller, the load side bus voltage %OS is biggest.

In Scenario-III, while the Controller-B is a SSFTPI controller, the PMDC motor load and load side bus voltage rise times are smallest. On the other hand, if there is no the SPF-GP system, the load voltage rise time is biggest. If the Controller-B is a FTSMC controller, the load side voltage rise time is biggest and %OS is smallest, but when the Controller-B is a PI controller, the load side voltage %OS is biggest.

5.1.2.2.4. Conclusion

In this study, novel switched power filter-green plug (SPF-GP) intelligent controllers for wave energy system are presented. A WEC system is emulated and then corresponding waveforms are observed. The power induced from WEC system is used to supply the dc load. The wave energy converter output voltage is rectified by the three phase full bridge uncontrolled rectifier and then the rectified voltage supplies the buck converter. The dc motor voltage is controlled with the buck converter for constant voltage and variable voltage trajectory references. The SPF-GP control system is proposed to provide stable voltage through the dc load. Four different control strategies (PI, SMC, FTSMC and SSFTPIC) are performed as SPF-GP controllers. The SPF-GP scheme improves the dc bus voltage so that the dc load performance is enhanced. While the dc load voltage control is realized for both constant reference and variable trajectory references with a classical PI controller, the dc bus voltage (dc load input voltage) control is carried out with different

control methods. When the reference voltage is near the dc load reference voltage, the SPF-GP control system performance decreases. On the other hand, when the reference voltage chosen is bigger, the SPF-GP control system performance is effectively improved.

The section has presented an approach to lessen discontinuity, sags and swells on voltage of WEC system. The experimental results are tabulated, graphed and show that the novel SPF-GP PI controller for wave energy converter system improves the load voltage quality. In the FTSMC, a slope of the sliding surface is dynamically changed by a fuzzy logic inference. The FTSMC solves the overshoot of a plant with PI controller in transient state and the chattering of a plant with SMC in the steady state. As shown in resulting graphs and tables, the steady state tracking error and chattering are reduced and also the overshoot is reduced. In addition to this, the FTSMC exhibits lower ISE, IAE and ITAE values compared with the PI, SSFTPIC and SMC methods. The proposed FTSMC is able to improve the system performance.

The proposed control algorithm consisting of both voltage and current dynamic error trajectory loops is able to smoothly regulate and manage the current or voltage of the DC bus voltage. A flexible FLC, whose interior parameters are easily accessible for interpretation and can be designed to be simulated in Matlab/Simulink environment for comprehensive use as a control tool. The simulation results show that the proposed fuzzy sliding mode controller has better performance than the others.

The advantages of FTSMC system in this study include: (1) constant switching frequency; (2) smaller error; (3) fast and robust voltage response; (4) smaller overshooting; (5) reduction of chattering;

The major contributions of this study are: 1) the successful development of a fuzzy logic SMC system, in which the fuzzy logic control rules are embedded into the classical SMC to improve performance; 2) the control methods designed in this study can be easily adapted to other electric drive applications; 3) the successful proposed FTSMC system, in which the rise time is decreased.

5.1.2.3. A Novel Switched Power Filter-Green Plug (SPF-GP) Scheme for Wave Energy System with Hybrid Loads

5.1.2.3.1. The Wave Energy Conversion with Hybrid Loads

The proposed wave energy conversion hybrid utilization system is shown in Figures 3.1 and 5.44 with and without the novel FACTS switched power filter-green plug (SPF-GP), respectively. The unified system comprised of a wave energy converter, rectifier, dc filter, SPF-GP system, DC-DC converter, backup battery, DC-DC chopper, DC/AC inverter, and ac and dc motors as the loads.

Due to the stochastic nature of the wave kinetic characteristics, the generated voltage show variations and extensive oscillations, which are not exactly periodic. In order to reduce these oscillations in the generated voltage with variable frequency and amplitude, the wave energy converter (WEC) output voltage is rectified and the power is collected on a load side bus. The idea of using a common load side bus is useful for collecting power from other similar WEC systems at one common bus for obtaining more power to supply larger loads. The rectified voltage is transformed and regulated by the SPF-GP converter and power is transmitted to a battery through a DC-DC buck converter.

Appropriate controllers for the SPF-GP converter, DC-DC buck converter, DC-DC chopper and DC/AC inverter are also developed in the scope of this study. The load side voltage is regulated and kept constant by means of using the SPF-GP converter controller and the DC-DC buck converter controller in the backup battery. Moreover, the PMDC motor and AC motor loads demands are assured by controlling the DC-DC chopper and the DC/AC inverter.

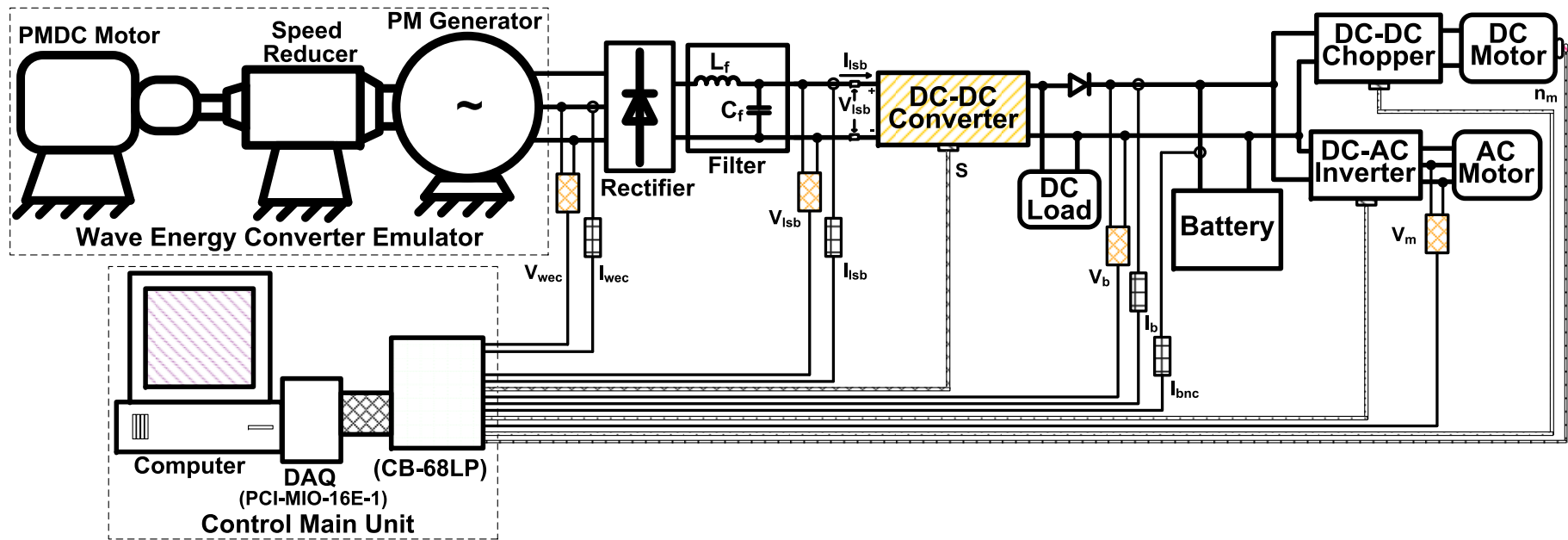


Figure 5.44. Wave Energy Conversion system without the SPF-GP

5.1.2.3.2. Controllers

In this study, there four controller systems, which are the three phase AC motor voltage control with a Self-Scaled Fuzzy Tuned PI Controller (SSFTPIC), the PMDC motor speed control with PID controller, the battery charge control with classical fuzzy logic controller (FLC), and the three-loop dynamic error driven control with PI controller for the SPF-GP system.

The ac motor electric load voltage ($V_{acmotor}$) is measured by a LV-25P voltage transducer and compared with the reference voltage ($V_{acmotor(ref)}$) to yield the voltage error signal ($e_{acmotor}$) and the dynamic change in error ($de(k)$) which are applied to a SSFTPIC to generate the required output as a shown in Figure 5.45. The output of the SSFTPIC controller is applied to PWM switching unit to generate required pulses (S_A, S_B, S_C) into the DC/AC inverter system.

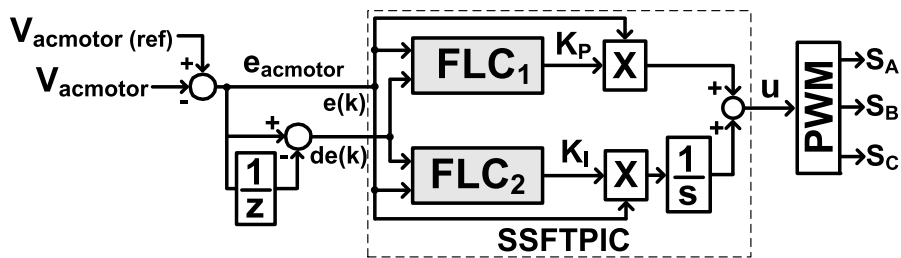


Figure 5.45. The three phase AC motor voltage control with SSFTPIC block diagram

The dc motor load speed is adjusted via regulating voltage by the DC-DC chopper with the single-loop controller shown in Figure 5.46. The speed error signal is applied to a PID controller to generate the required output control signal. The PWM switching unit generates required pulses into the DC-DC chopper circuit.

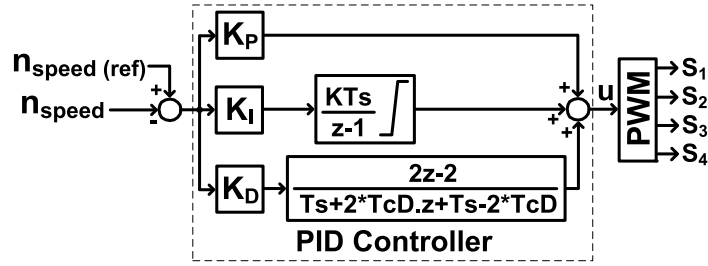


Figure 5.46. The PMDC motor speed control with PID controller block diagram

The battery voltage (V_{bat}) and the battery current (I_{bat}) are used as control variables in the battery charging control system and is shown in Figure 5.47. There are two different modes in the charging operation. The net current flowing in and out of the battery bank (I_{batnet}) is calculated to determine its SOC. While the SOC is lower than 90%, the battery will be under a constant current. On the other hand, while the SOC is higher than 90%, the battery will be charged under a constant voltage. The FLC is used to manage the battery charge system.

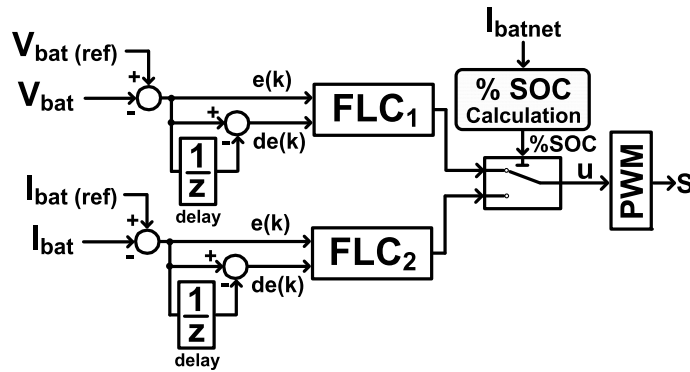


Figure 5.47. The battery charge control with FLC block diagram

The control scheme has a three-loop error driven dynamic structure as shown in Figure 5.48. The two controllers use the changes in the common load side bus current (I_{lsb}), common load side bus voltage (V_{lsb}) deviation from reference value and changes in common load side bus power (P_{lsb}) to generate a total error signal for a load side bus voltage control. The changes in load side bus current ($e_{I_{lsb}}$) and power error ($e_{P_{lsb}}$) are obtained by taking the differences, between the current and delayed real input values. The common load side bus current change, the common load side bus voltage error and the

power change multiplied by the related weighting factors ($\gamma_{I_{lsb}}, \gamma_{V_{lsb}}, \gamma_{P_{lsb}}$) and the output summation is the total control error (e_{tB}). The total error of the multi-loop structure goes into PI controller block shown in Figure 5.48.

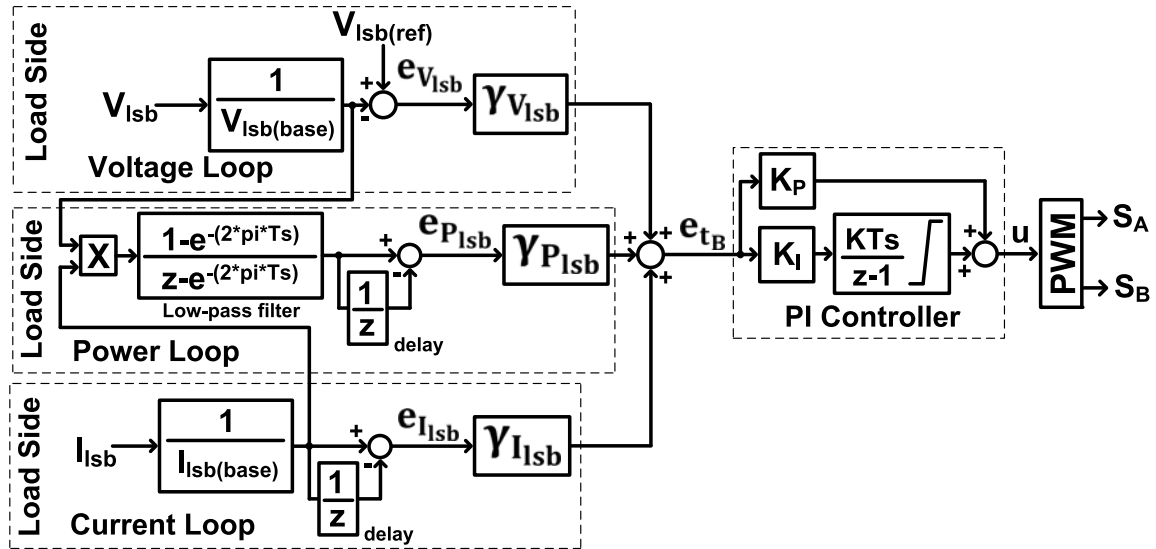


Figure 5.48. The three-loop dynamic error driven control with PI controller for the SPF-GP system diagram

5.1.2.3.3. Digital Simulation

The proposed Wave Energy Conversion hybrid system and all components including controller, filters and auxiliary devices are modeled in Matlab/Simulink and simulated for different operating conditions so the performance of the system elements can be evaluated. The operational dynamic blocks in Simulink/Simpower library are used in the modeling of the system for simulation studies as shown in Figures 5.49 and 5.50 without and with the SPF-GP, respectively. The data for the diodes, the capacitors and the other semiconductors are set to the same values given in the components datasheets. The simulation system parameters are given in Appendix 7.

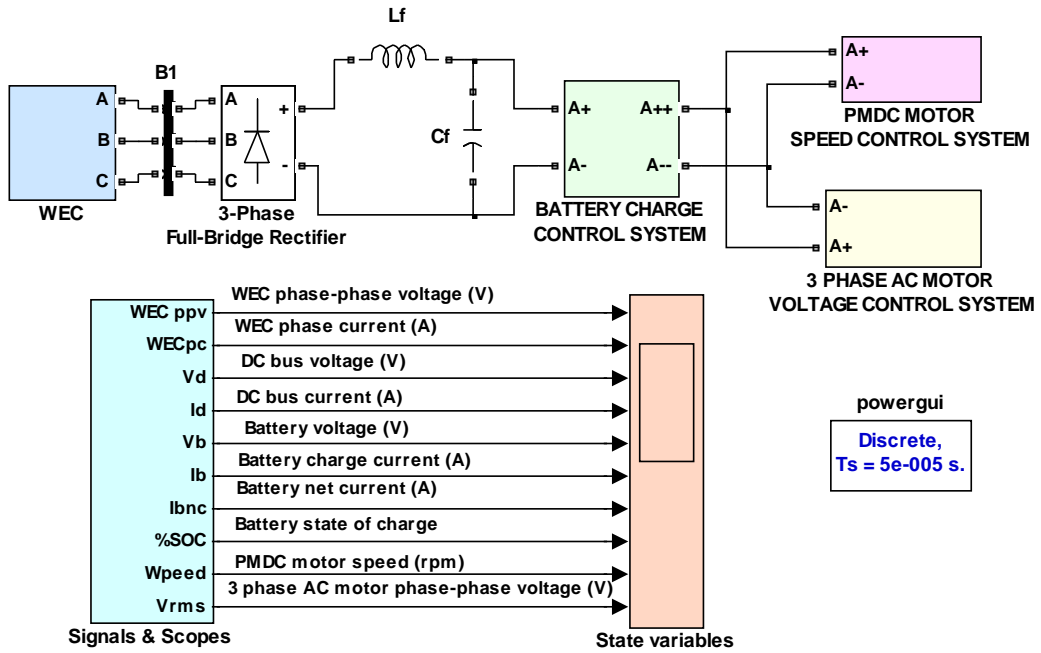


Figure 5.49. The Simulink operational block diagram of the system without the FACTS (SPF-GP)

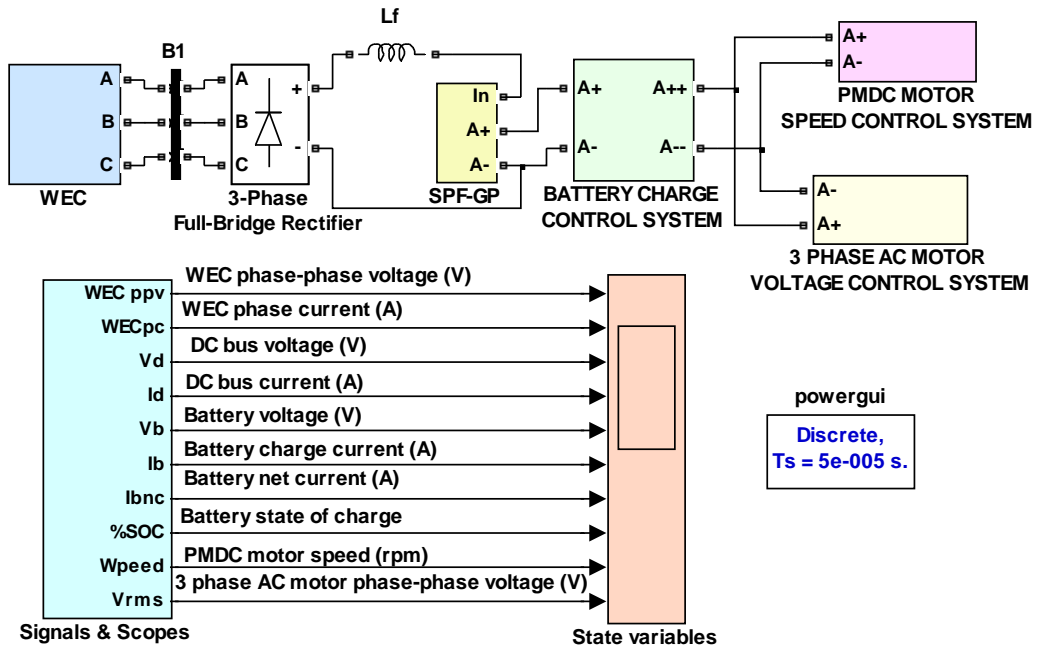


Figure 5.50. The Simulink dynamic block model of the system with the FACTS (SPF-GP)

5.1.2.3.4. Experimental Implementation

The real time implementation of the unified system is done using the RTWT available in Matlab/Simulink toolbox, which provides an opportunity to create and control real time executable commands for real time applications through Matlab/Simulink. A PCI-6070E DAQ card is used in this study in order to establish communication on data acquisition between the real time part of the study and the computer, which contains the digital modeling of the SPF-GP, the DC-DC converter, DC-DC chopper, DC/AC inverter and the controllers used in the complete system. The main control units of the system without SPF-GP are implemented through Matlab/Simulink as shown in Figure 5.51.

Since an individual driver circuit and an additional control algorithm are required for switching the semiconductors in the rectifier, a passive rectifier is used to reduce the cost and controller complexity while increasing the system robustness. The output voltage wave energy converter emulator is rectified by a three phase full bridge uncontrolled rectifier and then applied to the DC-DC buck converter, which is controlled for the battery charging. The DC-DC chopper and DC-AC inverter are used to control DC and AC loads demands, respectively. The system with the novel FACTS SPF-GP control main unit is modeled in the Matlab/Simulink software as shown in Figure 5.52.

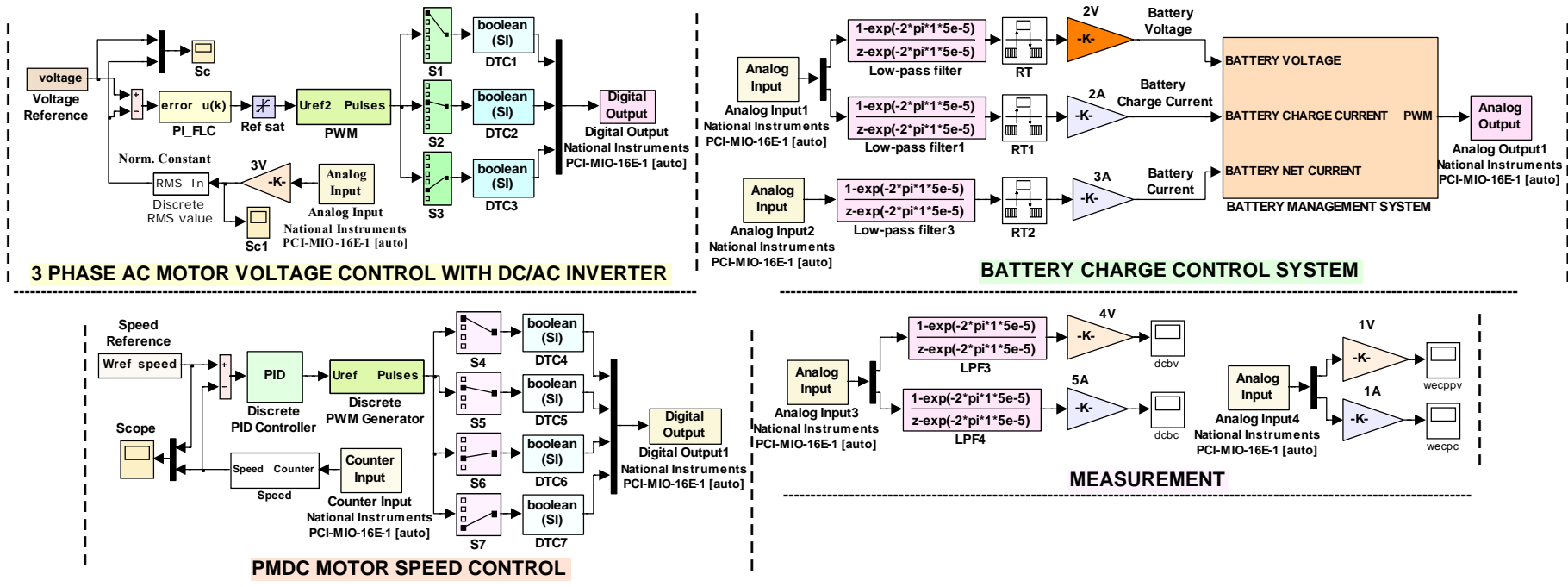


Figure 5.51. The main control stages of the test system without the FACTS (SPF-GP)

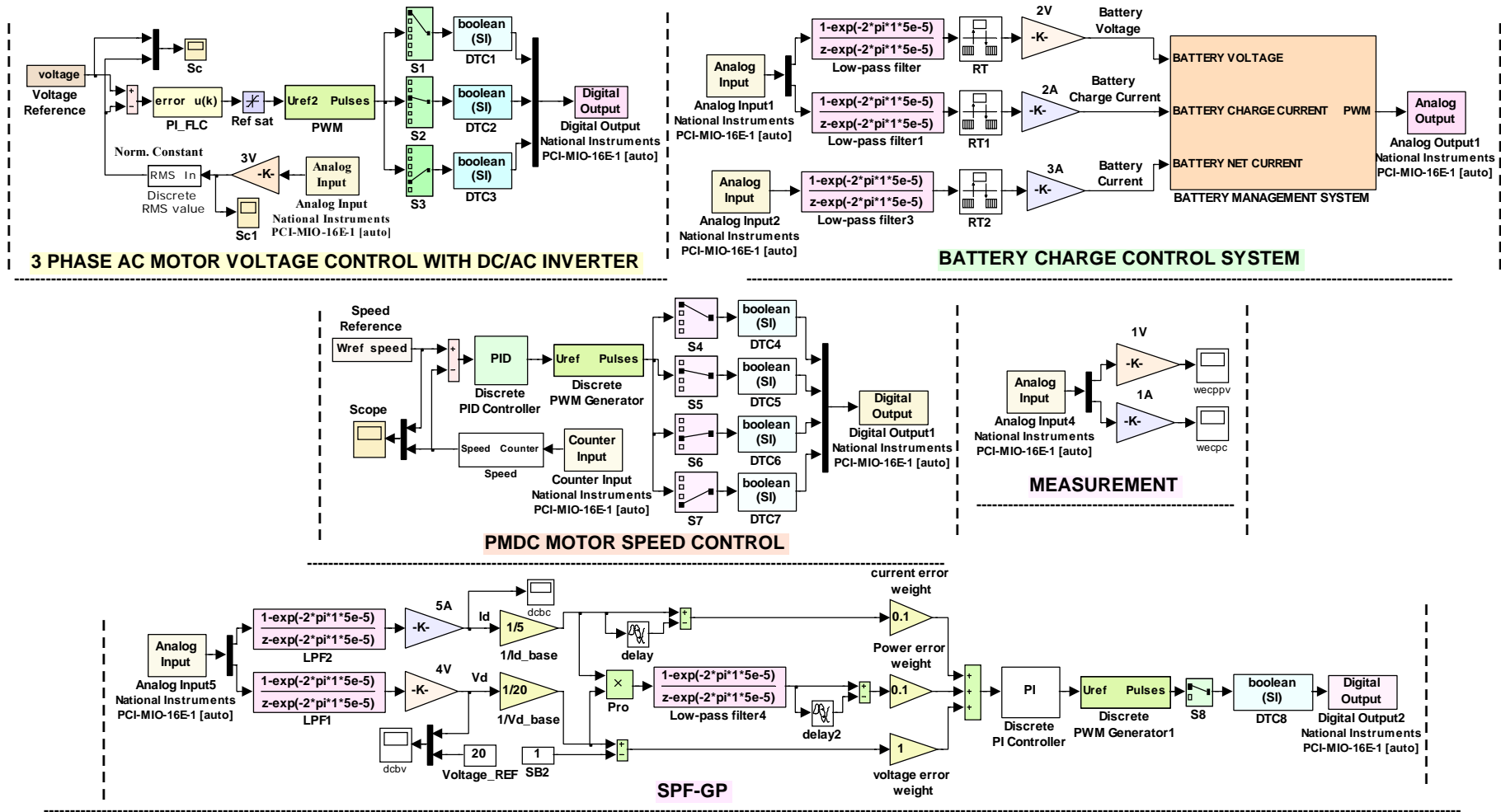


Figure 5.52. The main control stages of the test system with the FACTS (SPF-GP)

5.1.2.3.5. Digital Simulation and Experimental Results

The experimental setup shown in Figure 4.1 consists of the data acquisition system with four Hall Effect Current Sensors (LEM, LA-25NP), four Hall Effect Voltage Sensors (LEM, LV25-P), an encoder and an DAQ card (National Instruments PCI-6070E). The computational implementation part of the experimental setup runs in Matlab/Simulink environment, through the data acquisition. The parameters of the system for both simulation and experimental tests are given in Appendix 7.

In order to validate the simulation models of the proposed filters and control algorithms, an experimental set up has been established as shown in Figure 4.1. The experimental and digital simulation tests are done under four different cases tabulated in Table 5.3 for observing the systems under different operating conditions.

For different operating conditions, if the wave period is increased, the generated voltage waveform includes less discontinuity. On the other hand, if the period is decreased, voltage sags and swells become more, and the system performance is lowered. The wave period without the SPF-GP scheme is taken bigger than with the SPF-GP scheme to indicate the effectiveness of the SPF-GP control system. The system with the SPF-GP scheme is tested under more difficult circumstances.

Table 5.3. The three different system scenarios for the real time experimental studies

	Case I	Case II	Case III	Case IV
PMDC motor speed trajectory tracking reference ($w_{m(ref)}$)	Constant	Constant	Variable	Variable
3 phase AC motor voltage trajectory tracking reference ($V_{m(ref)}$)	Constant	Constant	Variable	Variable
Load side bus reference voltage ($V_{d(ref)}$)	20V	20V	20V	20V
SPF-GP model	Without	With	Without	With

Error energy based performance measures such as integral square error (ISE), integral of the absolute error (IAE) and integral of time multiplied by absolute error (ITAE) are used to compare the performance of the controllers in terms of parameter optimization. To realize a satisfying comparison between the controllers, the IAE and

ITAE are used to get information about operational characteristics of the controllers during transient and steady-state operation. Since the information about the error energy based performance indices can be found in any Optimal Control book, no details are given here.

First of all, the system performance is observed for constant PMDC motor load speed and AC motor load voltage trajectory tracking references with and without the SPF-GP model for a load side bus reference voltage of 20V. The results belonging to Case I and II are shown in Figures 5.53-5.62. Experimental and Simulation results without and with SPF-GP are depicted in the same figure for providing a better comparison and show the effect of the SPF-GP.

The peak values of the phase to phase voltage of WEC system shown in Figure 5.53 are over 20 Volts with SPF-GP while they are below 20 Volts without the SPF-GP. The peak values of the current waveform shown in Figure 5.54 are higher when the SPF-GP is used when they are compared with the results obtained without the SPF-GP since the increased voltage magnitude causes higher currents. While the SPF-GP is not used, the load side bus voltage shown in Figure 5.55 has higher drops for each starting instant of the wave cycles. The use of SPF-GP results in reduction of drop voltage on the load side bus while keeping a constant load side bus voltage at 20 Volts. Figure 5.56 shows the load side bus current variation with and without SPF-GP.

The battery voltage and charge current waveforms are shown in Figures 5.57 and 5.58, respectively. Since the SOC shown in Figure 5.60 is lower than 90%, the battery is under a constant current ($I_{bat(ref)} = 0.3A$). If the SOC was higher than 90%, the battery would be charged under constant voltage ($V_{bat(ref)} = 13.56V$). The battery charge current peak values are higher in Case II than Case I as shown in Figure 5.58. The battery SOC shown in Figure 5.60 decreases by the reason of that battery net current (I_{bnc}) values are negative as a shown in Figure 5.59. The PMDC motor load speed and AC motor load voltage waveforms are shown in Figures 5.61 and 5.62, respectively. The system performances for Case I and II have been determined by the means of ISE, IAE and ITAE as given in Appendix 12. The improvement is observed in the system performance.

The system performance for the Cases III and IV observed for variable PMDC motor load speed trajectory tracking reference and AC motor load voltage trajectory tracking reference with and without the SPF-GP model for a load side bus reference voltage of 20V are given in Figures 5.63-5.72.

Stepwise changes are given to the loads speed and voltage to analyze the performance of the SPF-GP and controller if the applied speed and voltage of the load changes due to variable power or torque control requirements. The effects of the SPF-GP on voltage and current are given in Figures 5.63 and 5.64, while the peak values of the WEC voltages are below 20 volts without SPF-GP, they are above 20 volts with the SPF-GP. Both voltages and the currents of the WEC show similar effects with the SPF-GP here as in the Cases I and II. The voltage of the WEC is kept constant when the reference speed applied to the PMDC motor and reference voltage adapted into the AC motor have changes as shown in Figures 5.71 and 5.72, respectively. Since the SOC shown in Figure 5.70 is lower than 90%, the battery is under a bulk charge mode (constant current).

The system performances have been determined by the means of ISE, IAE and ITAE as given in Appendix 12. The improvement is observed in the system performance.

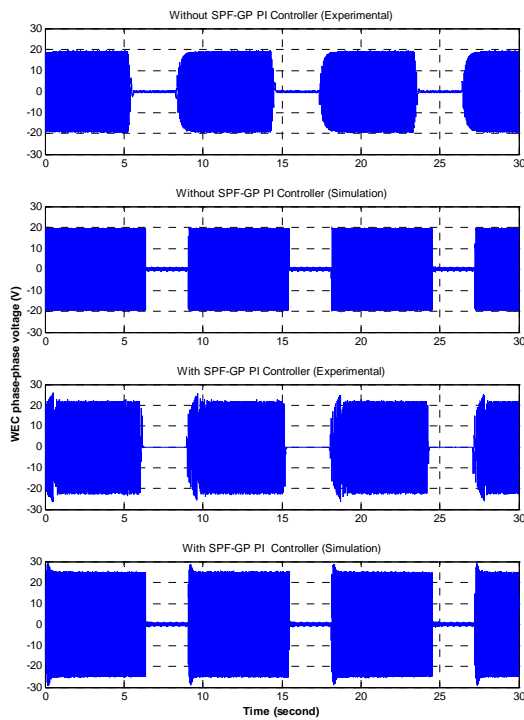


Figure 5.53. WEC phase-phase voltage

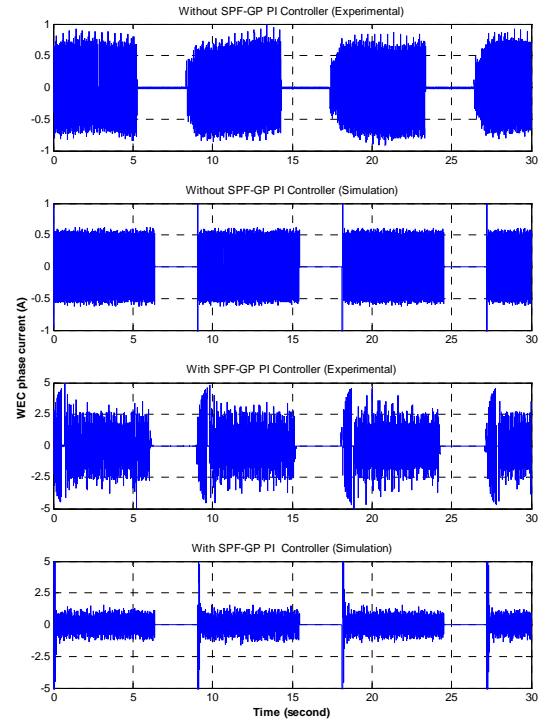


Figure 5.54. WEC phase current

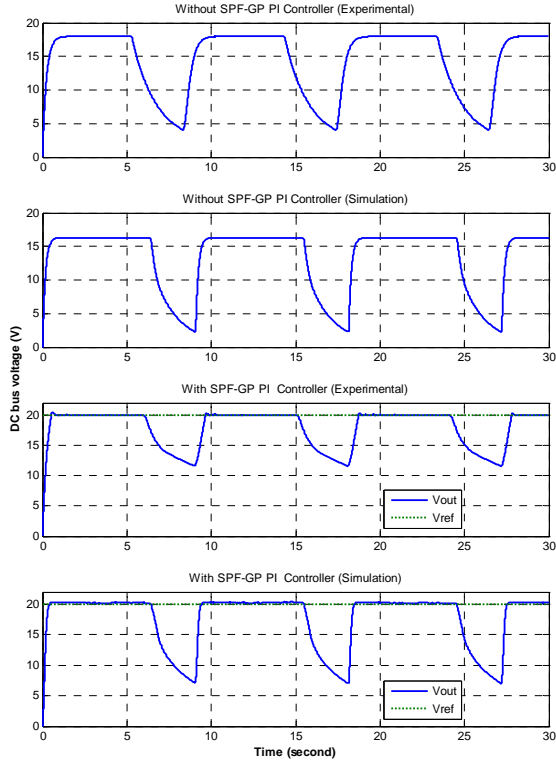


Figure 5.55. Load side bus voltage, V_{lsb}

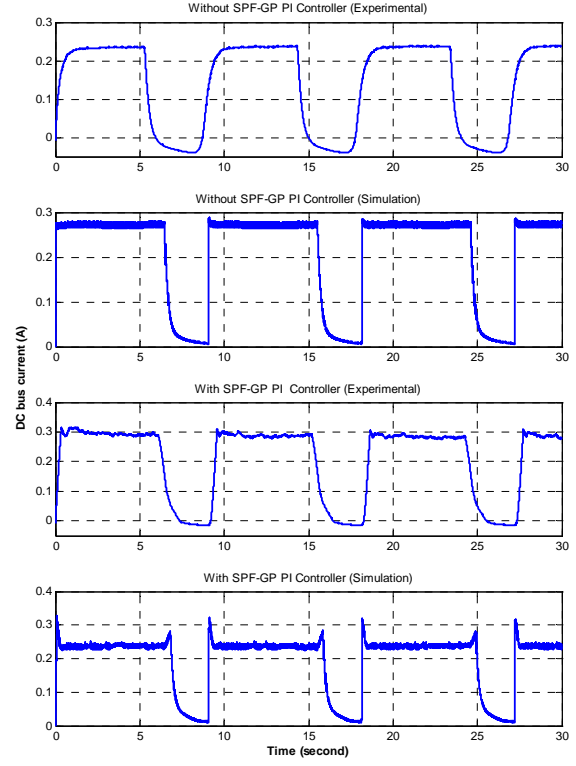


Figure 5.56. Load side bus current, I_{lsb}

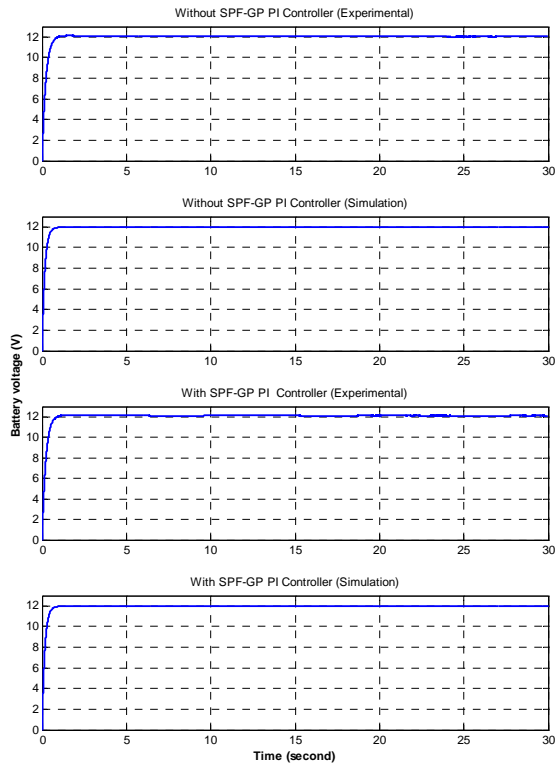


Figure 5.57. Battery voltage, V_b

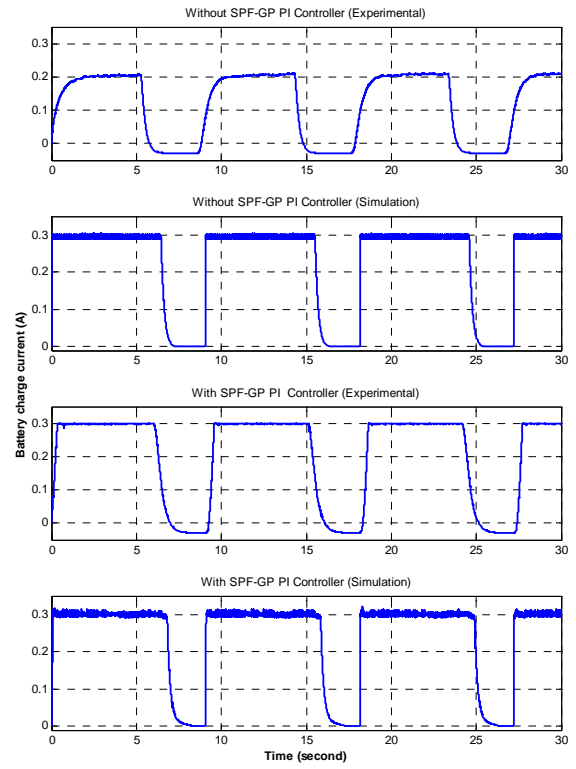


Figure 5.58. Battery charge current, I_b

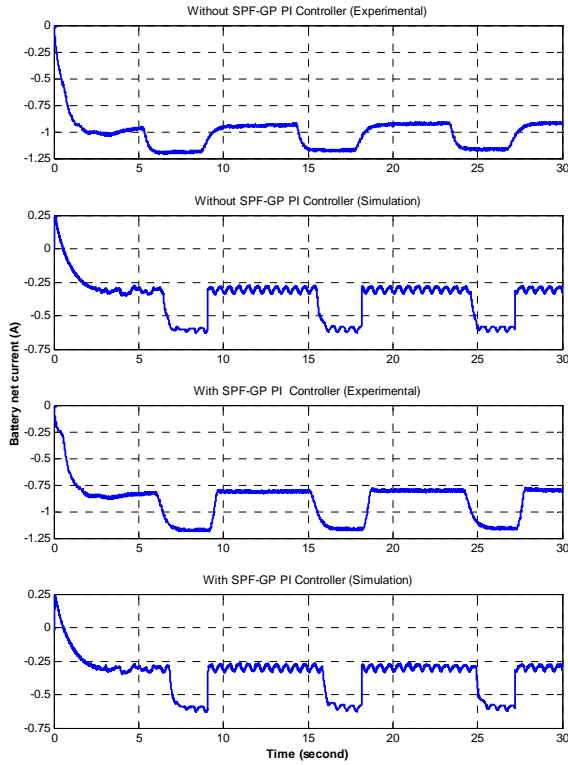


Figure 5.59. Battery net current, I_{bnc}

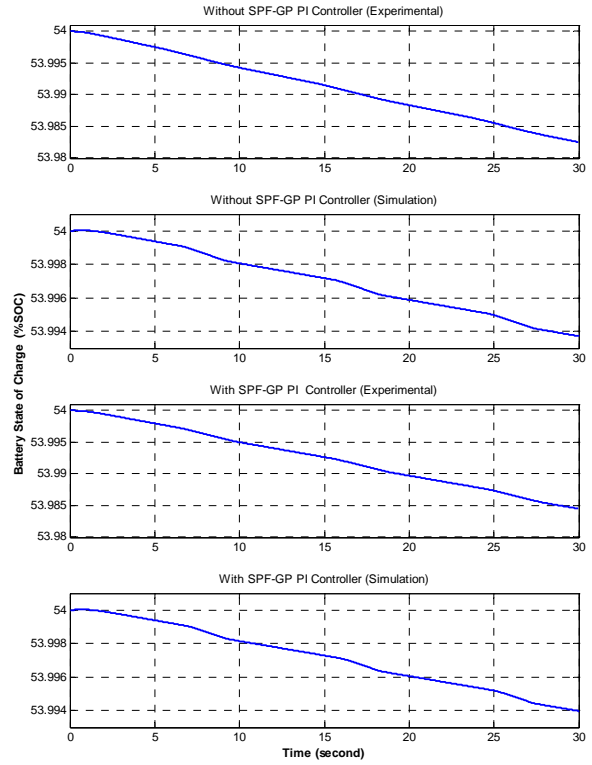


Figure 5.60. Battery SOC

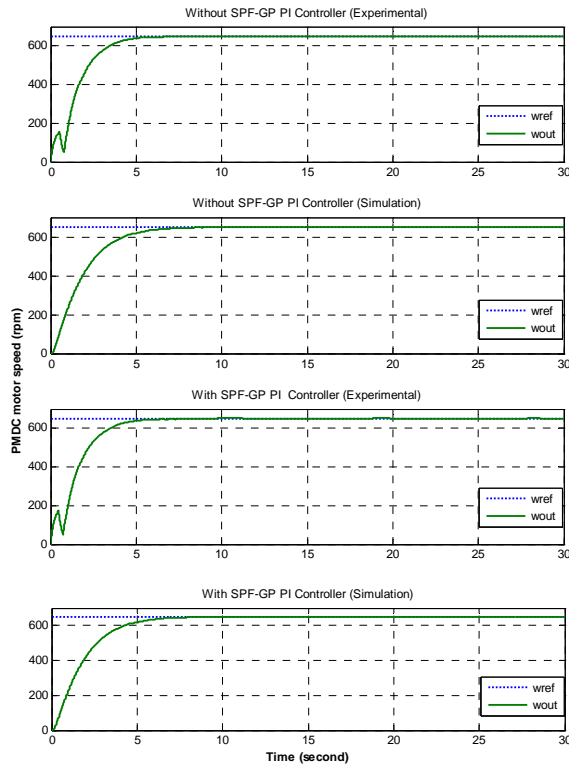


Figure 5.61. PMDC motor speed

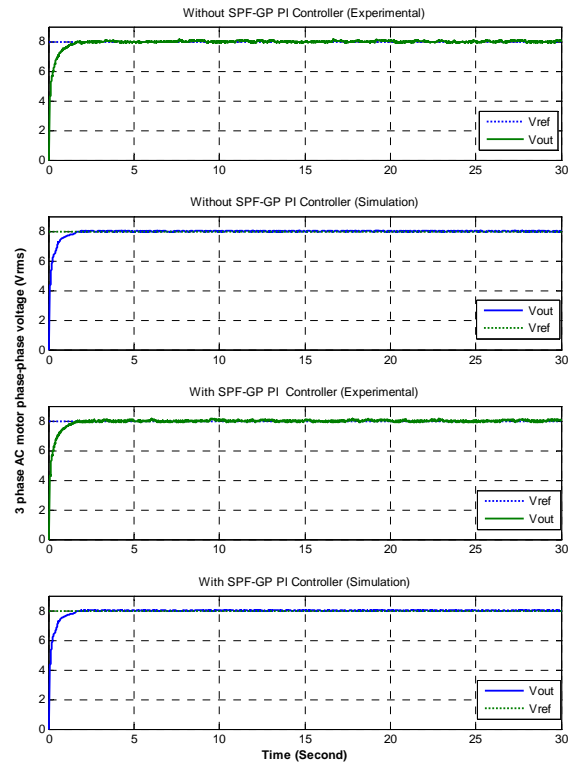


Figure 5.62. 3 phase AC motor phase-phase voltage (rms)

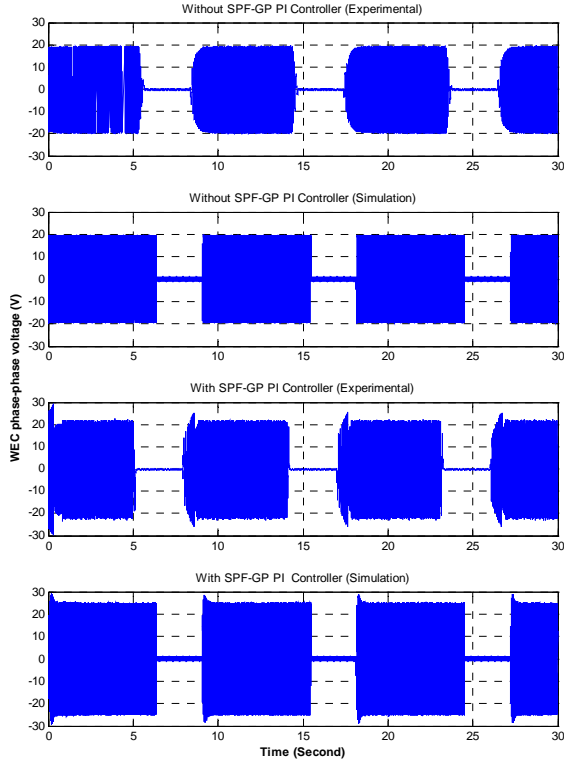


Figure 5.63. WEC phase-phase voltage

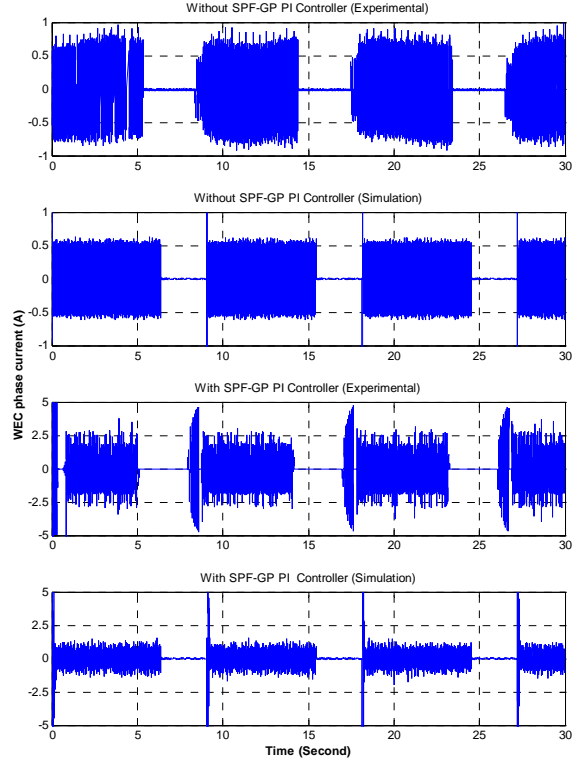


Figure 5.64. WEC phase current

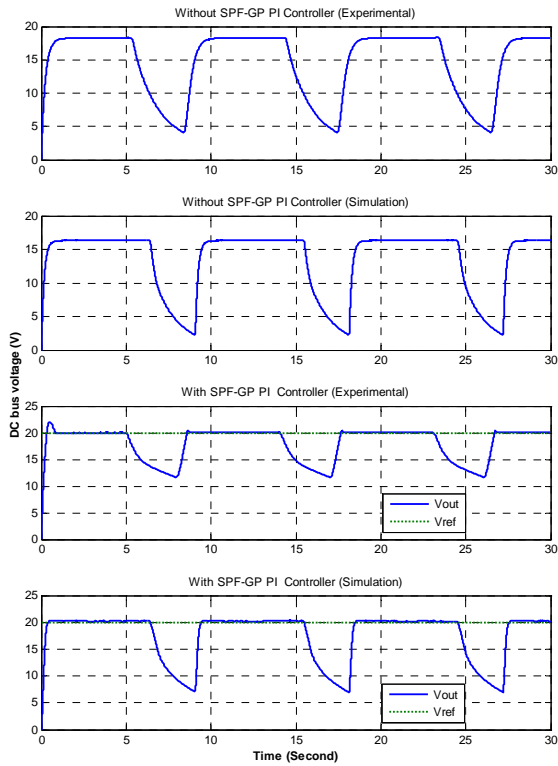


Figure 5.65. Load side bus voltage, V_{1sb}

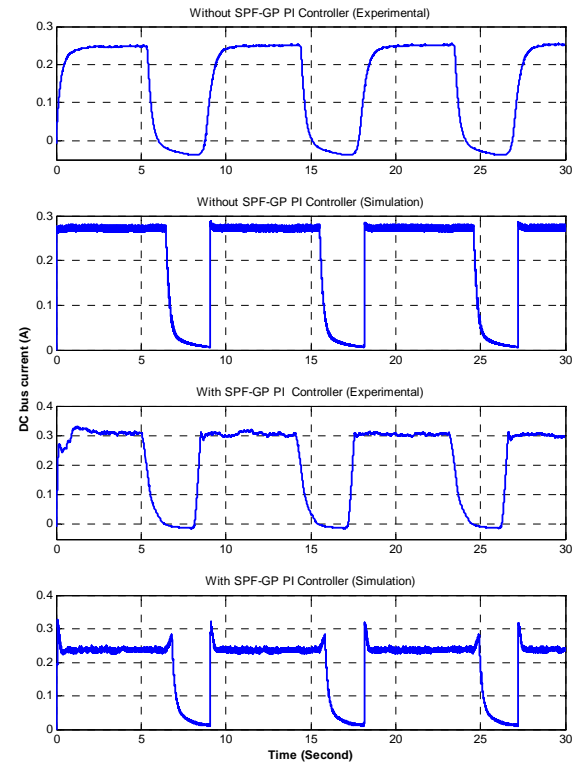


Figure 5.66. Load side bus current, I_{1sb}

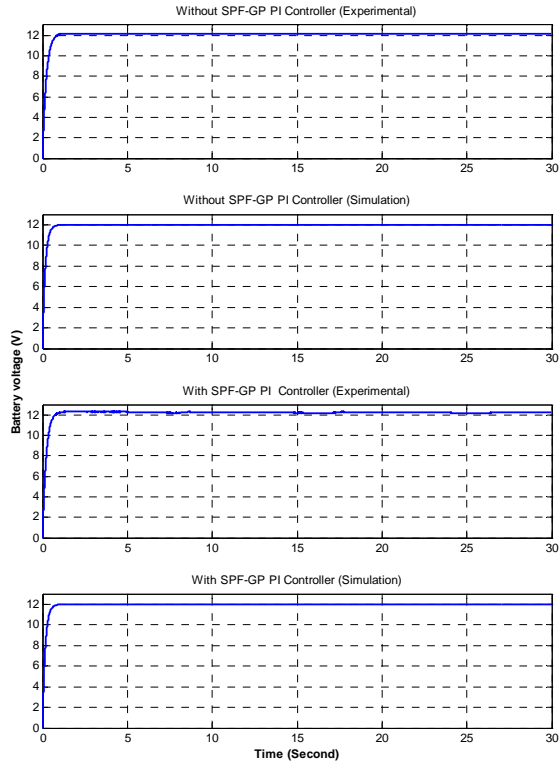


Figure 5.67. Battery voltage, V_b

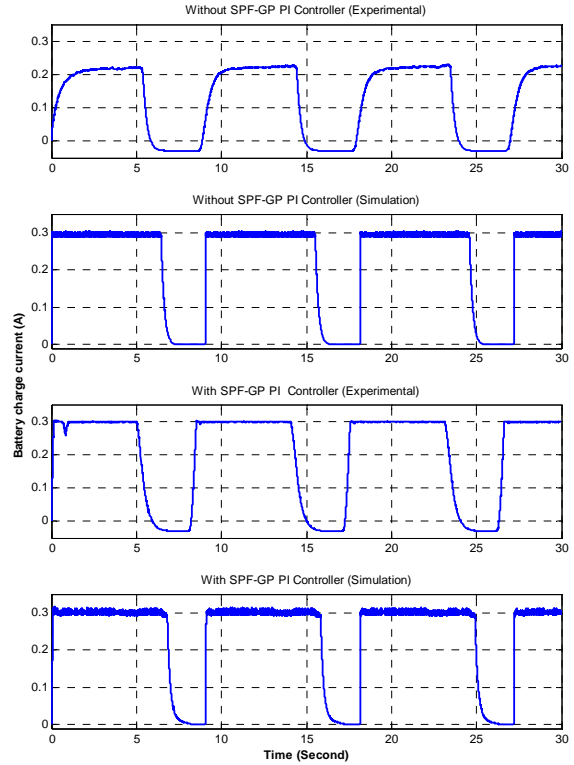


Figure 5.68. Battery charge current, I_b

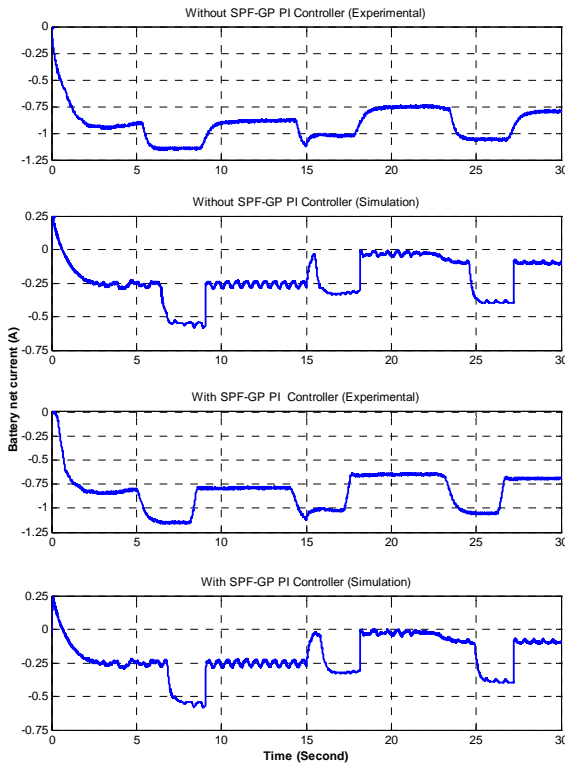


Figure 5.69. Battery net current, I_{bnc}

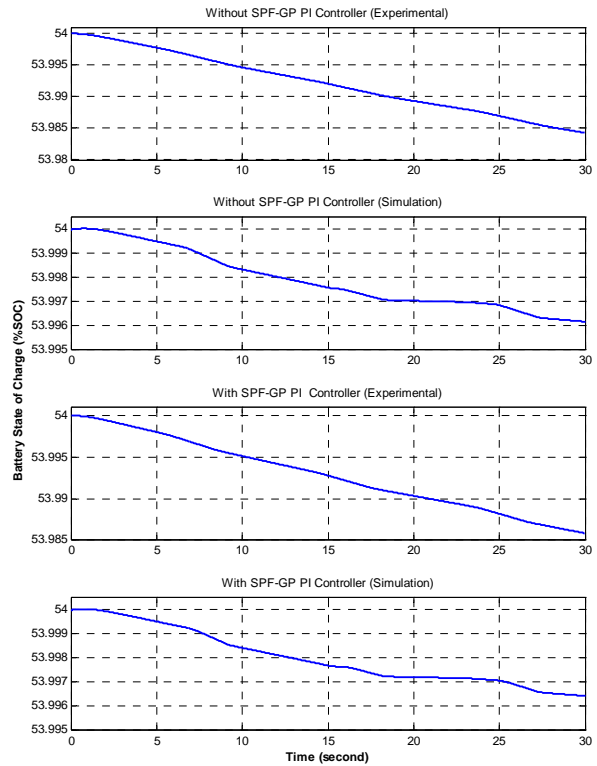


Figure 5.70. Battery SOC

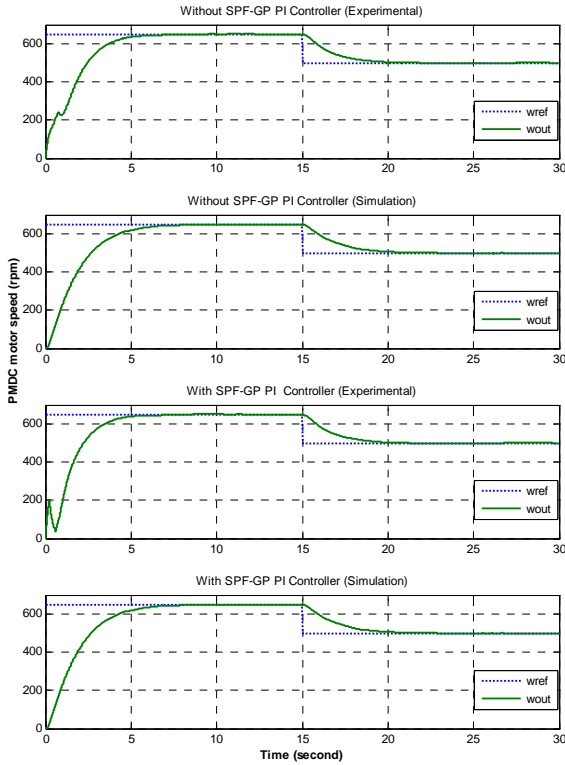


Figure 5.71. PMDC motor speed

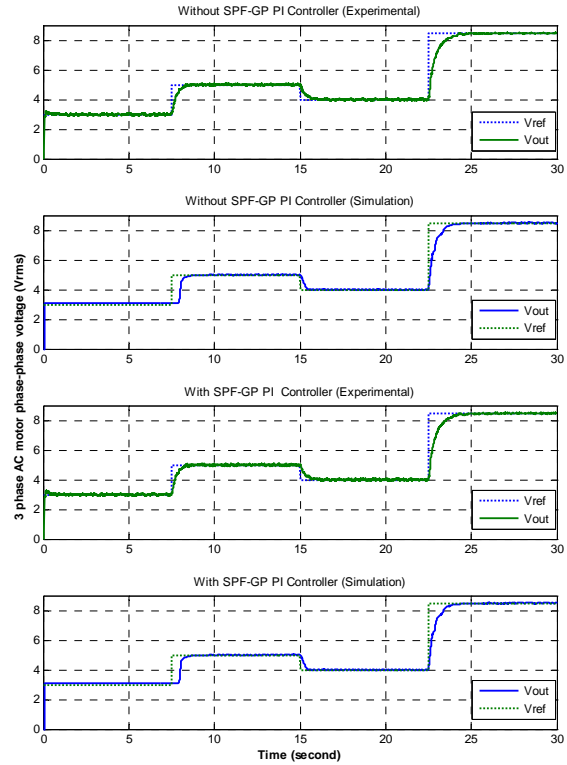


Figure 5.72. 3 phase AC motor phase-phase voltage (rms)

5.1.2.3.6. Conclusion

A novel FACTS based switched power filter-green plug (SPF-GP) scheme regulated by a tri-loop dynamic error driven control algorithm is used to stabilize the wave energy system as a standalone source with backup battery for both DC and AC loads. In order to control and compensate the power flow from wave source to electrical load, a PI controller is developed and used to generate the switching signals for the SPF-GP device, which acts as the power conditioner and stabilization device between the wave source and the load and also to regulate, store the load side bus energy into the battery and transfer power to the loads, an adaptive fuzzy logic controller is used to produce the signals for the DC-DC converter.

Interfacing devices are necessary to ensure power balance and voltage stabilization between the WEC system and the electrical loads since the magnitude, speed and cycle of the sea wave are not constant and unpredictable.

The generated AC voltage from WEC system is rectified and applied to SPF-GP system. The SPF-GP device is controlled for constant DC bus voltage whether the load

demands are constant or variable. The PI controlled SPF-GP device is fully utilized to provide a stable voltage regulation at the common load side bus. It is shown that the proposed controller used in the SPF-GP scheme improved the load side bus voltage stabilization so that energy utilization is enhanced. The dynamic error driven scheme uses the load side bus voltage error as the main regulating loop along with the dynamic current and power deviations as the two supplementary/auxiliary loops. The use of this novel control strategy enables the regulating system to react to any changes in load power and load current to generate the required control action for a constant load side bus voltage. The SPF-GP scheme regulated by the time-descaled dynamic error driven loops and PI controller is the main contribution of this study providing the required load side bus voltage stabilization.

One additional study, which is considered here, is the elimination of dc inrush current ripples that occur at the beginning of the each sea-wave cycle. This problem is solved using a backup battery storage such that the required load demand is managed effectively from the batteries during the beginning of each wave cycle. The magnitude of the DC voltage fluctuations is lessened.

The laboratory prototype experiments are done for four cases, which are constant load voltage and speed references tracking with and without SPF-GP scheme and variable PMDC motor speed and AC motor voltage trajectories with and without the SPF-GP scheme. It can be concluded from the comparison of the results from all the test cases that the application of the PI controlled SPF-GP scheme and the multi loop error driven PI control approach provides a mean constant load side bus voltage utilization for both constant and variable load speed and voltage trajectory test cases.

5.2. Summary

The novel FACTS SPF-GP systems are utilized to provide a stable voltage regulation at the common load side bus for the loads since interfacing devices between the WEC system and the electrical loads are required to have a power balance and a steady voltage magnitude. A properly controlled SPF-GP scheme improves the load side bus voltage so that the dc load performance is enhanced. A three loop dynamic error driven controller is used to regulate the novel FACTS SPF-GP scheme. The effects of the proposed scheme and the controller are examined using the developed simulation model of the overall

system and compared with those obtained from the experimental setup of the same system for model validation.

Both digital simulation and laboratory prototype experiments are done for variable cases. It can be concluded from the comparison of the results from all the cases that the application of the FACTS novel SPF-GP scheme associated with the three loops error driven control approach provide a constant load side bus voltage for both constant and variable load voltage trajectory cases.

One additional study, which is not considered here, may be the elimination of the current ripples that occur at the beginning of the each wave cycle. Actually this problem can easily be solved using backup batteries such that the required load power is managed to be supplied from the batteries during the beginning of each wave cycle. Since the worst case scenario is considered here, the positive support of the backup batteries are not considered at the first step and then the battery is connected into the power system to lessen voltage fluctuations.

6. CONCLUSIONS AND FUTURE WORKS

6.1. Conclusions

A novel FACTS based switched power filter-green plug (SPF-GP) scheme and effective novel control strategies are presented in this work to reduce the interfacing power quality problems and improve the energy utilization of WEC systems.

Emulator model of the wave energy conversion system is carried out in two different ways; one is a Computer Based Wave Energy Conversion Emulator (CBWECE) and the other one is Machine Based Wave Energy Conversion Emulator (MBWECE).

A wave energy converter system, a novel Switched Modulated Power Filter-Green Plug (SPF-GP) Scheme adapted into a wave energy converter system, loads exhibiting variable characteristics, multi loop error drivers, and intelligent controllers were modeled and simulated successfully using Matlab/Simulink.

The experimental prototype models of the wave energy converter system, the proposed SPF-GP system, multi loop error drivers, and the controllers were set up and tested experimentally.

Both the simulation and the experiments were done for different scenarios and results of the same operating conditions from both platforms are compared for model validation as well as system performances on load side voltage and load variations on source side. An investigation of reducing voltage sags and swells is also carried out. It can be concluded from the comparison of the results from all the cases that the application of the FACTS novel SPF-GP scheme associated with the novel multi loop error driven intelligent control approach provided a constant DC bus voltage for both constant and variable load voltage trajectory cases.

The experiments also provided several valuable insights into the operation of the proposed SPF-GP system and the estimation of the common bus system efficiency upon which future work can be built.

6.2. Future Work

The performance of the prototype could be enhanced by improving the controllers. The DAQ card is versatile and has many advantages and benefits. But, the DAQ card performance can be insufficient in power switching parts such as a DC-DC chopper, DC-DC converter and DC/AC inverter. An increase in speed can be achieved by using an FPGA to perform the bulk of the operation. Such an integrated circuit/architecture approach could significantly improve the performance of the test system.

Finally, the wave energy converter system was only tested in certain modes: There are power flows only from wave source to electrical loads, only from energy storage to electrical loads and from wave source to energy storage and electrical loads. These modes involve stand-alone power system frameworks. The alternative power system would be argued for a grid connected mode. Bidirectional power electronic topologies would be improved and adapted into the system to transfer power in either direction. Effective control strategies would need to be studied to ensure power balance and voltage stabilization, and also manage power flow direction.

Validation of the model in irregular wave conditions would be required. Physical experiments for a wave energy converter system model should be carried out. The results of such testing would be used to approve the simulation model.

The same novel SPF-GP would be utilized with other AC-DC Interface Schemes using wind-photovoltaics, wave-microhydro and hybrid green energy utilization systems. Other control strategies based using soft-computing Artificial-Intelligent Controllers would be utilized.

7. REFERENCES

1. Nelson, V., Introduction to Renewable Energy, CRC Press, 2011.
2. World Energy Outlook 2011: Executive Summary, International Energy Agency, 9 November 2011.
3. Jones, R.H., World Energy Outlook 2011 Presentation, Oslo, 14 November 2011.
4. Aswathanarayana, U., Harikrishnan, T. and Sahini, K.M.T., Green Energy Technology, Economics and Policy, CRC Press, 2010.
5. Renewables 2011 Global Status Report, REN21, 2011.
6. Khaligh, A. and Onar, O.C., Energy Harvesting: Solar, Wind, and Ocean Energy Conversion Systems, CRC Press, 2010.
7. Ghosh, T.K. and Prelas, M.A., Energy Resources and Systems: Volume 2: Renewable Resources, Springer, 2011.
8. Petrova, M.A.S., Determinants of Public Opinion on Renewable Energy: The Case of Wave Energy Development in Oregon, Phd Thesis, Oregon State University, 2011.
9. Cruz, J., Ocean Wave Energy: Current Status and Future Perspectives, Springer, Berlin, 2008.
10. Falnes, J., A Review of Wave-Energy Extraction, Marine Structures, 20 (2007) 185-201.
11. Drew, B., Plummer, A.R. and Sahinkaya, M.N., A Review of Wave Energy Converter Technology, Journal Proceedings of the Institution of Mechanical Engineers, Part A: Journal of Power and Energy, 223, 8 (2009) 887-902.
12. Falco, A.F.O., Wave Energy Utilization: A Review of the Technologies, Renewable and Sustainable Energy Reviews, 14 (2010) 899-918.
13. Lindroth, S. and Leijon, M., Offshore Wave Power Measurements-A Review, Renewable and Sustainable Energy Reviews, 15 (2011) 4274-4285.
14. Melo, A.B. and Bhuyan, G., 2008 Annual Report, International Energy Agency Implementing Agreement on Ocean Energy Systems (IEA-OES), 2009.
15. The Carbon Trust, Marine Energy Challenge, Oscillating Water Column Wave Energy Converter Evaluation Report, 2005.

16. Fodorean, D., Szabo, L. and Miraoui, A., Generator Solutions for Stand Alone Pico-Electric Power Plants, IEEE International Electric Machines and Drives Conference, 2009, IEMDC'09, 434-438.
17. Pop, E., Leba, M., Barbu, C.T. and Pop, M., Modeling, Simulation and Control of Pico-hydro Power Plant, 4th WSEAS/IASME International Conference on Dynamical Systems and Control (CONTROL'08), Corfu, Greece, 10 October 26-28, 2008, 103-108.
18. Alcom, R.G. and Beattie, W.C., Power Quality Assessment from a Wave-Power Station, 16th International Conference and Exhibition on Electricity Distribution, 2001, 238-238.
19. ISLAY LIMPET Wave Power Plant: Publishable Report 1 November 1998 to 30 April 2002, The Queen's University of Belfast.
20. Whittaker, T.J.T., Beattie, W., Folley, M., Boake, C., Wright, A., Osterried, M. and Heath, T., The Limpet Wave Power Project-The First Years of Operation, Renewable Energy, Queen's University Belfast, 2003.
21. Suzuki, M., Arakawa, C., Takahashi, S., Performance of Wave Power Generating System Installed in Breakwater at Sakata Port in Japan, Proc. of ISOPE, 2004, 202–209.
22. Enciso, Y.T., Ortubia, I., Aguilera, L.I.L. and Marques, J., Mutriku Wave Power Plant: From the Thinking out to the Reality, Proceedings of the 8th European Wave and Tidal Energy Conference, Uppsala, Sweden, 2009, 319-329.
23. Osawa, H. and Miyazaki, T., Wave-PV Hybrid Generation System Carried in The Offshore Floating Type Wave Power Device "Mighty Whale", IEEE Techno-Ocean'04, 4 (2004) 1860-1866.
24. Osawa, H., Washio, Y, Ogata, T. and Tsuritani, Y., The Offshore Floating Type Wave Power Device "Mighty Whale" Open Sea Tests: Performance of The Prototype, Proceedings of The Twelfth (2002) International Offshore and Polar Engineering Conference, Kitakyushu, Japan, May 26-31, 2002, 595-600.
25. Wave-Energy Buoy Wins Grant, Professional Engineering, 19 September 2007, 9.
26. Bradley, C. and Venezia, W., Spar Buoy Platform for Water Wave, Turbulence and Underwater Electric Field Sensors, Proceedings of the IEEE/OES/CWTM Tenth Working Conference on Current Measurement Technology, 2010, 190-197.
27. Wave Power, Modern Power Systems, December 2007, 44-47.
28. Oceanlinx Technical Facts Sheet, Oceanlinx, 2009, 1-4.
29. Blue Power: Turning Tides into Electricity, Environmental Health Perspectives, 115, 12 (2007) A590-A593.

30. Dunnett, D. and Wallace, J.S., Electricity Generation from Wave Power in Canada, Renewable Energy, 34 (2009) 179-195.
31. Weinstein, A., Fredrikson, G., Parks, M.J. and Nielsen, K., AquaBuOY-The Offshore Wave Energy Converter Numerical Modeling and Optimization, IEEE Techno-Ocean'04, 4 (2004) 1854-1859.
32. Payne, G.S., Taylor, J.R.M., Parkin, P. and Salter, S.H., Numerical Modelling of the Sloped IPS Buoy Wave Energy Converter, Proceedings of the Sixteenth (2006) International Offshore and Polar Engineering Conference, San Francisco, California, USA, May 28-June 2, 2006, 396.
33. Gomes, R.P.F., Henriques, J.C.C., Gato, L.M.C. and Falco, A.F.O., IPS 2-Body Wave Energy Converter: Acceleration Tube Optimization, International Journal of Offshore and Polar Engineering, 20, 4 (2010) 247-255.
34. Falcao, A.F.O., Candido, J.J., Justino, P.A.P and Henriques, J.C.C, Hydrodynamics of the IPS Buoy Wave Energy Converter Including the Effect of Non-uniform Acceleration Tube Cross Section, Renewable Energy, 41 (2012) 105-114.
35. Garnaud, X. and Mei, C.C., Comparison of Wave Power Extraction by a Compact Array of Small Buoys and by a Large Buoy, IET Renewable Power Generation, 4, 6 (2010) 519-530.
36. Knight, H., Offshore Device is Hydropower's Next Wave, The Engineer, 30 May-12 June 2003.
37. www.wavebob.com/key-features. 24.01.2012.
38. Wood, J., Racing the Waves, IEE Power Engineer, June/July 2004, 24-26.
39. Kime, P., Harnessing Wave Energy: Navy Program in Hawaii to See Fully Functional PowerBuoy this Year, Sea Power, 53, 3 (2010) 28-29.
40. Testing Time for the Navy Buoys, Modern Power Systems, 31, 9 (2011), 47.
41. Marine Renewables, www.sea-technology.com, July 2011, 67-68.
42. Dalton, G.J., Alcorn, R., and Lewis, T., Case Study Feasibility Analysis of the Pelamis Wave Energy Converter in Ireland, Portugal and North America, Renewable Energy, 35 (2010) 443-455.
43. Ahmed, T., Nishida, K. and Nakaoka, M., The Potential for Grid Power Integration of Offshore Ocean Wave Energy in the UK, The 2010 International Power Electronics Conference, 2010, 3204-3211.

44. Ahmed, T., Nishida, K. and Nakaoka, M., The Commercial Advancement of 16 MW Offshore Wave Power Generation Technologies in the Southwest of the UK, 8th International Conference on Power Electronics-ECCE Asia, May 30-June 3, 2011, The Shilla Jeju, Korea, 1476-1483.
45. Polinder, H. and Scuotto, M., Wave Energy Converters and their Impact on Power Systems, International Conference on Future Power Systems, 2005, 1-9.
46. Ahmed, T., Nishida, K. and Nakaoka, M., Grid Power Integration Technologies for Offshore Ocean Wave Energy, IEEE Energy Conversion Congress and Exposition (ECCE), 2010, 2378-2385.
47. Henderson, R., Design, Simulation, and Testing of a Novel Hydraulic Power Take-Off System for The Pelamis Wave Energy Converter, Renewable Energy, 31 (2006) 271-283.
48. McCabe, A.P., Bradshaw, A., Meadowcroft, J.A.C. and Aggidis, G., Developments in the Design of the PS Frog Mk 5 Wave Energy Converter, Renewable Energy, 31 (2006) 141-151.
49. Ruellan, M., Ahmed, H.B., Multon, B., Josset, C., Babarit, A. and Clement, A., Design Methodology for a SEAREV Wave Energy Converter, IEEE Transactions on Energy Conversion, 25, 3 (2010) 760-767.
50. Babarit, A., Clement, A., Ruer, J. and Tartivel C., SEAREV: A Fully Integrated Wave Energy Converter, Proceedings of the OWEMES'09.
51. Babarit, A. and Clement, A.H., Optimal Latching Control of a Wave Energy Device in Regular and Irregular Waves, Applied Ocean Research, 28 (2006) 77-91.
52. Wu, F., Zhang, X.P., Ju, P. and Sterling, M.H., Modeling and Control of AWS-Based Wave Energy Conversion System Integrated into Power Grid, IEEE Transactions on Power Systems, 23, 3 (2008) 1196-1204.
53. Polinder, H., Mecrow, B.C., Jack, A.G., Dickinson, P.G. and Mueller, M.A., Conventional and TFFM Linear Generators for Direct-Drive Wave Energy Conversion, IEEE Transactions on Energy Conversion, 20, 2 (2005) 260-267.
54. Valerio, D., Beirao, P. and Costa, J.S., Optimisation of Wave Energy Extraction with the Archimedes Wave Swing, Ocean Engineering, 34 (2007) 2330-2344.
55. Wood, K., Wave-Energy Conversion, Composites Technology, 9/30/2010, 30-31.
56. 1 MW Wave Energy Power Plant, Waveroller Technology, November 2007, 1-12.
57. Whittaker, T. and Folley, M., Nearshore Oscillating Wave Surge Converters and the Development of Oyster, Phil. Trans. R. Soc. A, 370 (2012) 345-364.

58. Collier, D., Whittaker, T. and Crowley, M., The Construction of Oyster A Nearshore Surging Wave Energy Converter, 2nd International Conference on Ocean Energy, 2008, 1-7.
59. Beels, C., Troch, P., Visch, K.D., Kofoed, J.P. and Backer, G.D., Application of the Time-Dependent Mild-Slope Equations for the Simulation of Wake Effects in the Lee of a Farm of Wave Dragon Wave Energy Converters, Renewable Energy, 35 (2010) 1644-1661.
60. Kofoed, J.P., Frigaard, P., Madsen, E.F. and Sorensen, H.Chr., Prototype Testing of the Wave Energy Converter Wave Dragon, Renewable Energy, 31 (2006) 181-189.
61. Tedd, J. and Kofoed, J.P., Measurements of Overtopping Flow Time Series on the Wave Dragon, Wave Energy Converter, Renewable Energy, 34 (2009) 711-717.
62. Zhou, Z., Knapp, W., MacEnri, J., Sorensen, H.Ch., Madsen, E.F., Masters, I. and Igetic, P., Permanent Magnet Generator Control and Electrical System Configuration for Wave Dragon MW Wave Energy Take-off System, IEEE International Symposium on Industrial Electronics, ISIE 2008, 2008, 1580-1585.
63. Ocean Energy Report, ABS Energy Research, 2007, 19-32.
64. Mehlum, E., Commercial Tapered Channel Wave Power Plants in Australia and Indonesia, Proceedings OCEANS'91, Ocean Technologies and Opportunities in the Pacific for the 90's, 1991, 535-538.
65. Vicinanza, D. and Frigaard, P., Wave Pressure Acting on a Seawave Slot-cone Generator, Coastal Engineering, 55 (2008) 553-568.
66. Vicinanza, D., Ciardulli, F., Buccino, M., Calabrese, M. and Koefed, J.P., Wave Loadings Acting on an Innovative Breakwater for Energy Production, Journal of Coastal Research, 64 (2011) 608-612.
67. Clement, A., McCullen, P., Falcao, A., Fiorentino, A., Gardner, F., Hammarlund, K., Lemonis, G., Lewis, T., Nielsen, K., Petroncini, S., Pontes, M.T., Schild, P., Sjöström, B.O., Sørensen, H.C. and Thorpe, T., Wave Energy in Europe: Current Status and Perspectives, Renewable and Sustainable Energy Reviews, 6 (2002) 405-431.
68. Langhamer, O., Haikonen, K. and Sundberg, J., Wave Power-Sustainable Energy or Environmentally Costly? A Review with Special Emphasis on Linear Wave Energy Converters, Renewable and Sustainable Energy Reviews, 14 (2010) 1329-1335.
69. Grecian, W.J., Inger, R., Attrill, M.J., Bearhop, S., Godley, B.J., Witt, M.J. and Votier, S.C., Potential Impacts of Wave-Powered Marine Renewable Energy Installations on Marine Birds, The International Journal of Avian Science, 152 (2010) 683-697.

70. Falnes, J., Optimum Control of Oscillation of Wave-Energy Converters, International Journal of Offshore and Polar Engineering, 12, 2 (2002) 147-155
71. Babarit, A., Duclos, G. and Clement, A.H., Comparison of Latching Control Strategies for a Heaving Wave Energy Device in Random Sea, Applied Ocean Research, 26 (2004) 227-238.
72. Falcao, A.F.O., Phase Control through Load Control of Oscillating-Body Wave Energy Converters with Hydraulic PTO System, Ocean Engineering, 35 (2008) 358-366.
73. Yavuz, H., Mistikoğlu, S. and Stallard, T., Processing Irregular Wave Measurements to Enhance Point Absorber Power Capture Performance, Ocean Engineering, 38 (2011) 684-698.
74. McCabe, A.P., Stallard, T.J., Baker, N.J. and Yavuz, H., Estimation of the Responses of Axisymmetric Bodies in Spread Irregular Waves, Ocean Engineering, 34 (2007) 1371-1382.
75. Rodriguez, G.R. and Soares, C.G., Correlation between Successive Wave Heights and Periods in Mixed Sea States, Ocean Engineering, 28 (2001) 1009-1030.
76. Nunes, G., Valerio, D., Beirao, P. and Costa, J.S., Modelling and Control of a Wave Energy Converter, Renewable Energy, 36 (2011) 1913-1921.
77. Korde, U.A., Performance of a Wave Energy Device in Shallow-Water Nonlinear Waves: Part II, Applied Ocean Research, 19 (1997) 13-20.
78. Eidsmoen, H., Tight-Moored Amplitude-Limited Heaving-Buoy Wave-Energy Converter With Phase Control, Applied Ocean Research 20 (1998) 157-161.
79. Korde, U.A., On Providing a Reaction for Efficient Wave Energy Absorption by Floating, Applied Ocean Research, 21 (1999) 235-248.
80. Falco, A.F.de O. and Justio, P.A.P., OWC Wave Energy Devices with Air Flow Control, Ocean Engineering, 26 (1999) 1275-1295.
81. Korde, U.A., Efficient Primary Energy Conversion in Irregular Waves, Ocean Engineering, 26 (1999) 625-651.
82. Korde, U.A., Control System Applications in Wave Energy Conversion, OCEANS 2000 MTS/IEEE Conference and Exhibition, 3 (2000) 1817-1824.
83. Korde, U.A., Latching Control of Deep Water Wave Energy Devices Using an Active Reference, Ocean Engineering, 29 (2002) 1343-1355.
84. Falco, A.F.de O., Control of an Oscillating-Water-Column Wave Power Plant for Maximum Energy Production, Applied Ocean Research, 24 (2002) 73-82.

85. Falco, A.F.de O. and Rodrigues, R.J.A., Stochastic Modelling of OWC Wave Power Plant Performance, Applied Ocean Research, 24 (2002) 59-71.
86. Babarit, A., Duclos, G. and Clement A.H., Comparison of Latching Control Strategies for a Heaving Wave Energy Device in Random Sea, Applied Ocean Research, 26 (2004) 227-238.
87. Sharmila, N., Jalihal, P., Swamy, A.K. and Ravindran, M., Wave Powered Desalination System, Energy, 29 (2004) 1659-1672.
88. Barnes, M., El-Feres, R., Kromlides, S. and Arulampalam, A., Power Quality Improvement for Wave Energy Converters Using a D-STATCOM with Real Energy Storage, First International Conference on Power Electronics Systems and Applications, 2004, 72-77.
89. Henderson, R., Design, Simulation, and Testing of a Novel Hydraulic Power Take-Off System for the Pelamis Wave Energy Converter, Renewable Energy, 31 (2006) 271-283.
90. Babarit, A. and Clement A.H., Optimal Latching Control of a Wave Energy Device in Regular and Irregular Waves, Applied Ocean Research, 28 (2006) 77-91.
91. Falco, A.F.de O., Modelling and Control of Oscillating-Body Wave Energy Converters with Hydraulic Power Take-Off and Gas Accumulator, Ocean Engineering, 34 (2007) 2021-2032.
92. Valerio, D., Beirao, P. and Costa, R.S da, Optimisation of Wave Energy Extraction with the Archimedes Wave Swing, Ocean Engineering, 34 (2007) 2330-2344.
93. Thorburn, K. and Leijon, M., Farm Size Comparison with Analytical Model of Linear Generator Wave Energy Converters, Ocean Engineering, 34 (2007) 908-916.
94. Falco, A.F.de O., Phase Control through Load Control of Oscillating-Body Wave Energy Converters with Hydraulic PTO System, Ocean Engineering, 35 (2008) 358-366.
95. Valerio, D., Mendes, M.J.G.C., Beirao, P. and Costa, J.S.da, Identification and Control of the AWS Using Neural Network Models, Applied Ocean Research, 30 (2008) 178-188.
96. Wang, L., Lee, D.J., Lee, W.J. and Chen Zhe, Analysis of a Novel Autonomous Marine Hybrid Power Generation/Energy Storage System with a High-Voltage Direct Current Link, Journal of Power Sources, 185 (2008) 1284-1292.
97. Lopes, M.F.P., Hals, J., Gomes, R.P.F., Moan, T., Gato, L.M.C. and Falcao, A.F.de O., Experimental and Numerical Investigation of Non-Predictive Phase-Control Strategies for a Point-Absorbing Wave Energy Converter, Ocean Engineering, 36 (2009) 386-402.

98. Babarit, A., Guglielmi, M. and Clement, A.H., Declutching Control of a Wave Energy Converter, Ocean Engineering, 36 (2009) 1015-1024.
99. Boström, C., Lejerskog, E., Stålberg, M., Thorburn, K. and Leijon, M., Experimental Results of Rectification and Filtration from an Offshore Wave Energy System, Renewable Energy, 34 (2009) 1381-1387.
100. Luan, H., Onar, O.C., Khaligh, A., Dynamic Modeling and Optimum Load Control of a PM Linear Generator for Ocean Wave Energy Harvesting Application, Twenty-Fourth Annual IEEE Applied Power Electronics Conference and Exposition, 2009, APEC 2009, Washington, DC, 739-743.
101. Wu, F., Zhang, X.P., Ju, P. and Sterling, M.J.H., Optimal Control for AWS-Based Wave Energy Conversion System, IEEE Transactions on Power Systems, 24, 4 (2009) 1747-1755.
102. Blanco, M., Navarro, G. and Lafoz, M., Control of Power Electronics Driving a Switched Reluctance Linear Generator in Wave Energy Applications, 13th European Conference on Power Electronics and Applications, 2009, EPE'09, 1-9.
103. Jayashankar, V., Anand, S., Geetha, T., Santhakumar, S., Kumar, V.J., Ravindran, Setoguchi, T., Takao, M., Toyota, K. and Nagata, S., A Twin Unidirectional Impulse Turbine Topology for OWC Based Wave Energy Plants, Renewable Energy, 34 (2009) 692-698.
104. Paulo R. Costa, Paula B. Garcia-Rosa, Segen F. Estefen, Phase Control Strategy for a Wave Energy Hyperbaric Converter, Ocean Engineering, 37 (2010) 1483-1490.
105. M.R. Belmont, Increases in the Average Power Output of Wave Energy Converters Using Quiescent Period Predictive Control, Renewable Energy, 35 (2010) 2812-2820.
106. Falco, A.F.de O, Pereira, P., Henriques, J.C.C. and Gato, L.M.C., Hydrodynamic Simulation of a Floating Wave Energy Converter by a U-Tube Rig for Power Take-Off Testing, Ocean Engineering, 37 (2010) 1253-1260.
107. Yang, L., Hals, J. and Moan, T., Analysis of Dynamic Effects Relevant for the Wear Damage in Hydraulic Machines for Wave Energy Conversion, Ocean Engineering, 37 (2010) 1089-1102.
108. Beatty, S.J., Wild, P. and Buckham, B.J., Integration of a Wave Energy Converter into the Electricity Supply of a Remote Alaskan Island, Renewable Energy, 35 (2010) 1203-1213.
109. Kara, F., Time Domain Prediction of Power Absorption from Ocean Waves with Latching Control, Renewable Energy, 35 (2010) 423-434.

110. Ruellan, M., BenAhmed, H., Multon, B., Josset, C., Babarit, A. and Clement, A., Design Methodology for a SEAREV Wave Energy Converter, IEEE Transactions on Energy Conversion, 25, 3 (2010) 760-767.
111. Shek, J.K.H., Marcepherson, D.E. and Mueller, M.A., Experimental Verification of Linear Generator Control for Direct Drive Wave Energy Conversion, IET Renew. Power Gener., 4, 5 (2010) 395-403.
112. Boström, C. and Leijon, M., Operation Analysis of A Wave Energy Converter under Different Load Conditions, IET Renew. Power Gener., 5, 3 (2011) 245-250.
113. Rahm, M., Boström, C., Svensson, Grabbe, M., Bülow, F. and Leijon, M., Offshore Underwater Substation for Wave Energy Converter Arrays, IET Renew. Power Gener., 4, 6 (2010) 602-612.
114. Amundarain, M., Alberdi, M., Garrido, A.J., Garrido, I., Maseda, J., Wave Energy Plants: Control Strategies for Avoiding the Stalling Behaviour in the Wells Turbine, Renewable Energy, 35 (2010) 2639-2648.
115. Kazmierkowski, M.P. and Jasiński, M., Power Electronics for Renewable Sea Wave Energy, 12th International Conference on Optimization of Electrical and Electronic Equipment, OPTIM 2010, 4-9.
116. Igetic, P., Zhou, Z., Kanpp, J., MacEnri, Sorensen, H.C. and Friis-Madsen, E., Multi-Megawatt Offshore Wave Energy Converters - Electrical System Configuration and Generator Control Strategy, IET Renew. Power Gener., 5, 1 (2011) 10-17.
117. Cho, B.H., Yang, D.S., Park, S.Y., Choi, K.S. and Lee, D.H., Modeling and Control of a 75 kw Class Variable Liquid-Column Oscillator for Highly Efficient Wave Energy Converter, Ocean Engineering, 38 (2011) 436-443.
118. Yang, L. and Moan, T., Dynamic Analysis of Wave Energy Converter by Incorporating the Effect of Hydraulic Transmission Lines, Ocean Engineering, 38 (2011) 1849-1860.
119. Candido, J.J. and Justino, P.A.P.S., Modelling, Control and Pontryagin Maximum Principle for a Two-Body Wave Energy Device, Renewable Energy, 36 (2011) 1545-1557.
120. Saulnier, J.B., Clement, A., Falco, A.F.de O., Pontes, T., Prevosto, M. and Ricci, P., Wave Groupiness and Spectral Bandwidth as Relevant Parameters for the Performance Assessment of Wave Energy Converters, Ocean Engineering, 38 (2011) 130-147.
121. Bracco, G., Giorcelli, E. and Mattiazzo, G., ISWEC: A Gyroscopic Mechanism for Wave Power Exploitation, Mechanism and Machine Theory, 46 (2011) 1411-1424.

122. Tedeschi, E., Carraro, M. and Mattavelli, P., Effect of Control Strategies and Power Take-Off Efficiency on the Power Capture From Sea Waves, IEEE Transactions on Energy Conversion, 26, 4 (2011) 1088-1097.
123. Nunes, G., Valerio, D., Beirao, P. and Costa, J.S.da, Modelling and Control of a Wave Energy Converter, Renewable Energy, 36 (2011) 1913-1921.
124. O'Sullivan, D., Griffiths, J., Egan, M.G. and Lewis, A.W., Development of an Electrical Power Take Off System for a Sea-Test Scaled Offshore Wave Energy Device, Renewable Energy, 36 (2011) 1236-1244.
125. D.Q. Truong, K.K. Ahn, Wave Prediction Based on a Modified Grey Model MGM(1,1) for Real-Time Control of Wave Energy Converters in Irregular Waves, Renewable Energy, 43 (2012) 242-255.
126. Kurniawan, A., Pedersen, E. and Moan, T., Bond Graph Modelling of a Wave Energy Conversion System with Hydraulic Power Take-Off, Renewable Energy, 38 (2012) 234-244.
127. Ahn, K.K., Truong, D.Q., Tien, H.H. and Yoon, J.I., An Innovative Design of Wave Energy Converter, Renewable Energy, 42 (2012) 186-194.
128. Flocard, F. and Finnigan, T.D., Increasing Power Capture of a Wave Energy Device by Inertia Adjustment, Applied Ocean Research, 34 (2012) 126-134.
129. Falco, A.F.de O., Candido, J.J., Justino, P.A.P. and Henriques, J.C.C., Hydrodynamics of the IPS Buoy Wave Energy Converter including the Effect of Non-Uniform Acceleration Tube Cross Section, Renewable Energy, 41 (2012) 105-114.
130. Sorensen, R.M., Basic Coastal Engineering, Springer, 2006.
131. Mohan, Ned, Advanced Electric Drives: Analysis, Control and Modeling Using Simulink, MNPERE, ISBN 0-9715292-0-5, 2001.
132. El Aroudi, A., Debbat, M., Giral, R., Olivar, G., Benadero, L. and Toribio, E., Bifurcations in DC-DC Switching Converters: Review of Methods and Applications, International Journal of Bifurcation and Chaos, 15, 5 (2005) 1549-1578.
133. Wens, M. and Steyaert, M., Design and Implementation of Fully-Integrated Inductive DC-DC Converters in Standard CMOS, Springer, 2011.
134. Kazimierczuk, M.K., Pulse-width Modulated DC-DC Power Converters, Wiley, 2008.
135. Luo, F.L. and Ye, H., Synchronous and Resonant DC/DC Conversion Technology, Energy Factor, and Mathematical Modeling, Taylor & Francis, 2006.

136. Tseng, C.Y. Wang, L.W. and Huang, P.C., An Integrated Linear Regulator with Fast Output Voltage Transition for Dual-Supply SRAMs in DVFS Systems, IEEE Journal of Solid-State Circuits, 45, 11 (2010) 2239-2249.
137. Hazucha, P., Karnik, T., Bloechel, B.A., Parsons, C., Finan, D. and Borkar, S., Area-Efficient Linear Regulator with Ultra-Fast Load Regulation, IEEE Journal of Solid-State Circuits, 40, 4 (2005) 933-940.
138. Wang, C.C. and Wu, J.C., Efficiency Improvement in Charge Pump Circuits, IEEE Journal of Solid-State Circuits, 32, 6 (1997) 852-860.
139. Ma, D., and Luo, F., Robust Multiple-Phase Switched-Capacitor DC-DC Power Converter with Digital Interleaving Regulation Scheme, IEEE Transactions on Very Large Scale Integration (VLSI) Systems, 16, 6 (2008) 611-619.
140. Adinolfi, G., Femia, N., Petrone, G., Spagnuolo, G. and Vitelli, M., Design of DC/DC Converters for DMPPT PV Applications Based on the Concept of Energetic Efficiency, Journal of Solar Energy Engineering, 132, 2 (2010) 021005-1-021005-10.
141. Lembeye, Y., Bang, V.D., Lefevre, G. and Ferrieux, J.P., Novel Half-Bridge Inductive DC-DC Isolated Converters for Fuel Cell Applications, IEEE Transactions on Energy Conversion, 24, 1 (2009) 203-201.
142. Ruan, X., Li, B., Chen, Q., Tan, S.C. and Tse, C.K., Fundamental Considerations of Three-Level DC-DC Converters: Topologies, Analyses, and Control, IEEE Transactions on Circuits and Systems-I: Regular Papers, 55, 11 (2008) 3733-3743.
143. Ayyanar, R. and Mohan, N., Novel Soft-Switching DC-DC Converter with Full ZVS-Range and Reduced Filter Requirement-Part II: Constant-Input, Variable-Output Applications, IEEE Transactions on Power Electronics, 16, 2 (2011) 193-200.
144. Canales, F., Barbosa, P. and Lee, F.C., A Zero-Voltage and Zero-Current Switching Three-Level DC/DC Converter, IEEE Transactions on Power Electronics, 17, 6 (2002) 898-904.
145. Bodur, H., and Bakan, A.F., An Improved ZCT-PWM DC-DC Converter for High-Power and Frequency Applications, IEEE Transactions on Industrial Electronics, 51, 1 (2004) 89-95.
146. Rashid, M.H., Power Electronics Handbook, Academic Press, 2001.
147. Sankaran, C., Power Quality, CRC Press, ISBN 0-8493-1040-7, 2002.
148. Dugan, R.C., McGranaghan, M.F., Santoso, S. and Beaty, H.W., Electrical Power Systems Quality, McGraw-Hill, 2004.
149. Vosen, S.R. and Keller, J.O., Hybrid Energy Storage Systems for Stand-Alone Electric Power Systems: Optimization of System Performance and Cost through Control Strategies, International Journal of Hydrogen Energy, 24 (1999) 1139-1156.

150. Brooking, P.R.M. and Mueller, M.A., Power Conditioning of the Output From A Linear Vernier Hybrid Permanent Magnet Generator for Use in Direct Drive Wave Energy Converters, IEE Proceedings-Generation, Transmission and Distribution, 152, 5 (2005) 673-681.
151. Ang, K.H., Chong, G. and Li, Y., PID Control System Analysis, Design, and Technology, IEEE Transactions on Control Systems Technology, 13, 4 (2005) 559-576.
152. Da, Z., Zhengyun R., Jian'an F. and Lei J., Computation of Stabilizing PI and PID Controllers by Using Kronecker Summation Method, Proceedings of the 27th Chinese Control Conference July 16-18, 2008, Kunming, Yunnan, China, 72-75.
153. Yu, C.C., Autotuning of PID Controllers: A Relay Feedback Approach, Second Edition, Springer-Verlag, Germany, 2006.
154. Lelic, M., PID Controllers in Nineties, Coming Incorporated Science and Technology Division, Coming, NY, 1999.
155. Desborough, L. and Miller, R., Increasing Customer Value of Industrial Control Performance Monitoring-Honeywell Experience, Arizona, USA: CPC-VI, 2001.
156. Wang, Q.G., Ye, Z., Cai, W.J. and Hang, C.C., PID Control for Multivariable Processes, Springer-Verlag, Berlin Heidelberg, 2008.
157. Sung, S.W., Lee, J. and Lee, I.B., Process Identification and PID Control, John Wiley & Sons, 2009.
158. Johnson, M.A. and Moradi, M.H., PID Control, New Identification and Design Methods, Springer-Verlag, London, 2005.
159. Yurkevich, V.D., Advances in PID Control, InTech, Croatia, 2011.
160. O'Dwyer, A., Handbook of PI and PID Controller Tuning Rules, Imperial College Press, London, 2009.
161. Moradi, M.H., New Techniques for PID Controller Design, Proceedings of 2003 IEEE Conference on Control Applications, CCA 2003, 2003, 2, 903-908.
162. Unar, M.A., Murray-Smith, D.J. and Shah, S.F.A., Design and Tuning of Fixed Structured PID Controllers A Survey, Technical Report, Glasgow University, 1996.
163. Van der Zalm, G.M.V., Tuning of PID-type Controllers: Literature Overview, DCT-report, 2004.
164. Panda, R.C., Yu, C.C. and Huang, H.P., PID Tuning Rules for SOPDT Systems: Review and Some New Results, ISA Transactions, 43 (2004) 283-295.

165. Li, Y., Ang, K.H. and Chong, G.C.Y., Patents, Software, and Hardware for PID Control: an Overview and Analysis of the Current Art, IEEE Control Systems Magazine, 26, 1 (2006) 42-54.
166. <http://gb.espacenet.com>, GB Esp@cenet, European Patent Office (EPO), 16.12.2011.
167. O'Dwyer, A., PI and PID Controller Tuning Rules: an Overview and Personal Perspective, IET Irish Signals and Systems Conference, ISSC 2006, 2006, 161-166.
168. O'Dwyer, A., PI and PID Controller Tuning Rules for Time Delay Processes: A Summary, Technical Report AOD-00-01, Edition 1, 2002.
169. Qin, S.J., "Control Performance Monitoring-A Review and Assessment", Computers and Chemical Engineering, 23 (1998) 173-186.
170. Adamy, J. and Flemming, A., Soft Variable-Structure Controls: a Survey, Automatica, 40 (2004) 1821-1844.
171. Tan, S.C., Lai, Y.M. and Tse, C.K., Sliding Mode Control of Switching Power Converters: Techniques and Implementation, CRC Press, 2012.
172. Kaynak, O., Erbatur, K. and Ertugrul, M, The Fusion of Computationally Intelligent Methodologies and Sliding-Mode Control-A Survey, IEEE Transactions on Industrial Electronics, 48, 1 (2001) 4-17.
173. Hung, J.Y., Gao, W. and Hung, J.C., Variable Structure Control: A Survey, IEEE Transactions on Industrial Electronics, 40, 1 (1993) 2-22.
174. Utkin, V., Guldner, J. and Shi, J., Sliding Mode Control in Electro-Mechanical Systems, Second Edition, CRC Press, 2009.
175. Spurgeon, S.K., Sliding Mode Observers: a Survey, International Journal of Systems Science, 39, 8 (2008) 751-764.
176. Fridman, L., Moreno, J. and Iriarte, R., Sliding Modes After the First Decade of the 21st Century: State of the Art, Springer, Berlin, 2011.
177. Bandyopadhyay, B., Deepak, F. and Kim, K.S., Sliding Mode Control Using Novel Sliding Surfaces, Springer, 2009.
178. Sabanovic, A., Variable Structure Systems with Sliding Modes in Motion Control-A Survey, IEEE Transactions on Industrial Informatics, 7, 2 (2011) 212-223.
179. Utkin, V., Variable Structure Systems with Sliding Modes, IEEE Transactions on Automatic Control, AC-22, 2 (1977) 212-222.

180. Shamsara, O., Mehrshad, N. and Zare, A., Application of Modern Nonlinear Control to Blood Glucose Regulation: A Comparative Study of Characteristics of Sliding Mode Control and Fuzzy Logic Technique, International Review of Automatic Control, 2, 5 (2009) 600-608.
181. Shahgholian, G., Rajabi, A. and Karimi, B., Analysis and Design of PSS for Multi-Machine Power System Based on Sliding Mode Control Theory, International Review of Electrical Engineering (I.R.E.E.), 5, 5 (2010) 2241-2250.
182. Bogosyan, S., Gadamsetty, B., Gokasan, M., Sabanovic, A. and Unel, M., Experimental Evaluation of Sliding Mode and EKF Observers for Network Delay Compensation in Bilateral Control, International Review of Electrical Engineering (I.R.E.E.), 5, 5 (2010) 2484-2493.
183. Ignaciuk, P. and Bartoszewicz, A., LQ Optimal and Reaching Law-Based Sliding Modes for Inventory Management Systems, International Journal of Systems Science, 43, 1 (2012) 105-116.
184. Wach, P., Dynamics and Control of Electrical Drives, Springer, Berlin, 2011.
185. Sabanovic, A., Fridman, L.M. and Spurgeon, S., Variable Structure Systems from Principles to Implementation, The Institution of Engineering and Technology, 2004.
186. Imine, H., Fridman, L., Shraim, H. and Djemai, M, Sliding Mode Based Analysis and Identification of Vehicle Dynamics, Springer, Berlin, 2011.
187. Tannuri, E.A., Agostinho, A.C., Morishita, H.M. and Moratelli Jr, L., Dynamic Positioning Systems: An Experimental Analysis of Sliding Mode Control, Control Engineering Practice, 18 (2010) 1121-1132.
188. Rigatos, G.G., Modelling and Control for Intelligent Industrial Systems: Adaptive Algorithms in Robotics and Industrial Engineering, Springer, 2011.
189. Bandyopadhyay, B. and Janardhanan, S., Discrete-time Sliding Mode Control: A Multirate Output Feedback Approach, Springer, Germany, 2006.
190. Yu, X. and Kaynak, O., Sliding-Mode Control with Soft Computing: A Survey, IEEE Transactions on Industrial Electronics, 56, 9 (2009) 3275-3285.
191. Tan, S.C., Lai, Y.M. and Tse, C.K., General Design Issues of Sliding-Mode Controllers in DC-DC Converters, IEEE Transactions on Industrial Electronics, 55, 3 (2008), 1160-117.
192. Bowong, S., Controlled Synchronization of Chaotic Systems with Uncertainties Via a Sliding Mode Control Design, Physical Review E, 70 (2004) 066217/1-066217/10.
193. Dal, M. and Teodorescu, R., Sliding Mode Controller Gain Adaptation and Chattering Reduction Techniques for DSP-Based PM DC Motor Drives, Turk. J. Elec. Eng. & Comp. Sci., 19 (2011) 531-549.

194. Govindaswamy, S., Spurgeon, S.K. and Floquet, T., Discrete-Time Output Feedback Sliding-Mode Control Design for Uncertain Systems Using Linear Matrix Inequalities, International Journal of Control, 84, 5 (2011) 916-930.
195. Koshkouei, A.J. and Burnham, K.J., Adaptive Backstepping Sliding Mode Control for Feedforward Uncertain Systems, International Journal of Systems Science, 42, 12 (2011) 1935-1946.
196. Bartoszewicz, A. and Leverton, A.N., Time-Varying Sliding Modes for Second and Third Order Systems, Springer, Berlin, 2009.
197. Agrachev, A.A., Morse, A.S., Sontag, E.D., Sussmann, H.J. and Utkin, V.I., Nonlinear and Optimal Control Theory, Springer, 2008.
198. Bartolini, G., Pisano, A., Punta, E. and Usai, E., A Survey of Applications of Second-Order Sliding Mode Control to Mechanical Systems, International Journal of Control, 76, 9 (2003) 875-892.
199. Bartolini, G., Punta, E., Zolezzi, T., Simplex Sliding Mode Control of Multi-Input Systems with Chattering Reduction and Mono-Directional Actuators, Automatica, 47 (2011) 2433-2437.
200. Li, H., Liao, X., Li, C. and Li, C., Chaos Control and Synchronization via a Novel Chatter Free Sliding Mode Control Strategy, Neurocomputing, 74 (2011) 3212-3222.
201. Edwards, C., Fossas Colet, E. and Fridman, L., Advances in Variable Structure and Sliding Mode Control, Springer, Berlin, 2006.
202. Savu, A., Radoi, C. and Florescu, A., Sliding Mode PWM Control for a Buck Converter Under DCM/CCM Boundary, International Review of Electrical Engineering (I.R.E.E.), 5, 5 (2010) 1963-1971.
203. Bartoszewicz, A., Sliding Mode Control, InTech, 2011.
204. Efe, M.O., Acay, L.D., Unsal, C. and Khosla, R.K., Adaptive Fuzzy Sliding Mode Control for a Class of Bipartite Modular Robotic Systems, Istanbul University–Journal of Electrical & Electronics Engineering, 3, 1 (2003) 645-661.
205. Lin, T.C., Kuo, C.H. and Balas, V.E., Uncertain Fractional Order Chaotic Systems Tracking Design via Adaptive Hybrid Fuzzy Sliding Mode Control, Int. J. of Computers, Communications & Control, VI, 3 (2011) 418-427.
206. Sage, H.G., Mathelin, M.F.De. and Ostertag, E., Robust Control of Robot Manipulators: A Survey, Int. J. Control, 72, 16 (1999) 1498-1522.
207. Kareem, A. and Azeem, M.F., A Novel Soft Computing Based Algorithm for the Control of Dynamic Uncertain Systems-An Application to DC-DC Converters, International Journal of Artificial Intelligence & Applications (IJAIA), 2, 2 (2011) 21-30.

208. Kaur, G. and Singh, M.L., A Survey of Recent Advances in Fuzzy Logic in Communication Systems, International Journal of Applied Engineering Research, 4, 2 (2009) 139-151.
209. Murshid, A.M., Loan, S.A., Abbasi, S.A. and Alamoud, A.R.M., VLSI Architecture of Fuzzy Logic Hardware Implementation: A Review, International Journal of Fuzzy Systems, 13, 2 (2011) 74-88.
210. Saghafinia, A., Ping, H.W., Rahman, M.A., High Performance Induction Motor Drive Using Hybrid Fuzzy-PI and PI Controllers: A Review, International Review of Electrical Engineering (I.R.E.E.), 5, 5 (2010) 2000-2012.
211. Askerzade, I.N. and Mahmud, M., "Design and Implementation of Group Traffic Control System Using Fuzzy Logic", IJRRAS, 6, 2 (2011) 196-202.
212. Ficili, G. and Panno, D., A Fuzzy Algorithm for Combined Control of Traffic Parameters: Assessment and Key Issues, Computer Communications, 22, 3 (1999) 199-210.
213. Kalogirou, S.A., Artificial Intelligence for the Modeling and Control of Combustion Processes: A Review, Progress in Energy and Combustion Science, 29 (2003) 515-566.
214. Monmasson, E. and Cirstea, M.N., FPGA Design Methodology for Industrial Control Systems-A Review, IEEE Transactions on Industrial Electronics, 54, 4 (2007) 1824-1842.
215. Perrot, N., Ioannou, I., Allais, I., Curt, C., Hossenlopp, J. and Trystram, G., Fuzzy Concepts Applied to Food Product Quality Control: A Review, Fuzzy Sets and Systems, 157 (2006) 1145-1154.
216. Jeong, K.S., Lee, W.Y. and Kim, C.S., Energy Management Strategies of A Fuel Cell/Battery Hybrid System Using Fuzzy Logics, Journal of Power Sources, 145 (2005) 319-326.
217. Lalouni, S., Rekioua, D., Rekioua, T. and Matagne, E., Fuzzy Logic Control of Stand-Alone Photovoltaic System with Battery Storage, Journal of Power Sources, 193 (2009) 899-907.
218. Vinodh, S. and Balaji, S.R., Fuzzy Logic Based Leanness Assessment and Its Decision Support System, International Journal of Production Research, 49, 13 (2011) 4027-4041.
219. Sproule, B.A., Naranjo, C.A. and Türksen, I.B., Fuzzy Pharmacology: Theory and Applications, TRENDS in Pharmacological Sciences, 23, 9 (2002) 412-417.
220. Kentli, A., Studies on Fuzzy Logic Control of Electrical Machines in Turkish Universities: an Overview, Mathematical and Computational Applications, 16, 1 (2011) 236-247.

221. Gad, A. and Farooq, M., An Overview of Fuzzy Logic in Power and Control Systems, *IEEE 46th Midwest Symposium on Circuits and Systems*, 3 (2003) 1047-1050.
222. Guclu, R., Fuzzy Logic Control of Vibrations of Analytical Multi-Degree-of-Freedom Structural Systems, *Turkish J. Eng. Env. Sci.*, 27 (2003) 157-167.
223. Mahfouf, M., Abbod, M.F. and Linkens, D.A., A Survey of Fuzzy Logic Monitoring and Control Utilisation in Medicine, *Artificial Intelligence in Medicine*, 21 (2001) 27-42.
224. Feng, G., A Survey on Analysis and Design of Model-Based Fuzzy Control Systems, *IEEE Transactions on Fuzzy Systems*, 14, 5 (2006) 676-697.
225. Yaqiong, L., Man, L.K. and Zhang, W., Fuzzy Theory Applied in Quality Management of Distributed Manufacturing System: A Literature Review and Classification, *Engineering Applications of Artificial Intelligence*, 24 (2011) 266-277.
226. Fisco, N.R. and Adeli, H., Smart Structures: Part II- Hybrid Control Systems and Control Strategies, *Scientia Iranica A*, 8, 3 (2011) 285-295.
227. Dote, Y. and Ovaska, S.J., Industrial Applications of Soft Computing: A Review, *Proceedings of the IEEE*, 89, 9 (2001) 1243-1265.
228. Precup, R.E. and Hellendoorn, H., A Survey on Industrial Applications of Fuzzy Control, *Computers In Industry*, 62 (2011) 213-226.
229. Wong, B.K. and Lai, V.S., A Survey of the Application of Fuzzy Set Theory in Production and Operations Management: 1998-2009, *Int. J. Production Economics*, 129 (2011) 157-168.
230. Cirstea, M.N., Dinu, A., Khor, J.G. and McCormick, M., Neural and Fuzzy Logic Control of Drives and Power Systems, Newnes, 2002.
231. Lee, K.H., First Course on Fuzzy Theory and Applications, Springer, 2005.
232. Zimmermann, H.J., Fuzzy Set Theory and its Applications, Kluwer Academic Publishers, 1992.
233. Baczynski, M. and Jayaram, B., Fuzzy Implications, Springer, 2008.
234. Jantzen, J., Foundations of Fuzzy Control, Wiley, 2007.
235. Kovacic, Z. and Bogdan, S., Fuzzy Controller Design Theory and Applications, Taylor & Francis, 2006.
236. Nguyen, H.T., Prasad, N.R., Walker, C.L. and Walker E.A., A First Course in Fuzzy and Neural Control, Chapman & Hall/CRC, 2003.

237. Passino, K.M. and Yurkovich, S., *Fuzzy Control*, Addison-Wesley, 1998.
238. Grigorie, T.L., *Fuzzy Controllers, Theory and Applications*, InTech, 2011.
239. Shin, Y.C. and Xu, C., *Intelligent Systems Modeling, Optimization, and Control*, CRC Press, 2009.
240. Zhang, H. and Liu, D., *Fuzzy Modeling and Fuzzy Control*, Birkhauser Boston, 2006.
241. Chen, G. and Pham, T.T., *Introduction to Fuzzy Sets, Fuzzy Logic, and Fuzzy Control Systems*, CRC Press, 2001.
242. Ross, T.J., *Fuzzy Logic with Engineering Applications*, John Wiley & Sons, 2010.
243. Ibrahim, A.M., *Fuzzy Logic for Embedded Systems Applications*, Newnes, 2004.
244. Feng, G., *Analysis and Synthesis of Fuzzy Control Systems: A Model-Based Approach*, CRC Press, 2010.
245. Harris, J., *Fuzzy Logic Applications in Engineering Science*, Springer, 2006.
246. Espinosa, J., Vandewalle, J. and Wertz, V., *Fuzzy Logic, Identification and Predictive Control*, Springer, 2005.
247. Bojadziev, G. and Bojadziev, M., *Fuzzy Logic for Business, Finance, and Management*, World Scientific, 2007.
248. Castillo, O., *Type-2 Fuzzy Logic in Intelligent Control Applications*, Springer, 2011.
249. Mamdani, E.H., *Application of Fuzzy Algorithms for Control of Simple Dynamic Plant*, *Proceedings of the Institution of Electrical Engineers*, 121, 12 (1974) 1585-1588.
250. Mamdani, E.H., Assilian, S., *An Experiment in Linguistic Synthesis with a Fuzzy Logic Controller*, *International Journal of Man-Machine Studies*, 7, 1 (1975) 1-13.
251. Rahman, S.M. and Ratrou, N.T., *Review of the Fuzzy Logic Based Approach in Traffic Signal Control: Prospects in Saudi Arabia*, *Journal of Transportation Systems Engineering and Information Technology*, 9, 5 (2009) 58-70.
252. Roychowdhury, S. and Pedrycz, W., *A Survey of Defuzzification Strategies*, *International Journal of Intelligent Systems*, 16 (2001) 679-695.
253. Tamir, D.E. and Kandel, A., *Axiomatic Theory of Complex Fuzzy Logic and Complex Fuzzy Classes*, *Int. J. of Computers, Communications & Control*, VI, 3 (2011) 562-576.

254. Gupta, R.A., Kumar, R. and Bansal, A.K., Artificial Intelligence Applications in Permanent Magnet Brushless DC Motor Drives, Artificial Intelligence Review, 33, 3 (2010) 175-186.
255. Isermann, R., On Fuzzy Logic Applications for Automatic Control, Supervision, and Fault Diagnosis, IEEE Transactions on Systems, Man, and Cybernetics-Part A: Systems and Humans, 28, 2 (1998) 221-235.
256. Mellit, A., Kalogirou, S.A., Hontoria, L. and Shaari, S., Artificial Intelligence Techniques for Sizing Photovoltaic Systems: A Review, Renewable and Sustainable Energy Reviews, 13 (2009) 406-419.
257. Naidu, D.S. and Rieger, C.G., Advanced Control Strategies for Heating, Ventilation, Air-Conditioning, and Refrigeration Systems-An Overview: Part I: Hard Control, HVAC&R Research, 17, 1 (2011) 2-21.
258. Mitra, S. and Hayashi, Y., Neuro-Fuzzy Rule Generation: Survey in Soft Computing Framework, IEEE Transactions on Neural Networks, 11, 3 (2000) 748-768.
259. Shahirinia, A.H., Tafreshi, S.M.M., Gastaj, A.H. and Moghaddamjoo, A.R., Optimal Sizing of Hybrid Power System Using Genetic Algorithm, International Conference on Future Power Systems, November, 2005.
260. Ghoneim, A.A., Design Optimization of Photovoltaic Powered Water Pumping Systems, Energy Conversion & Management, 47, 11-12 (2006) 1449-1463.
261. Altas, I.H. and Sharaf, A.M., A Novel GUI Modeled Fuzzy Logic Controller for a Solar Powered Energy Utilization Scheme, The 13th International Conference on Emerging Nuclear Energy Systems (ICENES2007), Istanbul, Turkey, June, 2007.
262. Altas, I.H. and Sharaf, A.M., A Photovoltaic Array Simulation Model for Matlab-Simulink GUI Environment, International Conference on Clean Electrical Power, ICCEP'07, Capri, Italy, May, 2007.
263. Altas, I.H. and Sharaf, A.M., A Fuzzy Logic Power Tracking Controller For A Photovoltaic Energy Conversion Scheme, Electric Power Systems Research Journal, 25, 3 (1992) 227-238.
264. Altas, I.H. and Sharaf, A.M., A Novel Maximum Power Fuzzy Logic Controller for Photovoltaic Solar Energy Systems, Renewable Energy, 33, 3 (2008) 388-399.
265. Buchmann, I., Batteries in a Portable World, Cadex Electronics Inc., Second Edition, ISBN 0-9682118-2-8.
266. Piller, S., Perrin, M. and Jossen, A., Methods for State-of-Charge Determination and Their Applications, Journal of Power Sources, 96 (2001) 113-120.
267. Pop, V., Bergveld, H.J., Danilov, D., Regtien, P.P.L. and Notten, P.H.L., Battery Management Systems, Springer, 2008.

268. Tremblay, O., Dessaint, L.-A. and Dekkiche, A.-I., A Generic Battery Model for the Dynamic Simulation of Hybrid Electric Vehicles, IEEE Vehicle Power and Propulsion Conference, VPPC 2007, 2007, 284-289.
269. Digitally-Controlled Phase Shift Using the DS1669, Feb 28, 2002, <http://pdfserv.maxim-ic.com/en/an/AN184.pdf>. January 6, 2012.
270. Smith S.W., The Scientist and Engineer's Guide to Digital Signal Processing, California Technical Publishing, 1999.
271. OPA549, <http://www.ti.com/product/opa549>. January 6, 2012.
272. LM 741 Operational Amplifier, <http://cache.national.com/ds/LM/LM741.pdf>. January 6, 2012.
273. IR2181 High and Low Side Driver Datasheet, International Rectifier Corporation, 2004.
274. Saglam, M., Calculating the Technical Potential of Wave Energy in Turkey, Case Studies for Project Feasibility and Design, Master of Science Thesis, Marmara University, 2004.
275. Dixon, W.E., Dawson, D.M., Costic, B.T. and Queiroz, M.S., Towards the Standardization of a MATLAB-Based Control Systems Laboratory Experience for Undergraduate Students, Proceedings of the 2001 American Control Conference, 2 (2001) 1161-1166.
276. Ramos-Carranza, H.A., Medina, A. and Chang, G.W., Real-Time Shunt Active Power Filter Compensation, IEEE Transactions on Power Delivery, 23, 4 (2008) 2623-2625.
277. Paja, C.A.R., Romero, A. and Giral, R., Evaluation of Fixed-Step Differential Equations Solution Methods for Fuel Cell Real-Time Simulation, International Conference on Clean Electrical Power, ICCEP '07, 2007, 480-487.
278. Bakhti, A. and Benbaouche, L., Simulink-Rtwtgt Co-Design of Real Time Digital Interfaces, Proceedings of the 44th IEEE Conference on Decision and Control, and the European Control Conference 2005, 2005, 7593-7596.
279. Miao, L., Zou, G., Shi, P. and Jiao, X., Development of Hardware Driver for MATLAB/Simulink Real-Time Simulation, International Workshop on Intelligent Systems and Applications, ISA 2009.
280. Park, M-W, Son, Y-J and Kim, J-H, Design of the Real Time Control System for Controlling Unmanned Vehicle, International Conference on Control, Automation and Systems, 2007. ICCAS '07, 2007, 1234-1237.

281. Uriarte, F.M. and Butler-Purry, K.L., Real-Time Simulation of a Small-Scale Distribution Feeder Using Simulink and a Single PC, Proceedings of the 37th Annual North American Power Symposium, 2005, 213-218.
282. Najib, M.S., Jadin, M.S. and Daud, M.R., Development of Real-Time Signal Generator Graphical User Interface Using Matlab 6.5, 7th WSEAS International Conference on Software Engineering, Parallel and Distributed Systems, 2008, 103-106.
283. Limin, S., Shijie, A., Hanbao, C. and Hongbin. G., Study on Real-Time Test-Bench of Speed Governor Using Matlab/Xpc Target, 8th International Conference on Electronic Measurement and Instruments, ICEMI '07, 2007, 3-27-3-31.
284. Yang, P., Li, Y., Zhang, Y. and Li, S., Real-Time Mixed Simulation Platform for Fuzzy Control System Based on MATLAB, 2006 Chinese Control Conference, 1-5 (2006) 280-283.
285. Pivonka, P. and Miksanek, V., Real-Time Communication between MATLAB/Simulink and PLC via Process Visualization Interface, 11th WSEAS International Conference on Circuits, 2 (2007) 28-32.
286. Teng, F.C., Real-time Control Using Matlab Simulink, IEEE International Conference on Systems, Man and Cybernetics, 2000, 2697-2702.

8. APPENDICES

Appendix 1. AC/DC Rectifier (Section 3.3.1), CBWECE (Section 4.2.1), Signal Amplification (Section 4.2.1.4)

Table A.1.1. The parameters of the 3-phase full bridge rectifier constituted with Matlab/Simulink for digital simulation

Snubber resistance, $R_s(\Omega)$	100k
Snubber capacitance, $C_s(F)$	Inf
Power electronic device (Diode)	
$R_{on}(\Omega)$	1m
$L_{on}(H)$	0
Forward voltage, $V_f(V)$	1.5

Table A.1.2. PCI-6070E DAQ card features

Analog Inputs	:	16SE / 8DI
Input resolution	:	12 bits
Max Sampling Rate	:	1.25 MS/s
Input Range	:	± 0.05 to $\pm 10 V$
Analog Outputs	:	2
Output Rate	:	1 MS/s
Output Range	:	$\pm 10 V$
Digital I/O	:	8
Counter/Timer	:	2, 24-bit
Trigger	:	Analog, Digital

Table A.1.3. The operational amplifier features

High Current Output	
8A Continuous	10A Peak
Wide Power Supply Range	
Single Supply: +8V - +60V	Dual Supply: $\pm 4V - \pm 30V$
Full Protected	
Thermal Shutdown	Adjustable Current Limit
Output Disable Control	
Thermal Shutdown Indicator	
Control Reference PIN	

Appendix 2. Signal Amplification (Section 4.2.1.4), Low-voltage/Low-current Power Stage (Section 4.2.1.5.1)

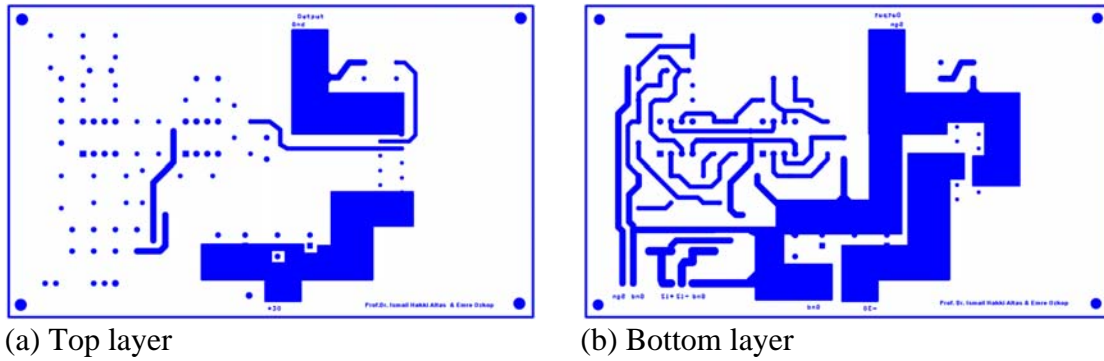


Figure A.2.1. The printed circuit boards of the system

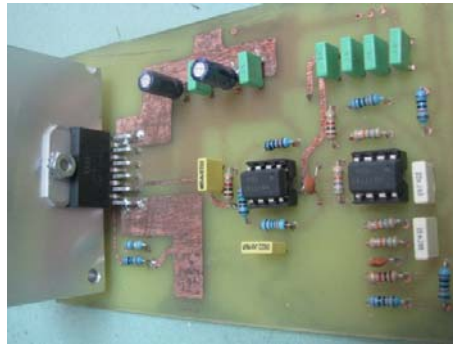


Figure A.2.2. The system photo (phase shift, signal filtering and amplification circuits)

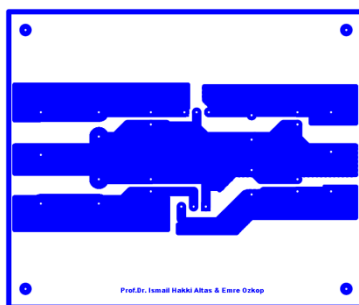


Figure A.2.3. The low power stage PCB

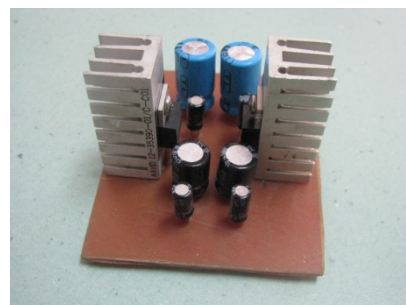


Figure A.2.4. The low power stage photo

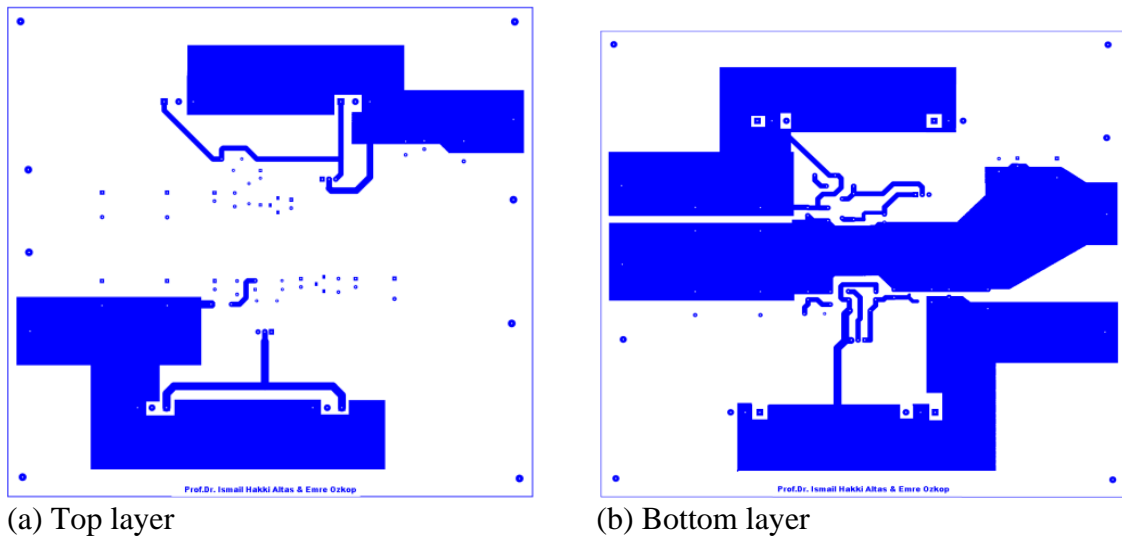
Appendix 3. High-voltage/High-current Power Stage (Section 4.2.1.5.2)

Figure A.3.1. The high power stage printed circuit board

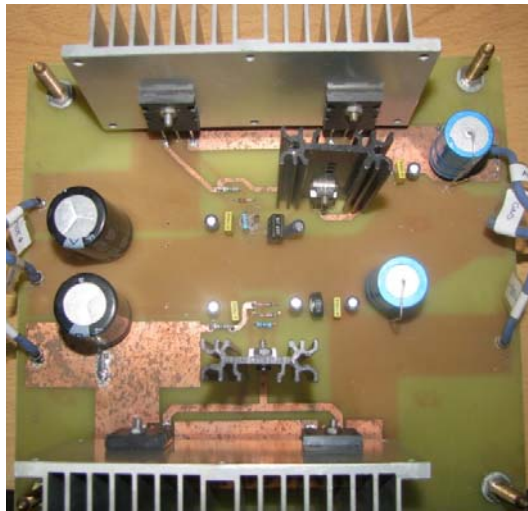


Figure A.3.2. The high power stage photo

Appendix 4. MBWECE (Section 4.2.2)

Table A.4.1. The Permanent Magnet DC (PMDC) motor parameters

Nominal Power (W)	:	250
Nominal Voltage (V)	:	24
Nominal Current (A)	:	12
Nominal Speed (rpm)	:	1500
Protection Class	:	<i>IP 44</i>
Operation Regime	:	S2- Intermittent
Isolation Class	:	<i>F – 155°C</i> (IEC 34-6)
Cooling Type	:	<i>IC – 40</i> (Self-cooling)

Table A.4.2. Three phase permanent magnet generator features

Nominal Power (W)	:	1500
Nominal Speed (rpm)	:	550
Required Moment at Nominal Power (Nm)	:	35
Phase Resistance (Ω)	:	5
Phase Inductance (mH)	:	18.2
Pole number	:	8
Torque constant (Nm/A)	:	1.1
Speed constant (rpm/V)	:	11.5
Rotor Inertia ($Kg.m^2$)	:	0.011
Starting Torque (Nm)	:	< 0.7
Magnet Type	:	<i>NdFeB</i>
Generator Arrangement	:	<i>3 phase star connection AA output</i>

Table A.4.3. Reducer features

Power (kW)	:	0.37
Conversion Rate	:	4
Output Speed (r/m)	:	359
Output Moment (Nm)	:	9.4
Service Factor	:	5.8

Appendix 5. DC-DC Buck Converter Design (Section 4.4.1), Power Supply (Section 4.4.2.1), DAQ Output Isolation Circuit (Section 4.4.3)

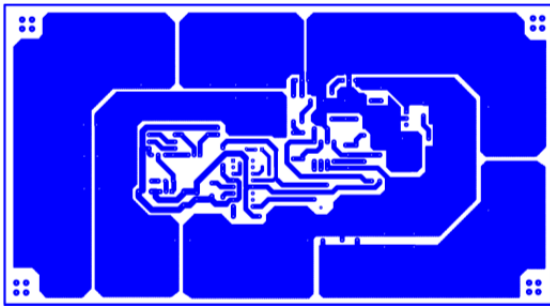


Figure A.5.1. The DC-DC buck converter printed circuit board



Figure A.5.2. The DC-DC buck converter general view

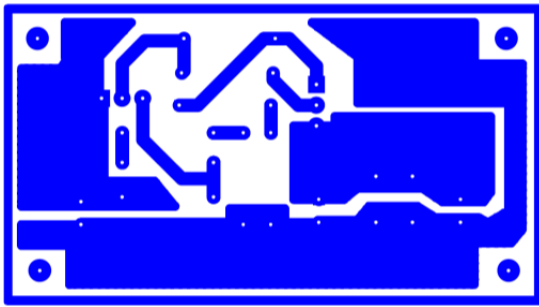


Figure A.5.3. The printed circuit board of chopper power supply



Figure A.5.4. The power supply photo chopper

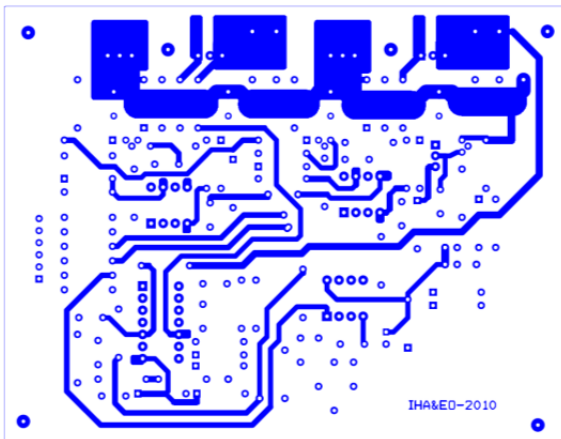


Figure A.5.5. The DC-DC chopper PCB (top layer)



Figure A.5.6. The DC-DC chopper photo

Appendix 6. Integrated Power Module (Section 4.4.4.1)

Table A.6.1. Switch states and current values for IPM

Parameter	Description	Max. Value	Units
V_{CES} / V_{RRM}	IGBT/Diode Blocking Voltage	600	V
V_+	Positive Bus Input Voltage	450	V
$I_O @ T_C=25^\circ\text{C}$	RMS Phase Current (Note 1)	20	A
$I_O @ T_C=100^\circ\text{C}$	RMS Phase Current (Note 1)	10	A
I_O	Pulsed RMS Phase Current (Note 2)	30	A
F_{PWM}	PWM Carrier Frequency	20	kHz
P_d	Power dissipation per IGBT @ $T_C = 25^\circ\text{C}$	38	W
V_{ISO}	Isolation Voltage (1min)	2000	V_{RMS}
T_J (IGBT&Diodes)	Operating Junction temperature Range	-40 to +150	$^\circ\text{C}$
T_J (Driver IC)	Operating Junction temperature Range	-40 to +150	$^\circ\text{C}$
T	Mounting torque Range (M3 screw)	0.5 to 0.6	Nm

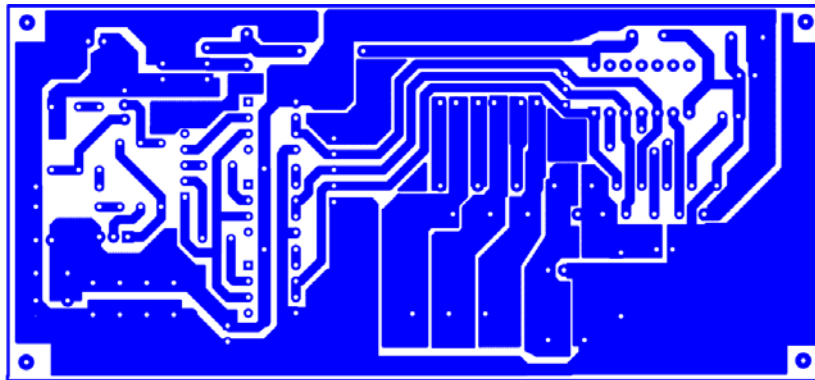


Figure A.6.1. The printed circuit board of the DC/AC inverter system



Figure A.6.2. The general view of inverter system

Appendix 7. Digital Simulation (Section 5.1.2.1.3), Digital Simulation and Experimental Results (Section 5.1.2.1.5), Digital Simulation (Section 5.1.2.3.3), Digital Simulation and Experimental Results (Section 5.1.2.3.5)

Table A.7.1. The parameters of the system with the SPF-GP control main unit constituted with Matlab/Simulink for digital simulation

3-phase full bridge rectifier				
	Snubber resistance, $R_s(\Omega)$			100k
	Snubber capacitance, $C_s(F)$			Inf
	Power electronic device (Diode)			
	$R_{on}(\Omega)$	1m	$L_{on}(H)$	0
	Forward voltage, $V_f(V)$			1.5
DC bus filter				
	DC bus filter inductance, $L_f(H)$			9.5u
	DC bus filter capacitor, $C_f(F)$			4700u
The Buck converter				
	The buck converter input filter capacitor, $C_1(F)$			220u
	The buck converter input filter inductor, $L_1(H)$			10.16u
	The buck converter input filter capacitor, $C_2(F)$			10u
	The buck converter freewheeling diode, D1			
	Resistance, $R_{on}(\Omega)$			0.001
	Inductance, $L_{on}(H)$			0
	Forward voltage, $V_f(V)$			1.8
	Snubber resistance, $R_s(\Omega)$			100
	Snubber capacitance, $C_s(F)$			10n
	The buck converter switch, Q1 (IGBT)			
	Internal resistance, $R_{on}(\Omega)$			0.001
	Snubber resistance, $R_s(\Omega)$			100
	Snubber capacitance, $C_s(F)$			10n
	The buck converter filter inductor, $L_2(H)$			32.4u
	The buck converter filter capacitor, $C_5(F)$			100u

Appendix 7 (continued)

Table A.7.1. The parameters of the system with the SPF-GP control main unit constituted with Matlab/Simulink for digital simulation (Cont.)

FACTS SPF-GP system				
The SPF-GP capacitor, $C_d(F)$				34000u
The SPF-GP switches, S_A, S_A (IGBTs)				
Internal resistance, $R_{on}(\Omega)$				0.001
Snubber resistance, $R_s(\Omega)$				100
Snubber capacitance, $C_s(F)$				10n
1-phase full bridge rectifier				
Snubber resistance, $R_s(\Omega)$				100k
Snubber capacitance, $C_s(F)$				Inf
Power electronic device (Diode)				
$R_{on}(\Omega)$	1m	$L_{on}(H)$	0	
Forward voltage, $V_f(V)$			1.5	
Controller-A				
The mono-loop PI controller parameters				
$K_{P(dcmlv)}$	3		$K_{I(dcmlv)}$	1
PWM generator				
Carrier frequency (Hz)			1000	
Sampling time (second)			50u	
Controller-B				
Loop weight gain of the current tracking loop, γ_{I_d}			0.1	
Loop weight gain of the voltage tracking loop, γ_{V_d}			1	
Loop weight gain of the power tracking loop, γ_{P_d}			0.1	
The multi-loop PI controller parameters				
K_P	500		K_I	50
PWM generator				
Carrier frequency (Hz)			1000	
Sampling time (Second)			50u	

Appendix 8. Digital Simulation and Experimental Results (Section 5.1.2.1.5)

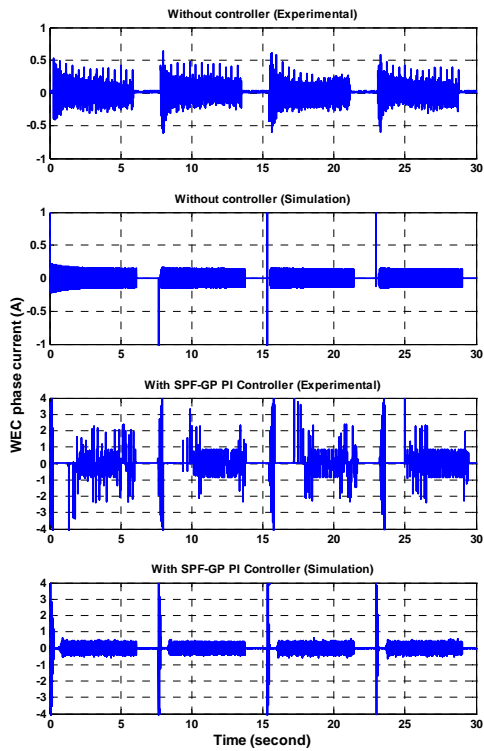


Figure A.8.1. WEC current (Case I-II)

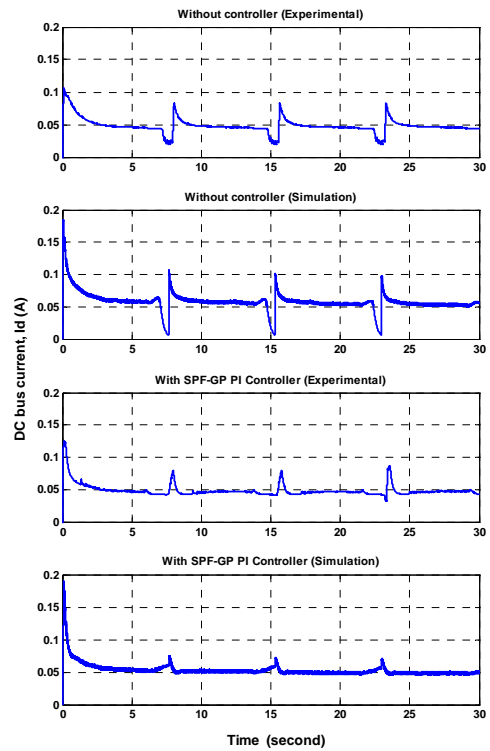


Figure A.8.2. DC bus current (Case I-II)

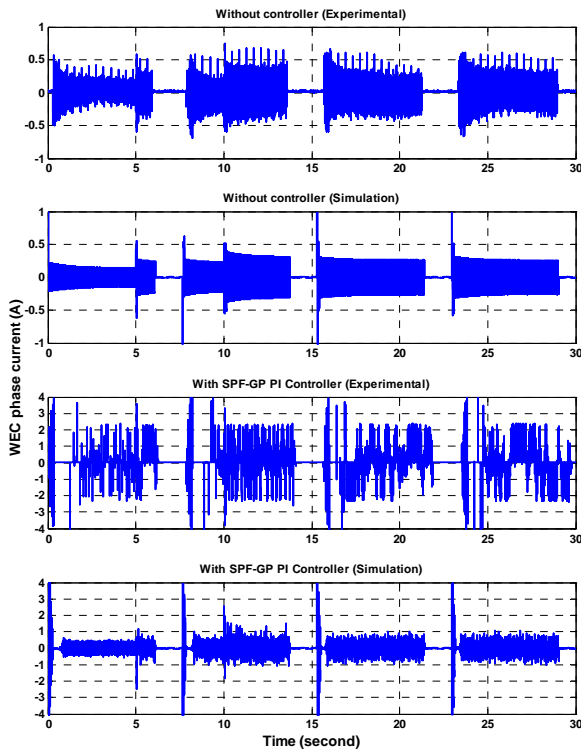


Figure A.8.3. WEC current (Case III-IV)

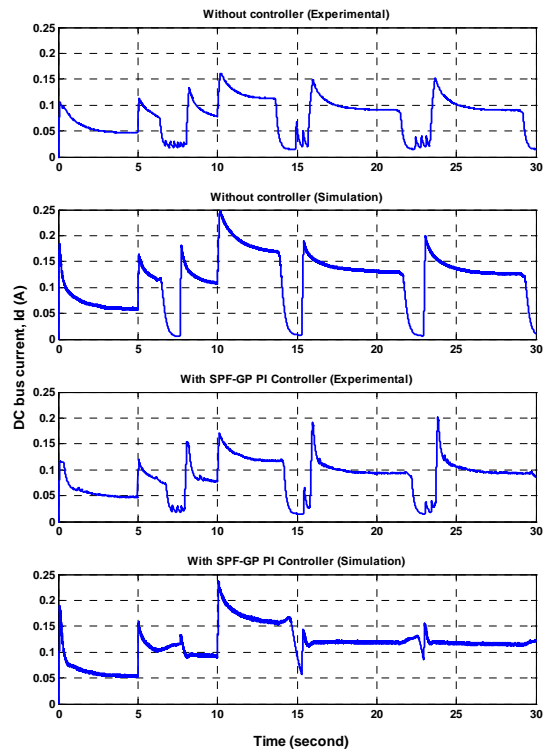


Figure A.8.4. DC bus current (Case III-IV)

Appendix 8 (continued)

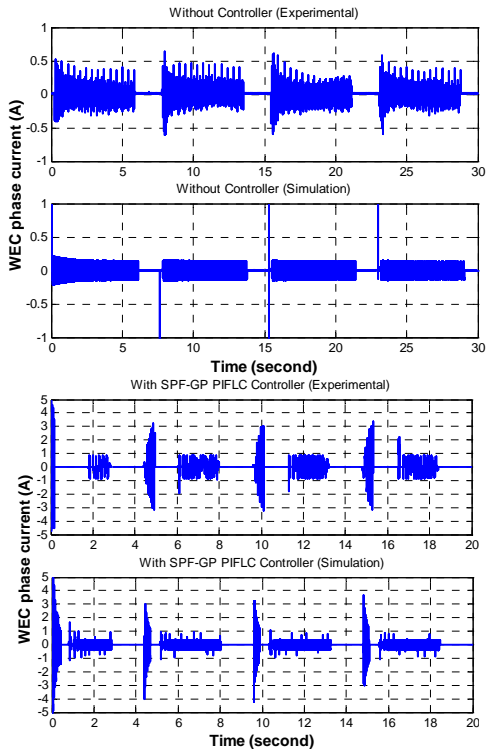


Figure A.8.5. WEC current Case I-II

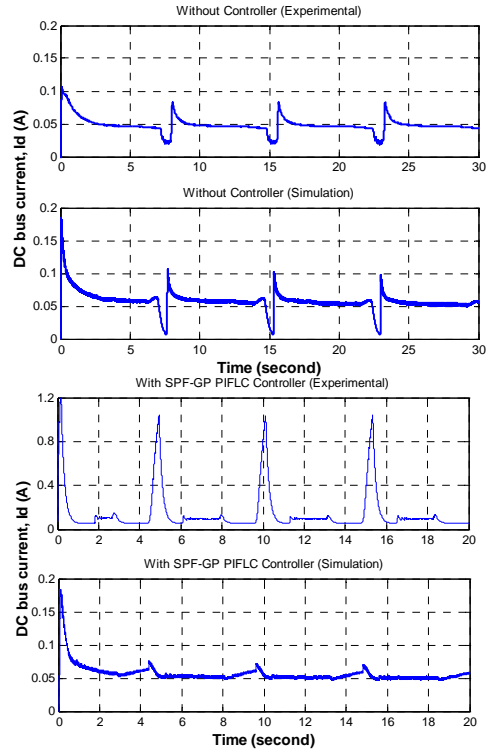


Figure A.8.6. DC bus current (Case I-II)

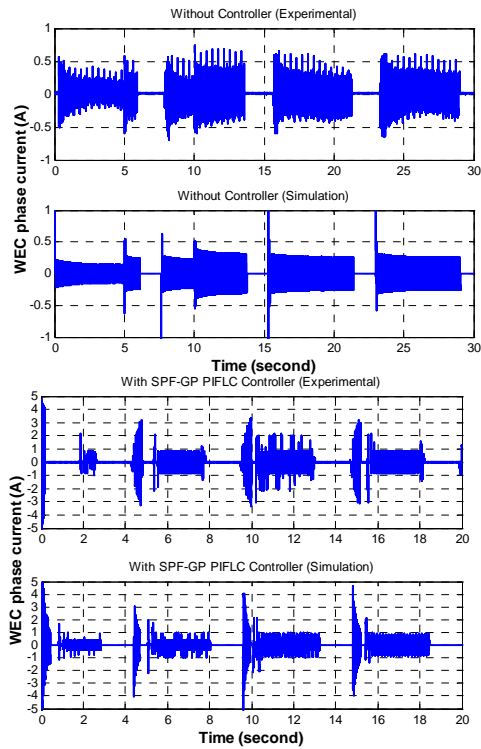


Figure A.8.7. WEC current (Case III-IV)

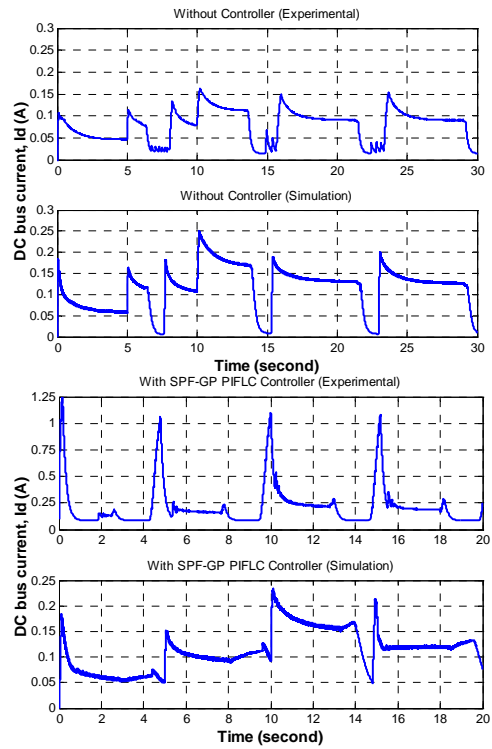


Figure A.8.8. DC bus current (Case III-IV)

Appendix 9. Digital Simulation and Experimental Results (Section 5.1.2.1.5)

Table A.9.1. DC Common Bus voltage under (Constant voltage control)

	FPI	ISE	IAE	ITAE
Without SPF-GP	Experimental	904.0326	133.3123	1953.3359
	Simulation	1407.7820	179.8697	2701.7281
With SPF-GP	Experimental	545.8469	75.8282	699.6841
	Simulation	241.6564	43.0775	435.1429

Table A.9.2. DC Motor load voltage under (Constant voltage control)

	FPI	ISE	IAE	ITAE
Without SPF-GP	Experimental	12.6079	8.7437	134.2657
	Simulation	5.4394	5.7263	86.0158
With SPF-GP	Experimental	0.5477	1.3291	10.3094
	Simulation	1.3244	1.3749	7.6363

Table A.9.3. DC Bus voltage under (Variable voltage control)

	FPI	ISE	IAE	ITAE
Without SPF-GP	Experimental	576.8663	112.0012	1583.1871
	Simulation	1572.4872	192.6991	2929.0777
With SPF-GP	Experimental	436.3712	65.3647	553.2747
	Simulation	391.8645	53.6663	589.4391

Table A.9.4. DC Motor load voltage under (Variable voltage control)

	FPI	ISE	IAE	ITAE
Without SPF-GP	Experimental	301.4509	46.1923	792.2616
	Simulation	76.0245	19.5800	318.9888
With SPF-GP	Experimental	224.7212	33.4801	479.1973
	Simulation	8.9981	4.3074	52.8773

Appendix 10. Experimental Results (Section 5.1.2.2.3)

Table A.10.1. The performance of the controllers ($V_{dcmlv(ref)}$), (Scenario-I)

Controller A	Controller B	tr (s) (10-90%)	%OS	ISE	IAE	ITAE
		0-2 sec.	0-2 sec.			
PI	Without controller	0.4391	0	681.0425	80.0832	823.3656
PI	PI	0.1298	65.2410	757.3827	93.4360	871.2591
PI	SSFTPIC	0.1325	58.3995	545.8469	75.8283	699.6843
PI	SMC	0.1439	29.9305	412.2266	54.5196	545.6171
PI	FTSMC	0.2786	0.24350	438.6005	53.6733	571.7985

Table A.10.2. The performance of the controllers ($V_{d(ref)}$), (Scenario-I)

Controller A	Controller B	tr (s) (10-90%)	%OS	ISE	IAE	ITAE
		0-2 sec.	0-2 sec.			
PI	Without controller	0.0616	0	11.6453	8.3003	85.8642
PI	PI	0.0418	0	4.90030	4.7716	50.7658
PI	SSFTPIC	0.0426	0	1.42360	1.9651	15.3270
PI	SMC	0.04275	0	1.42300	1.9537	15.2517
PI	FTSMC	0.05800	0	1.3089	1.7241	11.2317

Table A.10.3. The performance of the controllers ($V_{dcmlv(ref)}$), (Scenario-II)

Controller A	Controller B	tr (s) (10-90%)	%OS	ISE	IAE	ITAE
		0-2 sec.	0-2 sec.			
PI	Without controller	0.05995	0	284.6644	42.9635	590.8750
PI	PI	0.04250	0	257.1204	37.9983	539.5519
PI	SSFTPIC	0.04375	0	224.7214	33.4803	479.1981
PI	SMC	0.04090	0	230.2403	34.3774	492.9365
PI	FTSMC	0.05930	0	229.2448	33.9977	487.0221

Appendix 10 (continued)

Table A.10.4. The performance of the controllers ($V_{d(ref)}$), (Scenario-II)

Controller A	Controller B	tr (s) (10-90%)	%OS	ISE	IAE	ITAE
		0-2 sec.	0-2 sec.			
PI	Without controller	0.4242	0	500.6947	72.8395	696.8096
PI	PI	0.1331	62.528	517.0002	73.9713	629.6566
PI	SSFTPIC	0.1314	58.506	436.3712	65.3647	553.2747
PI	SMC	0.1386	32.1075	339.6065	50.5886	472.3016
PI	FTSMC	0.2791	0.2785	319.1388	46.0691	448.4086

Table A.10.5. The performance of the controllers ($V_{dcmlv(ref)}$), (Scenario-III)

Controller A	Controller B	tr (s) (10-90%)	%OS	ISE	IAE	ITAE
		0-2 sec.	0-2 sec.			
PI	Without controller	0.0599	0	284.6644	42.9635	590.8750
PI	PI	0.0398	0	0.746000	0.77679	6.52261
PI	SSFTPIC	0.0395	0	0.72040	0.75243	6.17892
PI	SMC	0.0413	0	0.81670	0.73877	5.88066
PI	FTSMC	0.0420	0	0.77065	0.68228	4.82701

Table A.10.6. The performance of the controllers ($V_{d(ref)}$), (Scenario-III)

Controller A	Controller B	tr (s) (10-90%)	%OS	ISE	IAE	ITAE
		0-2 sec.	0-2 sec.			
PI	Without controller	-----	-----	22871.0692	672.8395	6696.8096
PI	PI	0.4696	9.957	2397.84000	140.1632	1586.6157
PI	SSFTPIC	0.4682	7.4962	2139.02094	132.8928	1503.6316
PI	SMC	0.5106	1.2630	2130.39458	120.2130	1347.6857
PI	FTSMC	0.5144	0.0902	2128.62562	120.0451	1340.7657

Appendix 11. Experimental Results (Section 5.1.2.2.3)

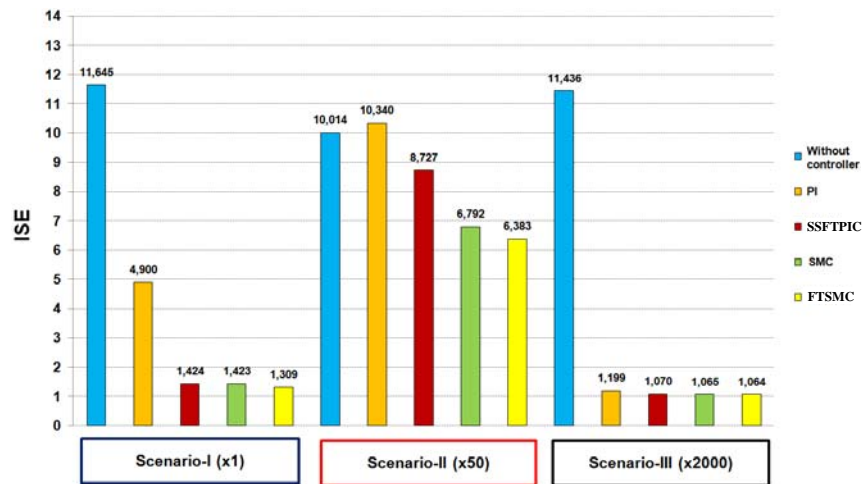


Figure A.11.1. The performance analysis of the Controller-B (ISE)

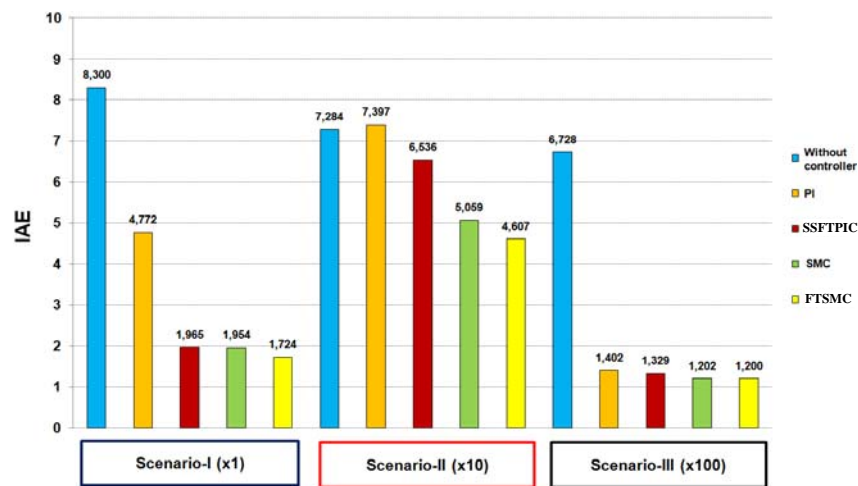


Figure A.11.2. The performance analysis of the Controller-B (IAE)

Appendix 11 (continued)

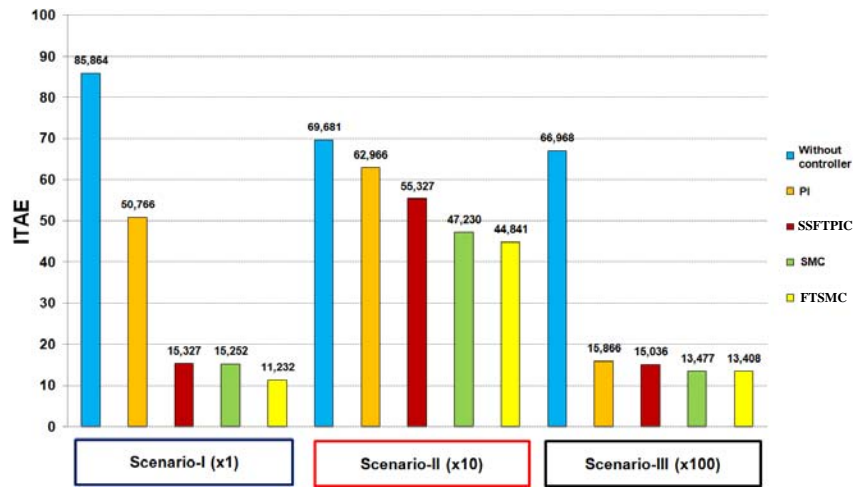


Figure A.11.3. The performance analysis of the Controller-B (ITAE)

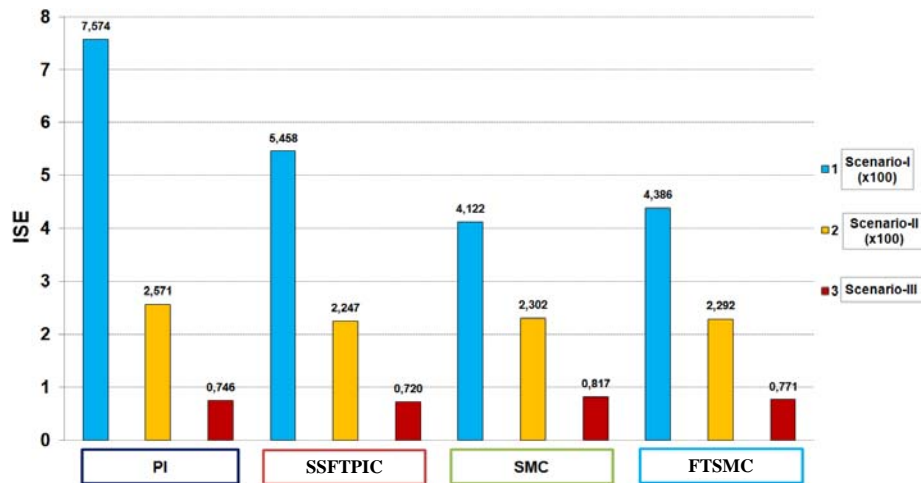


Figure A.11.4. The performance analysis of the Controller-A (ISE)

Appendix 11 (continued)

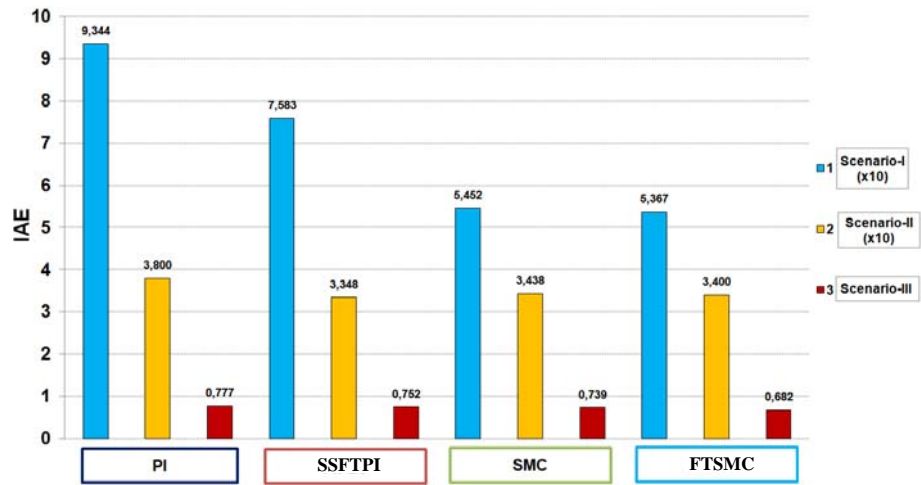


Figure A.11.5. The performance analysis of the Controller-A (IAE)

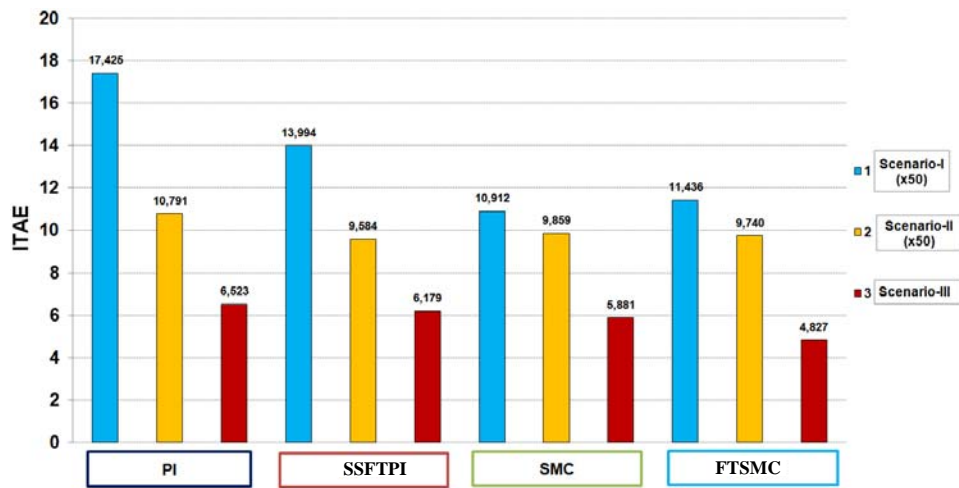


Figure A.11.6. The performance analysis of the Controller-A (ITAE)

Appendix 12. Digital Simulation and Experimental Results (Section 5.1.2.3.5)

Table A.12.1. Load side Common Bus voltage under (Case I-II)

		ISE	IAE	ITAE
Without SPF-GP	Simulation	2066.4879	201.2764	3167.4853
	Experimental	1675.6597	167.6058	2609.6729
With SPF-GP	Simulation	815.3542	83.9701	1379.5972
	Experimental	443.0999	65.1803	1048.0260

Table A.12.2. Battery voltage (Case I-II)

		ISE	IAE	ITAE
Without SPF-GP	Simulation	91.8504	49.1455	706.6137
	Experimental	90.6249	47.4235	678.2052
With SPF-GP	Simulation	91.6499	49.0811	705.3173
	Experimental	87.1054	46.2500	660.0712

Table A.12.3. Battery charge current (Case I-II)

		ISE	IAE	ITAE
Without SPF-GP	Simulation	0.6424	2.3402	39.1887
	Experimental	1.3294	5.4964	84.4805
With SPF-GP	Simulation	0.5421	1.9687	33.3295
	Experimental	0.8757	2.9514	49.1683

Table A.12.4. PMDC motor speed (Case I-II)

		ISE	IAE	ITAE
Without SPF-GP	Simulation	450385.6530	1217.6408	2056.3861
	Experimental	418202.2294	1074.3715	1729.7244
With SPF-GP	Simulation	450376.6776	1217.3161	2050.2660
	Experimental	402170.0597	1064.3084	1826.6001

Table A.12.5. Three phase AC motor phase-phase voltage (Vrms) (Case I-II)

		ISE	IAE	ITAE
Without SPF-GP	Simulation	8.2764	2.2339	3.8899
	Experimental	8.5699	3.1708	18.0389
With SPF-GP	Simulation	8.2760	2.2228	3.8117
	Experimental	8.5662	3.1862	18.0737

Appendix 12 (continued)

Table A.12.6. Load side bus voltage under (Case III-IV)

		ISE	IAE	ITAE
Without SPF-GP	Simulation	2066.4358	201.2800	3167.3933
	Experimental	1642.7692	161.8944	2530.9217
With SPF-GP	Simulation	818.6631	84.1860	1383.1333
	Experimental	420.1973	63.3190	963.0640

Table A.12.7. Battery voltage (Case III-IV)

		ISE	IAE	ITAE
Without SPF-GP	Simulation	91.5390	49.0460	704.4595
	Experimental	83.9412	45.1840	642.3103
With SPF-GP	Simulation	91.3428	48.9829	703.1887
	Experimental	74.9666	42.1109	597.0610

Table A.12.8. Battery charge current (Case III-IV)

		ISE	IAE	ITAE
Without SPF-GP	Simulation	0.6424	2.3409	39.2080
	Experimental	1.2698	5.2123	80.4256
With SPF-GP	Simulation	0.5433	1.9728	33.3811
	Experimental	0.8678	2.9138	45.9646

Table A.12.9. PMDC motor speed (Case III-IV)

		ISE	IAE	ITAE
Without SPF-GP	Simulation	474471.6283	1492.7427	6592.8171
	Experimental	388075.5433	1309.6179	5784.3085
With SPF-GP	Simulation	474462.6209	1492.7023	6595.0042
	Experimental	430370.8547	1306.5143	5695.6610

Table A.12.10. Three phase AC motor phase-phase voltage (Vrms)
(Case III-IV)

		ISE	IAE	ITAE
Without SPF-GP	Simulation	6.5450	4.1039	55.9237
	Experimental	5.8755	3.8769	65.2523
With SPF-GP	Simulation	6.5509	4.1067	55.9188
	Experimental	5.8490	3.8492	64.5019

CURRICULUM VITAE

Emre Özkop was born in Trabzon, Turkey on May 8, 1980. He graduated from Affan Kitapçıoğlu High School in 1998. Emre Özkop received his B.Sc.E in Electrical and Electronics Engineering from Gazi University and M.Sc.E from Karadeniz Technical University (KTU), Turkey, in 2003 and 2006, respectively. He also took part in the Erasmus Programme at the department of EESA, EELAB at Gent University in Gent, Belgium in 2005.

From 2004 to 2011, he was a research assistant in Electrical and Electronics Engineering Department, KTU, Turkey. Since January 2012, he has been a lecturer in the same department.

He is the author and co-author over forty scientific publications in journals and conference proceedings. He is a member of the Chamber of Electrical Engineers (EMO) and student member of the Institute of Electrical and Electronics Engineers (IEEE).

He got the Scientific and Technical Research Council of Turkey (TUBITAK) BAYG Scholarship for MSc studies from 2005-2007 and has gotten TUBITAK BAYG Scholarship for PhD studies since 2008. His research interests include analysis, control, and design of power electronic systems, intelligent control of power systems and utilization of renewable energy.

- [1]. **Ozkop, E.**, Altas, I.H. and Sharaf, A.M., A Novel Switched Power Filter-Green Plug (SPF-GP) Scheme for Wave Energy Systems, Renewable Energy, 44 (2012) 340-358.